Somerville, P.G., J.P. McLaren, L.V. LeFerre, R.W. Burger, and D.V. Helmburger 1987. Comparison of source scaling relations of Eastern and Western North American earthquakes, BSSA, 77, #2, 322-346.

Stephenson, D.E., R.C. Lee, and J.K. Kimball, 1993. Savannah River Site Disaggregated Seismic Spectra, in Fourth DOE Natural Phenomena Hazards Mitigation Conference.

Stepp, J.C., 1997. Moment Magnitude - Stress Drop Estimates for the Charleston Earthquake of 1886. Letter to R.C. Lee from J.C. Stepp of 2/19/97.

Stieve, A.L., C. Coruh, and J. Costain 1994. Confirmatory Drilling Project Final Report, WSRC-RP-94-0136.

Stokoe, Kenneth H., II, Hwang, Seon-Keun, Darendeli, Mehment, and N. K. James Lee, 1995. *Correlation Study of Nonlinear Dynamic Soil Properties: Savannah River Site, Aiken, South Carolina*, Rev. 0, File No. SRS-FR-CDP-95, University of Texas at Austin, Department of Civil Engineering, September 13, 1995.

Toro, G.R., N.A. Abrahamson, and J.F. Schneider, 1994. Engineering model of strong ground motions from earthquakes in the central and eastern United States, submitted to Earthquake Spectra, March 1994.

Toro, G.R., 1996. Probabilistic Models of Site Velocity Profiles at the Savannah River Site, Aiken, South Carolina, draft report November 4, 1996.

URS/John A. Blume and Associates, Engineers, 1982. "Update of Seismic Criteria for the Savannah River Plant, Vol. 1 of 2", Geotechnical: URS/JAB 8144, San Francisco CA, prepared for E.I. du Pont de Nemours and Company, DPE 3699, 293 pp.

U.S. Department of Energy, 1989. General Design Criteria, DOE Order 6430.1A Washington, D.C.

U.S. Department of Energy, 1992. Natural Phenomena Hazards Design Requirements Draft DOE Order 5480.NPH, Washington, D.C.

U.S. Department of Energy, 1989. General Design Criteria, DOE Standard 1020, Natural Phenomena Hazards Design and Evaluation Criteria for Department of Energy Facilities U.S. Department of Energy, Washington, D.C.

U.S. Department of Energy, 1992. General Design Criteria, DOE Standard 1024. Guidelines for Use of Probabilistic Seismic Hazard Curves at Department of Energy Sites, U.S. Department of Energy, Washington, D.C. 20585

U. S. Department of Energy, 1995. *DOE Standard: Natural Phenomena Hazards Assessment Criteria.* DOE-STD-1023-95, Change Notice #1, Washington, D. C. January 1996.

U.S. Nuclear Regulatory Commission, 1977. Regulatory Guide 1.60 Design Response Spectra for Seismic Design of Nuclear Power Plants, Washington, D.C.

WSRC, 1994. In Tank Processing (ITP) Geotechnical Summary Report, Rev. 0, WSRC-TR-94-0369.

WSRC, 1995. Engineering Standards Manual, Structural Design Criteria, Std. No. 1060, WSRC-TM-95-1, 8/1/95.

WSRC, 1996a. Conduct of Engineering and Technical Support Engineering Manual, E7.

WSRC, 1996b. F/H Canyon Ground Response Analysis, letter from L.A. Salomone to B.J. Gutierrez, ECSD-SGS-96-0225, June 28, 1996.

WSRC, 1996c. SRS Design Basis Response Spectrum, Status as of 12/31/96. Letter report to B.J. Gutierrez from L.A. Salomone, 12/31/96. PECD-SGS-96-0438.

WSRC, 1996d. Determination of Acceleration Time Histories and Response Spectra for F-Canyon, Appendix B- LAYERSH documentation, Calculation No. K-CLC-F-00011.

WSRC, 1997a. Determination of Soil Surface Uniform Hazard Spectrum for SRS Geologic Conditions Using SRS Mean Spectral Amplification Functions, Calculation number K-CLC-G-00029.

WSRC, 1997b. Computation of Soil Hazard by Application of SRS Spectral Amplification Functions to EPRI Bedrock Hazard, Calculation number K-CLC-G-00028.

Zoback and Moos, 1989. In situ stress measurements at the Savannah River Site.

16.0 TABLES

TABLE 4.1 - Performance Category 3 Bedrock Design Basis Spectrum

Frequency (Hz)	5% Damped Response (g)	Frequency (Hz)	5% Damped Response (g)	Frequency (Hz)	5% Damped Response (g)
0.1	0.0002772	5	0.1652	28	0.1893317
0.2	0.0020445	6	0.1747	31	0.1837419
0.3	0.0052704	7	0.1816	34	0.1778419
0.4	0.0102714	8	0.18637	40	0.1659168
0.5	0.0168325	9	0.1902	45	0.1564396
0.6	0.0227327	10	0.1929	50	0.1477262
0.7	0.0290546	11	0.1952	55	0.1399159
0.8	0.0369375	12	0.1972	60	0.1330411
0.9	0.043226	13	0.1985	65	0.1270767
1	0.0482713	14	0.1996	70	0.1219522
1.1	0.055	14.5	0.1998	75	0.1175789
1.25	0.0648	15	0.2004	80	0.1138581
1.5	0.0772	16	0.2001831	85	0.1106881
1.75	0.088	17	0.2006463	90	0.1079623
2	0.0989	18	0.2007362	95	0.1055485
2.5	0.1171	20	0.1999783	100	0.1031972
3	0.131	22	0.1982369		
4	0.1511	25	0.1943077		

TABLE 4.2 - Performance Category 4 Bedrock Design Basis Spectrum

Frequency (Hz)	5% Damped Response (g)	Frequency (Hz)	5% Damped Response (g)	Frequency (Hz)	5% Damped Response (g)
0.1	0.0012566	4	0.357	28	0.4868542
0.2	0.009044	5	0.383	31	0.4792033
0.3	0.0210028	6	0.4034	34	0.4697532
0.4	0.0372613	7	0.4176	40	0.4476758
0.5	0.0565381	8	0.4311	45	0.4278605
0.6	0.0718682	8.5	0.4375	50	0.4080071
0.7	0.0873354	9	0.4425	55	0.3888318
0.8	0.1066482	10	0.452	60	0.3707935
0.9	0.1210048	11	0.4597	65	0.3541422
1	0.1355	12	0.4657	70	0.3389912
1.1	0.1493	14	0.4757	75	0.3253537
1.25	0.17	16	0.483	80	0.3131722
1.5	0.2031	18	0.4889	85	0.3023209
1.75	0.23	20	0.4916649	90	0.2925963
2	0.252	22	0.4933728	95	0.283595
2.5	0.2917	25	0.4919316	100	0.2742803
3	0.32				

TABLE 5.1 Velocity Profiles Used in this Study

Area	Prof. No.	Name	Lat.	Lon.	Min. Depth (m)	Max. Depth (m)
A	1505	ACPT-1	33.344	81.739	2.74	38.10
A	1506	ACPT-2	33.344	81.738	2.74	37.49
A	1507	ACPT-4	33.344	81.737	2.74	36.27
A	1508	ACPT-7	33.346	81.738	2.74	36.27
A	1509	ACPT-8	33.345	81.739	2.74	37.19
CFD	1537	CFD-18	33.240	81.632	2.71	310.90
CFD	1538	CFD-1	33.238	81.630	0.91	292.61
F	1388	F-SEP-C2	33.288	81.678	7.62	52.43
F	1389	F-SEP-C3	33.288	81.675	2.74	35.36
F	1390	F-SEP-C4	33.287	81.676	2.74	33.53
F	1391	F-SEP-C5	33.287	81.676	3.05	34.75
F	1392	F-SEP-C6	33.288	81.676	4.57	54.56
F	1393	F-SEP-C7	33.289	81.676	3.05	51.51
F	1394	F-SEP-C8	33.286	81.678	4.88	36.88
F	1395	F-SEP-C9	33.288	81.679	3.05	46.03
F	1396	F-SEP-C10	33.290	81.678	3.05	46.03
F	1397	F-SEP-C11	33.289	81.677	3.05	52.43
F	1398	F-SEP-C12	33.288	81.679	3.05	54.25
F	1399	F-SEP-C13	33.289	81.678	2.74	52.12
F	1400	F-SEP-C14	33.287	81.679	3.05	46.94
F	1401	F-SEP-C15A	33.287	81.677	3.05	48.77
F	1402	F-SEP-C16	33.287	81.674	3.05	47.85
F	1403	F-SEP-C17	33.288	81.678	4.57	55.47
F	1404	F-SEP-C1	33.288	81.680	3.05	48.46
F	1407	F-TNK-C3	33.282	81.678	3.05	48.77
F	1409	F-TNK-C5	33.283	81.679	3.05	26.82
F	1410	F-TNK-C6	33.282	81.676	3.35	50.60
F	1412	F-TNK-C8	33.283	81.678	3.05	24.99
F	1413	F-TNK-C9	33.282	81.676	5.79	41.76
F	1414	F-TNK-C10	33.282	81.677	3.05	38.41
F	1415	F-TNK-C11	33.283	81.676	3.05	36.88
F	1416	F-TNK-C12	33.284	81.676	3.35	45.11
F	1417	F-TNK-C13	33.275	81.669	3.05	40.54
F	1419	F-TNK-C15	33.283	81.677	3.05	24.08
F	1420	F-TNK-C16	33.281	81.678	3.05	38.71
F	1421	F-TNK-C17	33.284	81.678	3.05	40.23
F	1511	235F-CPT1	33.291	81.676	3.66	46.33
F	1512	235F-CPT2	33.290	81.676	3.66	44.50
F	1513	235F-CPT3	33.291	81.676	3.66	49.99
F	1514	235F-CPT5	33.291	81.676	3.66	47.24
F	1539	F-51	33.289	81.676	3.05	35.66
GCB2	1649	GCB-2, interp	33.322	81.720	43.01	194.49
H	1422	htf-c18	33.284	81.639	3.05	34.14
H	1424	cpt-05	33.285	81.639	2.77	61.27
H	1425	cpt-06	33.285	81.639	2.80	44.50
H	1426	cpt-07	33.285	81.640	2.68	60.35
H	1427	cpt-10	33.285	81.640	5.91	42.37

TABLE 5.1 Velocity Profiles Used in this Study (continued)

Area	Prof. No.	Name	Lat.	Lon.	Min. Depth (m)	Max. Depth (m)
H	1428	cpt-11	33.285	81.639	15.24	60.96
H	1430	cpt-16	33.284	81.640	2.62	33.53
H	1431	cpt-18	33.284	81.639	2.84	53.04
H	1432	cpt-20	33.285	81.638	10.15	32.92
H	1433	cpt-20.1	33.285	81.638	21.73	33.83
H	1434	cpt-20.2	33.285	81.638	3.69	30.21
H	1435	cpt-23	33.286	81.639	4.15	33.22
H	1436	cpt-25	33.286	81.639	2.80	44.50
H	1437	cpt-26	33.285	81.639	2.77	47.55
H	1438	cpt-28.2	33.285	81.638	2.56	37.19
H	1439	cpt-29	33.285	81.640	6.52	60.96
H	1440	cpt-30	33.285	81.639	2.90	62.79
H	1441	cpt-31	33.284	81.640	11.00	41.15
H	1442	H-CYN-C01	33.290	81.641	3.05	41.45
H	1443	H-CYN-C02	33.289	81.643	6.71	44.20
H	1445	H-CYN-C04	33.99	81.651	3.05	54.25
H	1446	H-CYN-C05	33.288	81.641	4.88	49.68
H	1447	H-CYN-C06	33.290	81.643	3.05	51.51
H	1448	H-CYN-C07	33.290	81.639	3.05	46.03
H	1449	H-CYN-C08	33.290	81.638	3.05	45.11
H	1450	H-CYN-C09	33.291	81.642	3.96	57.00
H	1451	H-CYN-C10	33.289	81.640	2.74	58.22
H	1452	H-CYN-C12	33.287	81.639	2.74	57.30
H	1453	H-CYN-C13	33.287	81.641	2.74	58.22
H	1454	HTF-C05	33.286	81.640	3.05	60.66
H	1455	HTF-C06	33.286	81.640	5.79	61.57
H	1456	HTF-C07	33.28	81.640	3.05	65.53
H	1457	HTF-C08	33.285	81.641	5.79	56.08
H	1458	HTF-C09	33.286	81.641	3.05	57.00
H	1459	HTF-C10	33.285	81.645	3.96	12.19
H	1460	HTF-C11	33.285	81.644	7.50	12.07
H	1461	HTF-C12	33.285	81.646	3.05	12.19
H	1462	HTF-C13	33.285	81.645	3.96	44.20
H	1463	HTF-C14	33.284	81.642	4.88	45.11
H	1464	HTF-C15	33.284	81.641	4.88	46.94
H	1465	HTF-C16	33.285	81.641	5.79	43.28
H	1466	HTF-C17	33.286	81.642	4.88	31.39
H	1467	H244-C01	33.286	81.645	3.69	53.34
H	1468	H244-C02	33.286	81.645	2.77	49.07
H	1469	HCPT-32	33.285	81.643	2.74	57.91
H	1470	HCPT-34	33.284	81.643	3.72	57.61
H	1471	HCPT-37	33.285	81.644	2.68	57.61
H	1472	HCPT-38	33.284	81.643	4.69	58.52
H	1477	RHLWE-C1	33.285	81.645	0.00	50.29
H	1478	RHLWE-C5	33.285	81.645	0.00	50.29
H	1479	RHLWE-C10	33.285	81.645	0.00	50.29
H	1480	RHLWE-C12	33.285	81.645	2.74	54.86

TABLE 5.1 Velocity Profiles Used in this Study (continued)

Area	Prof. No.	Name	Lat.	Lon.	Min. Depth (m)	Max. Depth (m)
H	1481	H-NWT-C1	33.284	81.643	8.23	39.32
H	1482	H-NWT-C2	33.284	81.643	10.97	47.55
H	1483	H-NWT-C3	33.284	81.642	3.66	52.12
H	1484	H-NWT-C4	33.284	81.643	3.66	53.04
H	1485	HMMC-B02	33.284	81.644	3.05	53.34
H	1487	HMMC-C02	33.284	81.644	3.05	30.79
H	1488	HCIFC06A	33.291	81.639	2.74	25.15
H	1489	HCIFC06B	33.291	81.639	2.74	53.34
H	1490	HCIFC07	33.291	81.639	3.05	54.25
H	1491	HCIFC08	33.291	81.640	4.27	36.88
H	1492	HCIFC09	33.291	81.640	2.74	47.85
H	1493	HCIFC10	33.291	81.640	2.74	43.28
H	1494	HLWFC01	33.286	81.638	4.57	54.25
H	1495	HLWFC02	33.286	81.638	2.44	53.34
H	1496	HLWFC04	33.287	81.638	2.74	47.55
H	1540	B3 & B10	33.290	81.646	1.52	60.35
H	1541	B10 & B11	33.290	81.646	1.52	60.35
H	1542	B1 & B8	33.289	81.646	1.52	60.35
H	1543	B8 & B9	33.289	81.646	1.52	60.35
H	1545	SCPT-01	33.285	81.640	3.66	55.79
H	1547	SCPT-14	33.284	81.640	3.68	48.45
H	1589	SCPTU-1	33.290	81.646	5.33	49.53
H	1591	SCPTU7	33.290	81.647	3.81	48.46
H	1592	SCPTU-11	33.289	81.647	5.03	49.99
H	1608	RTRCPT04	33.290	81.646	3.69	50.35
H	1611	RTFCPT15	33.289	81.646	3.68	50.30
H	1615	MMP-2A-SB(R1-R2)	33.284	81.644	1.00	289.00
K	1318	P-25	33.211	81.657	0.00	121.92
K	1544	P-25B & P-25TB	33.211	81.657	0.00	94.49
K	1550	K-1012	33.212	81.666	4.60	57.90
K	1551	K-1008	33.211	81.664	3.00	57.60
K	1552	K-1003	33.213	81.663	3.00	57.90
K	1561	KC-2	33.213	81.663	2.30	37.30
K	1562	KC-RT3	33.213	81.663	2.30	36.60
K	1565	KC-9	33.212	81.662	2.29	37.34
K	1566	KC-10	33.211	81.663	2.29	41.68
K	1567	KC-15	33.213	81.664	2.29	49.71
K	1568	KC-18	33.213	81.664	2.33	28.19
K	1569	KC-20	33.211	81.663	2.29	38.86
K	1570	KR-1	33.210	81.665	3.90	30.97
K	1571	KR-2A	33.211	81.664	3.87	26.73
K	1572	KR-3	33.211	81.664	3.81	29.75
K	1573	KR-5	33.211	81.666	3.81	23.56
K	1574	KR-6	33.211	81.666	5.33	38.86
K	1576	KR-9	33.212	81.664	3.93	38.89
K	1577	KR-12B	33.212	81.666	6.86	22.49
K	1616	MMP-3-SB (R1-R2)	33.211	81.657	1.00	313.00

TABLE 5.1 Velocity Profiles Used in this Study (continued)

Area	Prof. No.	Name	Lat.	Lon.	Min. Depth (m)	Max. Depth (m)
L	1515	LREC-C01	33.210	81.627	3.96	29.57
L	1517	LREC-C03	33.214	81.624	3.05	34.14
L	1518	LREC-C04	33.210	81.625	3.05	49.68
L	1519	LREC-C05	33.212	81.626	3.05	48.77
L	1520	LREC-C06	33.211	81.624	3.05	52.43
L	1521	LREC-C07	33.211	81.624	3.05	46.03
L	1522	LREC-C08	33.210	81.624	3.05	51.51
L	1523	LREC-C11	33.211	81.623	3.05	7.62
L	1524	LREC-C12	33.210	81.622	3.05	50.50
L	1525	LREC-C13	33.210	81.623	3.96	5.79
L	1526	LREC-C14	33.210	81.623	3.05	48.46
L	1527	LREC-C16	33.210	81.621	3.05	43.28
L	1528	LREC-C17	33.213	81.622	3.05	37.80
L	1529	LREC-C20	33.210	81.621	3.05	44.20
L	1530	LREC-C21	33.214	81.624	3.05	47.85
L	1531	LREC-C22	33.210	81.621	3.05	44.20
L	1532	LREC-C23	33.209	81.621	2.74	43.28
L	1533	LREC-C24	33.209	81.621	3.05	49.68
L	1578	L205 AND L206	33.212	81.626	3.05	51.82
MMP4	1510	MMP-4C	33.338	81.708	3.66	39.93
MMP4	1617	MMP-4-SB (R1-R2)	33.338	81.708	1.00	221.00
NPR	1347	NPR M12A-17	33.253	81.638	0.00	78.94
NPR	1348	NPR M12A-18	33.252	81.637	0.00	42.98
NPR	1349	NPR M12A-19	33.253	81.637	0.00	63.09
NPR	1351	NPR M12A-21	33.253	81.637	0.00	70.41
NPR	1352	NPR M12A-22	33.253	81.636	0.00	79.55
NPR	1353	NPR M12A-25	33.254	81.637	0.00	53.04
NPR	1354	NPR M12A-26	33.251	81.638	0.00	41.15
NPR	1355	NPR M12A-27	33.253	81.639	0.00	44.81
NPR	1356	NPR M12A-28	33.254	81.636	0.00	66.75
NPR	1357	NPR M12A-29	33.252	81.636	0.00	59.44
NPR	1358	NPR M12A-30	33.252	81.635	0.00	64.92
NPR	1553	AFR-E24	33.257	81.627	3.00	91.40
NPR	1554	AFR-E25	33.258	81.628	1.50	91.40
NPR	1555	AFR-E26	33.259	81.630	1.50	91.40

TABLE 5.2 Summary of Deeper Profiles

Profiles Deeper Than 75m

Area	Prof. No.	Name	Lat.	Lon.	Max. Depth (m)
CFD	1537	CFD-18	33.240	81.632	310.90
CFD	1538	CFD-1	33.238	81.630	292.61
GCB2	1649	GCB-2, interp	33.322	81.720	194.49
H	1615	MMP-2A-SB (R1-R2)	33.284	81.644	289.00
K	1318	P-25	33.211	81.657	121.92
K	1544	P-25B & P-25TB	33.211	81.657	94.49
K	1616	MMP-3-SB (R1-R2)	33.211	81.657	313.00
MMP4	1617	MMP-4-SB (R1-R2)	33.338	81.708	221.00
NPR	1347	NPR M12A-17	33.253	81.638	78.94
NPR	1352	NPR M12A-22	33.253	81.636	79.55
NPR	1553	AFR-E24	33.257	81.627	91.40
NPR	1554	AFR-E25	33.258	81.628	91.40
NPR	1555	AFR-E26	33.259	81.630	91.40

Profiles Deeper Than 100m

Area	Prof. No.	Name	Lat.	Lon.	Max. Depth (m)
CFD	1537	CFD-18	33.240	81.632	310.90
CFD	1538	CFD-1	33.238	81.630	292.61
GCB2	1649	GCB-2, interp	33.222	81.720	194.49
H	1615	MMP-2A-SB (R1-R2)	33.284	81.644	289.00
K	1318	P-25	33.211	81.657	121.92
K	1616	MMP-3-SB (R1-R2)	33.211	81.657	313.00
MMP4	1617	MMP-4-SB (R1-R2)	33.338	81.708	221.00

Profiles Deeper Than 200m

Area	Prof. No.	Name	Lat.	Lon.	Max. Depth (m)
CFD	1537	CDF-18	33.240	81.632	310.90
CFD	1538	CFD-1	33.238	81.630	292.61
H	1615	MMP-2A-SB (R1-R2)	33.284	81.644	289.00
K	1616	MMP-3-SB (R1-R2)	33.211	81.657	313.00
MMP4	1617	MMP-4-SB (R1-R2)	33.338	81.708	221.00

TABLE 5.3 - SRS Well Data Used to Derive Soil Column Thickness

Well ID	UTM north	UTM east	Surface Elevation (ft)	Depth to Top of Rock (ft)	Ref. Source	Notes
AIK454	3709940.00	412737.40	470	680	7	
AIK830	3707695.00	431346.50	480	541	7	
AIK831	3707880.00	431347.90	505	538	7	
AIK832	3710384.00	434357.90	480	515	7	
AIK858	3696882.00	434372.10	435	651	1	
ALL27	3655603.00	454404.60	186	1476	1	
ALL324	3665301.00	449082.20	203	1355	1	
C1	3690555.00	424736.00	235	567	1	
C10	3653933.00	464096.00	289.6	1725.6	1	
C15	3581376.26	538147.82	65	2758	5	
C2	3699924.00	428347.50	418.8	553	1	
C3	3711255.00	454998.80	295.2	523	1	
C5	3686712.00	462042.40	265.6	1073	1	
C6	3670906.00	470604.70	208.7	1374	1	
C7	3663770.00	452781.20	252	1416	1	
CFD-1	3677663.24	441304.80	268.8	979	10	991 TD
CFD-18	3677879.59	441176.71	248.4	1072	10	1085 TD
CPC1	3679081.25	437361.81	285.1	1096	1	
DRB-1	3684171.28	437524.32	266.5	877	11	versus database
DRB-10	3673729.08	446088.37	250	1170	12	TD 4212, location est.
DRB-11	3676727.82	443943.08	274.3	1071	12	3279.11 TD. location scaled
DRB-2	3682229.00	438710.00	279.5	977	5	
DRB-3	3682955.00	438181.00	285.4	934	11	versus database
DRB-4	3681931.00	437630.00	249.9	924	11	
DRB-5	3683426.00	438803.00	286	930	11	
DRB-6	3683130.00	439247.00	268	900	2	delta with Table 5
DRB-7	3682833.00	439474.00	276.5	965	5	
DRB-8	3682396.01	439666.13	260	960	13	1965 TD, elev. est., scaled
DRB-9	3678515.00	442591.00	293.5	1034	12	elev. est., TD 2694
GCB-1	3687046.38	431141.65	336.2	749	5	
GCB-2	3687061.02	433006.03	221.2	659	5	
GCB-3	3689597.85	432841.86	255.7	621	5	
GCB-4	3679654.53	440617.80	306.2	1056	6	
GCB-5.1	3685563.64	443370.93	308.8	973	5	
GIRARD	3658532.00	432761.90	250	1375	7	
MILLERSPD	3676951.00	416551.40	245	852	1	
MMP-2A	3682741.36	440041.13	287.4	982	6	
MMP-3B	3674679.41	438731.52	264.58	1088	6	
MMP-4B	3688771.48	434068.64	354.14	785	6	
NPR-5	3679842.85	441336.26	322	1094	5	DH-1, elev. est. NPR Phase3
P12R	3676845.82	443801.78	295	1088	?	TD approx 1222, elev. est.
P30	3688762.74	434053.53	357.39	772	3	
P4R	3679131.49	425158.28	105.3	690	2	
P5R	3667525.45	443356.43	207	1235	5	elev. well inv.

TABLE 5.3 - SRS Well Data Used to Derive Soil Column Thickness (cont.)

P6R	3682009.21	431351.37	253.4	842	11	elev. well inv.
P7R	3688205.73	444313.88	273	888	11	
P8R	3687564.00	430814.00	357.6	831	5	
P9R	3686765.92	431978.53	322	680	5	estimated by log correlation
PBF1	3683749.00	450624.60	276.1	1053	1	
PBF2	3682966.00	451079.20	268	995.6	1	
PBF3	3679455.00	442063.40	317	1119.3	1	
PBF4	3673852.00	434686.40	208	1069	1	
PBF5	3672789.00	435586.00	241	1050	1	
PBF6	3670150.00	430909.50	93	874.5	1	
PBF8	3678609.00	442465.60	292	993	1	
PPC1	3676536.00	446358.10	313	1158	1	
PW53A	3689122.00	431400.40	381	738.2	7	
SSW-1	3677651.00	433105.30	311	1023	4	TD 1400
SSW-2	3678541.00	434695.80	167.3	860	4	TD 1308
SSW-3	3678790.00	435066.50	179	912.5	4	TD 1116
SSW-4	3678993.11	440381.23	290	1059	9	vert. array, delta database
SSW-5	3696926.33	434262.58	440	652	8	New Ellenton, TD 260m
SSW-6	3638250.76	539201.67	68.9	2424	8	Walterboro, 800m (2624)

Notes: Source of Basement "Top of Rock" Picks

1. Aadland et al., 1995, Hydrogeologic Framework of West-Central South Carolina, SCDNR Water Resources Report 5
2. Christl, R.J., 1964, Storage of Radioactive Wastes in Basement Rock Beneath the Savannah River Plant, DP-844
3. Bledsoe et al., 1990, Baseline Hydrogeologic Investigation - Summary Report, WSRC-RP-90-1010
4. WEGS Report, Geophysical log Figures, Top of Rock Picks by D.E. Wyatt
5. Top of Rock by D. E. Wyatt from geophysical logs
6. Top of Rock by D. E. Wyatt from geophysical and OYO suspension logs
7. Top of Rock from database
8. Top of Rock by D. Stephenson
9. Top of Rock from USGS Field Geological Log (Fred Falls)
10. Stieve et al., 1991, Pen Branch Fault Program: Consolidated Report, WSRC-RP-91-87
11. Benedict et al., 1969, Permanent Storage of Radioactive Separations Process Wastes in Bedrock, SRTC
12. Bradley and Cory, 1976, Technical Assessment of Bedrock Waste Storage, DP-1438
13. Top of Rock from Zoback and Moos, 1989, In Situ Stress Measurements at the Savannah River Site.

TABLE 5.4 - Basecase Stratigraphic Layering (Typical H-Area)

LAYER	AVERAGE LAYER THICKNESS (ft)
Upland	1*
Tobacco Rd	76
Shallow Clay	6
Dry Branch/Santee	54
Four Mile/Shallow Sand	20
Snapp	20
Four Mile/Shallow Sand	87
Shallow Clay	10
Deep Sand	54
Deep Clay	15
Deep Sand	209
Deep Clay	18
Deep Sand	11
Deep Clay	10
Deep Sand	106
Deep Clay	6
Deep Sand	192

* Typical Upland thickness in H-Area is about 28 ft.

TABLE 8.1 Selected PGA - Controlling Earthquake Median Magnitude-Distance Pairs with 5% and 95% Confidence Range

	Target Magnitudes (Mw)			Target Distance (km)		
PGA(g)	5%	M-bar	95%	5%	D-bar	95%
0.05	4.8	5.7	6.8	36	42	79
0.10	4.8	5.7	6.8	17	36	43
0.20	5.0	5.9	7.2	8	21	36
0.25	5.0	5.9	7.2	4	17	32
0.30	5.0	6.0	7.2	9	19	58
0.40	5.0	6.0	7.2	6	15	43
0.50	5.5	6.2	7.8	7	13	54
0.75	5.5	6.2	7.8	5	9	24

Note: The target distances are associated with different source depths.

TABLE 8.2 - Crystalline Bedrock Control Motion Spectral (log) Averages Over the 1-2.5 hz and 5-10 hz Frequency Ranges

	Magnitude (Mw)	PGA (g)	Average Sa 1 to 2.5 hz (g)	Average Sa 5 to 10 hz (g)
ML	4.8	0.05	0.010	0.065
ML	4.8	0.10	0.018	0.120
ML	5.0	0.20	0.052	0.267
ML	5.0	0.25	0.063	0.326
ML	5.0	0.30	0.078	0.383
ML	5.0	0.40	0.102	0.502
ML	5.5	0.50	0.203	0.693
ML	5.5	0.75	0.297	1.020
MM	5.7	0.05	0.027	0.082
MM	5.7	0.10	0.051	0.160
MM	5.9	0.20	0.110	0.307
MM	5.9	0.25	0.134	0.378
MM	6.0	0.30	0.180	0.464
MM	6.0	0.40	0.231	0.604
MM	6.2	0.50	0.309	0.760
MM	6.2	0.75	0.446	1.110
MH	6.8	0.05	0.051	0.098
MH	6.8	0.10	0.083	0.176
MH	7.2	0.20	0.173	0.352
MH	7.2	0.25	0.210	0.431
MH	7.2	0.30	0.307	0.577
MH	7.2	0.40	0.373	0.732
MH	7.8	0.50	0.525	0.965
MH	7.8	0.75	0.643	1.290

TABLE 8.3 - Triassic Bedrock Control Motion Spectral (log) Averages Over the 1-2.5 hz and 5-10 hz Frequency Ranges

	Magnitude (Mw)	PGA (g)	Average Sa 1 to 2.5 hz (g)	Average Sa 5 to 10 hz (g)
ML	4.8	0.05	0.010	0.065
ML	4.8	0.10	0.019	0.121
ML	5.0	0.20	0.053	0.271
ML	5.0	0.25	0.065	0.332
ML	5.0	0.30	0.075	0.377
ML	5.0	0.40	0.099	0.499
ML	5.5	0.50	0.198	0.689
ML	5.5	0.75	0.379	1.095
MM	5.7	0.05	0.027	0.082
MM	5.7	0.10	0.051	0.159
MM	5.9	0.20	0.109	0.306
MM	5.9	0.25	0.134	0.378
MM	6.0	0.30	0.169	0.448
MM	6.0	0.40	0.221	0.591
MM	6.2	0.50	0.298	0.747
MM	6.2	0.75	0.598	1.283
MH	6.8	0.05	0.056	0.101
MH	6.8	0.10	0.083	0.175
MH	7.2	0.20	0.171	0.348
MH	7.2	0.25	0.208	0.428
MH	7.2	0.30	0.261	0.526
MH	7.2	0.40	0.336	0.687
MH	7.8	0.50	0.450	0.884
MH	7.8	0.75	1.009	1.590

TABLE 8.4 Source Parameters Used To Develop Bedrock Control Motion

PGA	Magnitude	Distance	Depth	Corner Freq.
		(km)	(km)	(Hz)
0.05	4.8	34.59	15	1.862
	5.7	40.85	15	0.6608
	6.8	93.39	10	0.1746
0.10	4.8	19.24	15	1.8624
	5.7	34.64	15	0.6608
	6.8	41.57	15	0.1862
0.20	5.0	10.42	10	1.387
	5.9	10.1	10	0.492
	7.2	34.03	10	0.1101
0.25	5.0	7.76	10	1.387
	5.9	17.24	10	0.492
	7.2	30.09	10	0.1101
0.30	5.0	8.59	5	1.293
	6.0	13.23	5	0.4089
	7.2	32.33	5	0.1027
0.40	5.0	7.03	5	1.293
	6.0	11.21	3	0.4089
	7.2	27.61	3	0.1027
0.50	5.5	7.82	5	0.727
	6.2	10.67	5	0.3248
	7.8	31.03	5	0.0515
0.75	5.5	8.44	3	0.5058
	6.2	22.13	2	0.2259
	7.8	74.05	3	0.0358

TABLE 10.2 Parameters Varied to Generate Charleston 84th Percentile Ground Motions

Parameter	50th	Standard Error	84th %
Stress Drop ($\Delta\sigma$) (event 1)	150	$\sigma_{ln} = 0.50$	247
Stress Drop ($\Delta\sigma$) (event 2)	130	$\sigma_{ln} = 0.50$	214
Stress Drop ($\Delta\sigma$) (event 3)	70	$\sigma_{ln} = 0.50$	115
Stress Drop ($\Delta\sigma$) (event 4)	40	$\sigma_{ln} = 0.50$	66
Kappa (κ)	0.006	fixed	fixed
Quality Factor (Q)	670	$\sigma_{ln} = 0.18$	802
Frequency exponent (η)	0.33	$\sigma_{ln} = 0.05$	0.347

Source Depth	4, 10, 15, 20, 25 km	
Soil Profile Thickness (uniform distribution)	Crystalline	Triassic
	600-800 ft	900-1100 ft
	800-1000 ft	1100-1300 ft
	1000-1200 ft	1300-1500 ft

TABLE 13.1 PC3 Design Basis Envelope Spectrum (Interpolated spectral values using log frequency and linear spectral acceleration)

Frequency	Response Spectral Acceleration (g's)				
(Hz)	0.5%	2.0%	5%	7%	10%
100	0.16	0.16	0.16	0.16	0.16
33	0.1756	0.1676	0.16	0.1568	0.153
14	0.3922	0.3375	0.30	0.2727	0.2526
6.5	0.5930	0.4687	0.375	0.3361	0.2983
1.6	0.5382	0.4221	0.340	0.2994	0.2646
0.6	0.2482	0.1990	0.1677	0.1456	0.1300
0.5	0.1986	0.1604	0.1303	0.1185	0.1062
0.4	0.1112	0.0908	0.0747	0.0682	0.0615
0.3	0.0566	0.0470	0.0362	0.0361	0.0328
0.2	0.0286	0.0244	0.0209	0.0195	0.018
0.1			0.0043		

TABLE 13.2 PC4 Design Basis Envelope Spectrum (Interpolated spectral values using log frequency and linear spectral acceleration)

Frequency	Response Spectral Acceleration (g's)				
(Hz)	0.5%	2.0%	5%	7%	10%
100	0.227	0.227	0.227	0.227	0.227
33	0.2516	0.2396	0.227	0.2238	0.2183
18	0.4471	0.3946	0.350	0.3308	0.3105
7	1.0107	0.8030	0.655	0.5800	0.5160
1.5	1.1825	0.9275	0.760	0.6579	0.5814
0.7	0.7401	0.5899	0.4813	0.4279	0.3813
0.5	0.5209	0.4206	0.3411	0.3107	0.2786
0.4	0.2404	0.1963	0.1519	0.1474	0.1329
0.3	0.0998	0.0827	0.0632	0.0636	0.0578
0.2	0.0426	0.0363	0.0311	0.029	0.0268
0.1			0.0067		

17.0 FIGURES

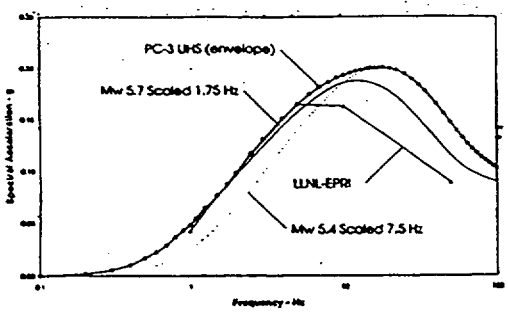

(a) SRS Broadened Rock Uniform Hazard Spectra (UHS) are the basis for generating a Soil UHS (free surface).

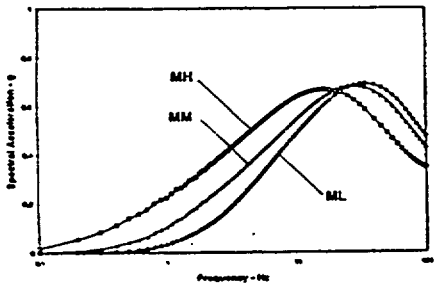

(b) Three bedrock control motion spectra representing low (ML), medium (MM), and high (MH) magnitude were generated for each suite of Peak Ground Acceleration (PGA) levels (0.05, 0.1, 0.2, 0.25, 0.3, 0.4, 0.5 and 0.75g) and each SRS bedrock type (crystalline and Triassic). The bedrock control motion PGA levels and magnitudes, are based on the EPRI de-aggregation. The distances were varied to produce the desired PGA levels.

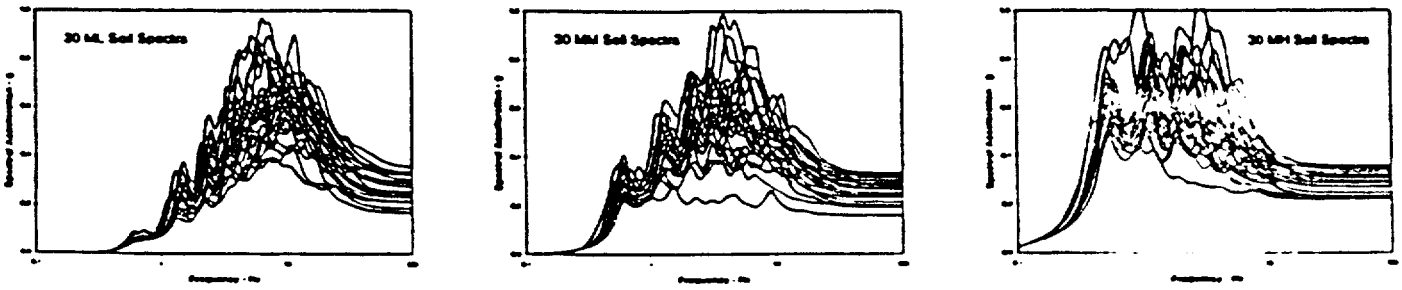

(c) Thirty convolution analyses (corresponding to 30 different soil profiles) are performed for each bedrock control motion (30 convolution analyses x 9 PGA levels x 3 magnitudes x 2 bedrock types) The convolution analyses are also performed for 3 depth ranges

Figure 2.1 - Flow chart and diagrams describing design basis spectra approach

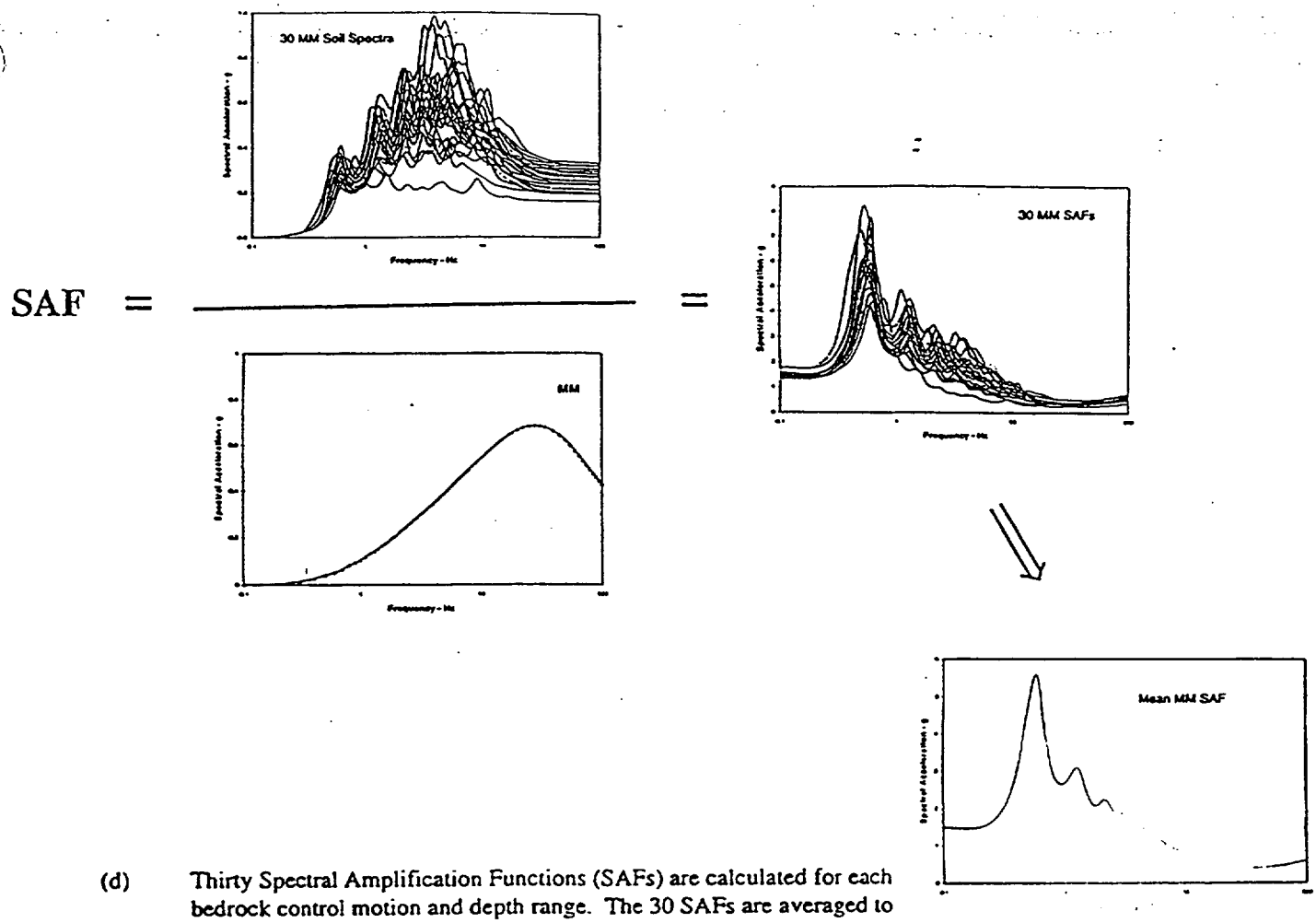

(d) Thirty Spectral Amplification Functions (SAFs) are calculated for each bedrock control motion and depth range. The 30 SAFs are averaged to get a mean SAF for each bedrock control motion, PGA level and depth range.

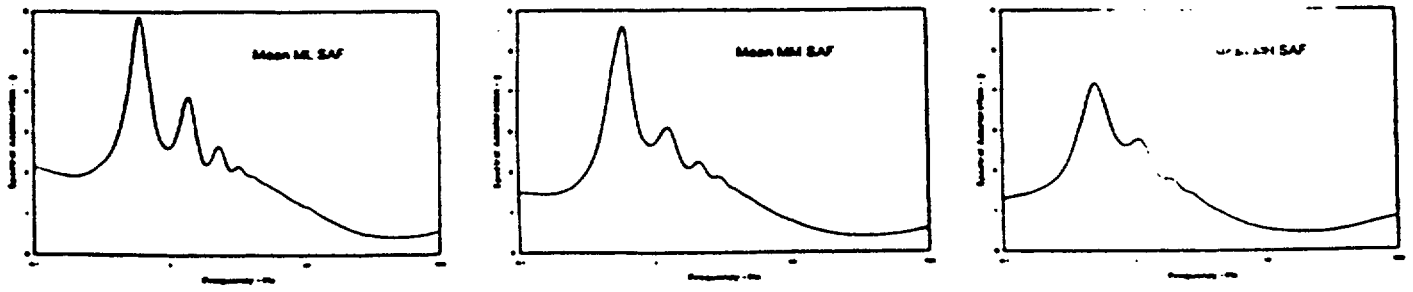

(e) Each PGA level, bedrock type and depth range has three mean SAFs representing low, medium, and high magnitude.

Figure 2.1 (continued) - Flow chart and diagrams describing design basis spectra approach

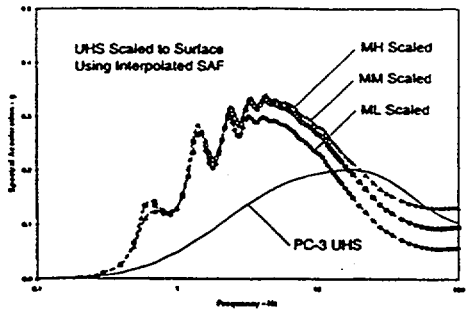

(f) The appropriate mean SAFs are interpolated to provide SAFs to scale the UHS to surface.

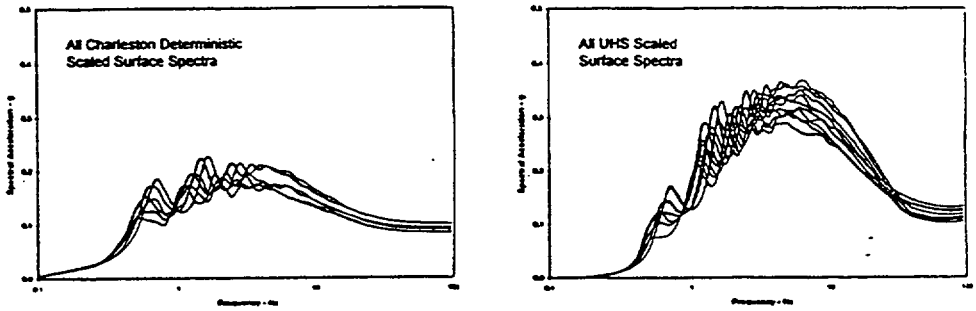

(g) The same scaling process is repeated for the Charleston deterministic check. Soil response for UHS scaling and Charleston scaling can then be compared.

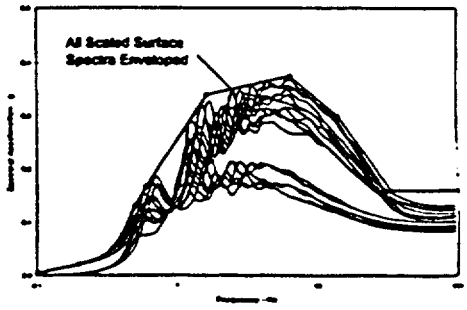

(h) The UHS and Charleston surface responses (low, medium, and high magnitude surface responses for each bedrock type and depth range) are then enveloped.

Figure 2.1 (continued) - Flow chart and diagrams describing design basis spectra approach

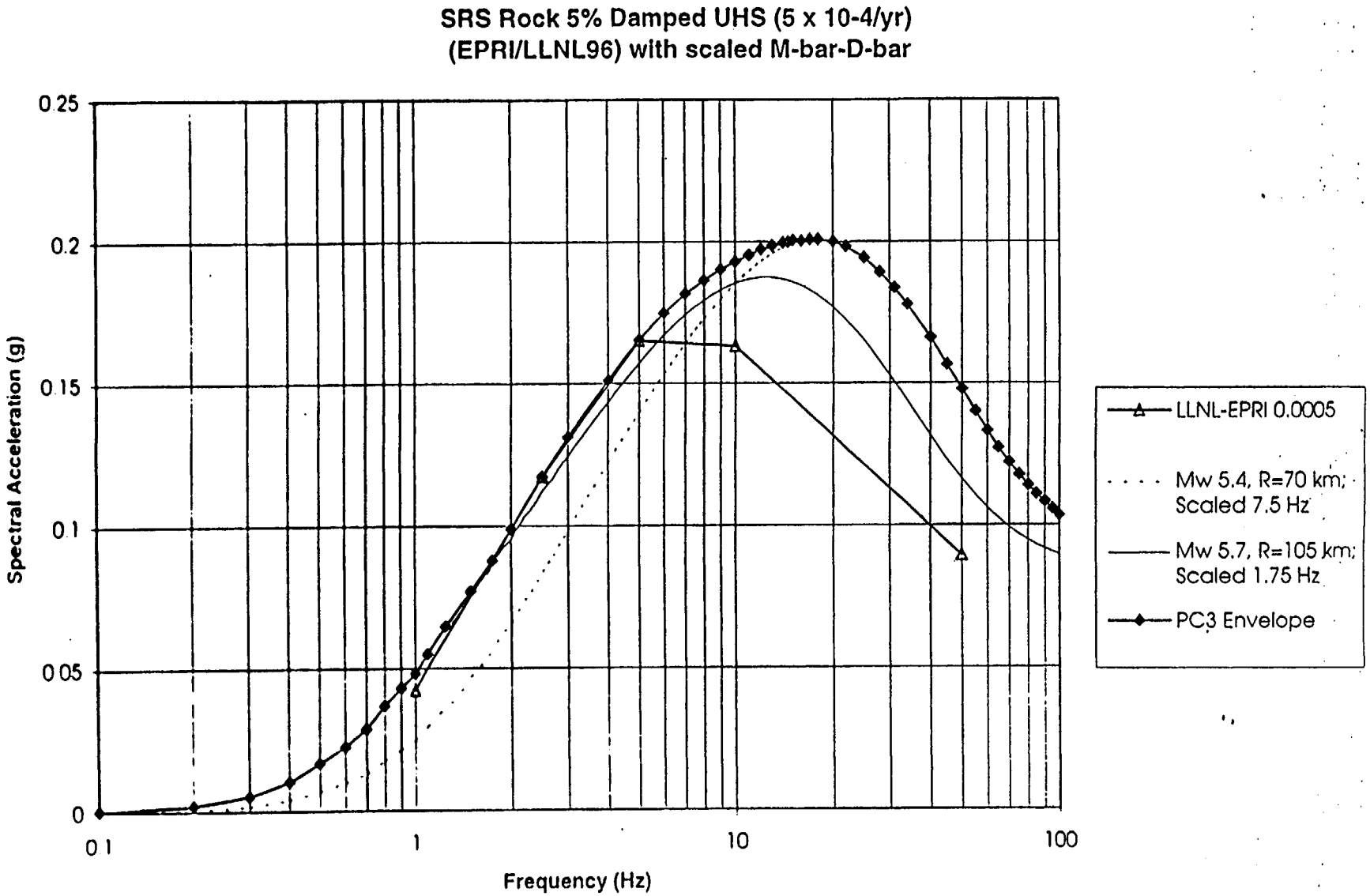

Figure 4.1 - Bedrock Performance Category 3 (PC3) envelope spectrum meeting requirements of DOE-STD-1023 (diamonds). Combined EPRI and LLNL bedrock UHS with annual probability of exceedance of $5x10^{-4}$ (triangles). RVT site specific spectra used for broadening UHS shown with solid (scaled to the UHS spectrum at 1.75 Hz) and dashed (scaled to the UHS spectrum at 7.5 Hz) lines.

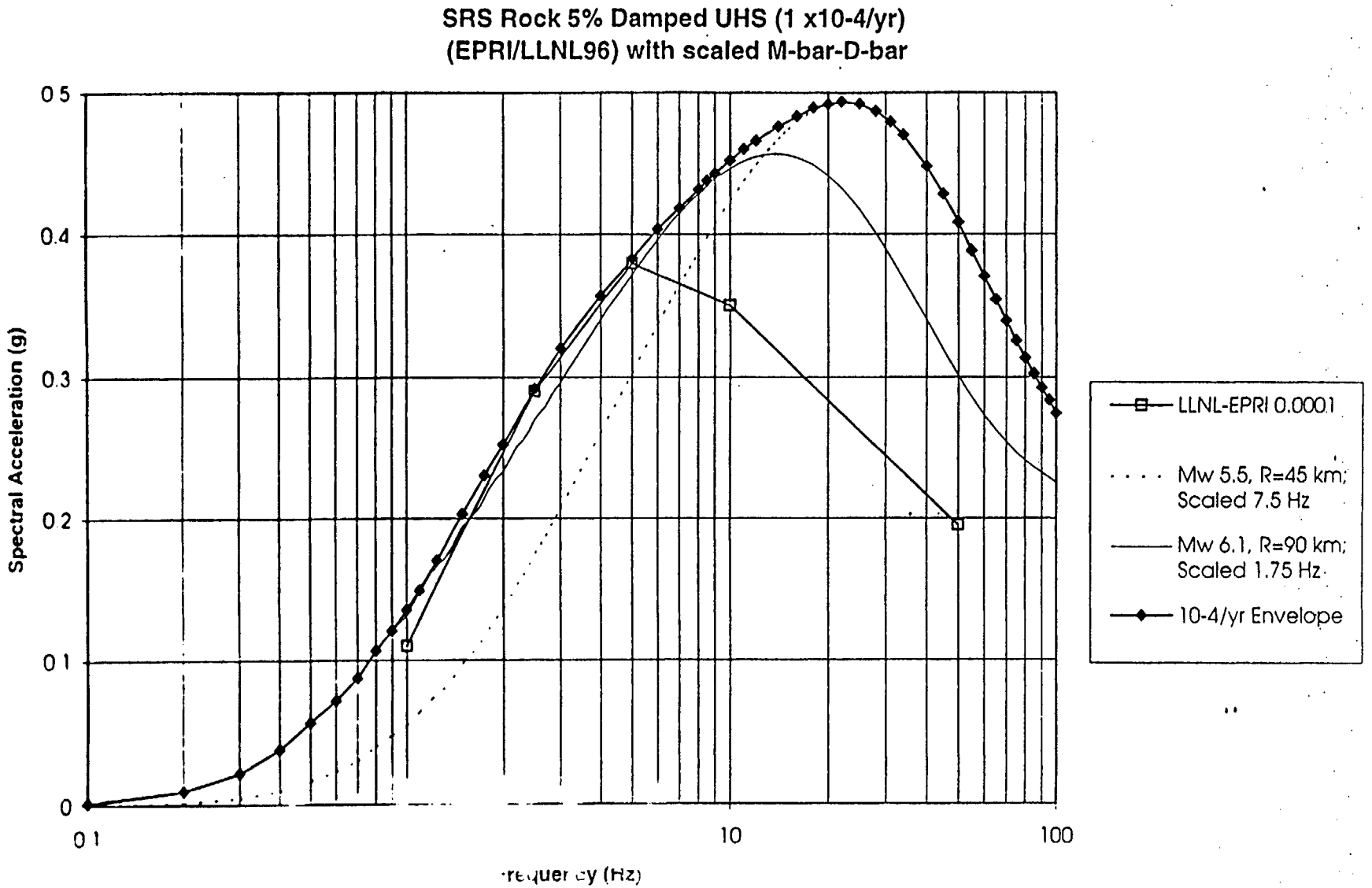

Figure 4.2 - Bedrock Performance Category (1x10-4) envelope spectrum meeting requirements of DOE-STD-1023 (diamonds). Combined EPRI and LLNL bedrock uniform hazard spectrum at annual probability of exceedance of $1x10^{-4}$ (triangles). Scaled RVT site specific spectra used for broadening UHS shown with solid (scaled to the UHS spectrum at 1.75 Hz) and dashed (scaled to the UHS spectrum at 7.5 Hz) lines.

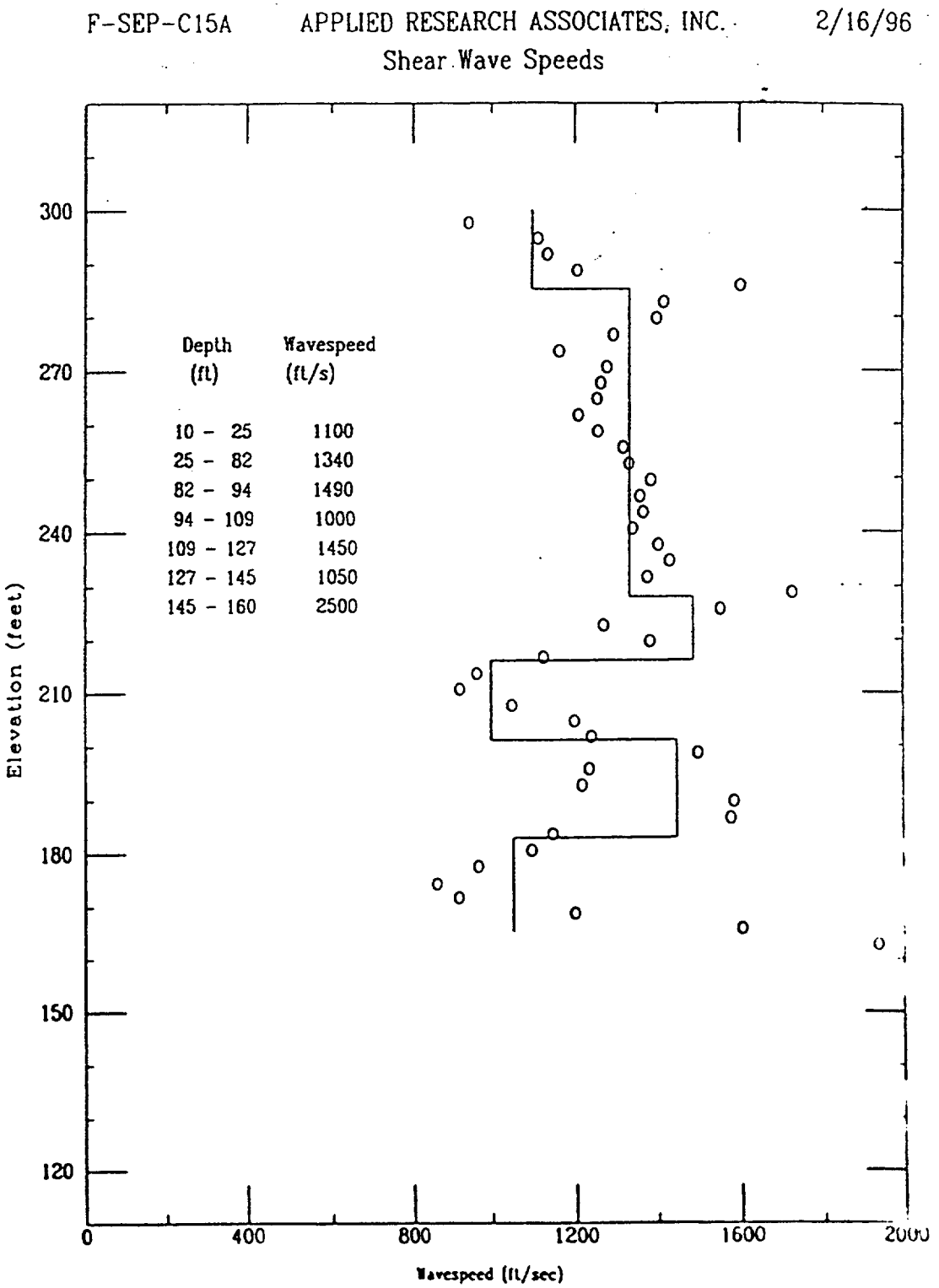

Figure 5.1 - Example seismic cone penetrometer S-wave interpretation (solid lines) Measurements taken in F-area.

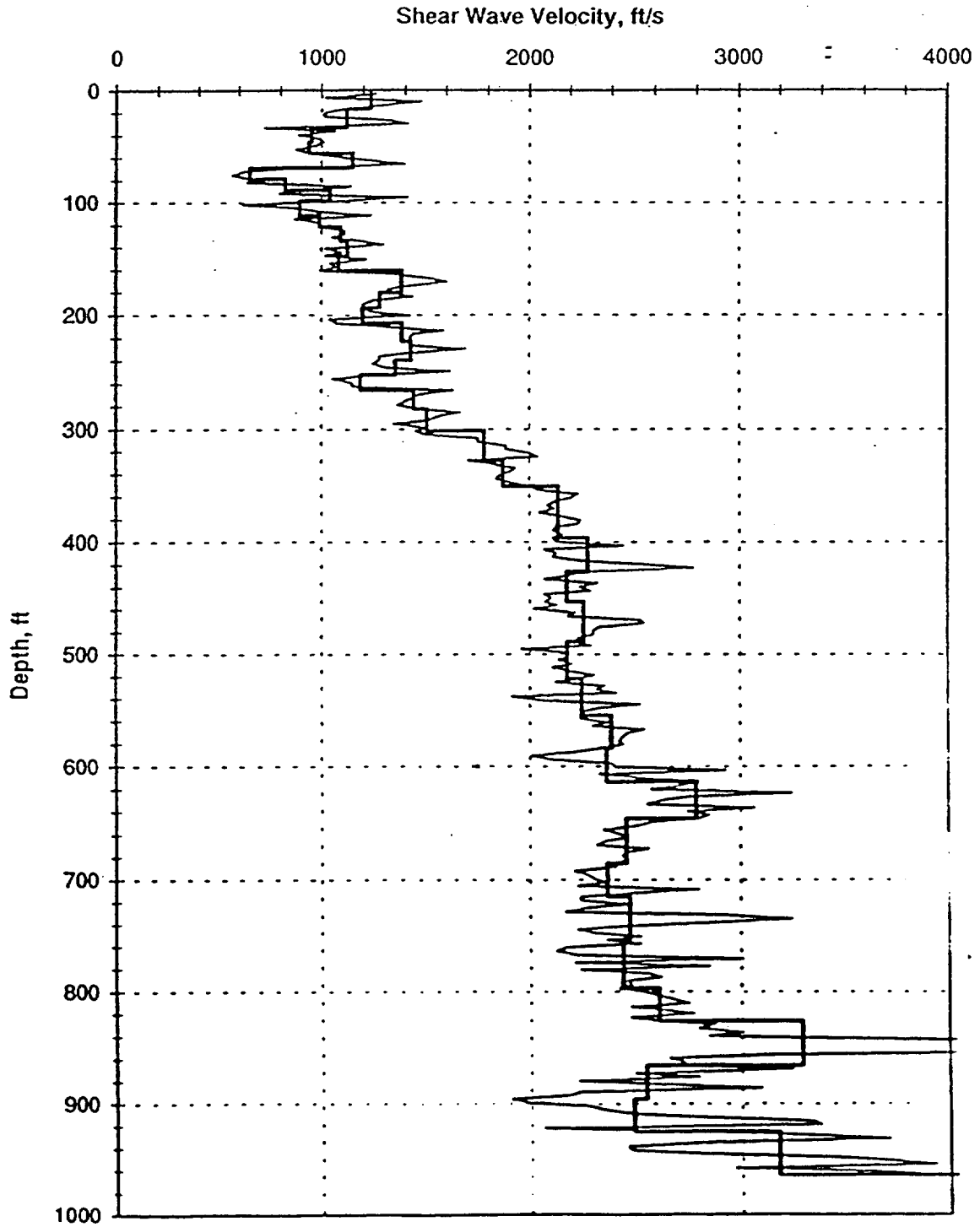

Figure 5.2 - Example Oyo S-wave velocity logger profile (thin solid lines). Measurements taken in vicinity of F- and H-areas. Low-pass filtered (using Program LAYERSH) velocity model shown by heavy line

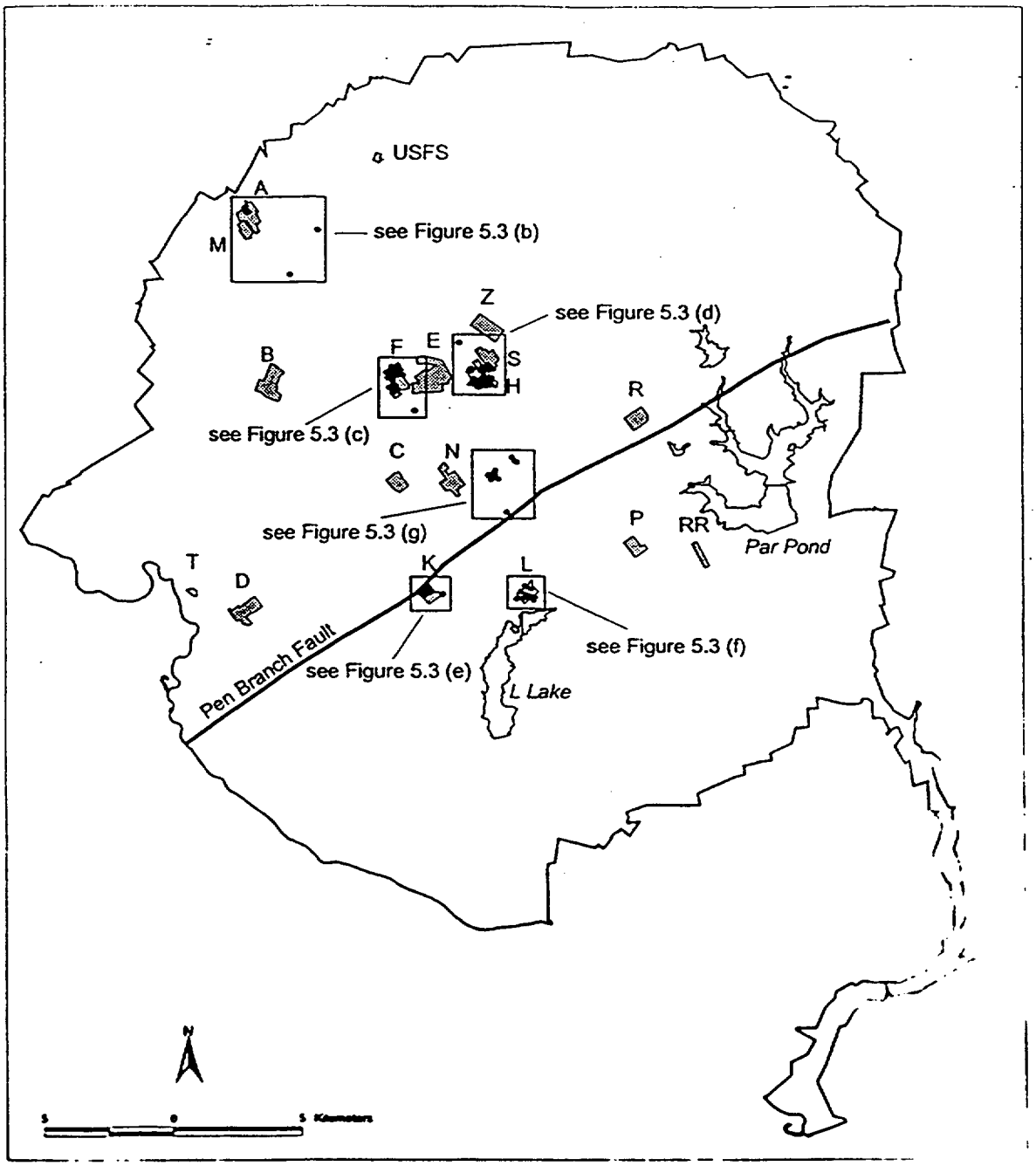

Figure 5.3 (a) - SRS map showing locations of existing facility areas and locations of shear-wave measurements (dots). Areas shown in rectangles are expanded in Figures 5.3 (b) - 5.3 (g).

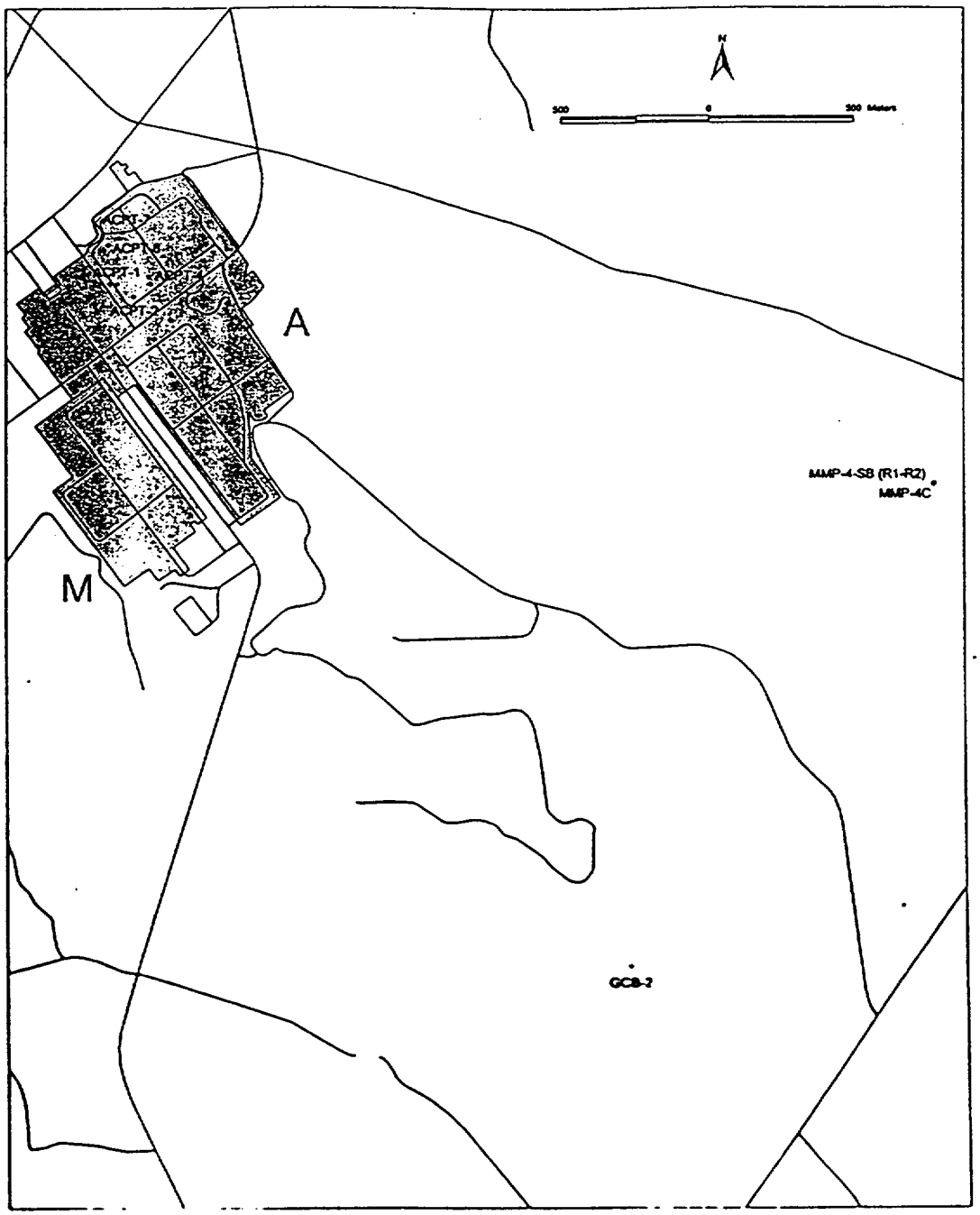

Figure 5.3 (b) - SRS A- and M-Areas with names and locations of shear-wave measurements (dots).

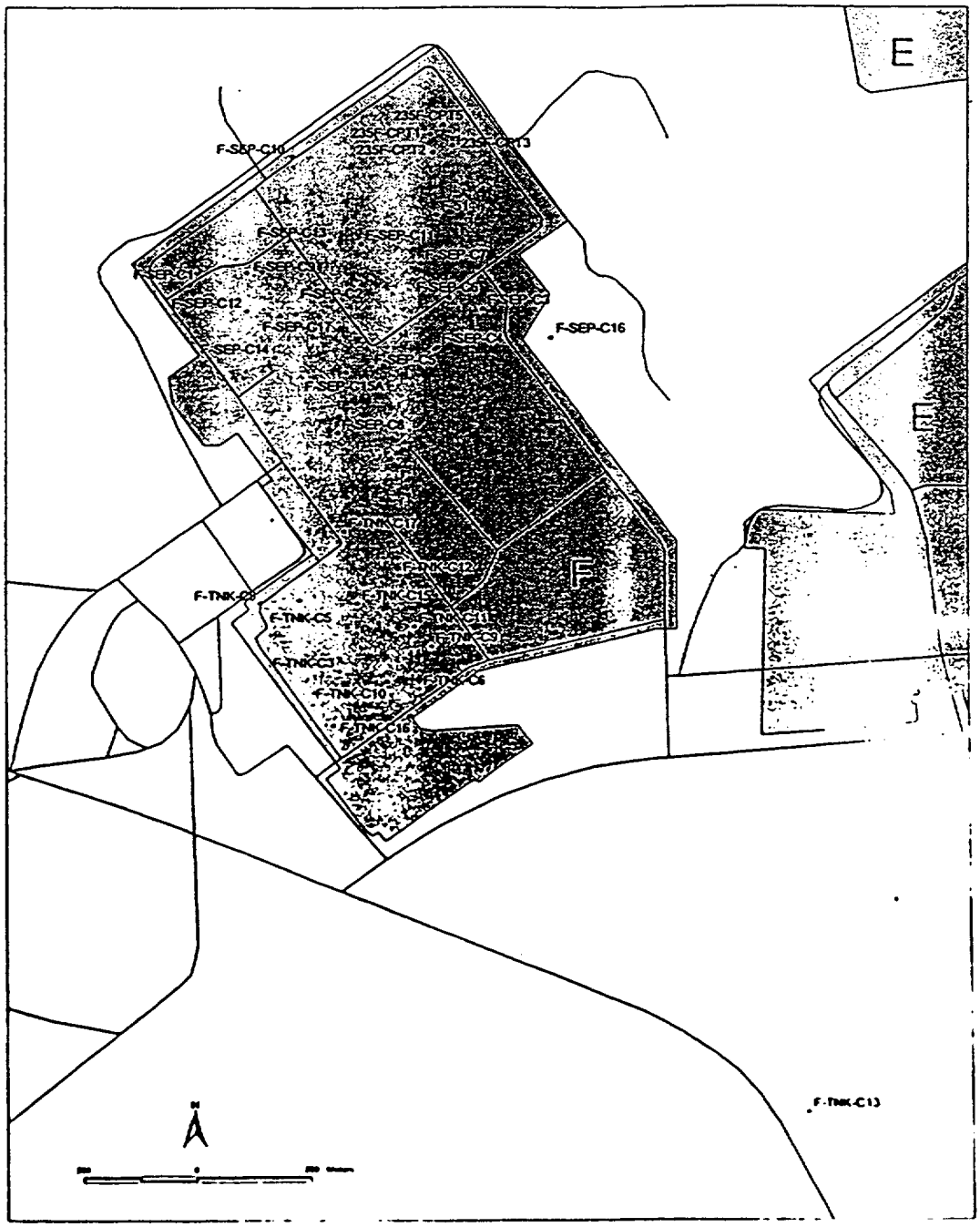

Figure 5.3 (c) - SRS F-Area with names and locations of shear-wave measurements (dots)

Figure 5.3 (d) - SRS H-Area with names and locations of shear-wave measurements (cont.)

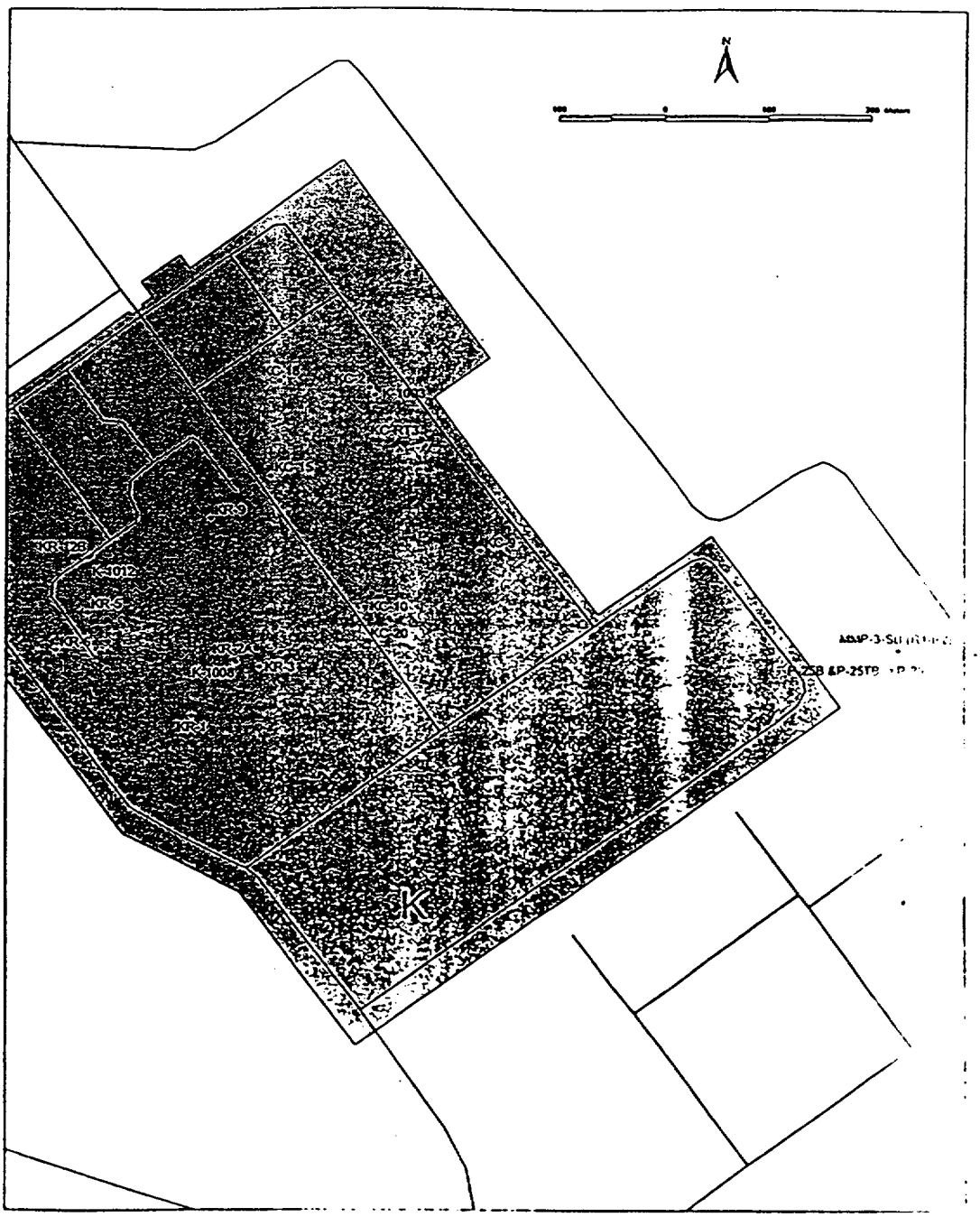

Figure 5.3 (e) - SRS K-Area with names and locations of shear-wave measurements (Lots).

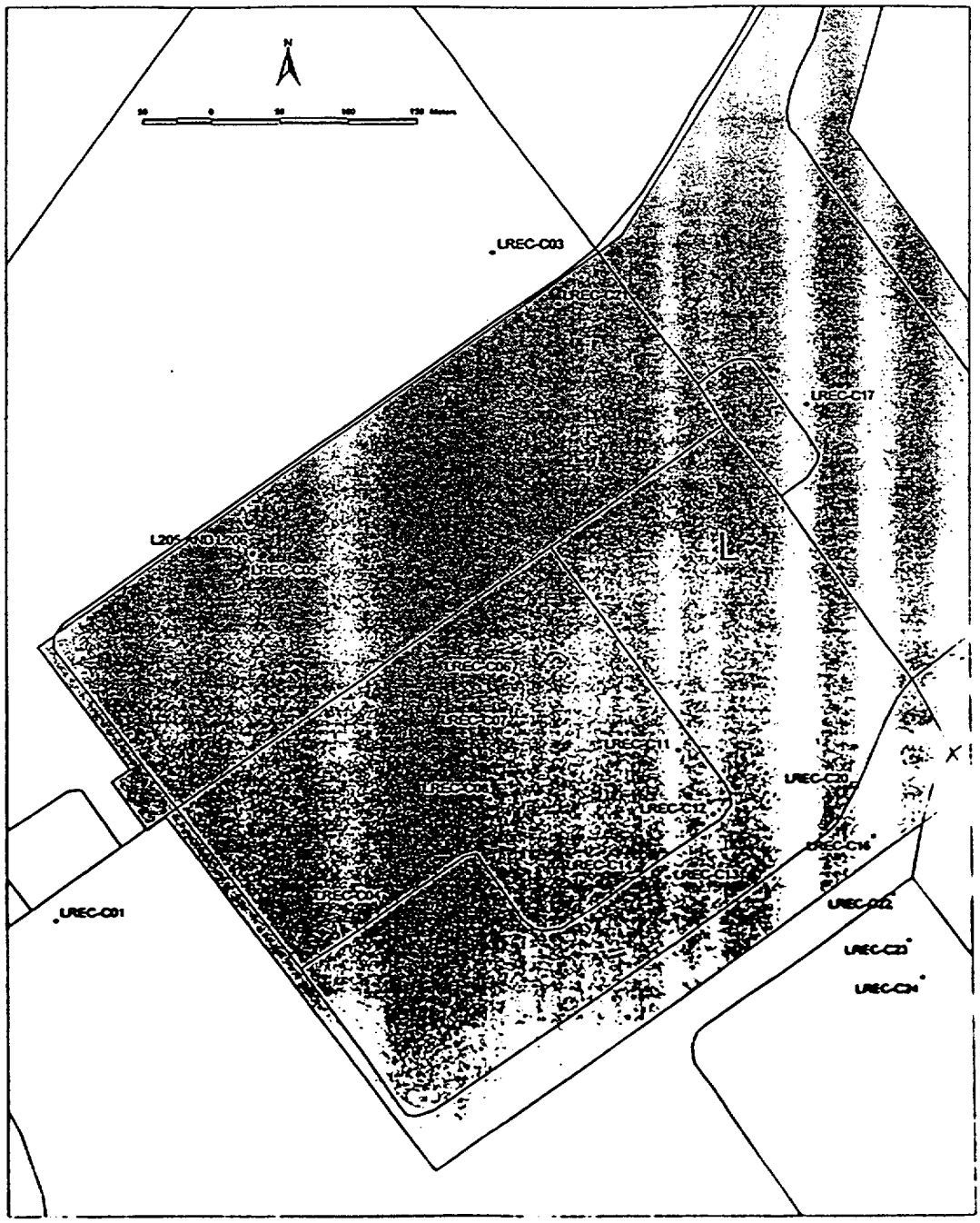

Figure 5.3 (f) - SRS L-Area with names and locations of shear-wave measurements (dots)

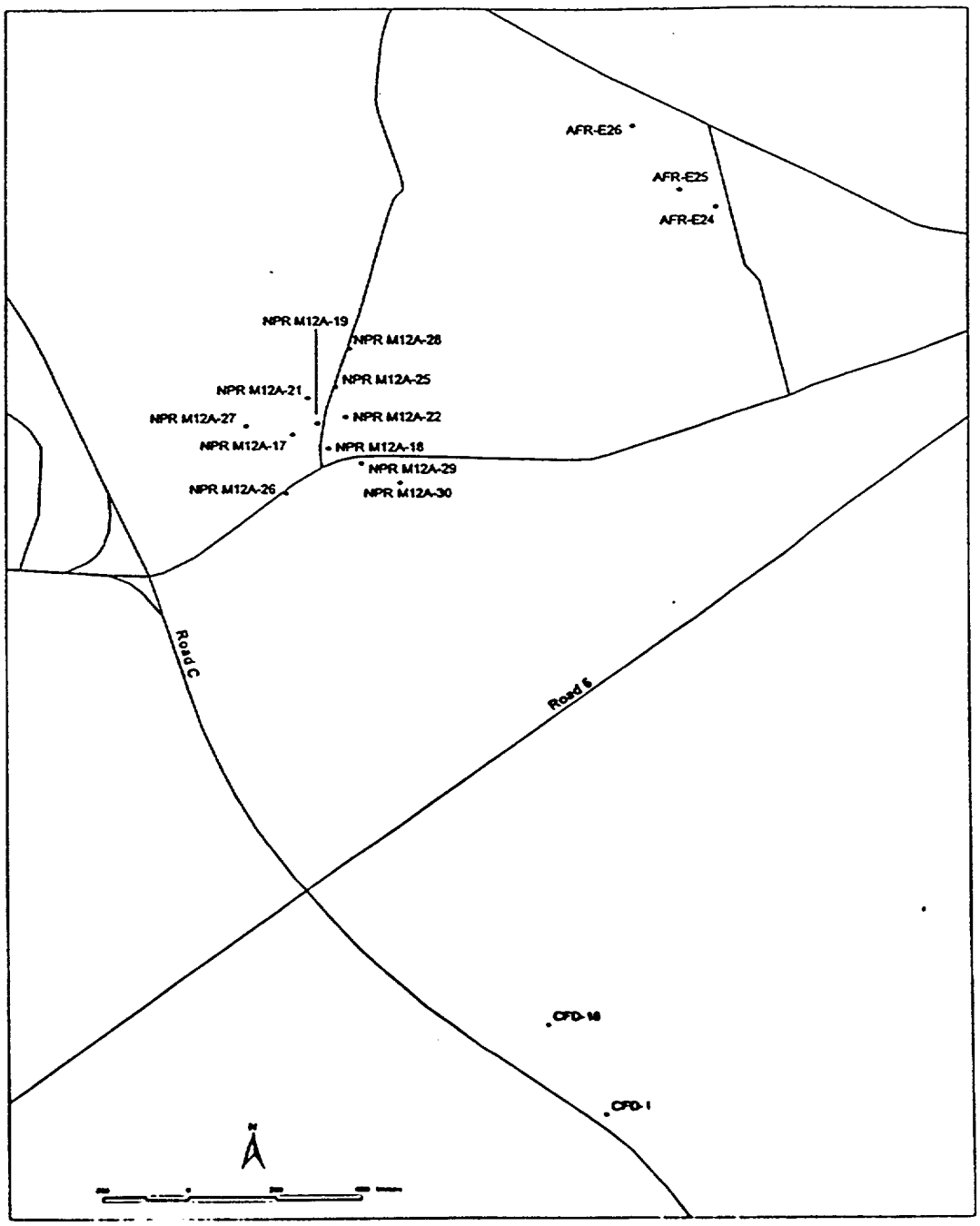

Figure 5.3 (g) - SRS NPR- and AFR-Areas with names and locations of shear-wave measurements (dots).

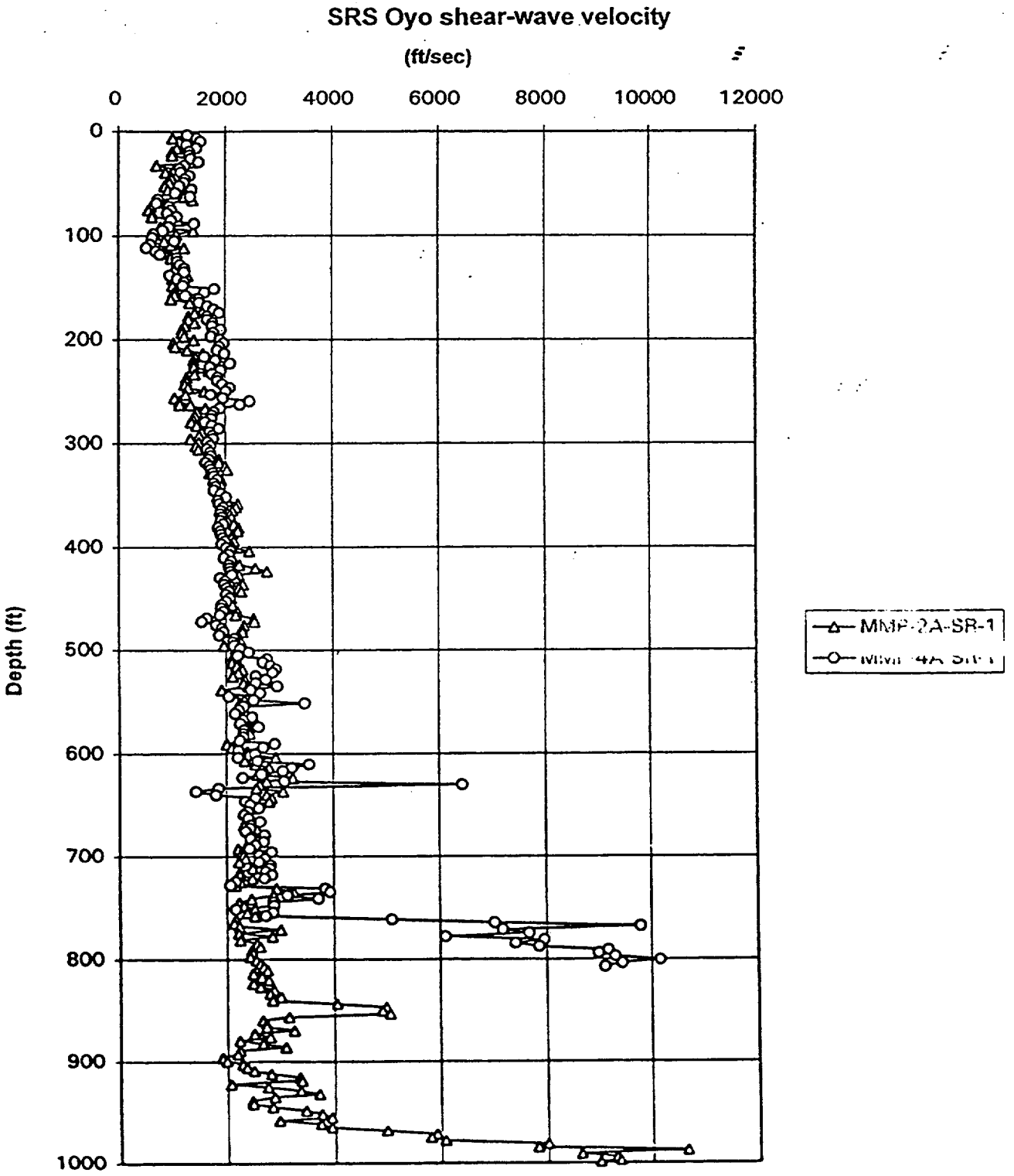

Figure 5.4 - Oyo velocity profile obtained in borehole GCB.

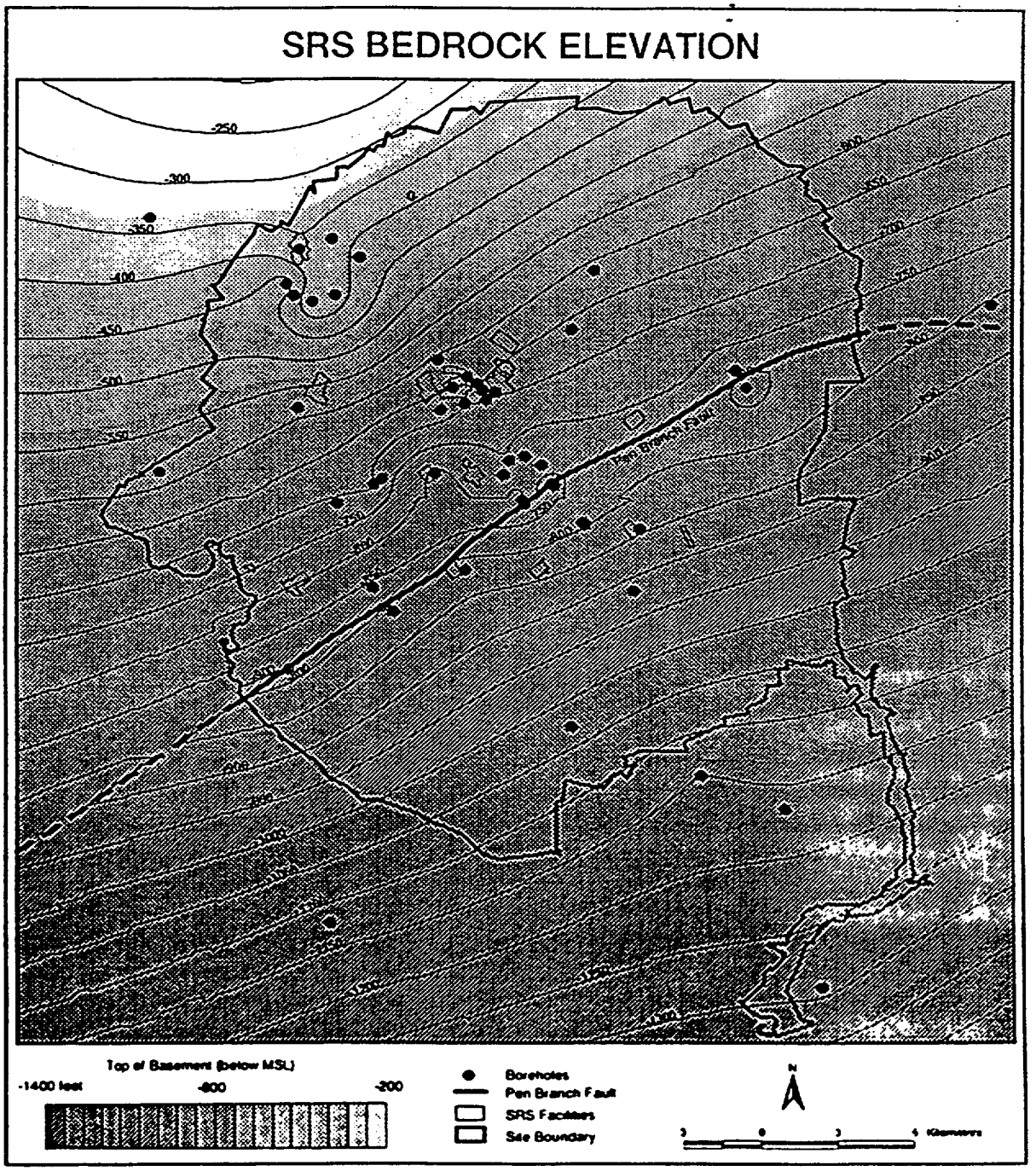

Figure 5.5(a) - Bedrock elevation map developed by interpolating between the boreholes which contacted bedrock using Kriging methods

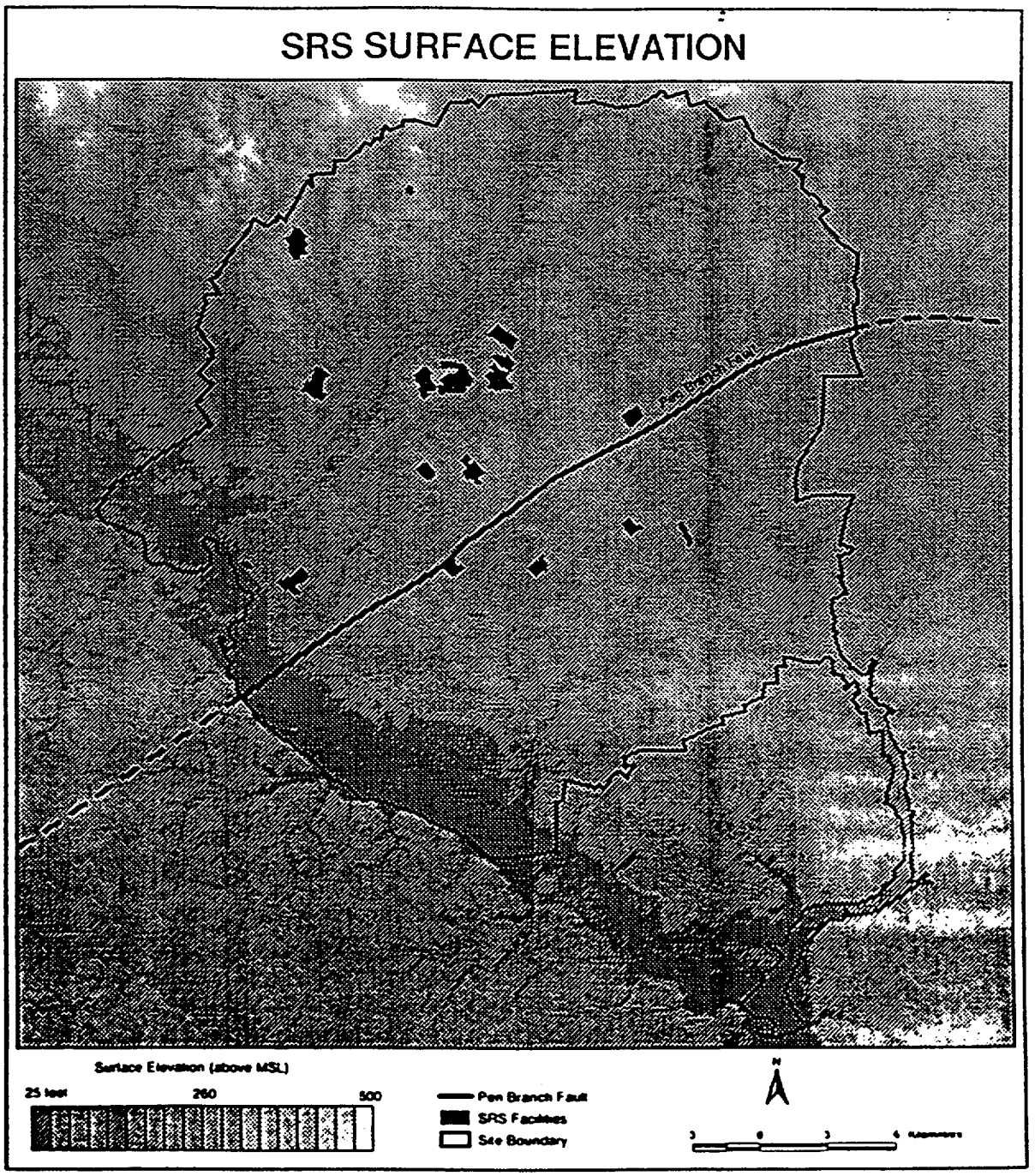

Figure 5.5(b) - USGS digital surface elevation map for the SRS

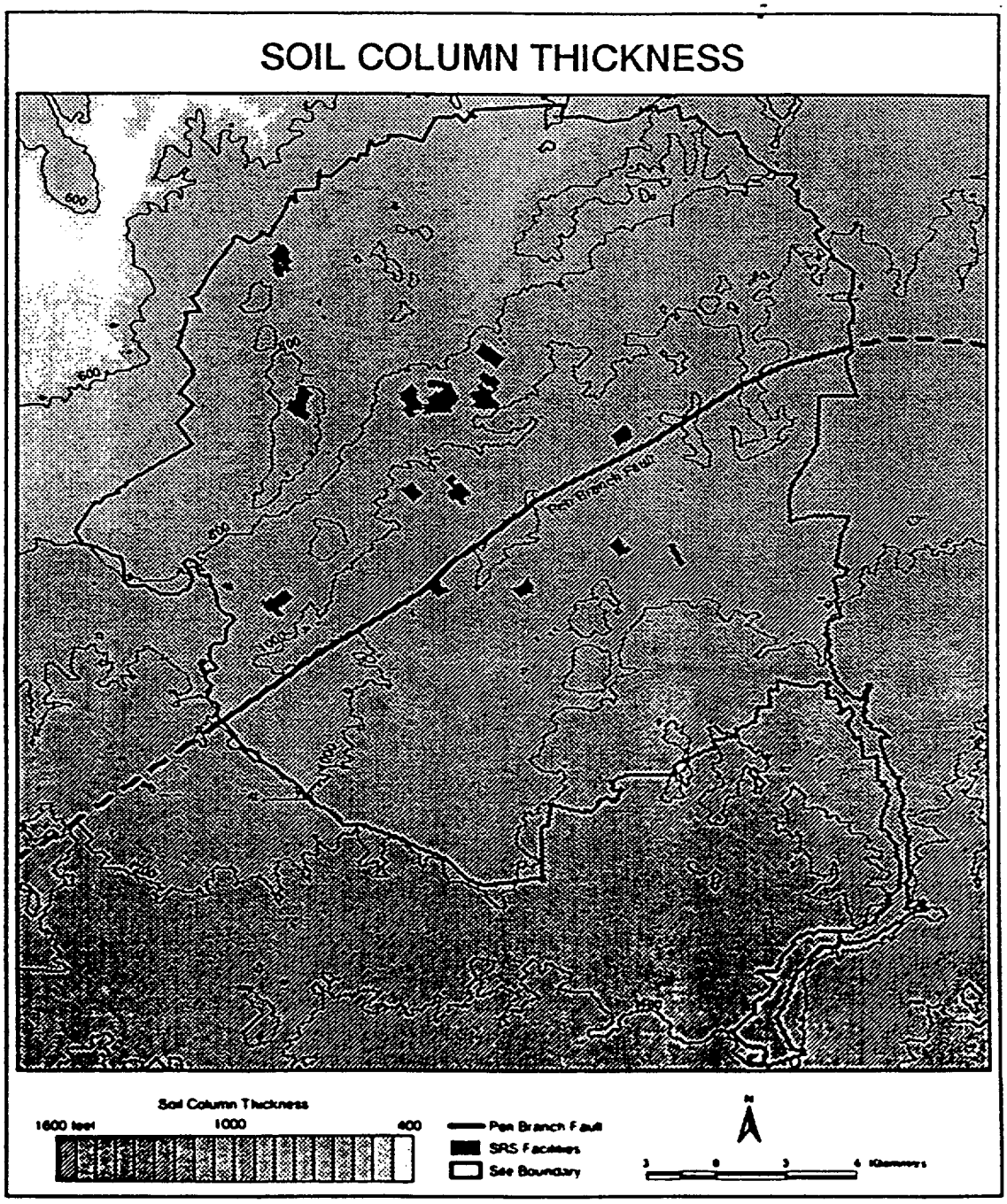

Figure 5.5 (c) - SRS contours of soil column thickness

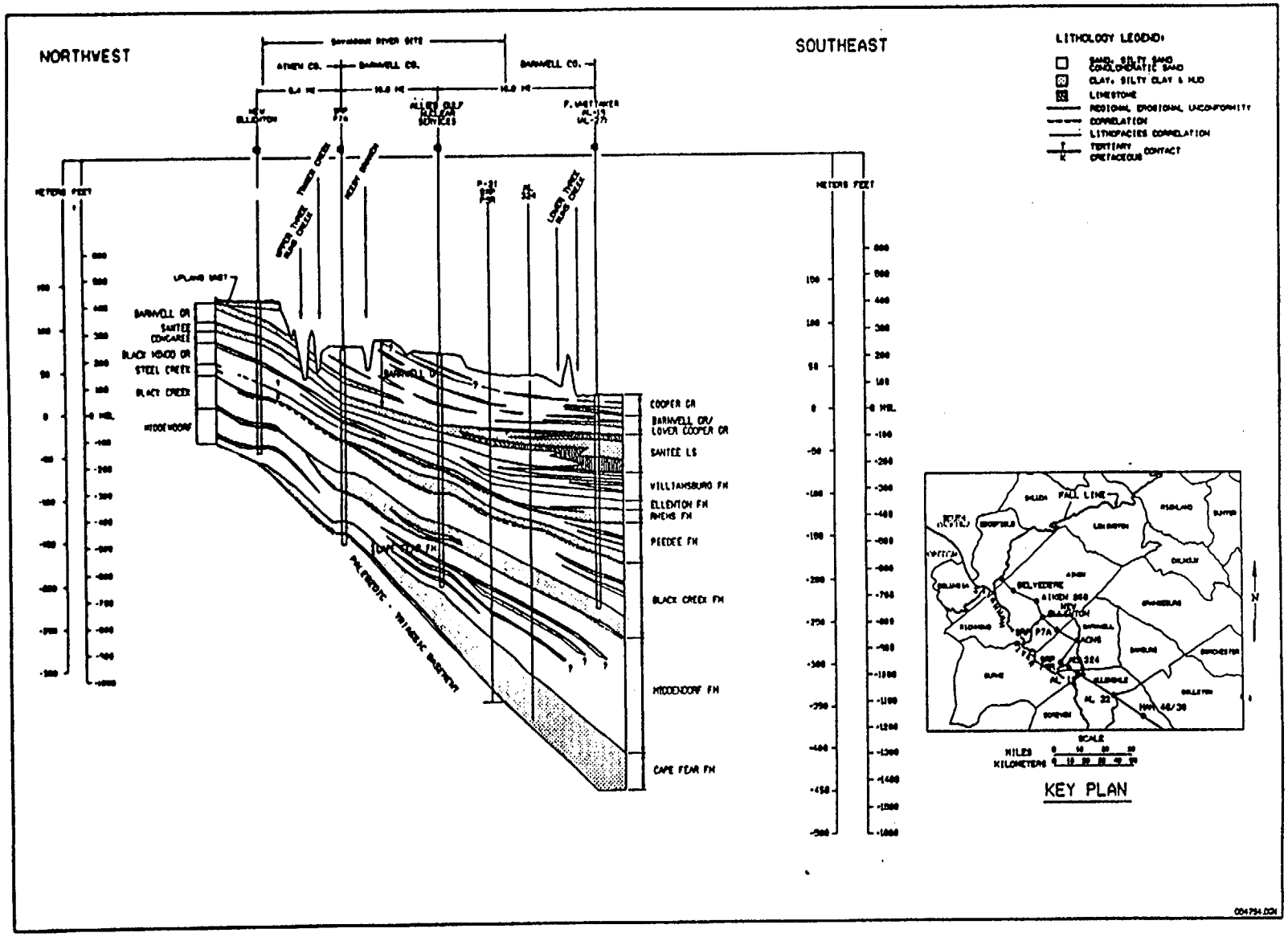

Figure 5.6 - Generalized Stratagraphic Cross Section for SRS (after Aadland et al., 1989).

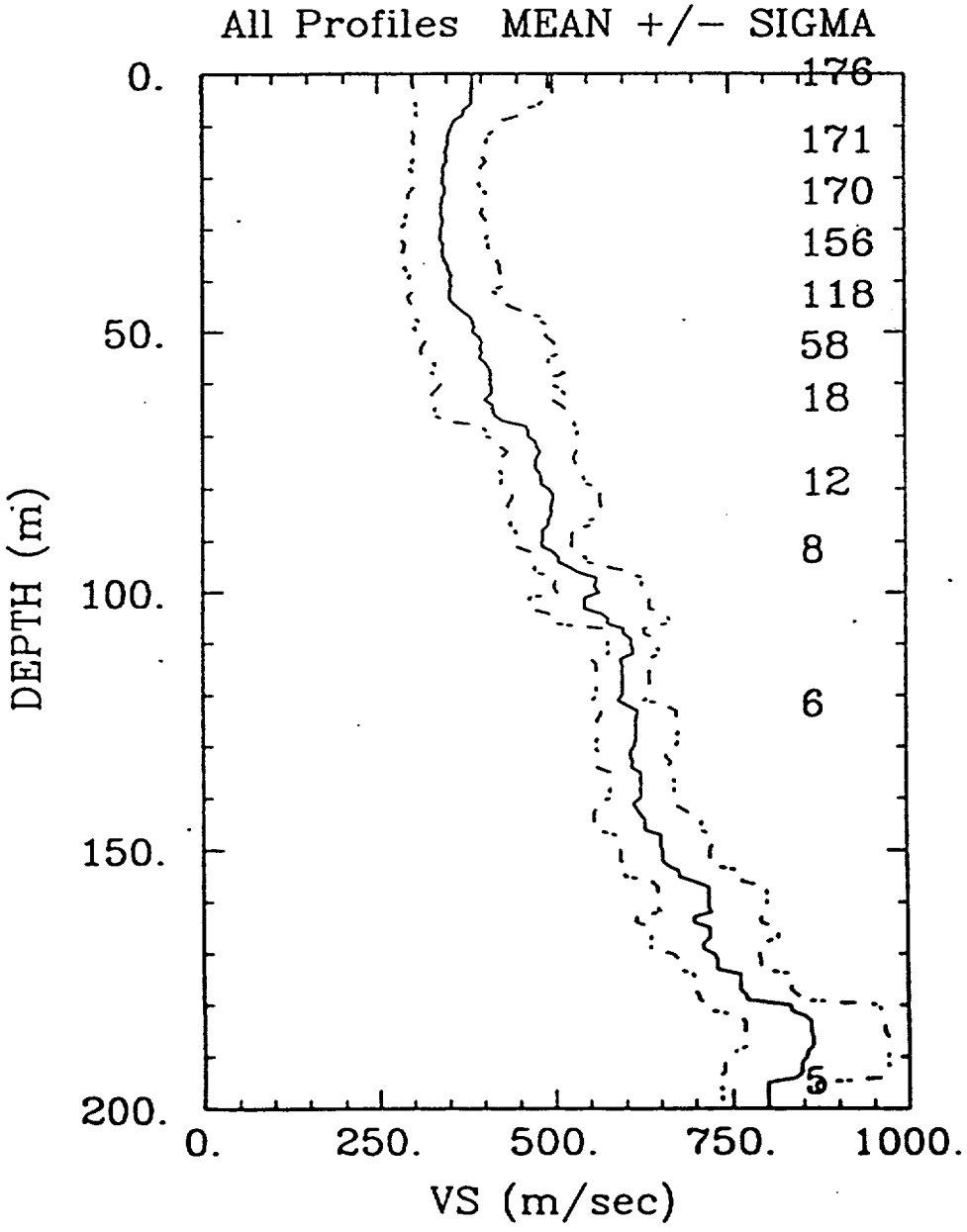

Figure 6.1 - SRS generic shear-wave velocity model based on all SRS shear-wave velocity data. Solid line is median velocity; dashed lines, median ± logarithmic standard deviation (σ_{lnV}). Numbers on right side axis are number of profiles used to compute statistics at the corresponding depth (Figure taken from Toro (1996))

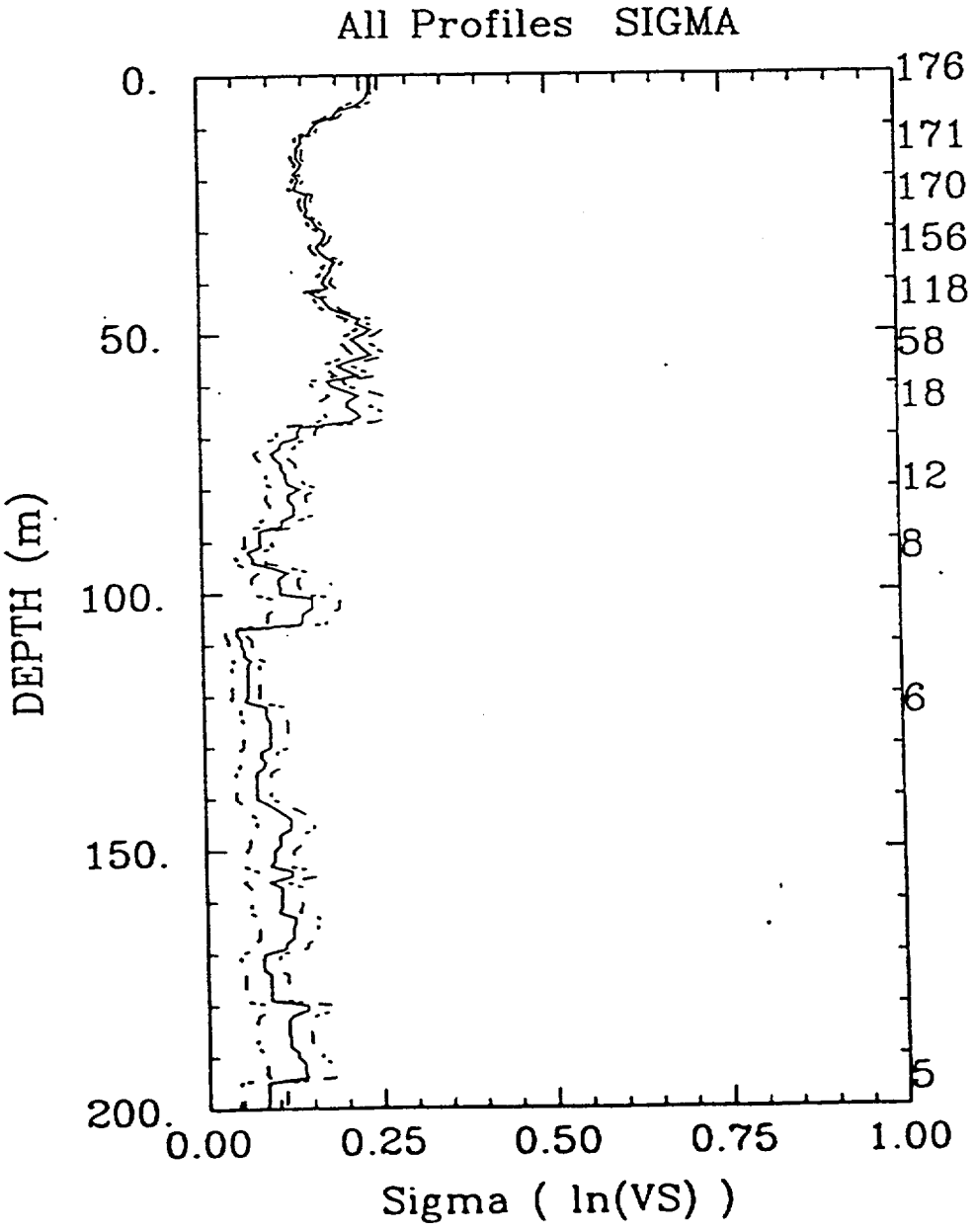

Figure 6.2 - SRS generic shear-wave velocity standard deviation derived from all SRS shear-wave velocity data. Solid line is best estimate σ_{lnV} vs. depth; dashed line, best estimate σ_{lnV} ± standard error of estimation. Numbers on right side axis are number of profiles used to compute statistics at the corresponding depth (Figure taken from Toro (1996))

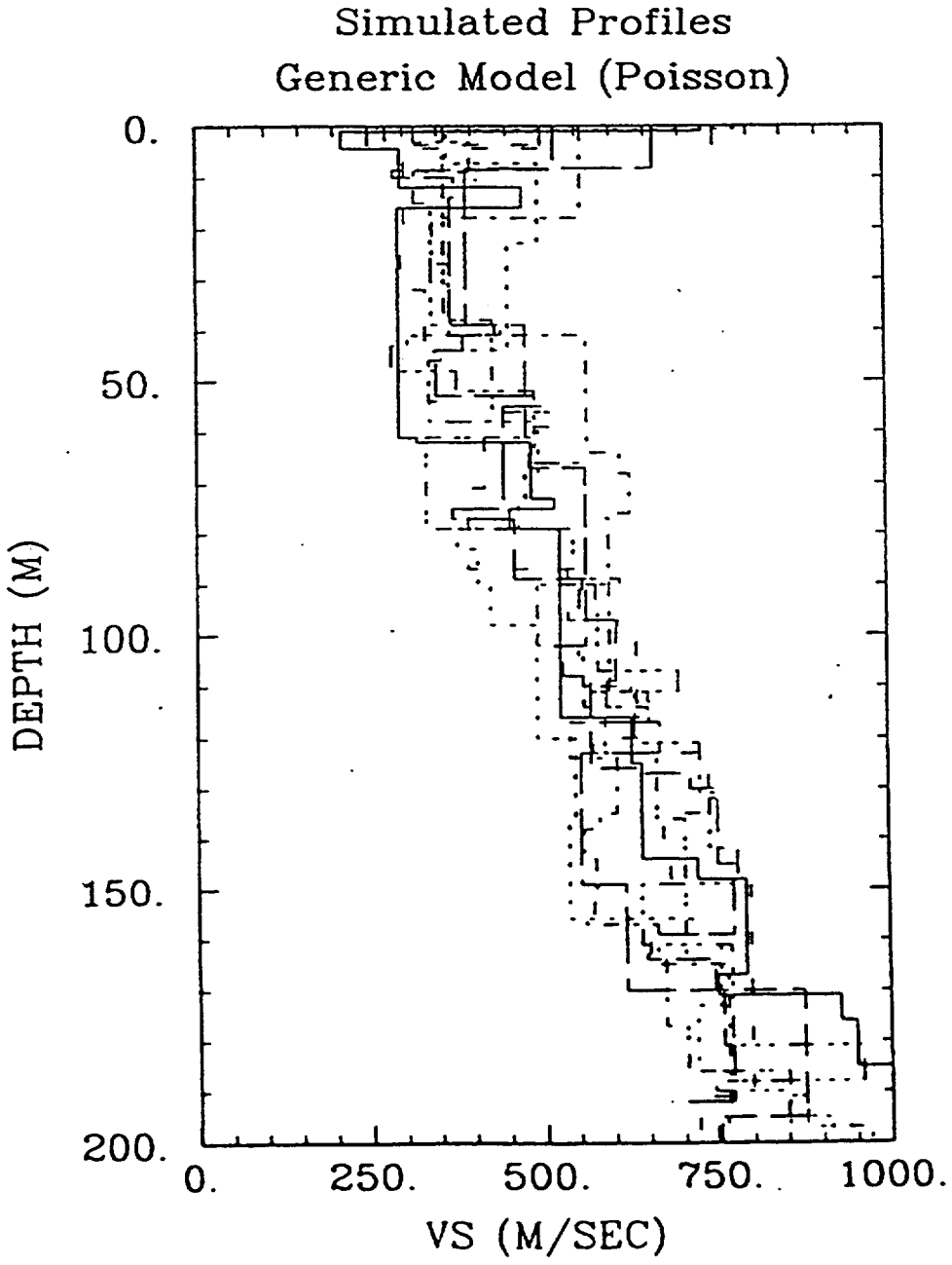

Figure 6.3 (a) - Simulated shear-wave velocity profiles using SRS generic model and a non-homogeneous Poisson model for layer thickness (Figure taken from Toro (1996))

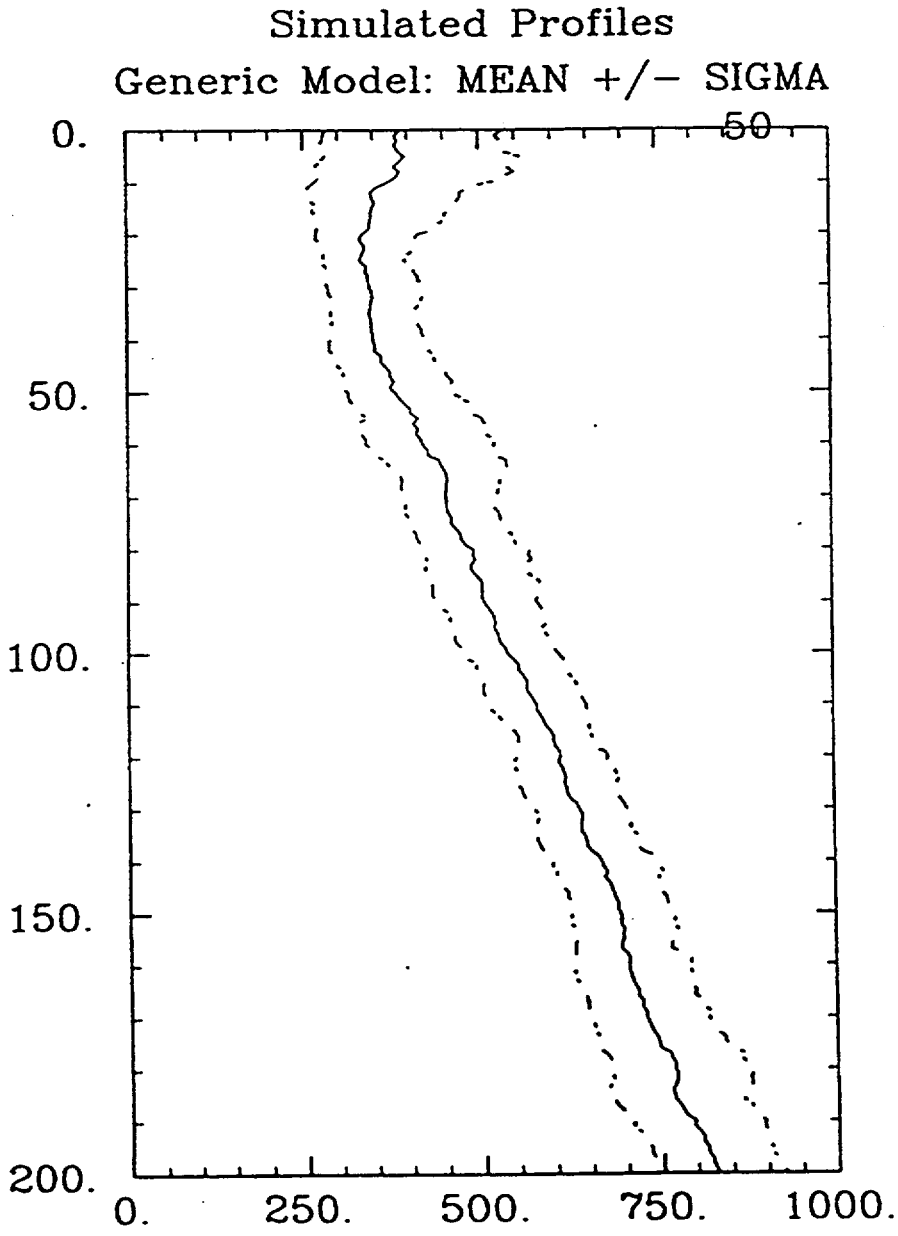

Figure 6.3 (b) - Median shear-wave profile from 50 profiles simulated using the SRS generic velocity model (Figure taken from Toro (1996)).

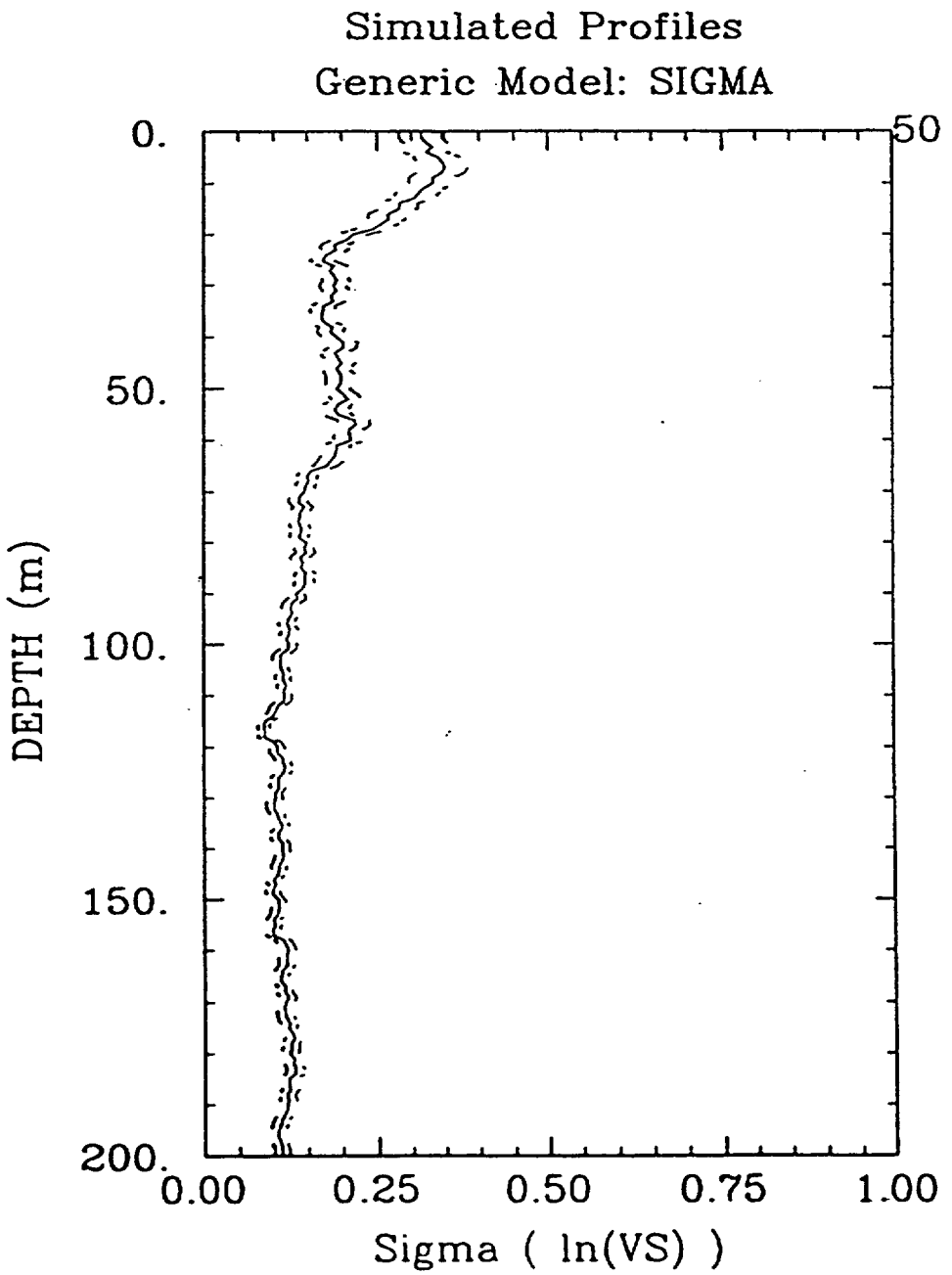

Figure 6.3 (c) - σ_{lnV} and its error of estimation vs. depth from 50 profiles simulated using the SRS generic velocity model (Figure taken from Toro (1996)).

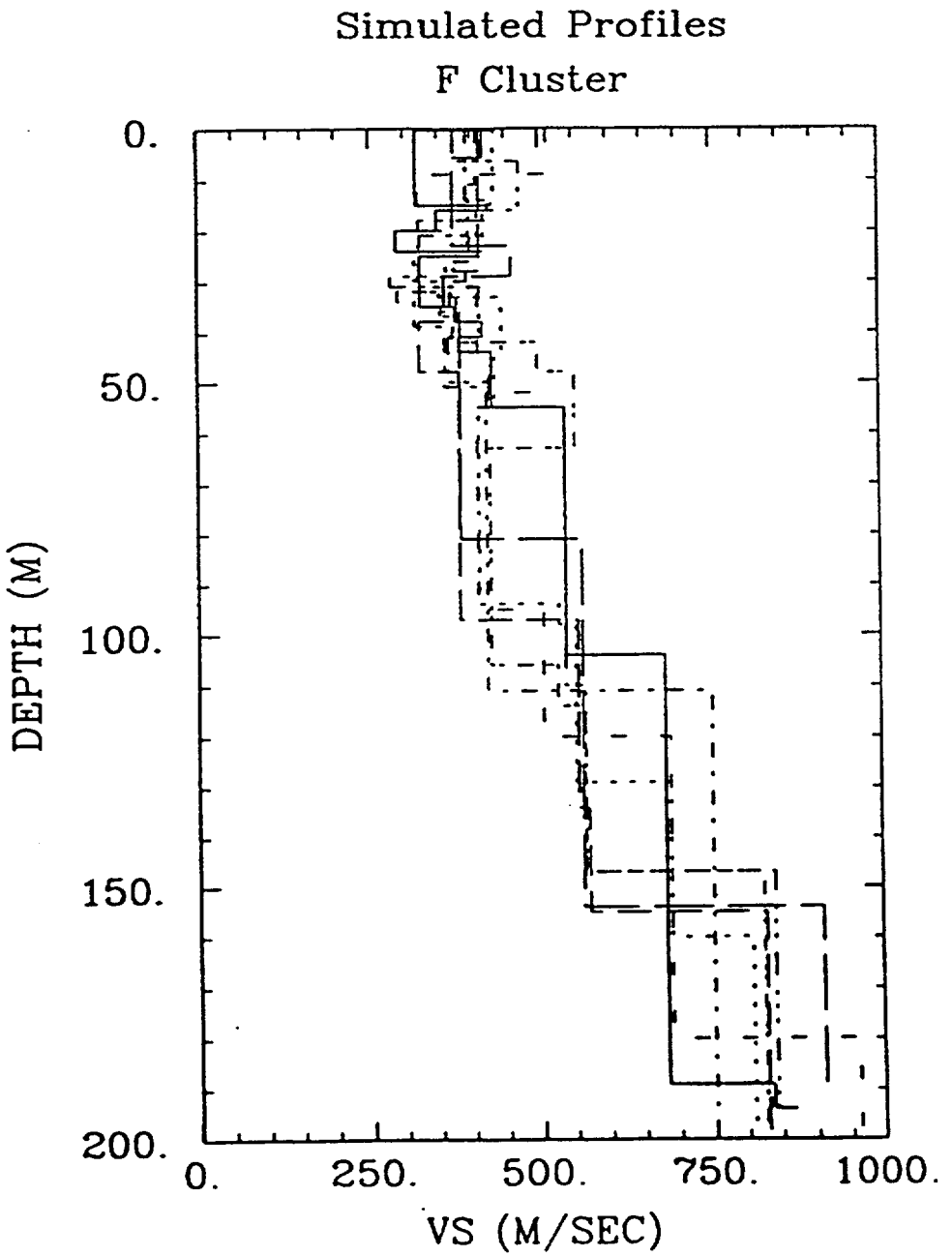

Figure 6.4 (a) - Simulated shear-wave velocity profiles for F-Area using F-Area-specific shear-wave data (Figure taken from Toro (1996)).

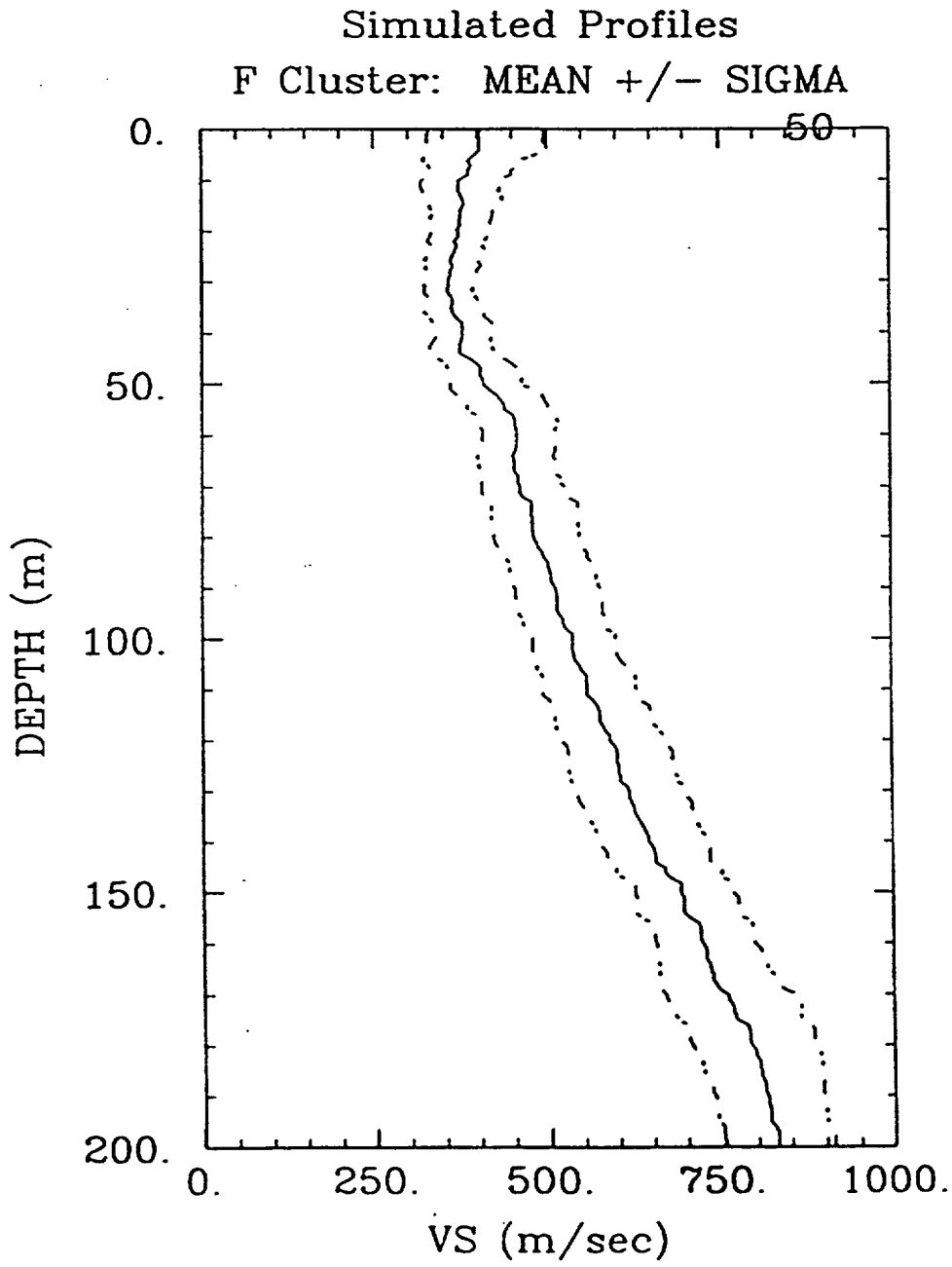

Figure 6.4 (b) - Median shear-wave profile from 50 profiles simulated using the F-Area specific shear-wave data and its error of estimation (Figure taken from Toro (1996))

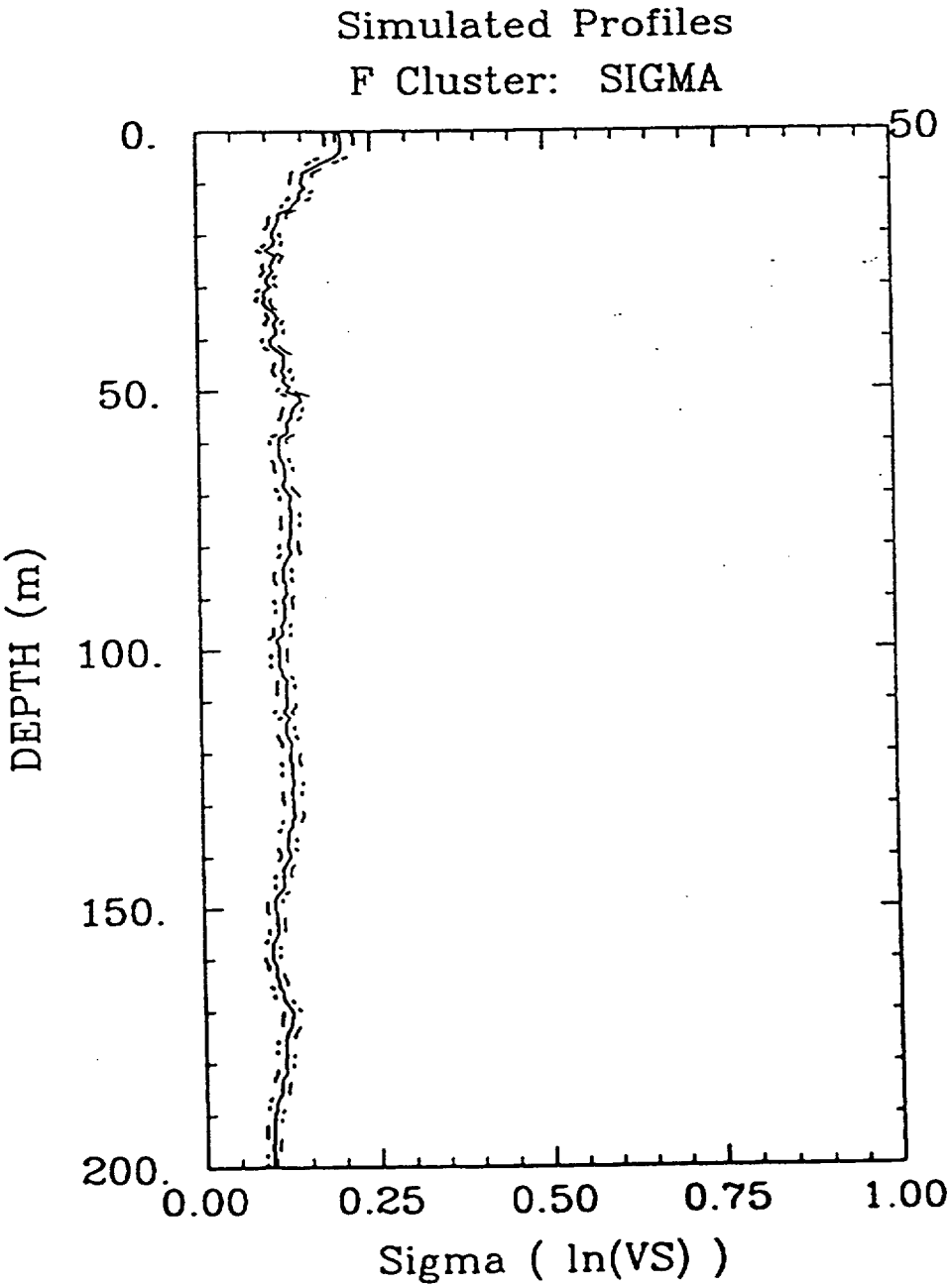

Figure 6.4 (c) - σ_{lnV} and its error of estimation vs. depth from 50 profiles simulated using the F-Area specific shear-wave data (Figure taken from Toro (1996))

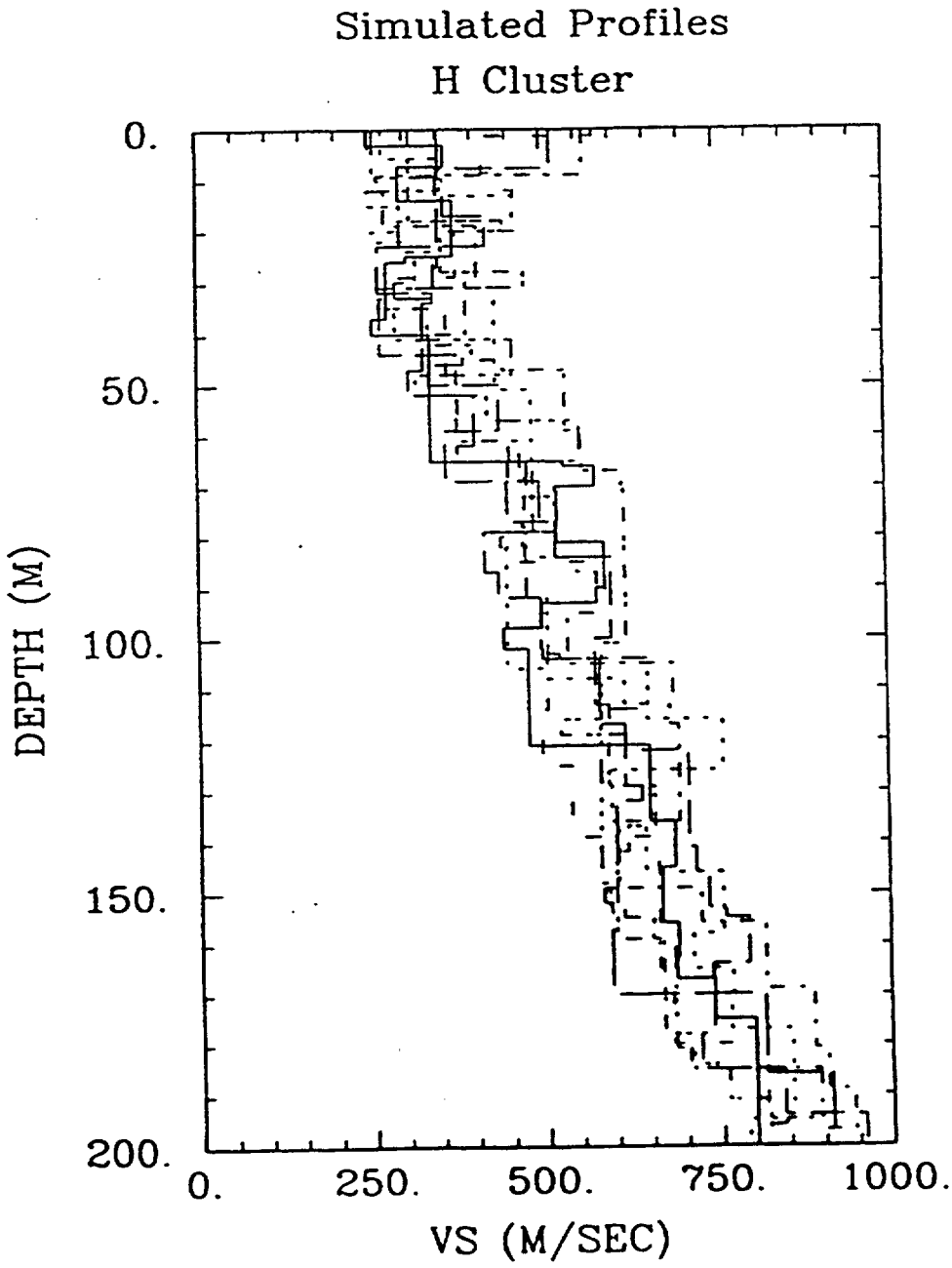

Figure 6.5 (a) - Simulated shear-wave velocity profiles for H-Area using H-Area-specific shear-wave data (Figure taken from Toro (1996)).

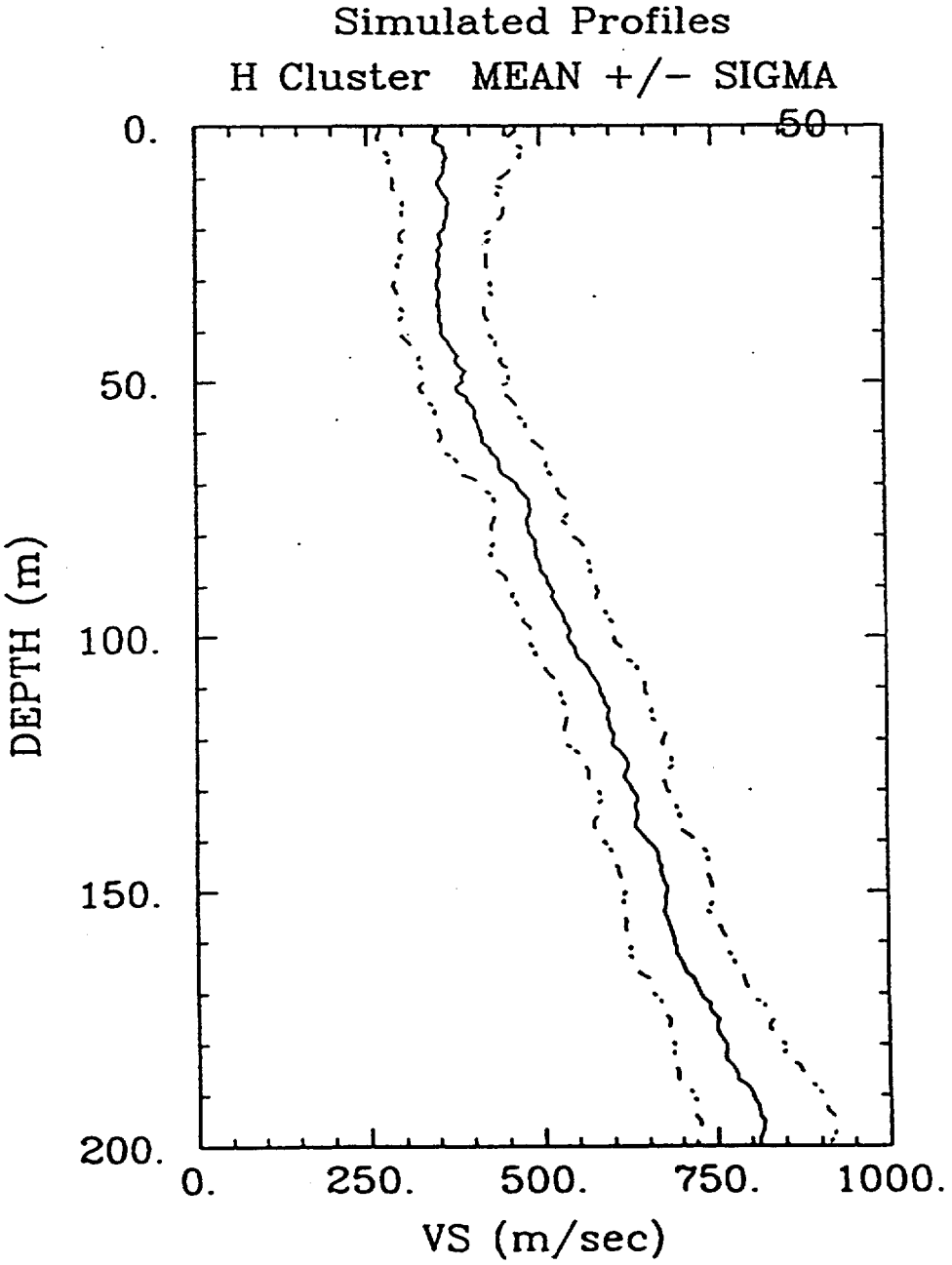

Figure 6.5 (b) - Median shear-wave velocity profile and its standard deviation from 50 profiles simulated using the H-Area specific shear-wave data (Figure taken from Toro (1996))

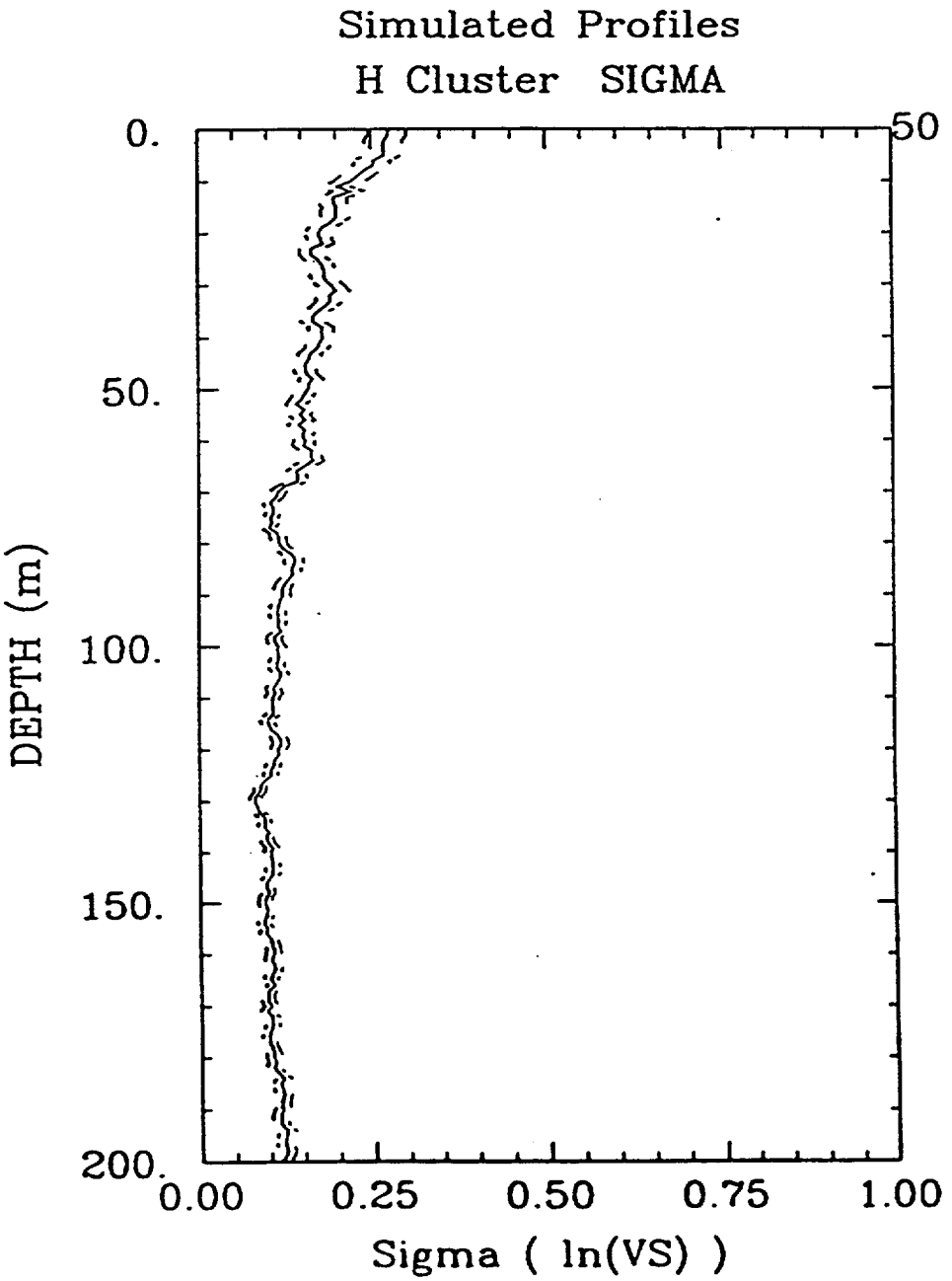

Figure 6.5 (c) - σ_{lnV} and its error of estimation vs. depth from 50 profiles simulated using the H-Area specific shear-wave data (Figure taken from Toro (1996)).

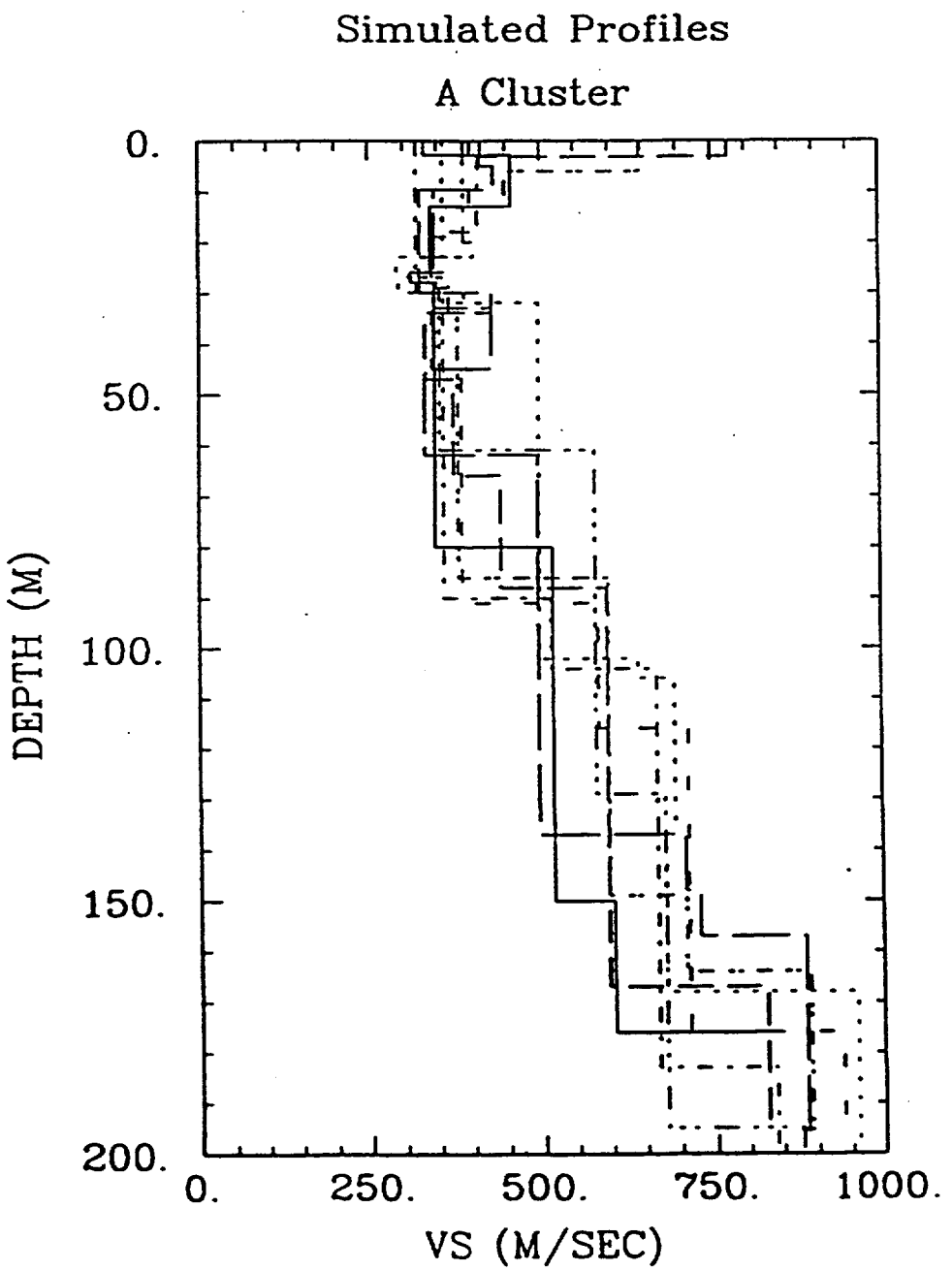

Figure 6.6 (a) - Simulated shear-wave velocity profiles for A-Area using A-Area-specific shear-wave data (Figure taken from Toro (1996)).

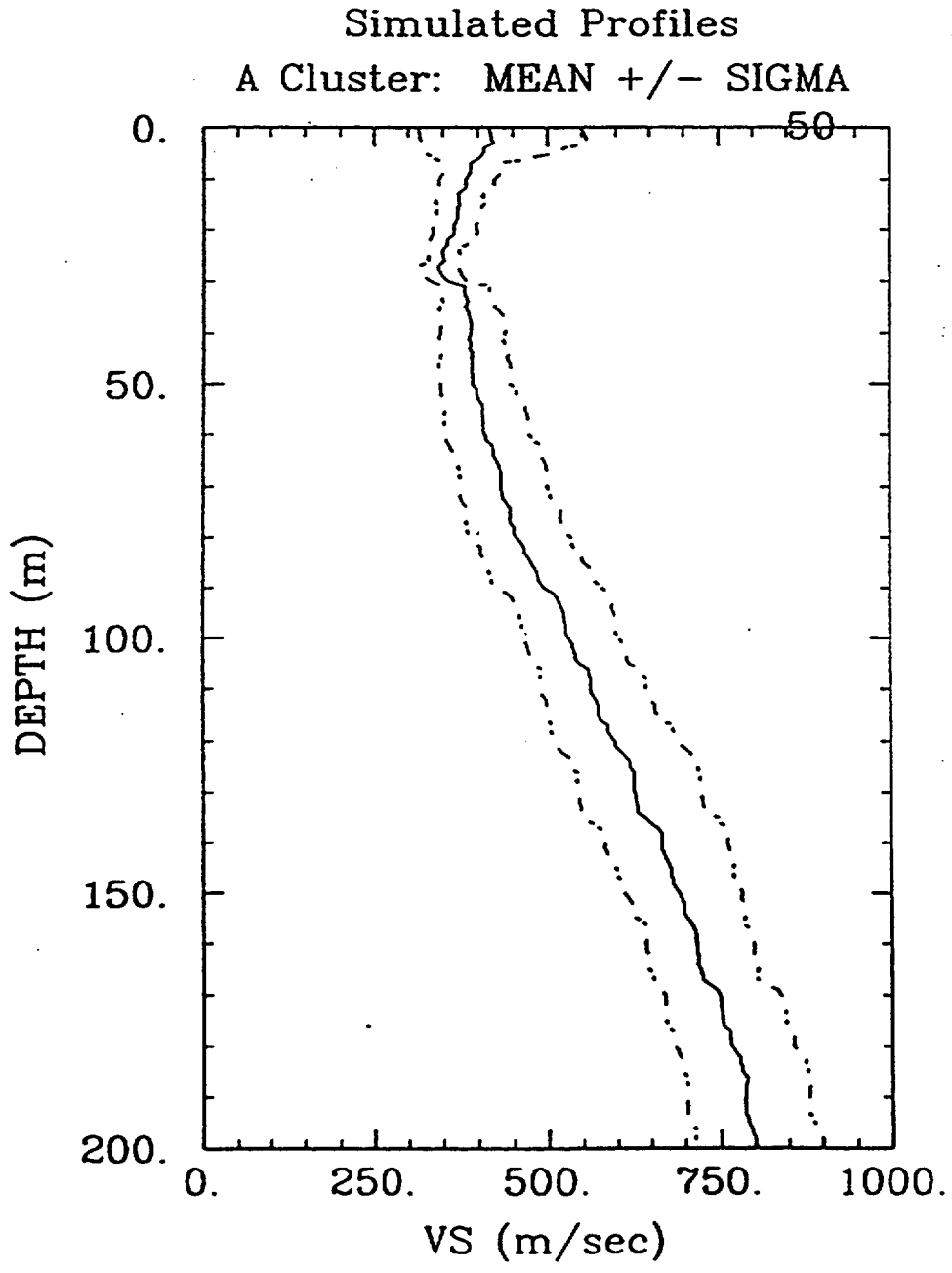

Figure 6.6 (b) - Median shear-wave velocity profile from 50 profiles simulated using the A-Area specific shear-wave data (Figure taken from Toro (1996)).

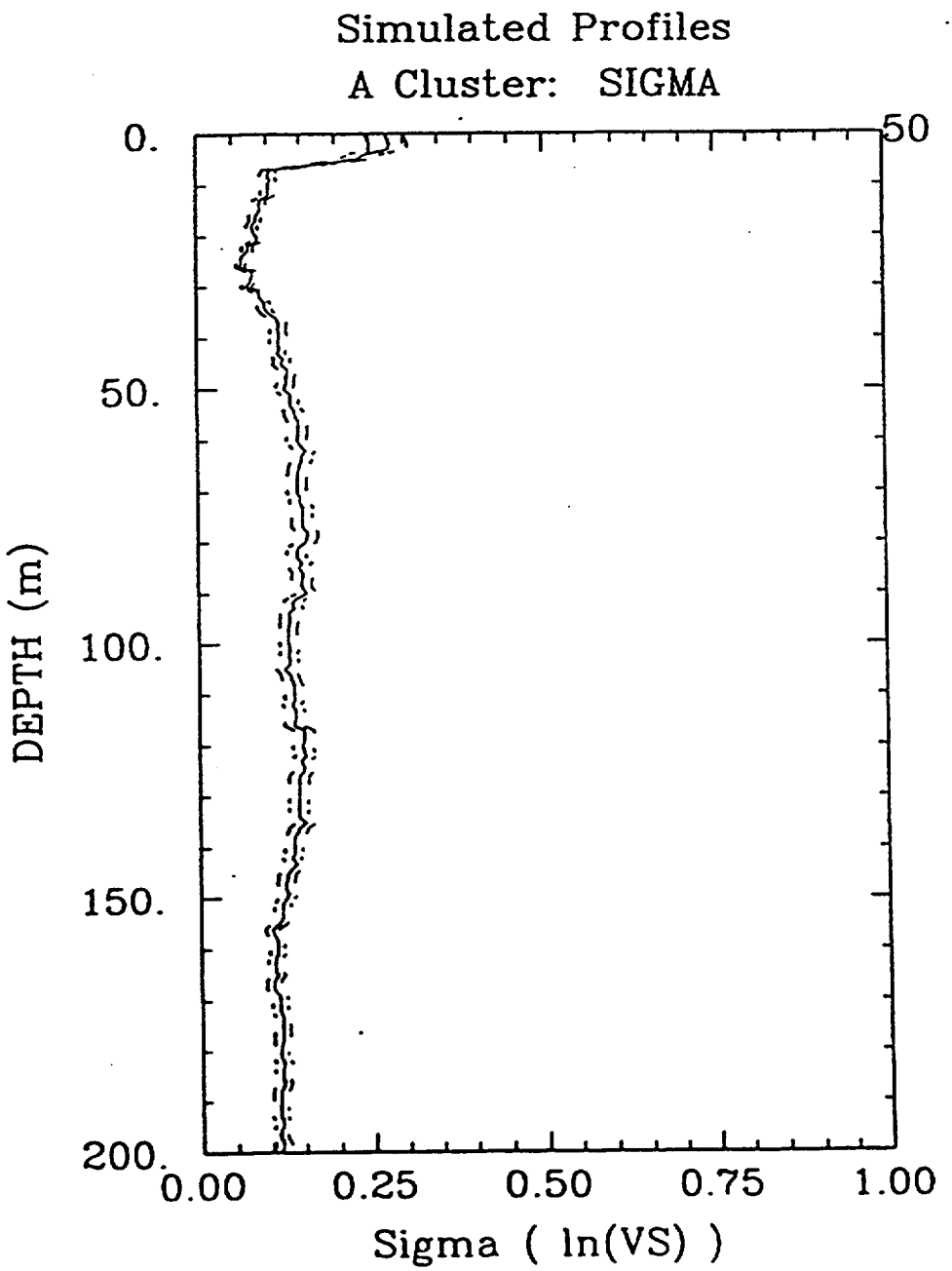

Figure 6.6 (c) - σ_{lnV} and its error of estimation vs. depth from 50 profiles simulated using the A-Area specific shear-wave data (Figure taken from Toro (1996)).

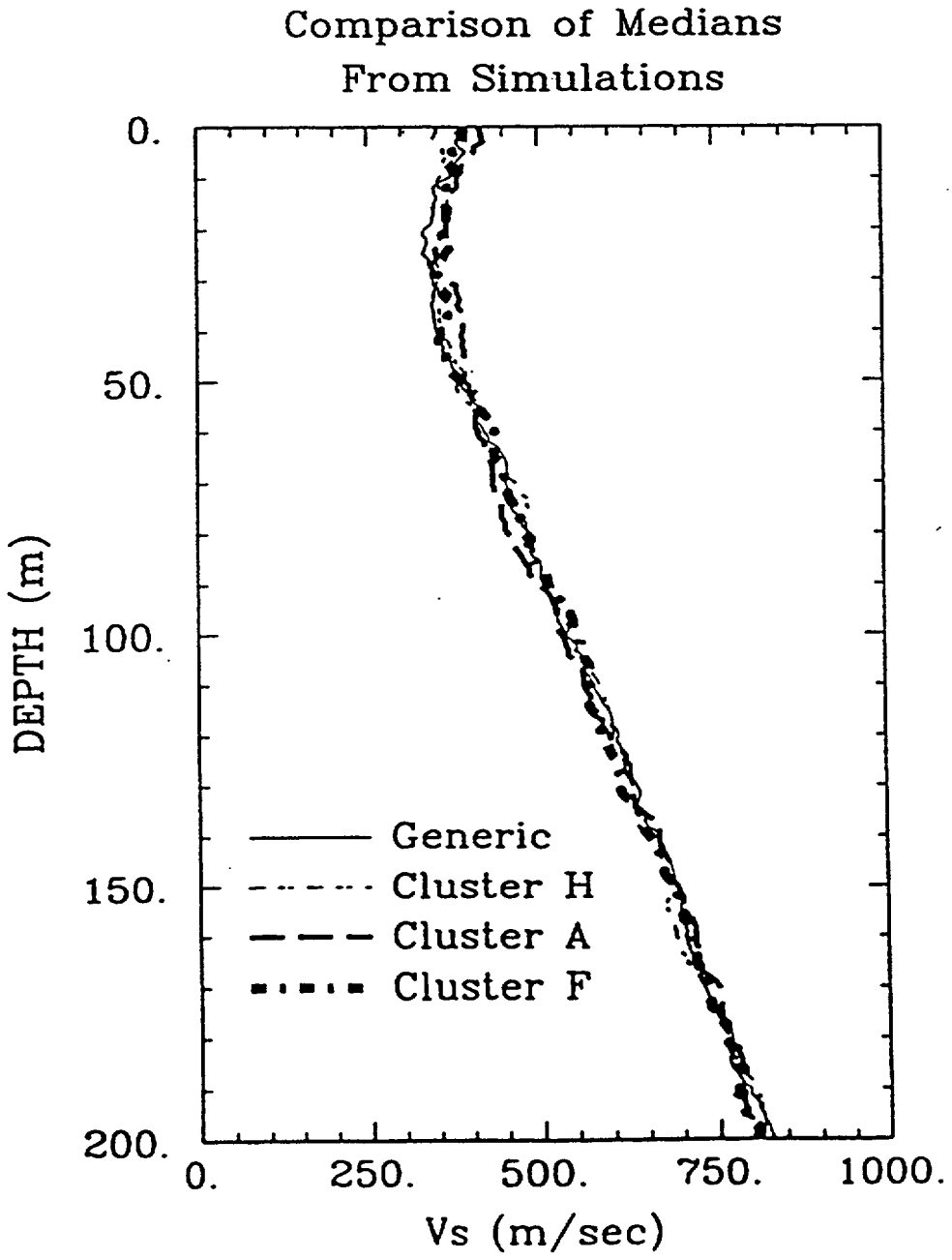

Figure 6.7 - Comparison of median shear-wave velocity profiles from simulations for A-, F-, and H-Areas.

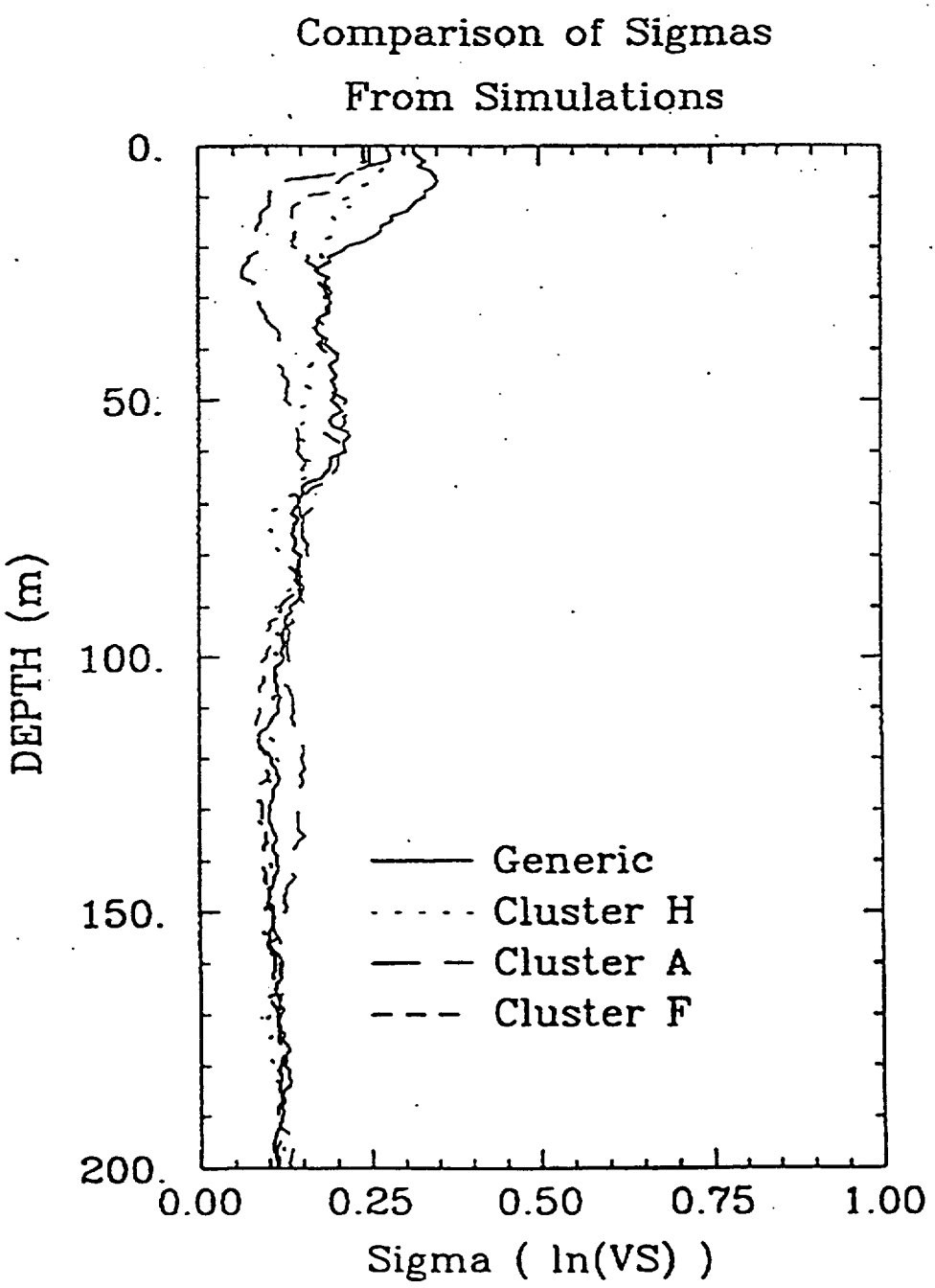

Figure 6.8 - Comparison of σ_{lnV} vs. depth from shear-wave velocity simulations for A-, F-, and H-Areas.

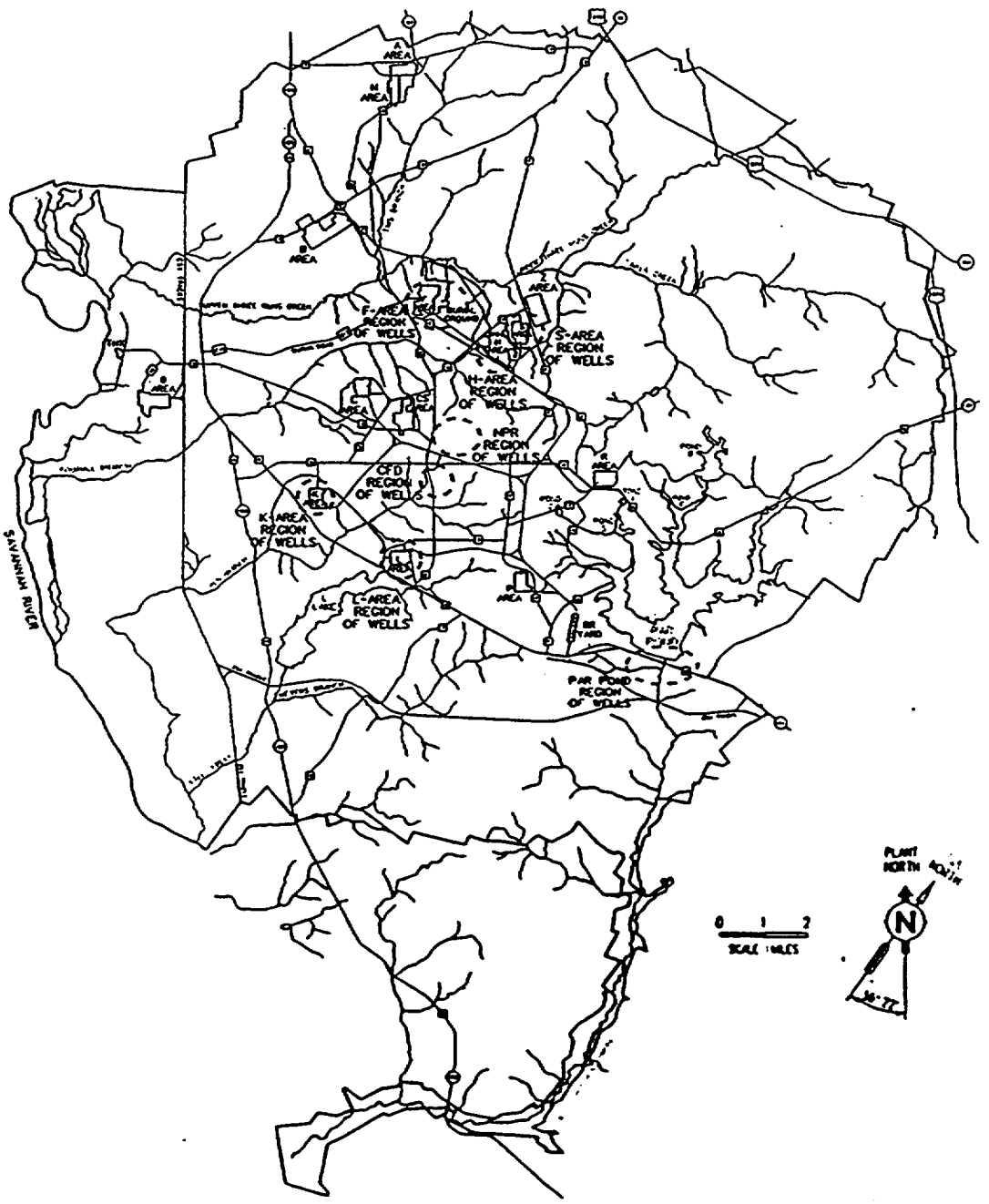

Figure 7.1 - Map of SRS showing the general boring (well) locations of all specimens used in the dynamic property correlation database.

Elevation (ft)	Geologic Formation	Depth (ft)	Number of Specimens	
			Sand	Clay
248		0	(3)	(0)
218	Upland	30	(18)	(1)
	Tobacco Road			
174		74	(13)	(2)
	Dry Branch			
125		123		
	Santee		(16)	(0)
58		190	(2)	(0)
43	Warley Hill	205		
	Congaree		(1)	(0)
-4		252	(0)	(0)
-30	Four Mile	278	(4)	(1)
-55	Snapp	303		
	Sawdust Landing		(0)	(0)
-122		370		
	Steel Creek		(0)	(1)
-242		490		
	Black Creek		(4)	(1)
-517		765		
	Middendorf		(1)	(1)
-657		905		
	Cape Fear		(3)	(0)
-795		1043		
	Basement			

Note: Stratigraphic profile taken from boring CFD 18.

Figure 7.2 - Representative stratigraphic profile of the SRS showing locations of soil samples used for dynamic testing.

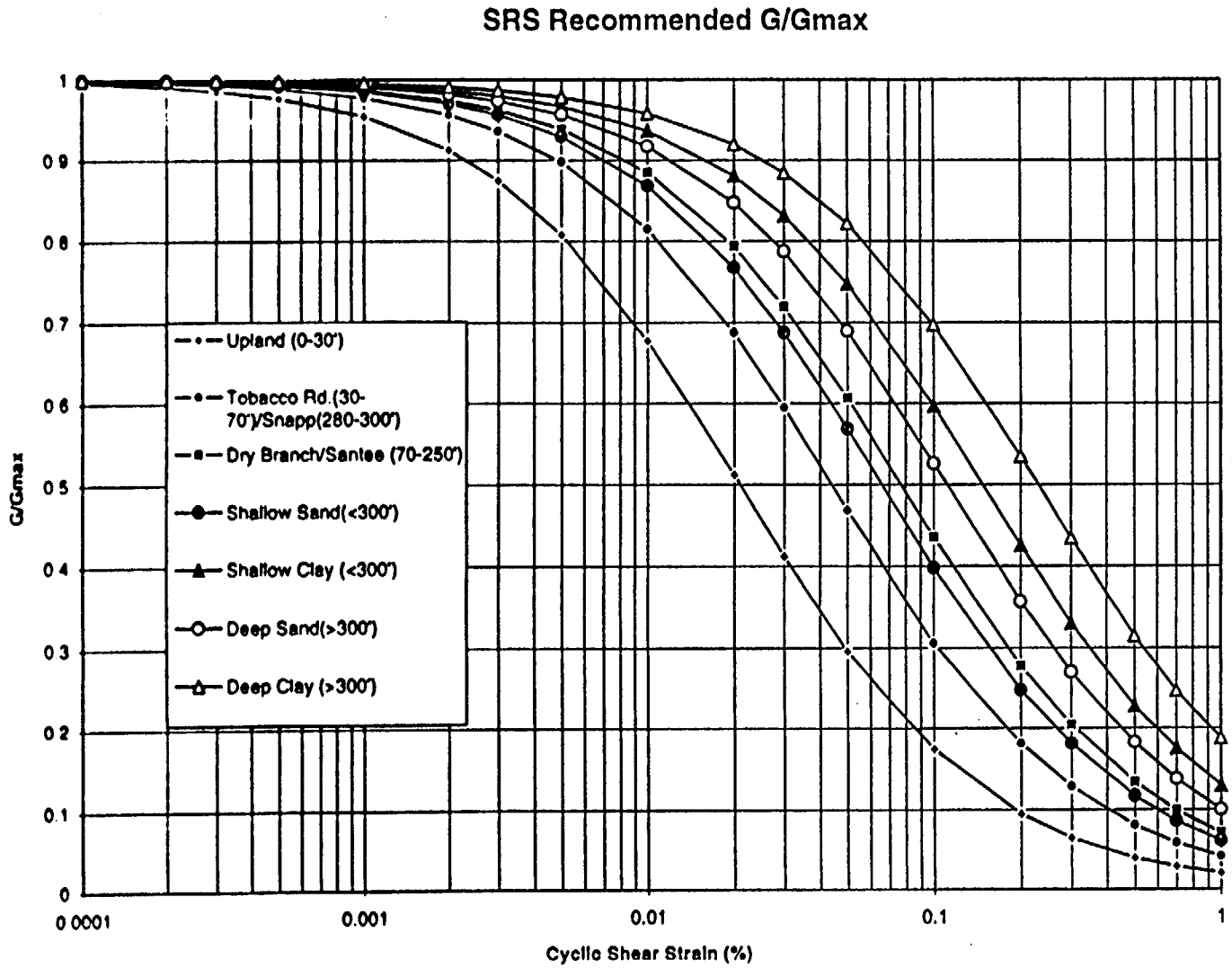

Figure 7.3 - Recommended generic strain-dependent shear modulus degradation curves for SRS soils (formations shown in Figure 7.2) (Stokoe et al., 1995).

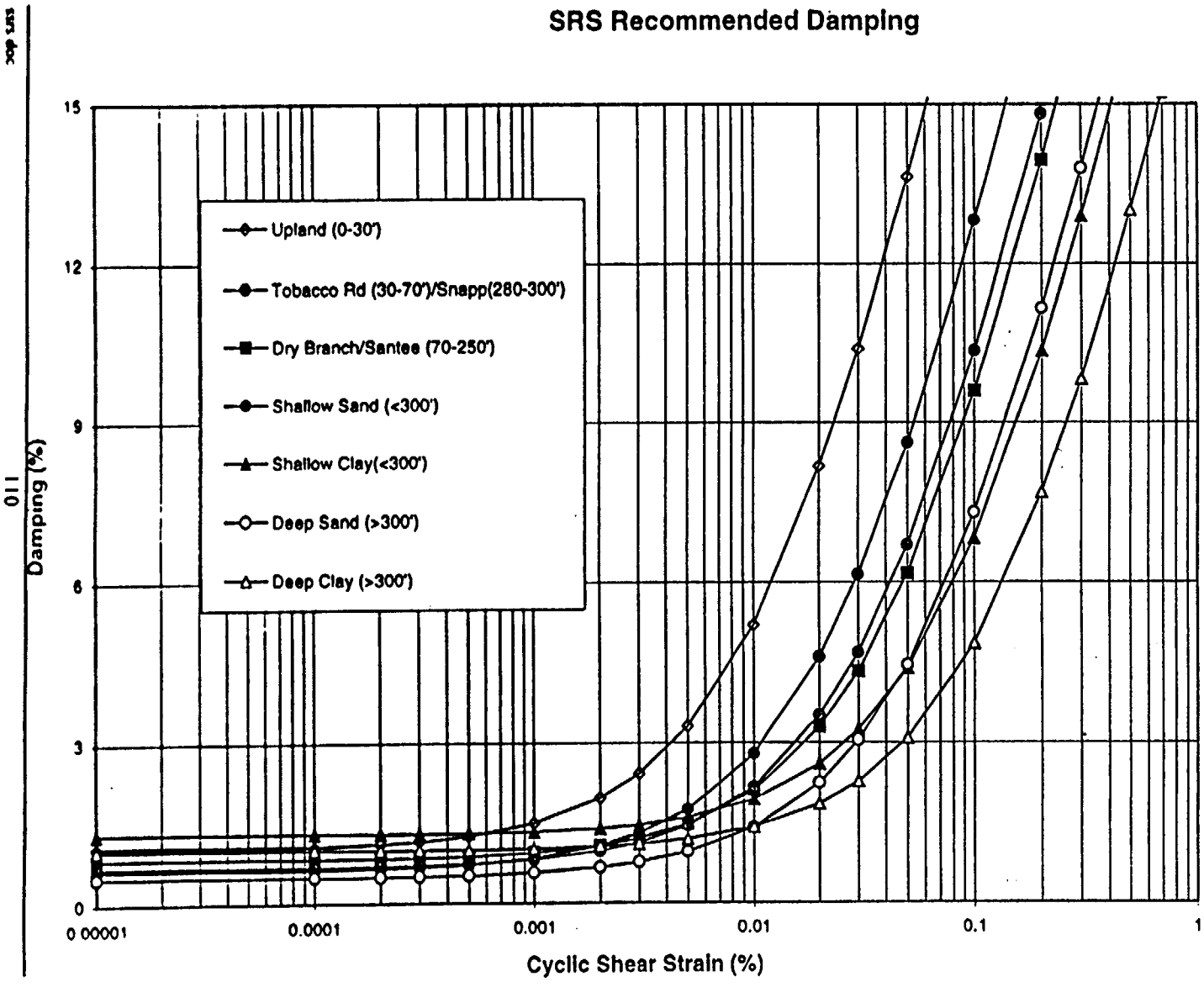

Figure 7.4 - Recommended generic strain-dependent soil damping curves for SRS soils (formations shown in Figure 7.2) (Stokoe et al., 1995).

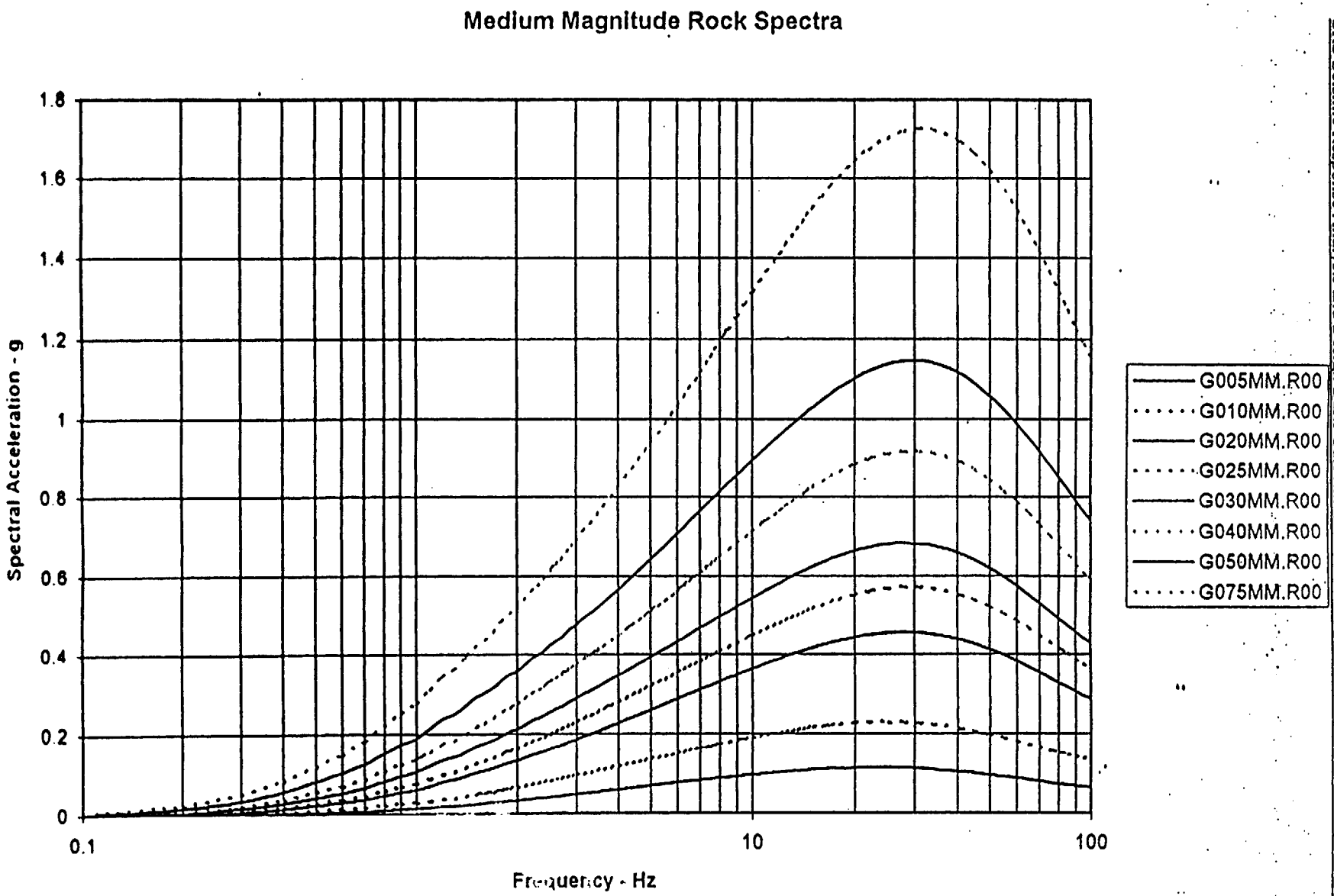

Figure 8.1(a) - 5 % damped response spectra for medium magnitude (M-bar) crystalline bedrock control motions used to generate generic soil response for soil category Z. Bedrock peak ground acceleration (PGA) ranges from 0.05g (G005MM.R00) to 0.75g (G075MM.R00) (see Table 8.2).

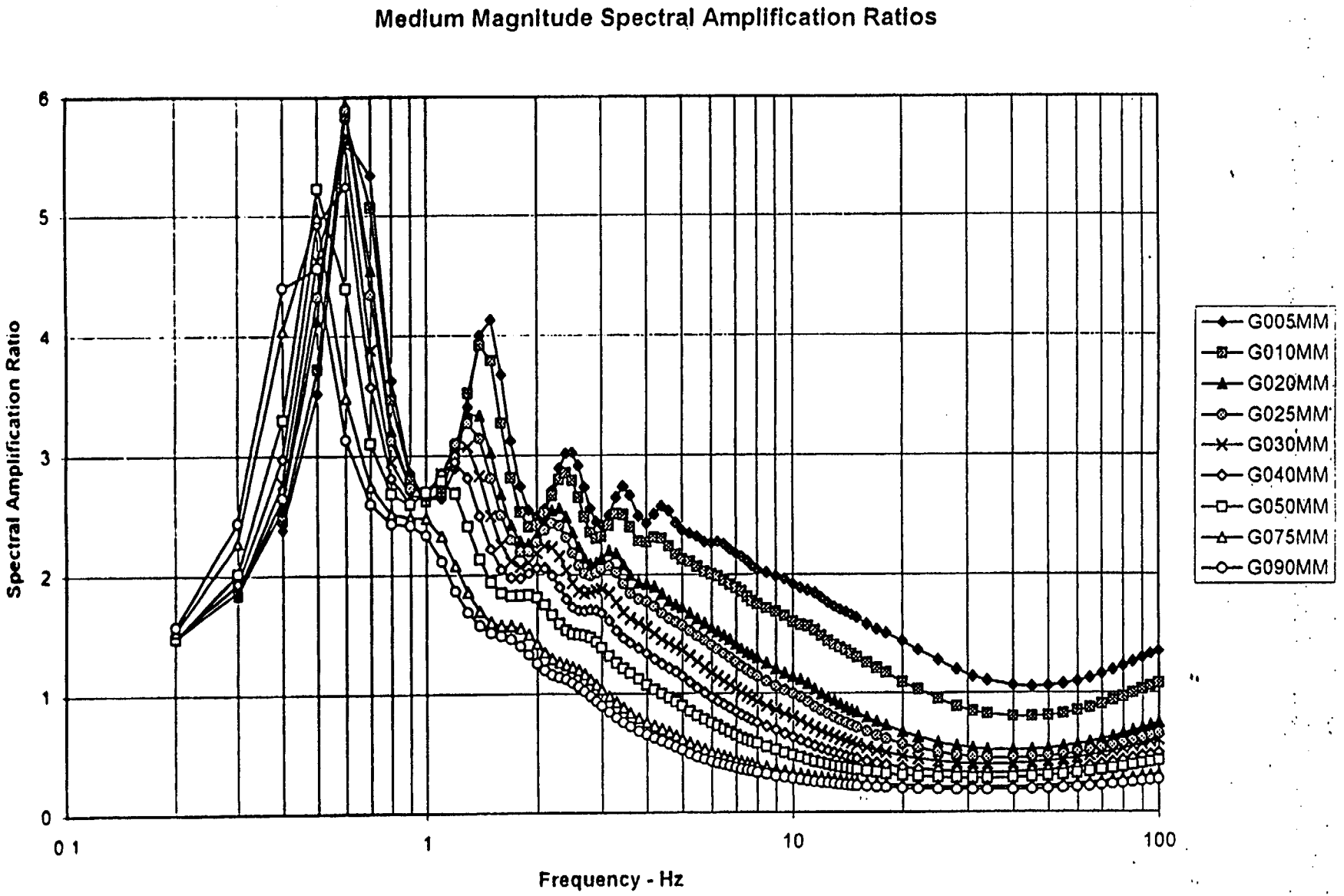

Figure 8.1(b) - Mean 5 % damped SRS generic amplification spectra for medium magnitude (M-bar) soil category 2 and crystalline response. Corresponding bedrock peak ground acceleration (PGA) ranging from 0.05g (G005MM) to 0.75g (G075MM) (see Table 8.2).

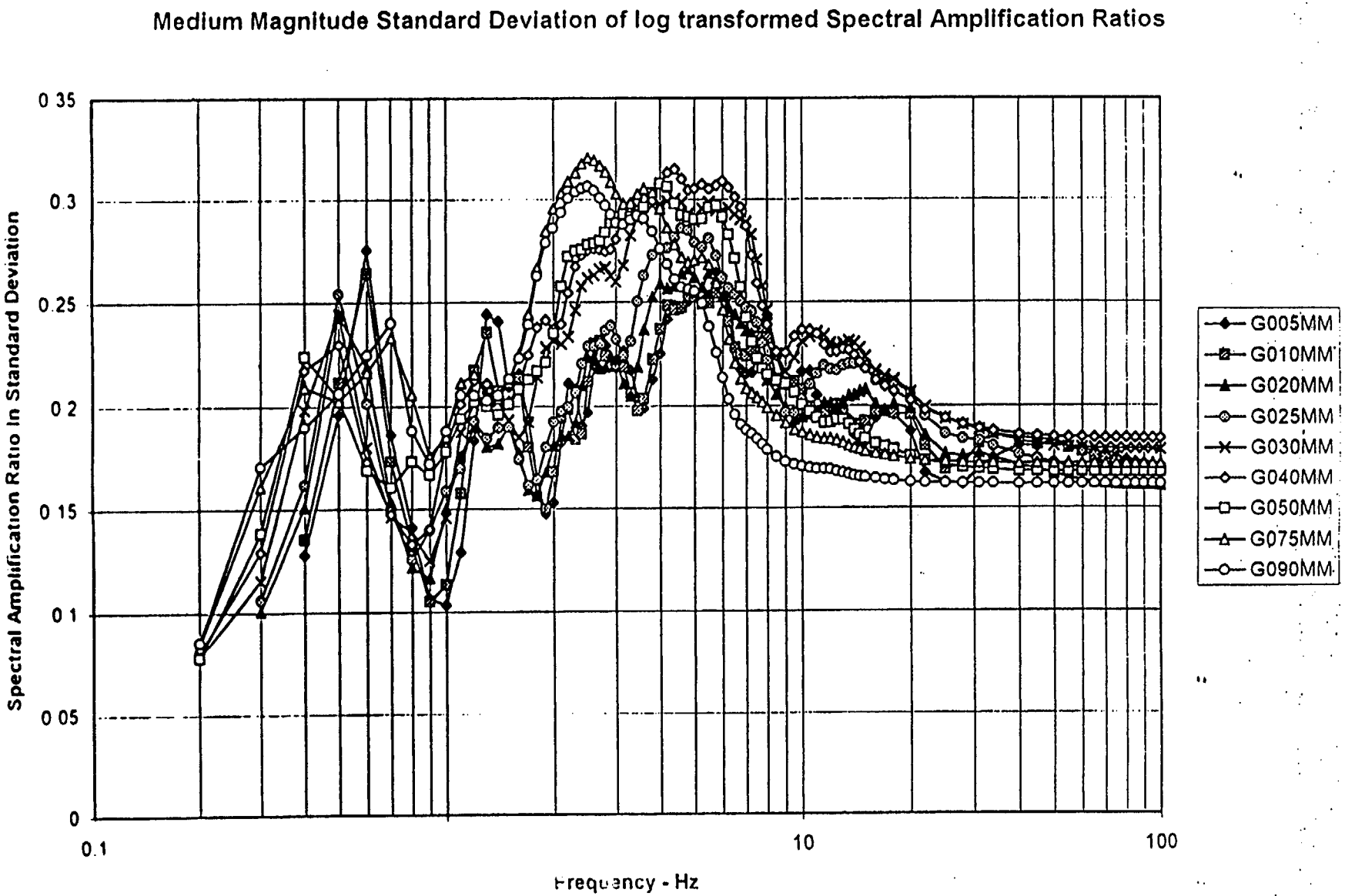

Figure 8.1(c) - Logarithmic standard deviation of 5 % damped SRS generic amplification spectra for medium magnitude (M-bar) soil category 2 response. Corresponding bedrock peak ground acceleration (PGA) ranging from 0.05g (G005MM) to 0.75g (G075MM) (see Table 8.2).

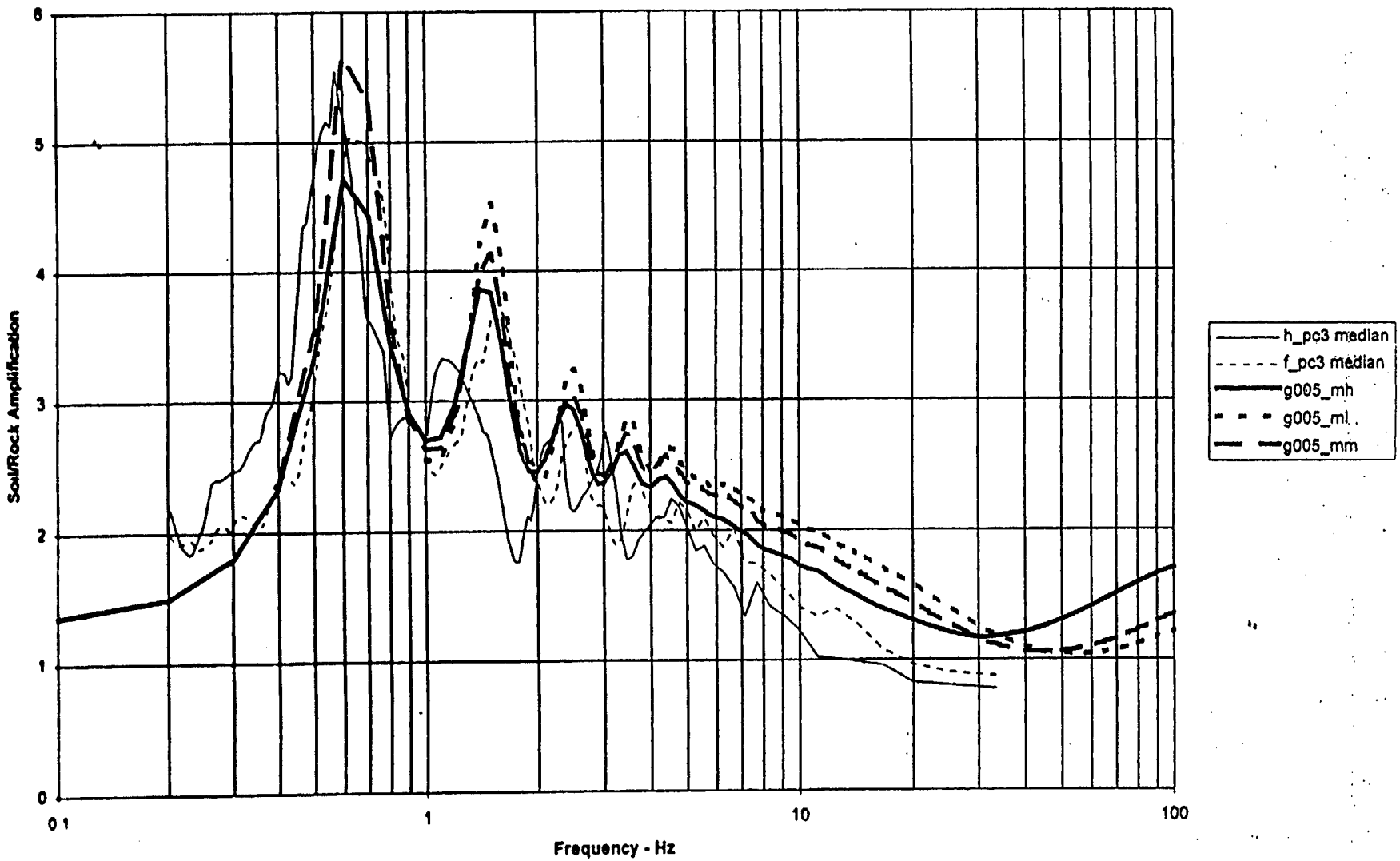

Figure 8 1(d) - Comparison of crystalline depth category 2 SAFs (PGA=0.05g; ML, MM, MH) to F- and H-Canyon median SAF spectra (light lines).

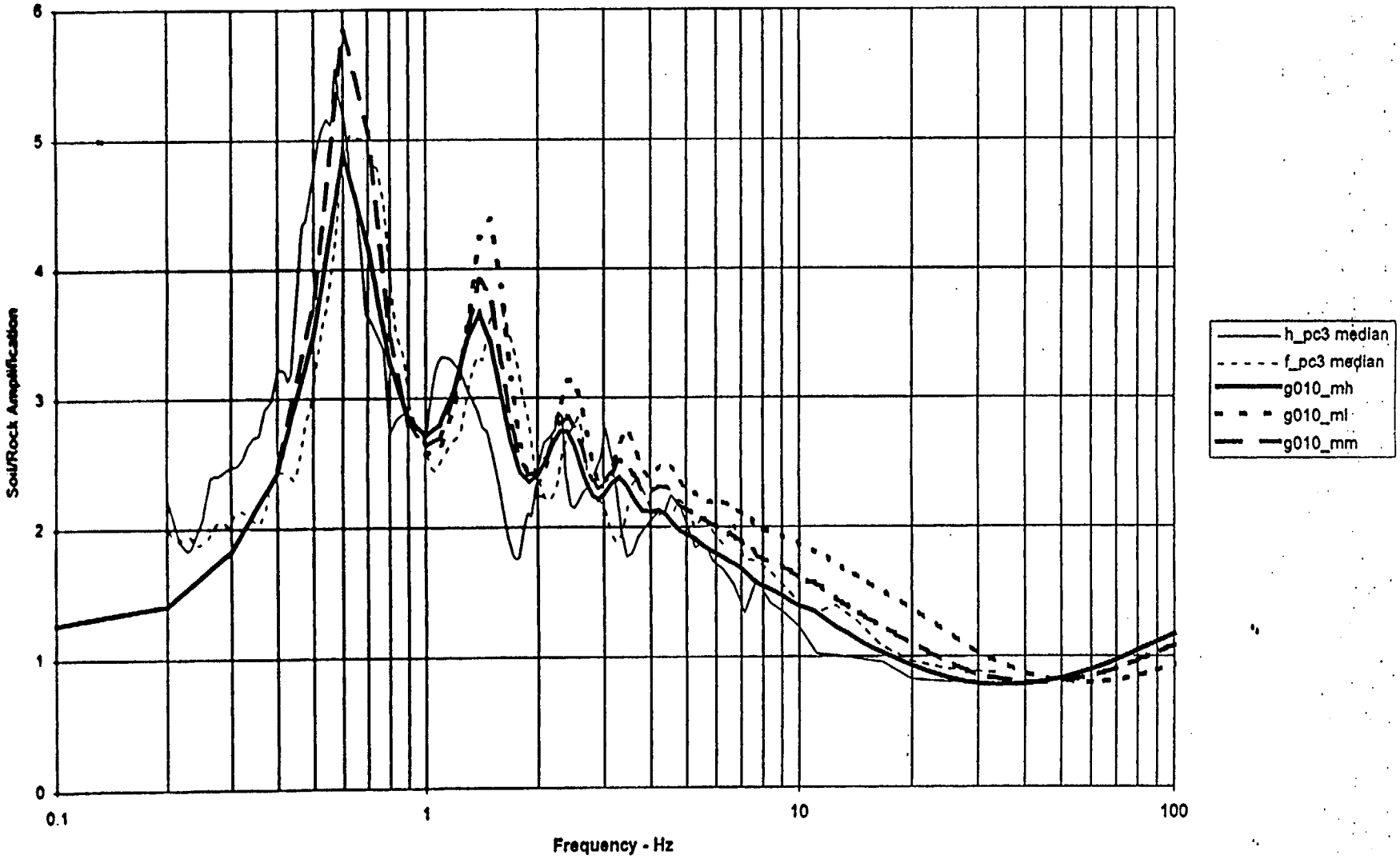

Figure 8.1(e) - Comparison of crystalline depth category 2 SAFs (PGA=0.10g; ML, MM, MH) to F- and H-Canyon median SAF spectra (light lines).

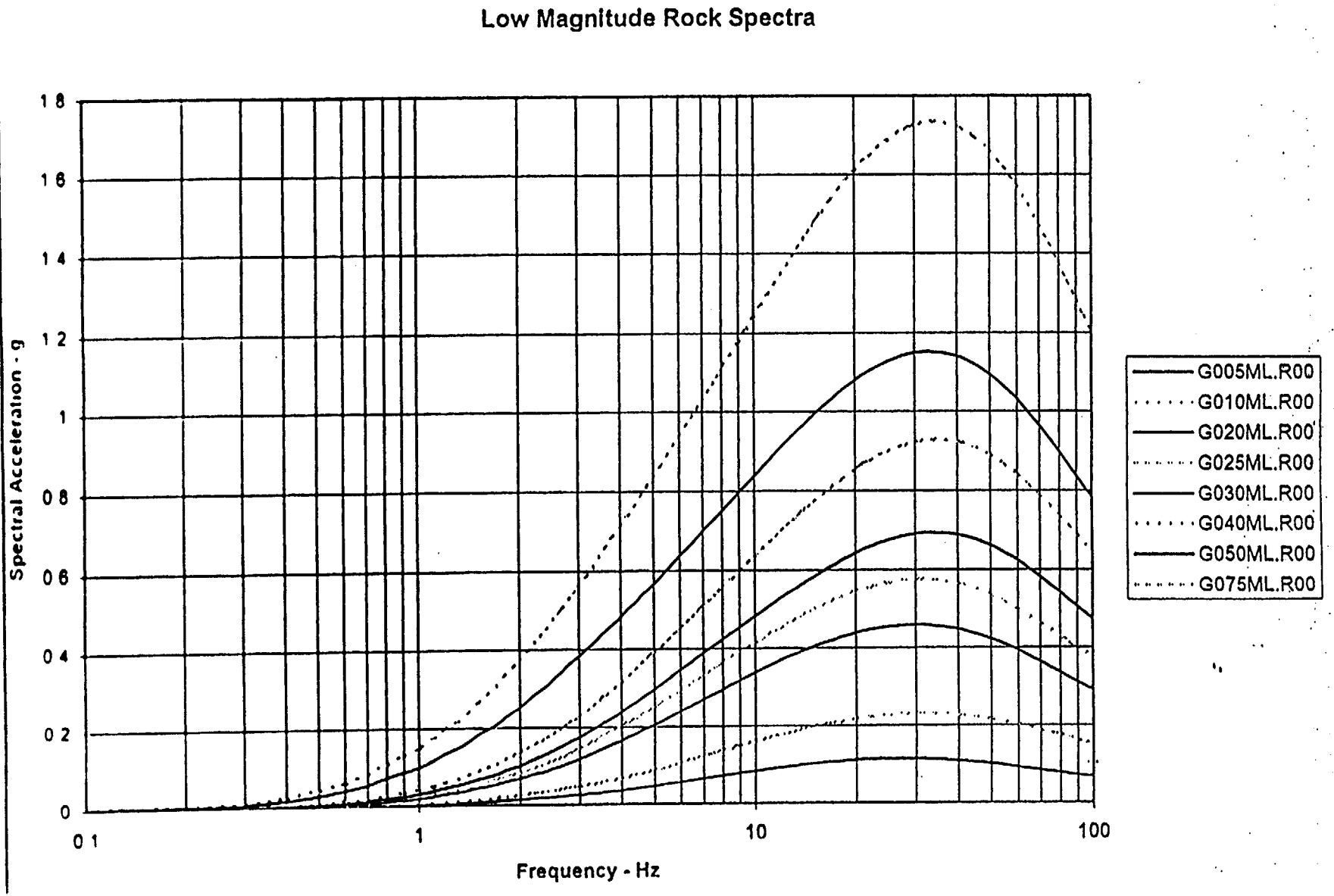

Figure 8.2 (a) - 5 % damped response spectra of low magnitude (ML) crystalline bedrock control motions used to generate soil response. Bedrock peak ground acceleration (PGA) ranges from 0.05g (G005ML.R00) to 0.75g (G075ML.R00) (see Table 8.2).

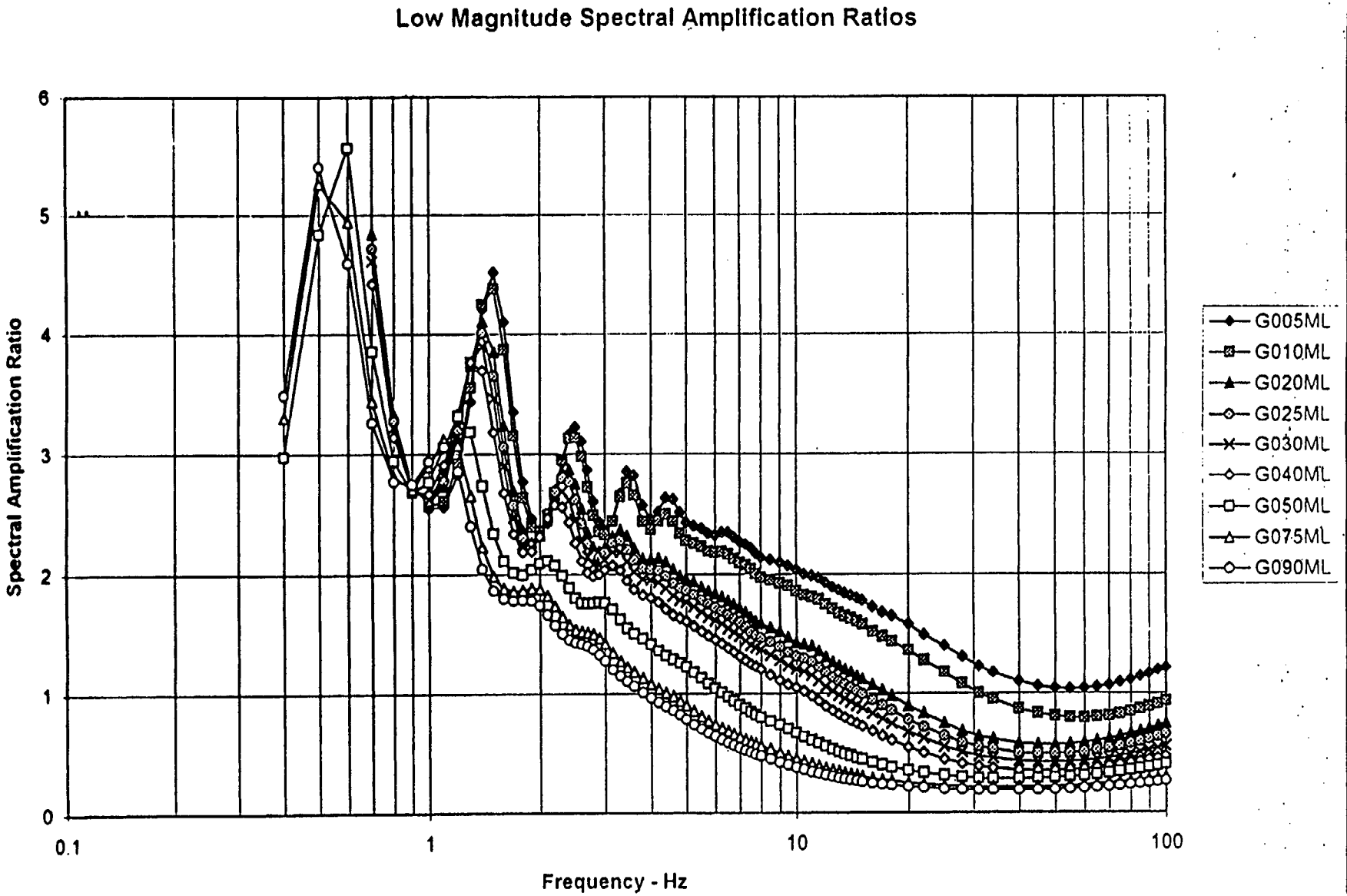

Figure 8.2 (b) - Mean 5 % damped response spectra of low magnitude soil category 2 spectral amplification for crystalline rock. Corresponding bedrock peak ground acceleration (PGA) ranges from 0.05g (G005ML) to 0.75g (G075ML).

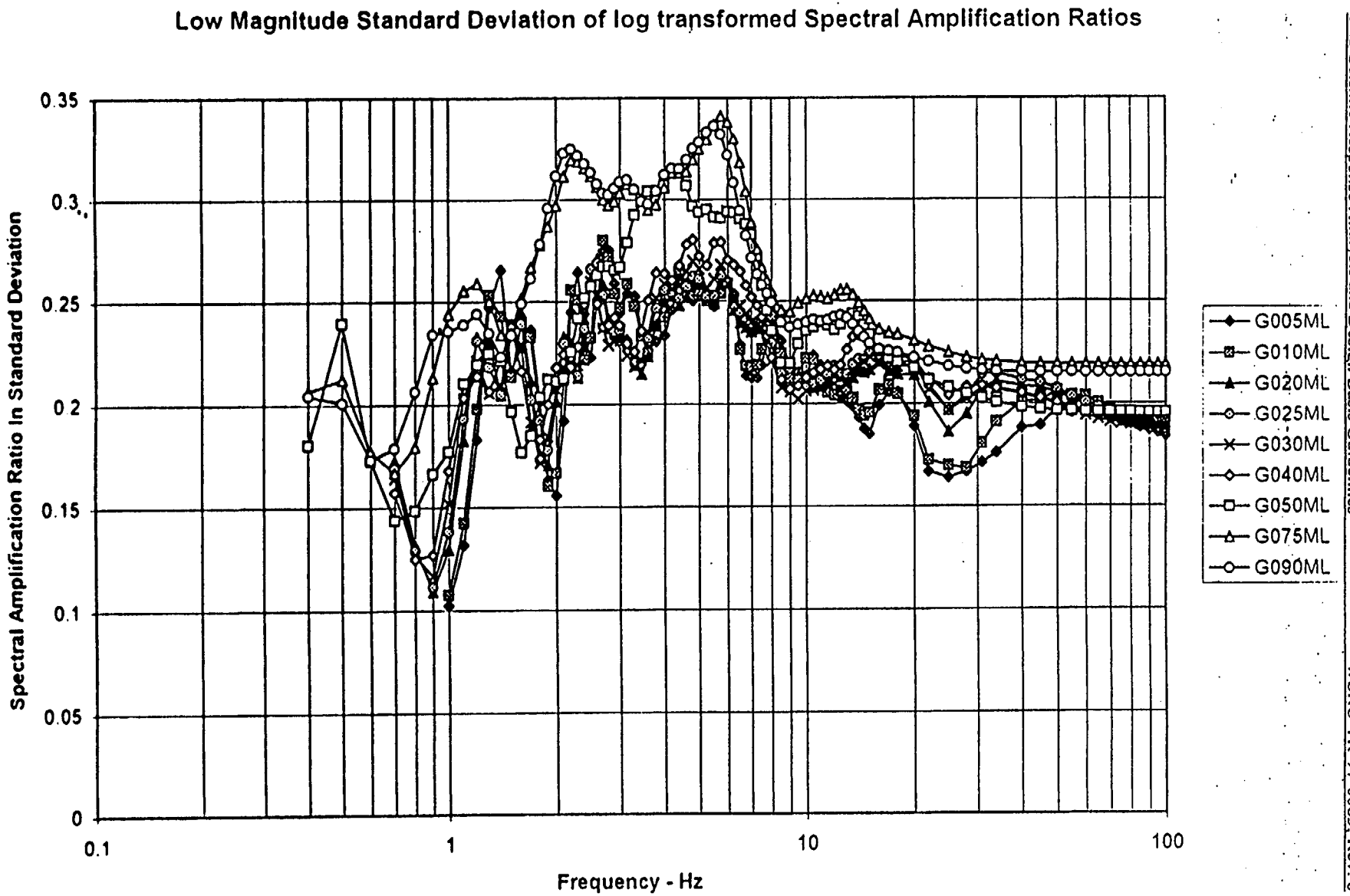

Figure 8.2 (c) - Logarithmic standard deviation of 5 % damped spectral amplification spectra for low magnitude soil category 2 response for crystalline rock. Corresponding bedrock peak ground acceleration (PGA) ranges from 0.05g (G005ML) to 0.75g (G075ML).

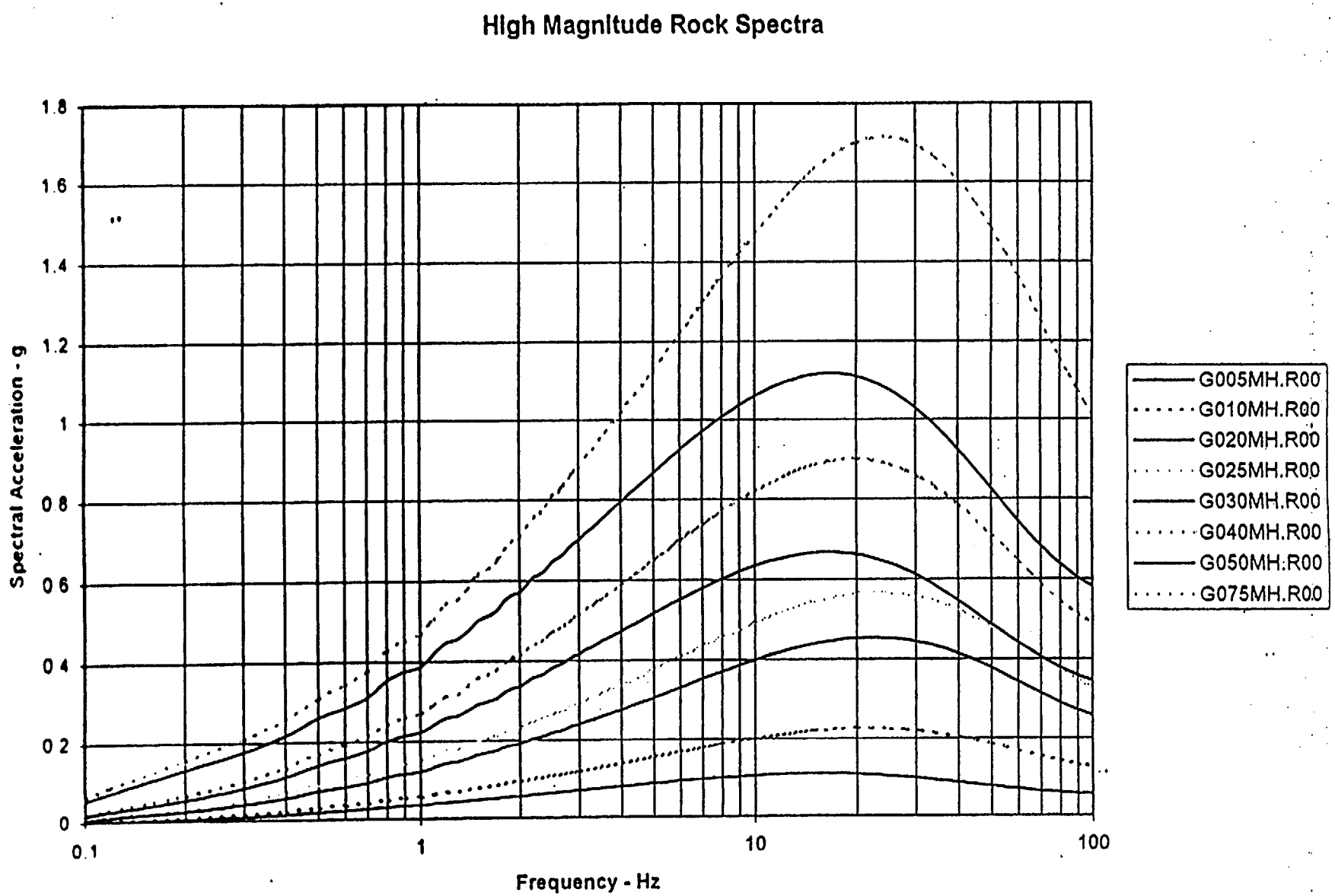

Figure 8 3 (a) - 5 % damped amplification response spectra for high magnitude crystalline bedrock control motions used to generate soil category 2 response. Bedrock peak ground acceleration (PGA) ranges from 0.05g (G005MH.R00) to 0.75g (G075MH.R00) (see Table 8.2).

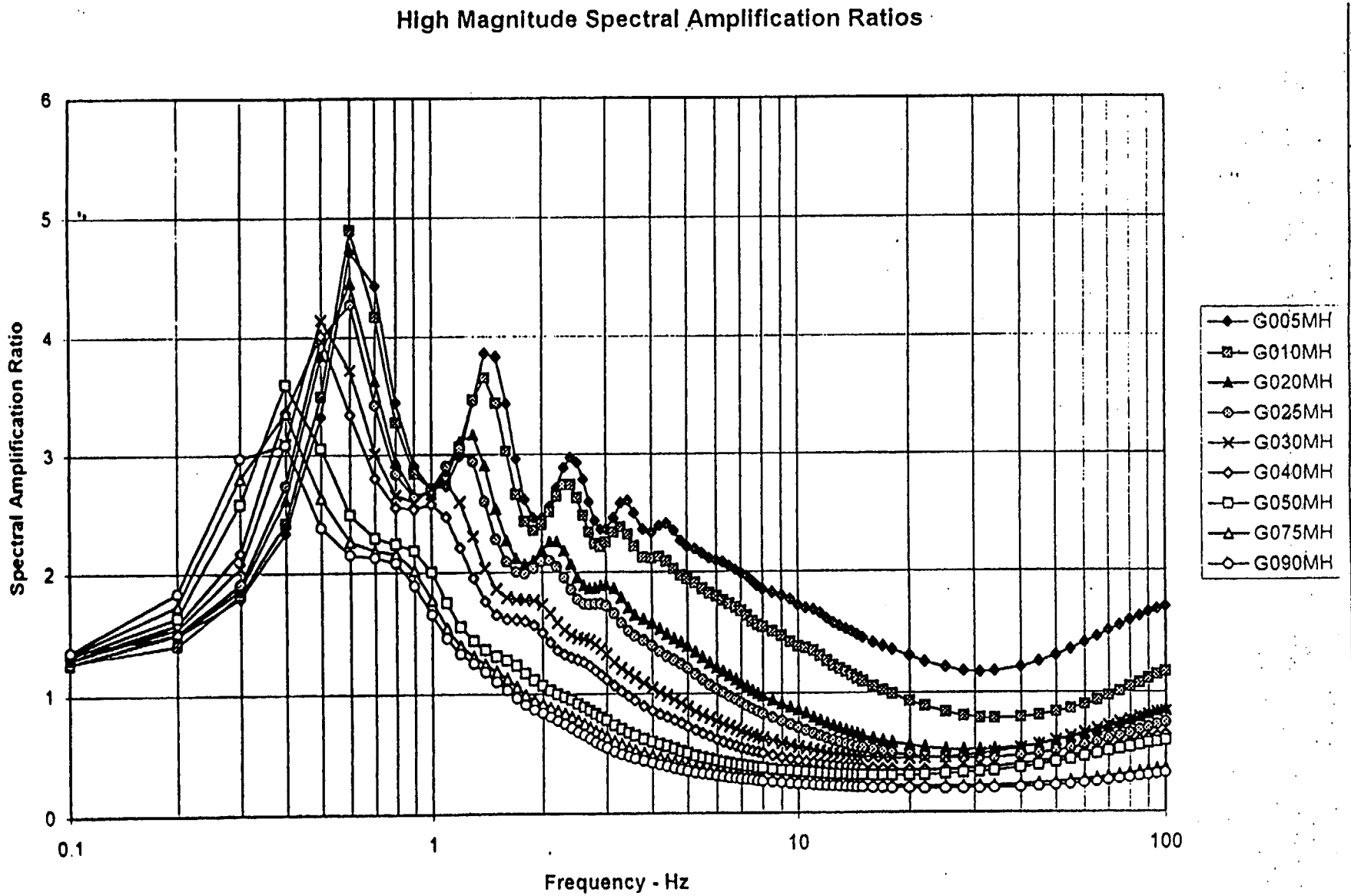

Figure 8.3 (b) - Mean 5 % damped response spectra of high magnitude soil category 2 response for crystalline rock. Corresponding bedrock peak ground acceleration (PGA) ranges from 0.05g (G005MH) to 0.75g (G075MH) (see Table 8.2).

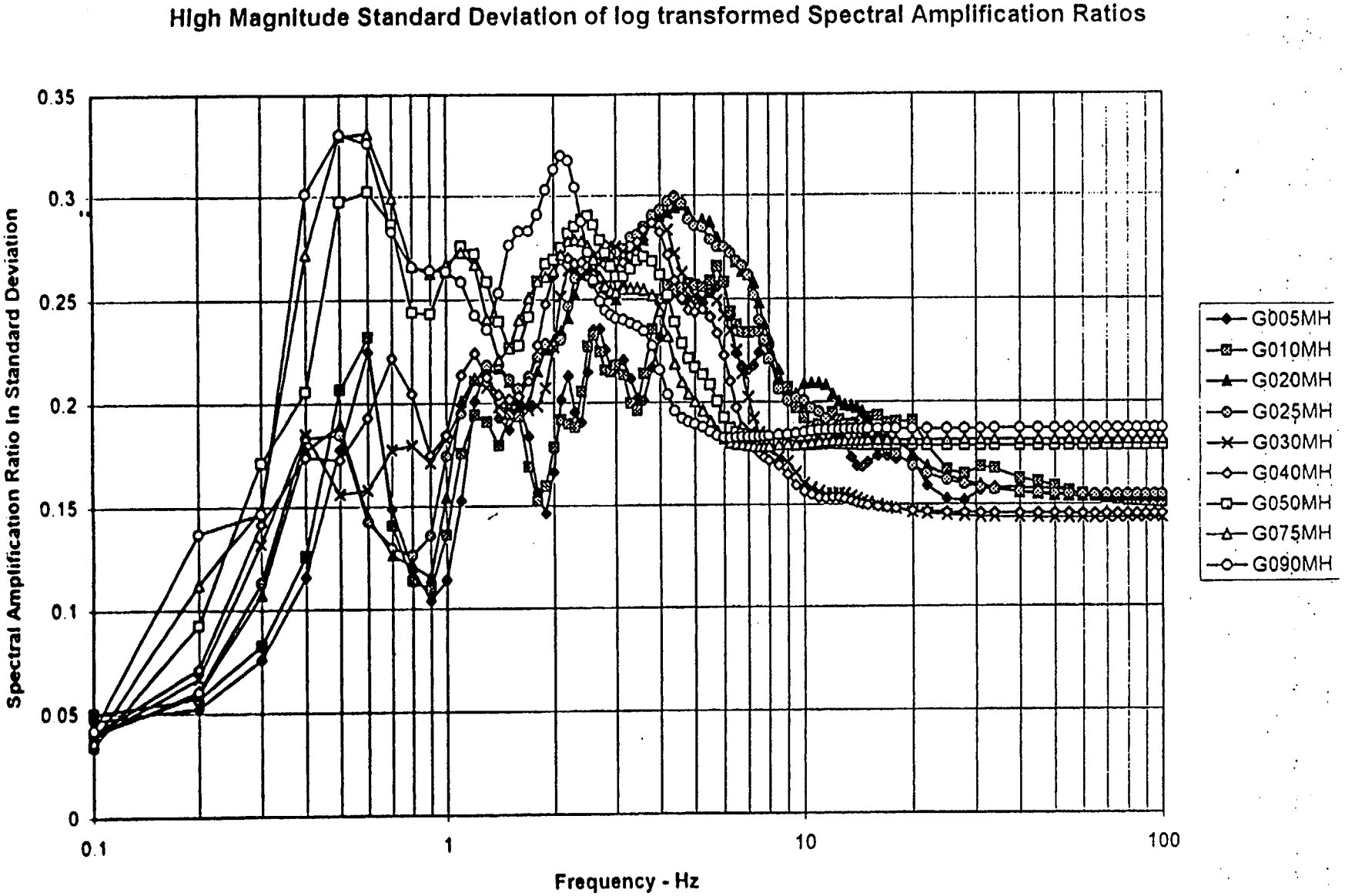

Figure 8.3 (c) - Logarithmic standard deviation of 5 % damped response spectra of high magnitude soil category 2 response for crystalline rock. Corresponding bedrock peak ground acceleration (PGA) ranges from 0.05g (G005MH) to 0.75g (G075MH) (see Table 8.2).

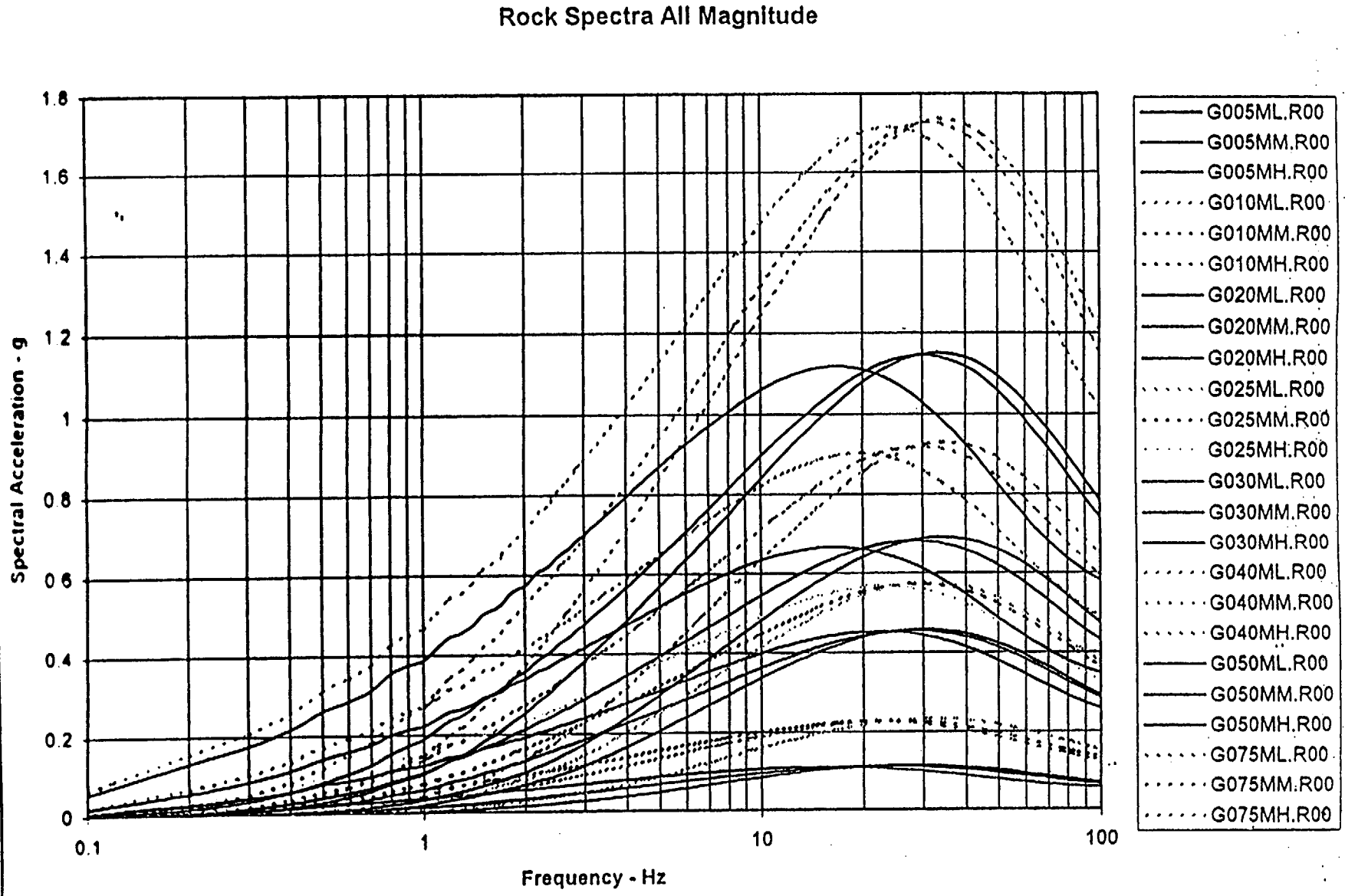

Figure 8.4 - Comparison of high, medium, and low magnitude 5 % damped response spectra of crystalline bedrock control motions used to generate soil category 2 response. Bedrock peak ground acceleration (PGA) ranging from 0.05g (G005M*.R00) to 0.75g (G075M*.R00) (see Table 8.2).

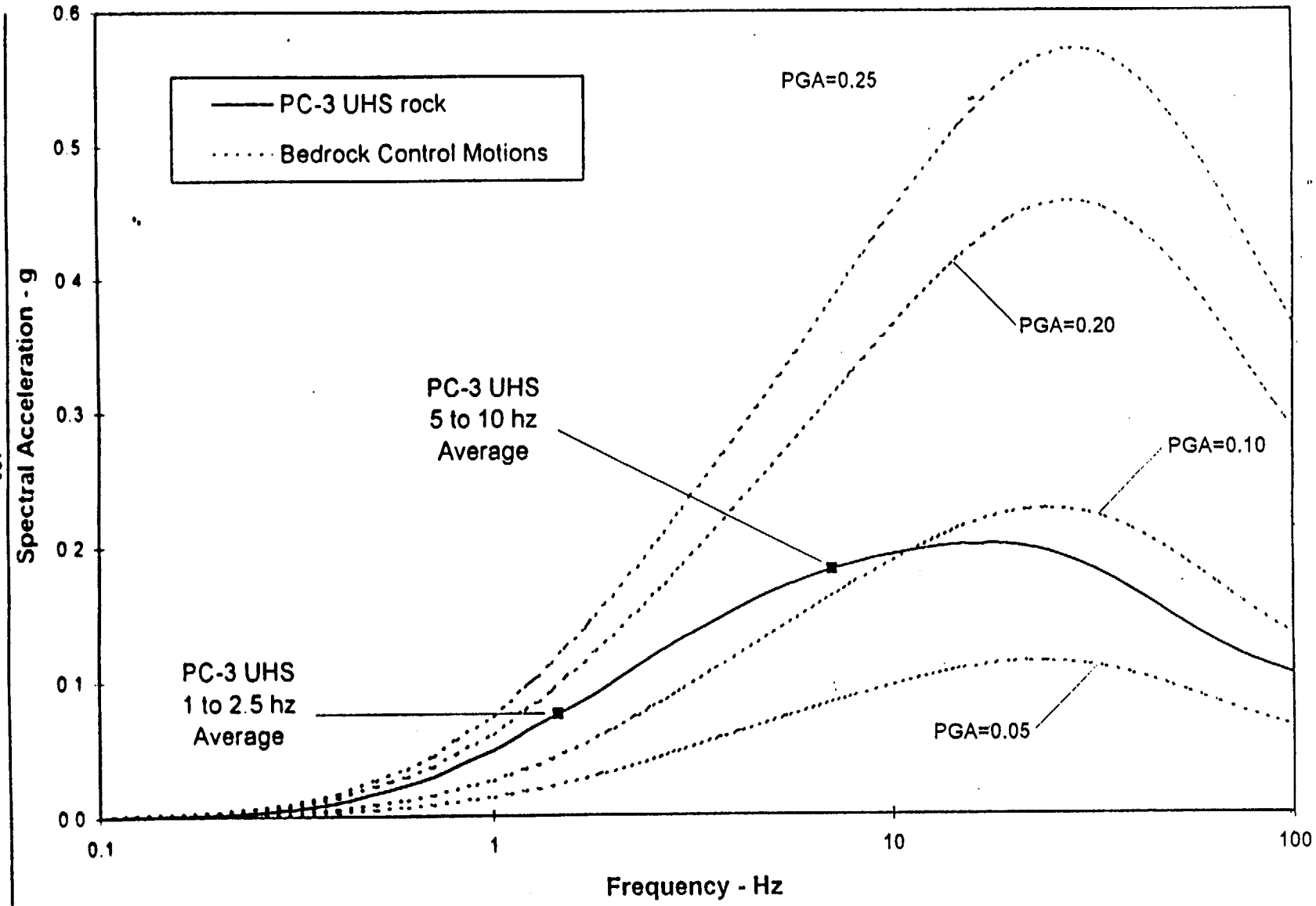

Figure 8.5 - Illustration of PC3 bedrock UHS (solid line) and four bedrock control motion spectra derived from M-bar that bracket the PC3 spectra (dashed lines, PGA=0.05, 0.10, 0.20, 0.25). The computed 1-2.5 and 5-10 Hz spectral averages of the bedrock UHS are identified by the symbols. The SAFs corresponding to bedrock control motions PGA=0.1 and PGA=0.2 are used (interpolated) to define the soil response in this case.

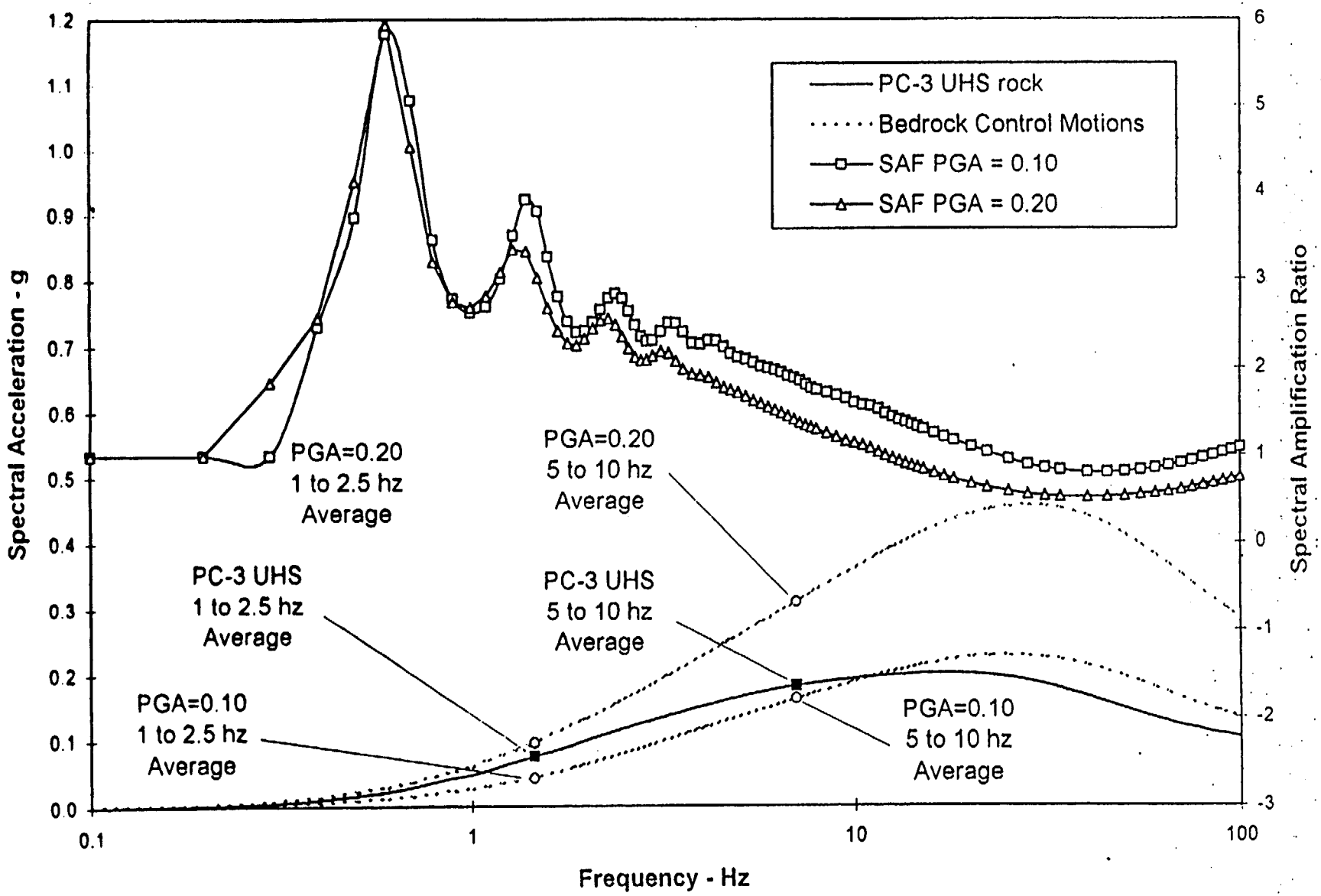

Figure 8.6 - Illustration of PC3 bedrock UHS (solid line) and two control motion spectra used to interpolate the two corresponding SAFs (solid lines with symbols-scale on right vertical axis). Note the relative position of the 1-2.5 and 5-10 Hz spectral averages between the control motion spectra and the UHS.

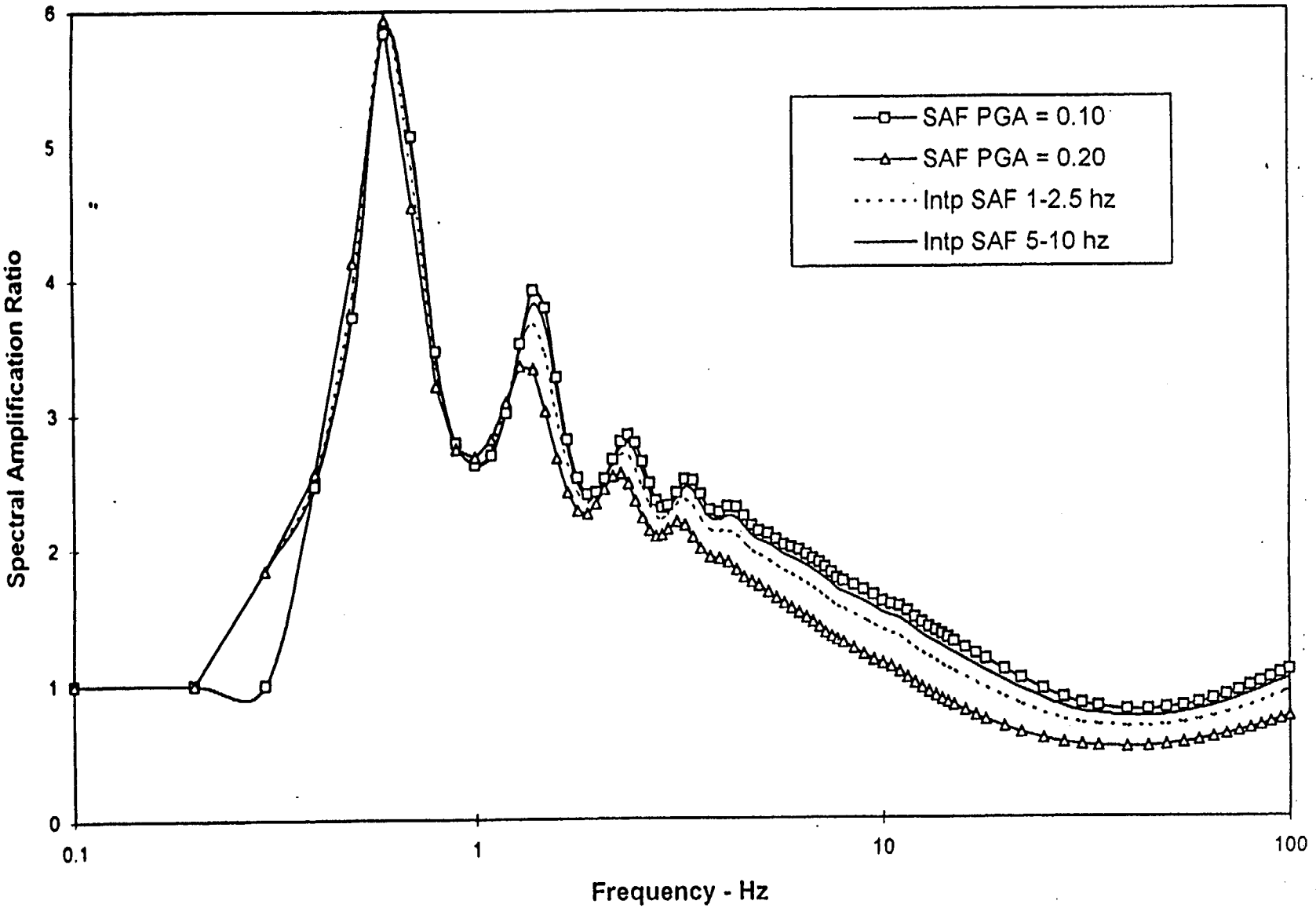

Figure 8.7 - Comparison of the two SAFs of Figure 8.6 and the interpolated SAFs for the 1-2.5 and 5-10 Hz spectral averages (solid and dashed lines).

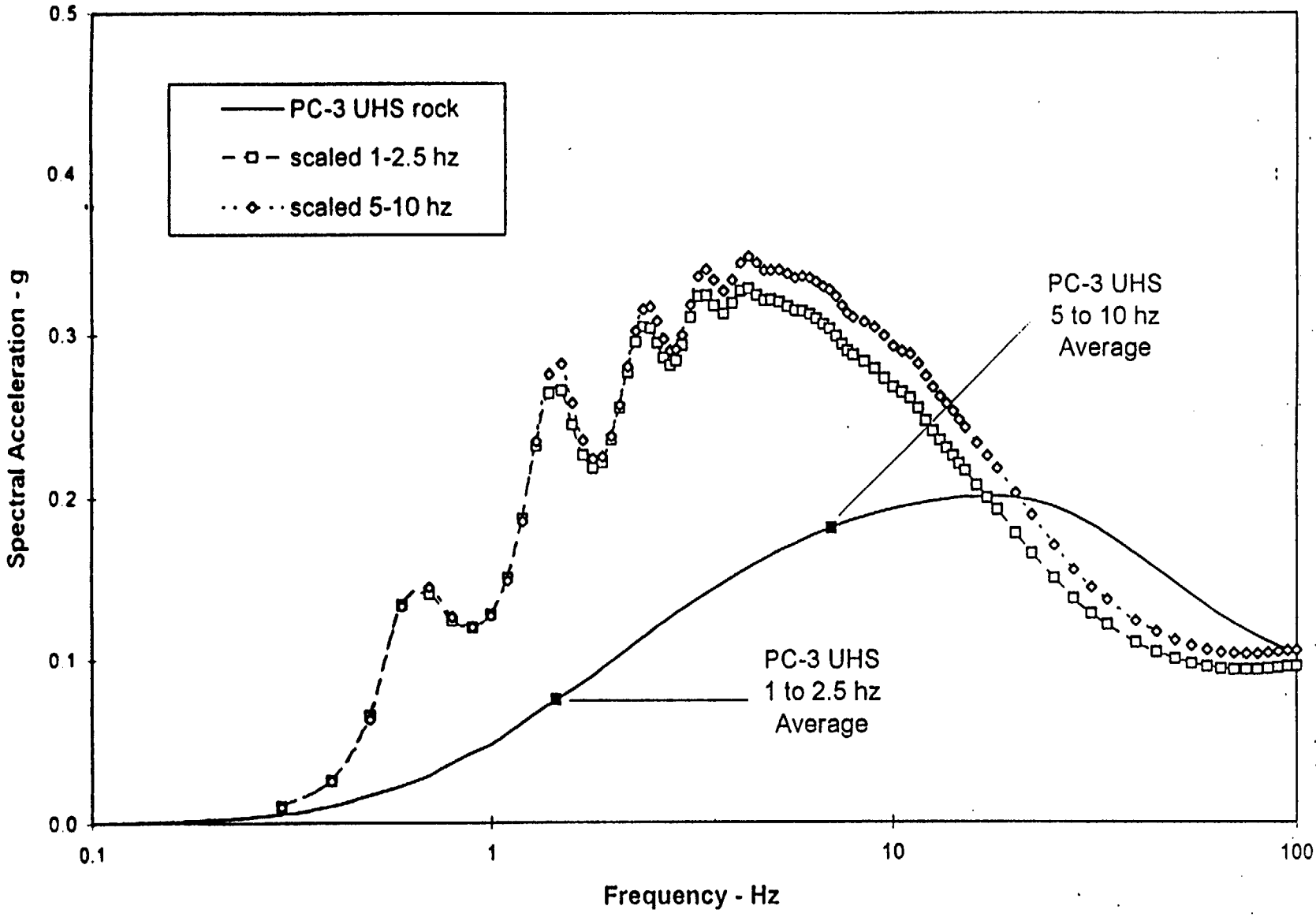

Figure 8.8 - Soil response for the 1-2.5 and 5-10 Hz spectral averages (SAF(f)*UHS(f) = SOIL RESPONSE(f)).

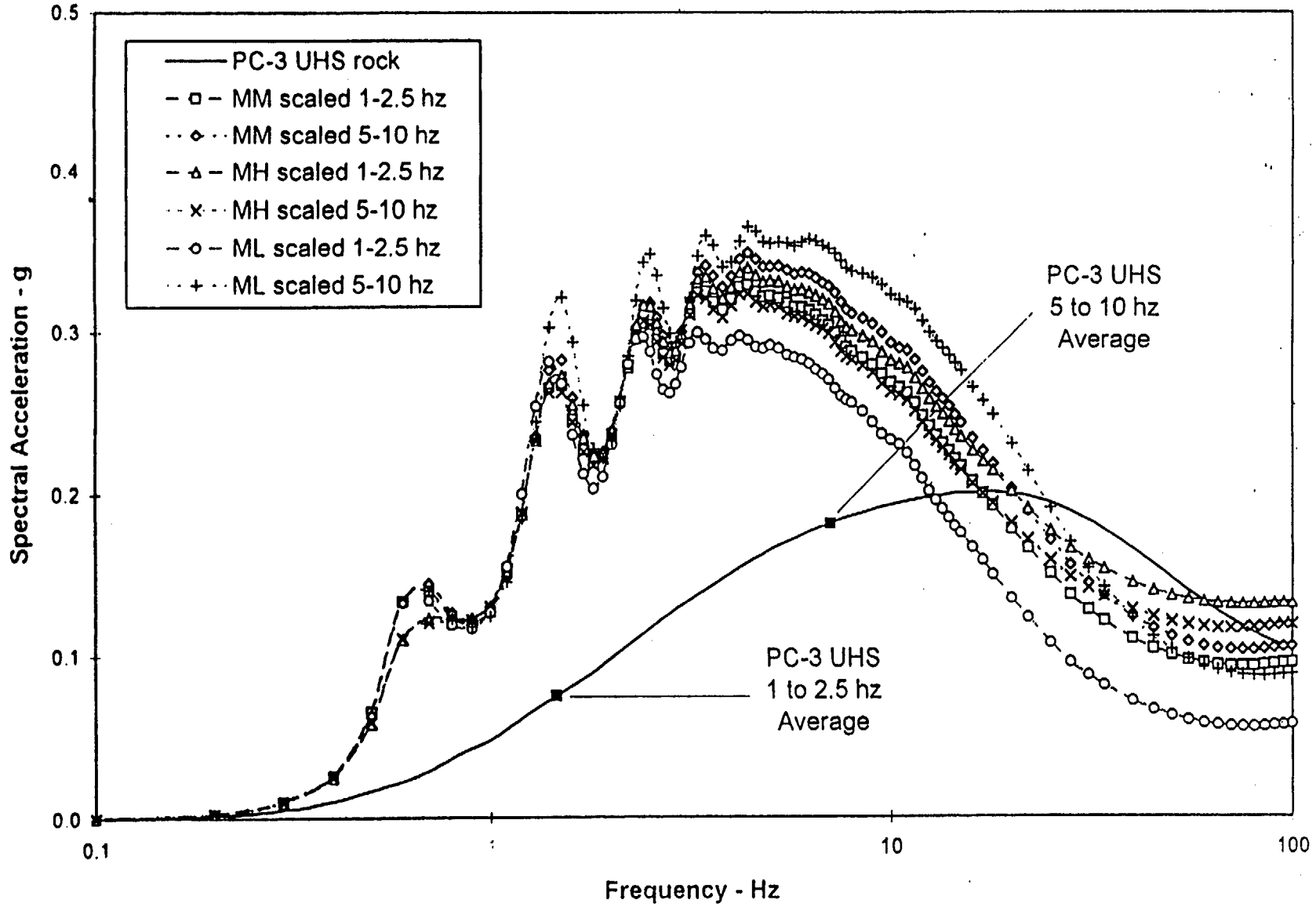

Figure 8.9 - Soil response for ML, MM, MH shown with broadened UHS.

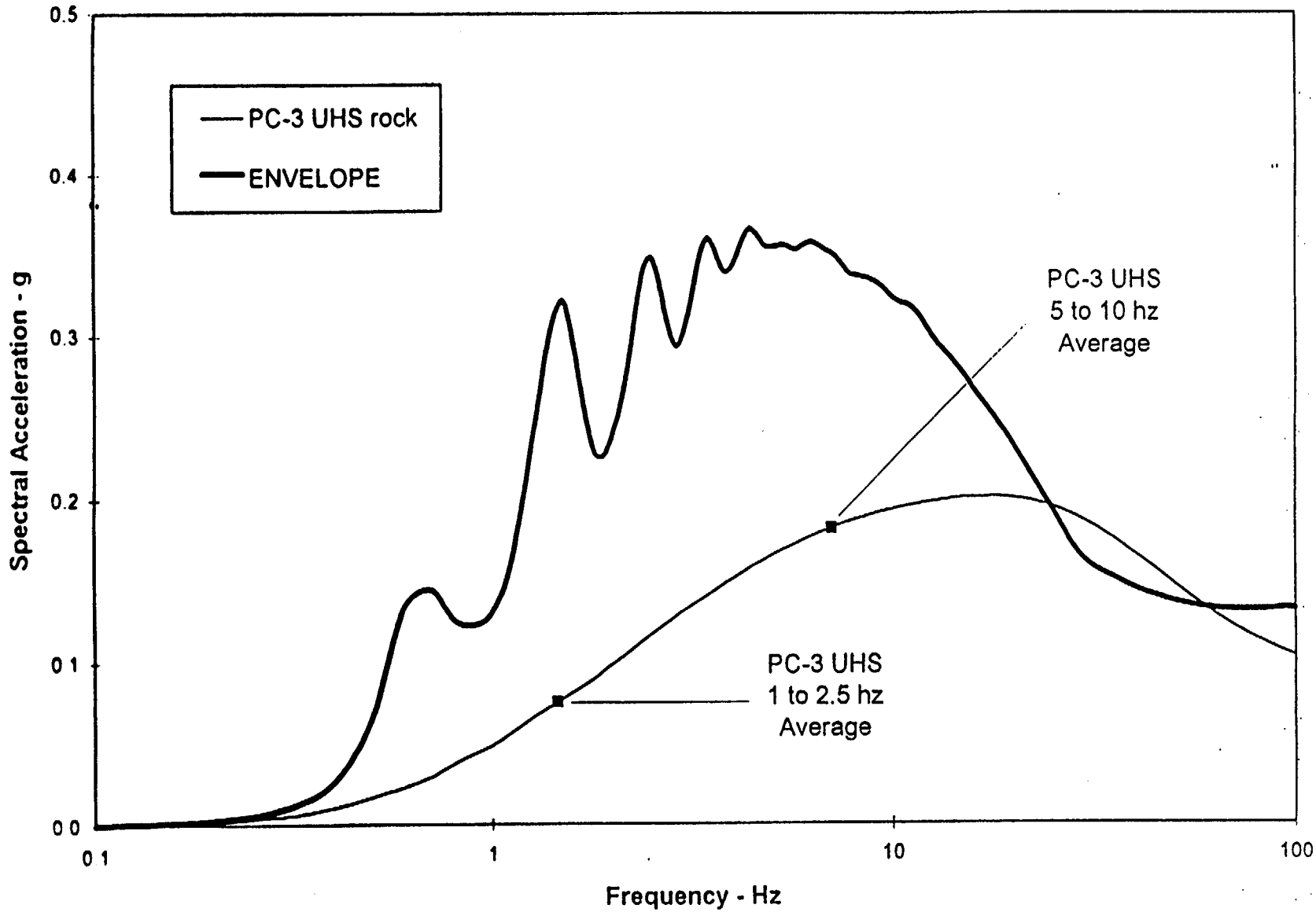

Figure 8.10 - The envelope of the responses shown in Figure 8.9.

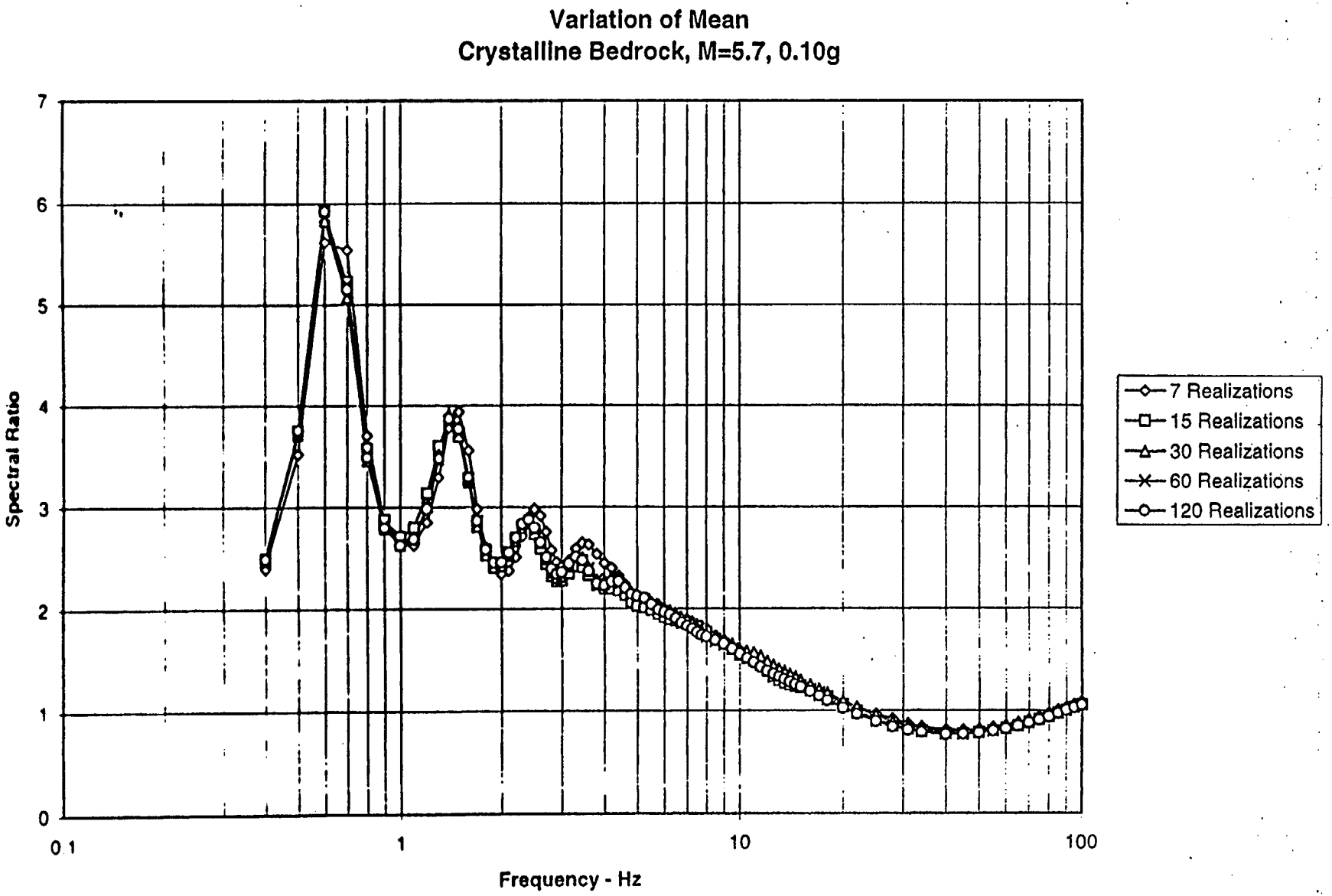

Figure 8.11 - Sensitivity of the median SAF to the selected number of soil velocity profile randomizations. SAFs were computed using 7, 15, 30, 60, and 120 velocity profiles for M-bar and 10%g for soil category 2.

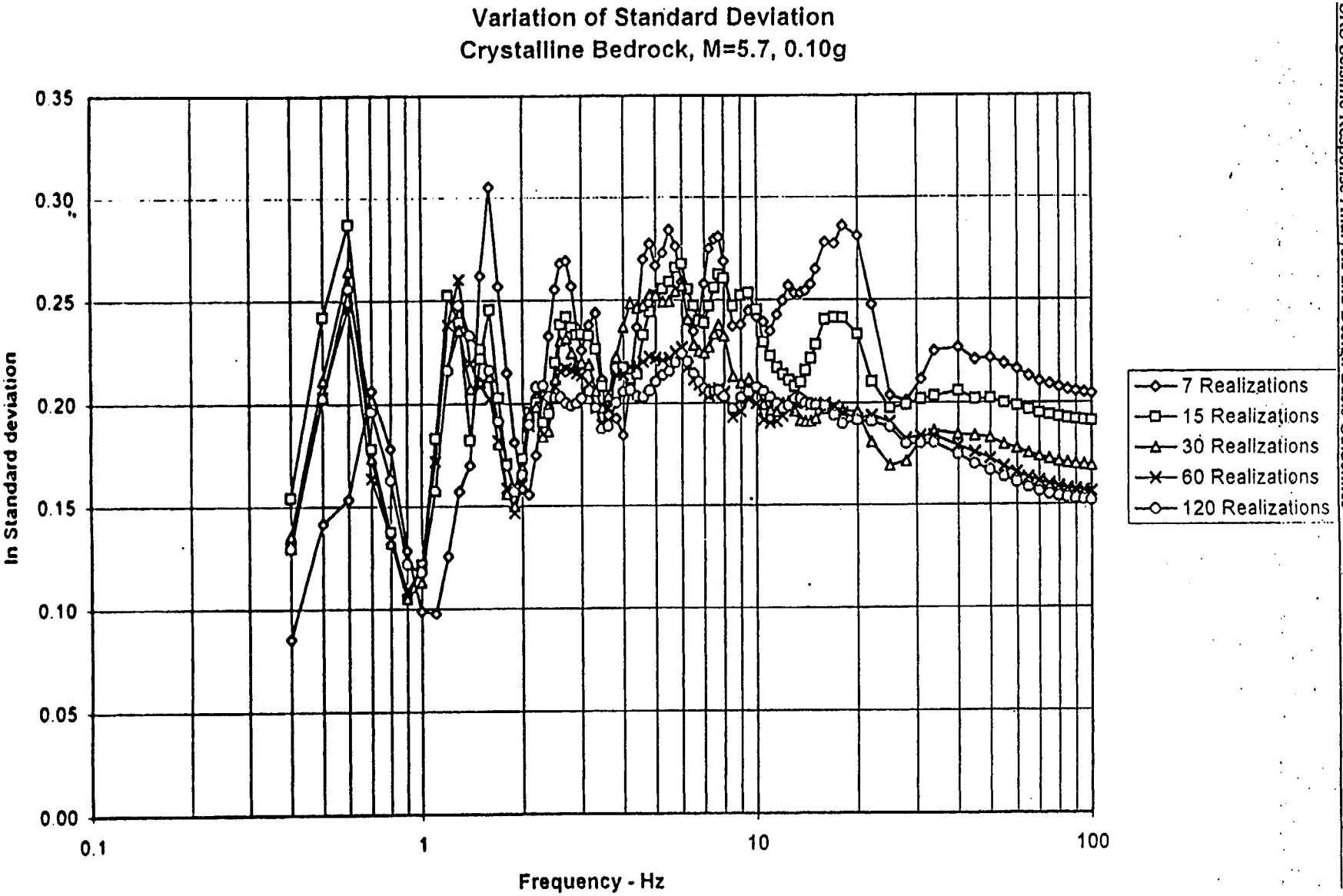

Figure 8.12 - Sensitivity of the SAF sigma to the selected number of soil velocity profile randomizations. SAFs were computed using 7, 15, 30, 60, and 120 velocity profiles for M-bar and 10%g for soil category 2.

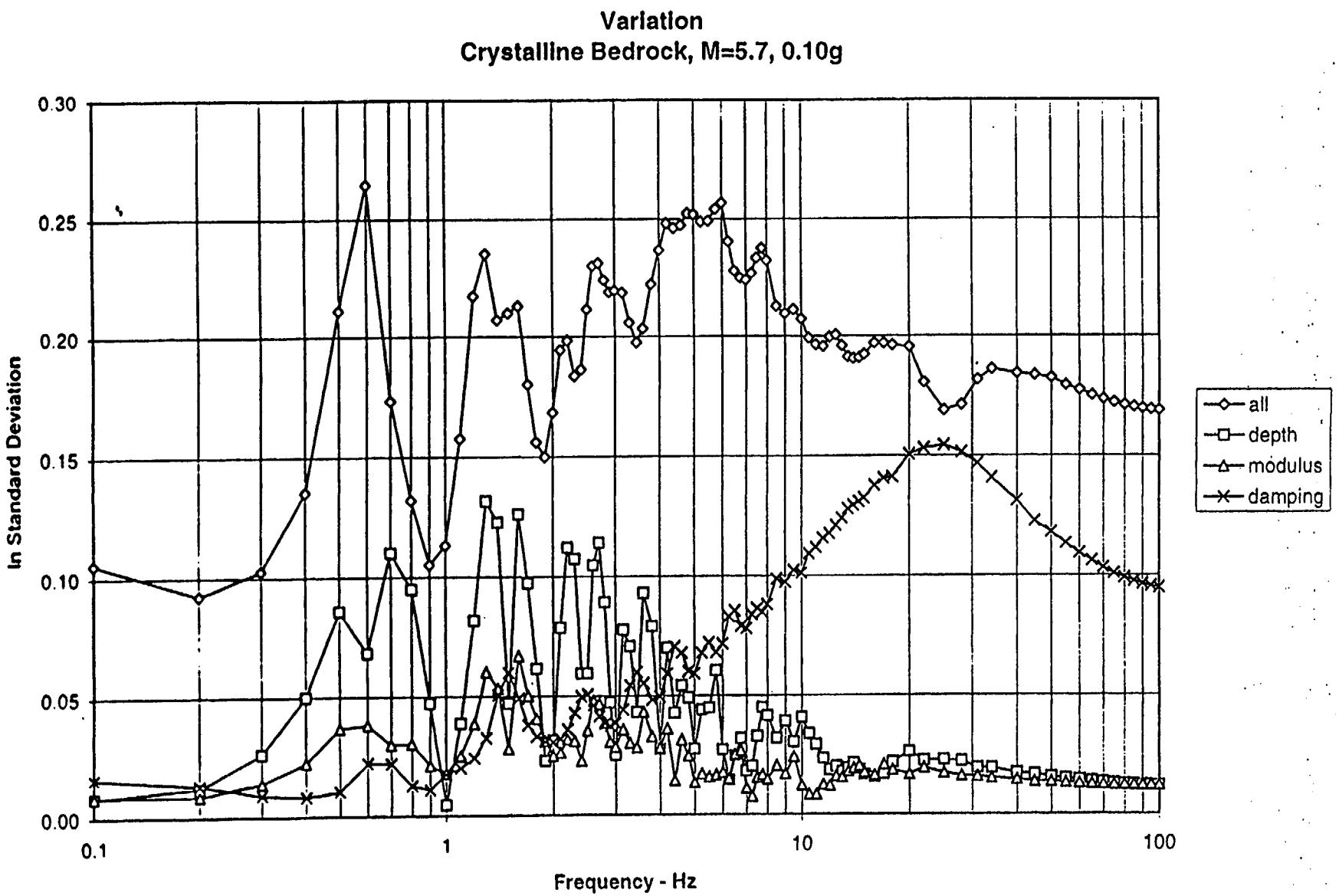

Figure 8.13 - Composition of SAF sigma by comparison of total sigma to individual randomizations of soil column depth, modulus reduction, and damping.

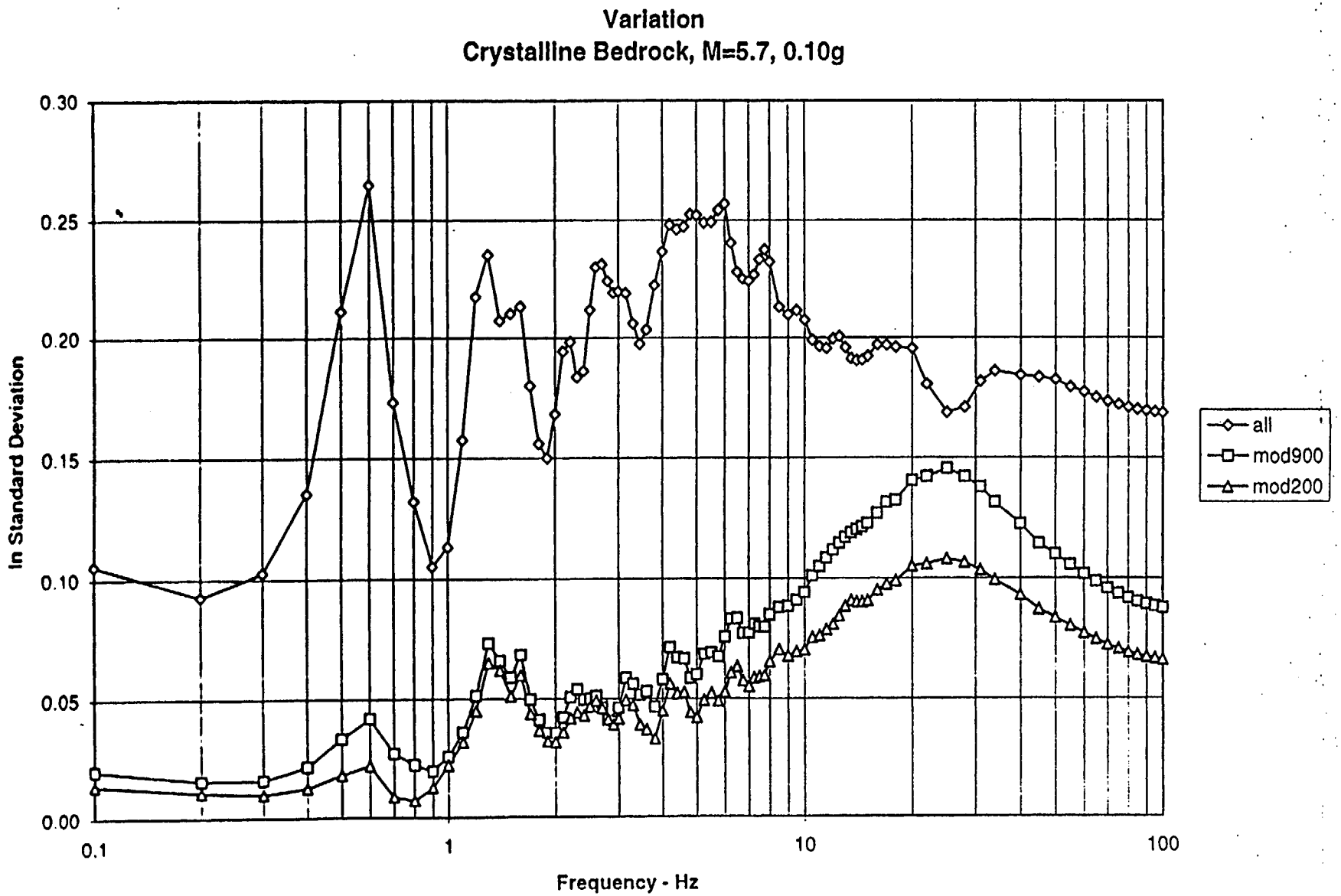

Figure 8.14 - Composition of SAF sigma by comparison of total sigma to individual randomizations of modulus and damping, modulus and damping in upper 200 ft.

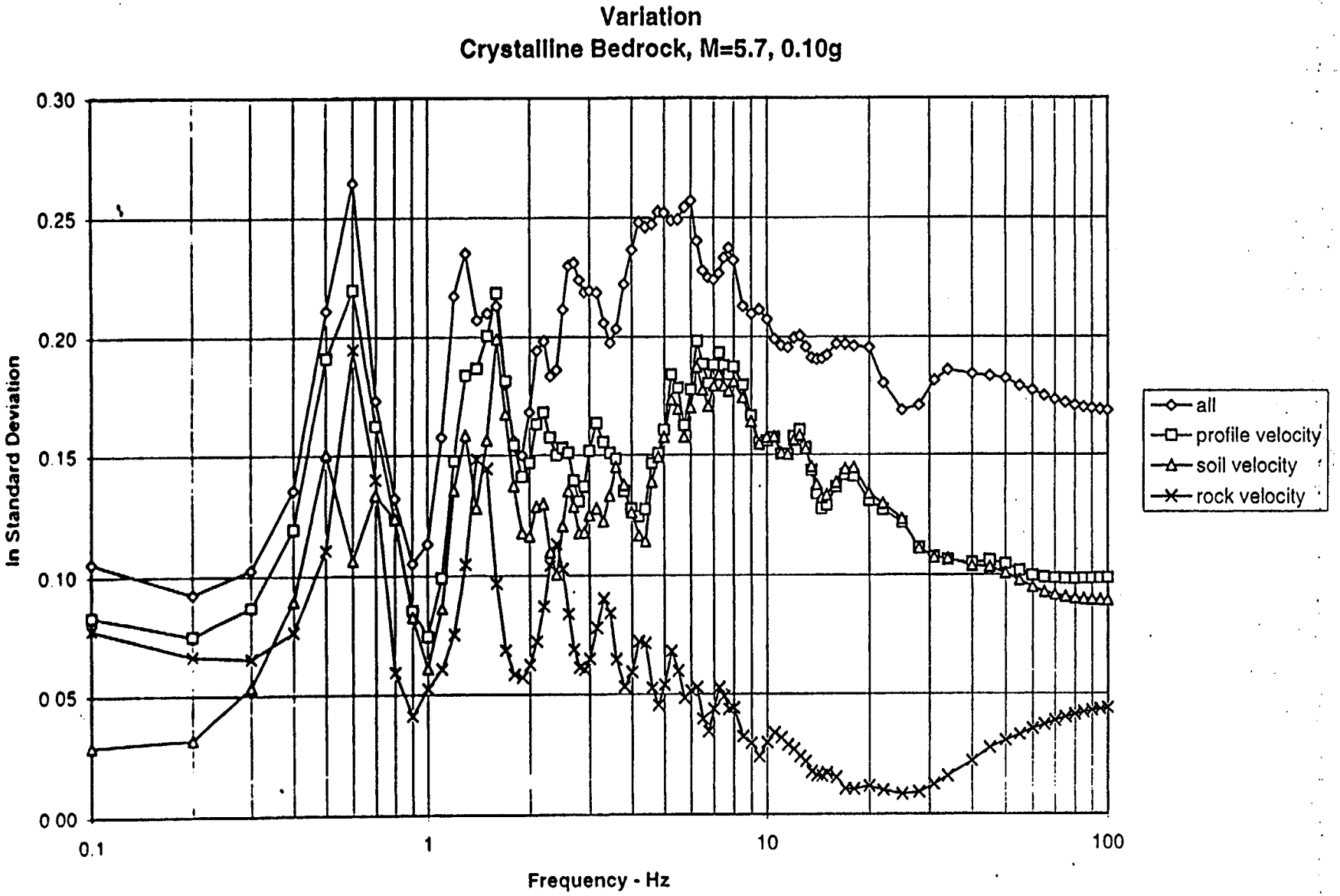

Figure 8.15 - Composition of SAF sigma by comparison of total sigma to individual randomizations of rock velocity, soil velocity, and rock and soil velocity.

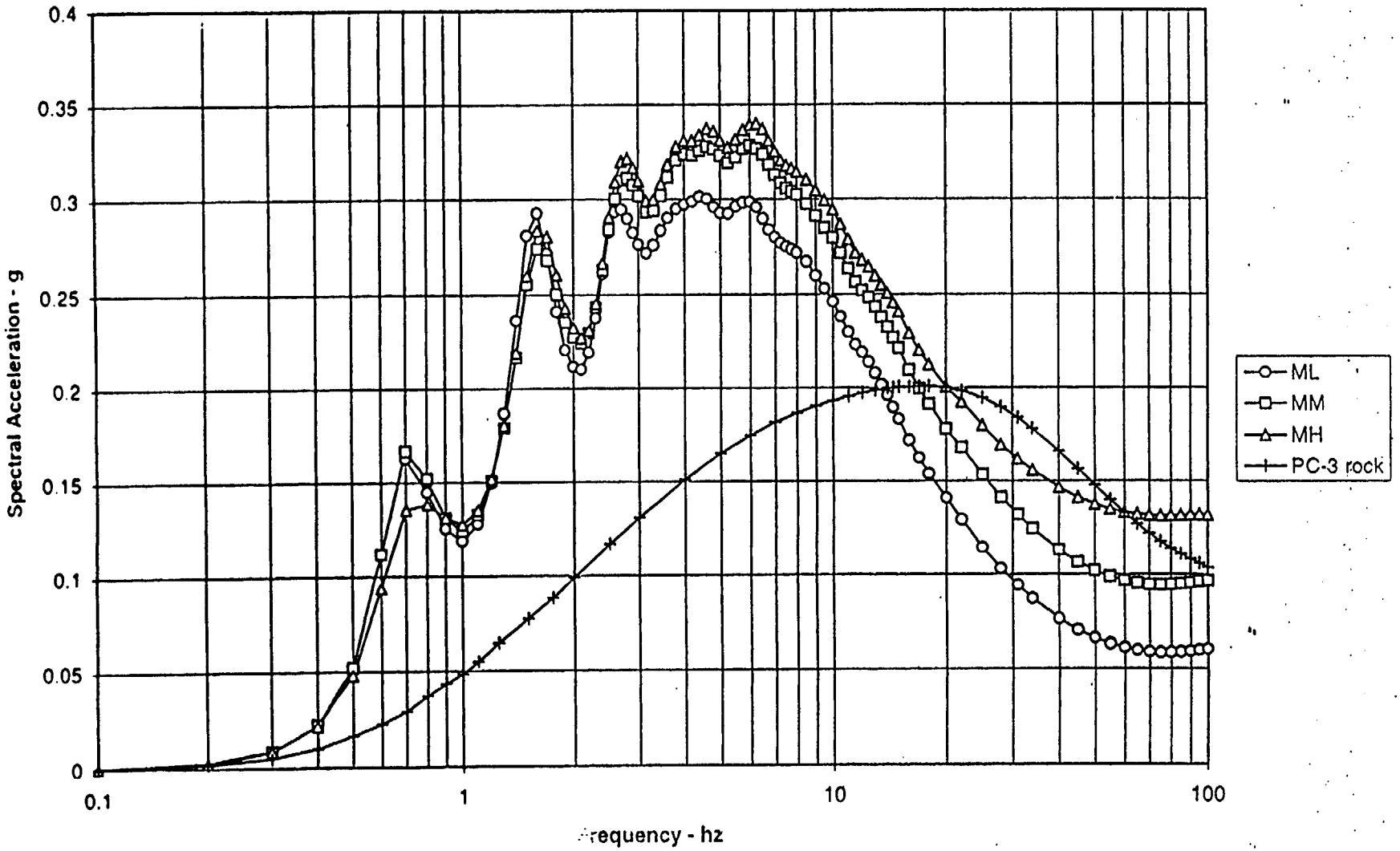

Figure 9.1(a) - Performance Category 3 5% d[illegible]ed soil response spectra from 1-2.5 Hz mean based scaling of broadened bedrock UHS (PC-3 rock). Response shown using low (ML), medium (MM), and high (MH) magnitude scaling. Soil category 1 (600-800 ft) over crystalline bedrock.

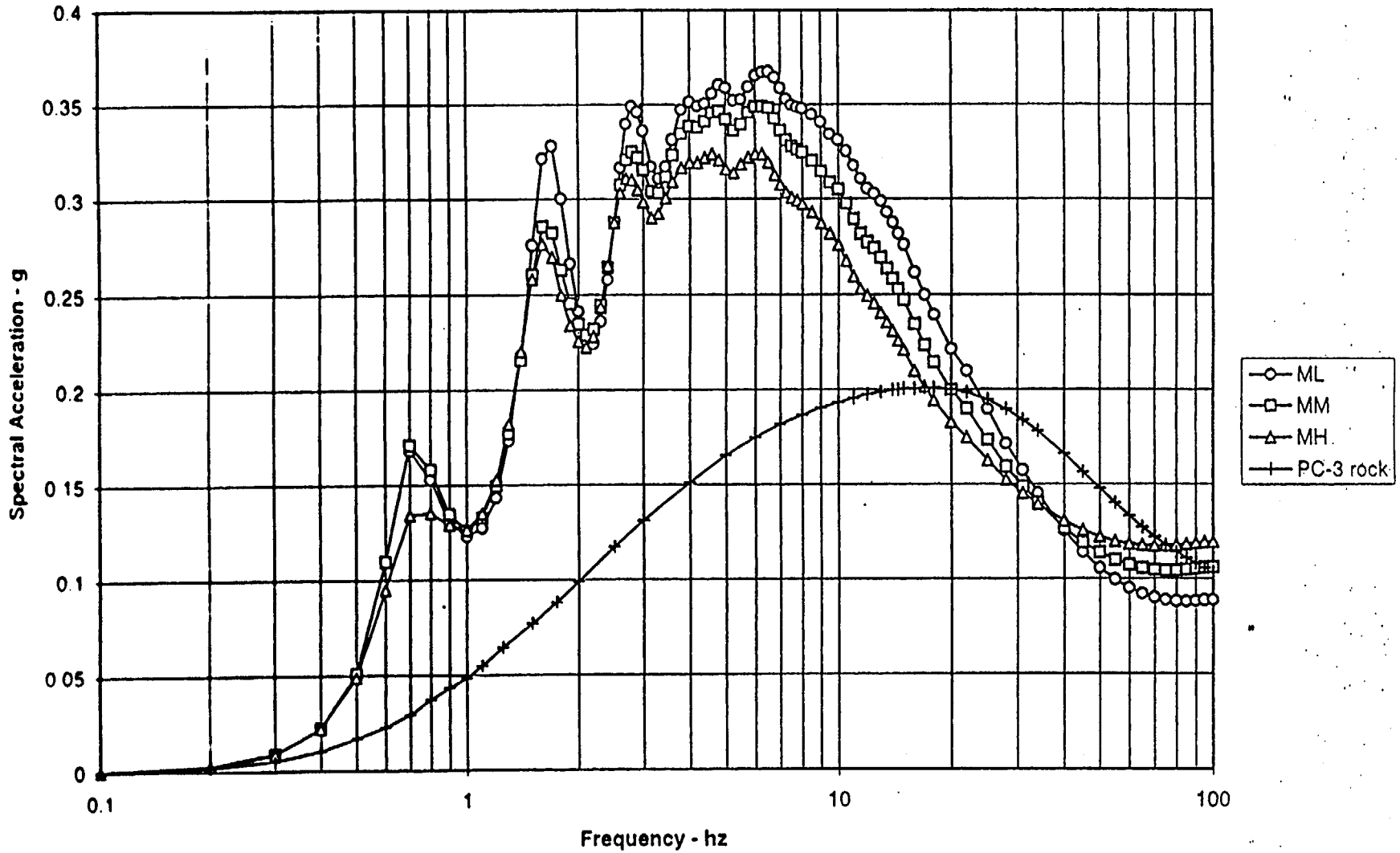

Figure 9.1(b) - Performance Category 3 5% damped soil response spectra from 5-10 Hz mean based scaling of broadened bedrock UHS (PC-3 rock). Response shown using low (ML), medium (MM), and high (MH) magnitude scaling. Soil category 1 over crystalline bedrock.

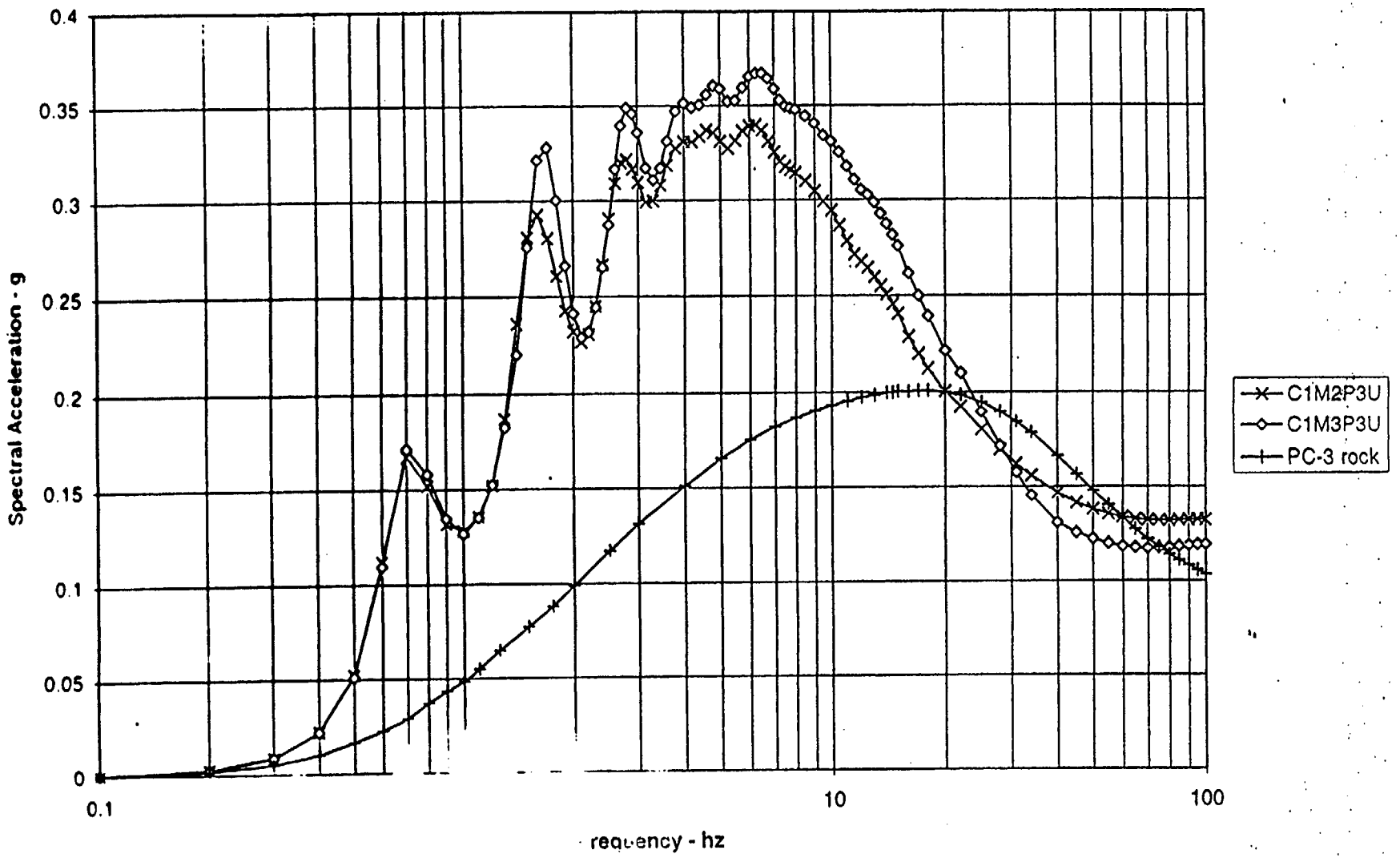

Figure 9.1(c) - Enveloping of Performance ... by 3 ... damped soil response spectra from 1-2.5 Hz (C1M2P3U) and 5-10 Hz (C1M3P3U) mean based scaling of ... bedrock UHS (PC-3 rock). Envelopes of low, medium, and high magnitude scaled spectra are shown. Soil category 1 over crystalline bedrock.

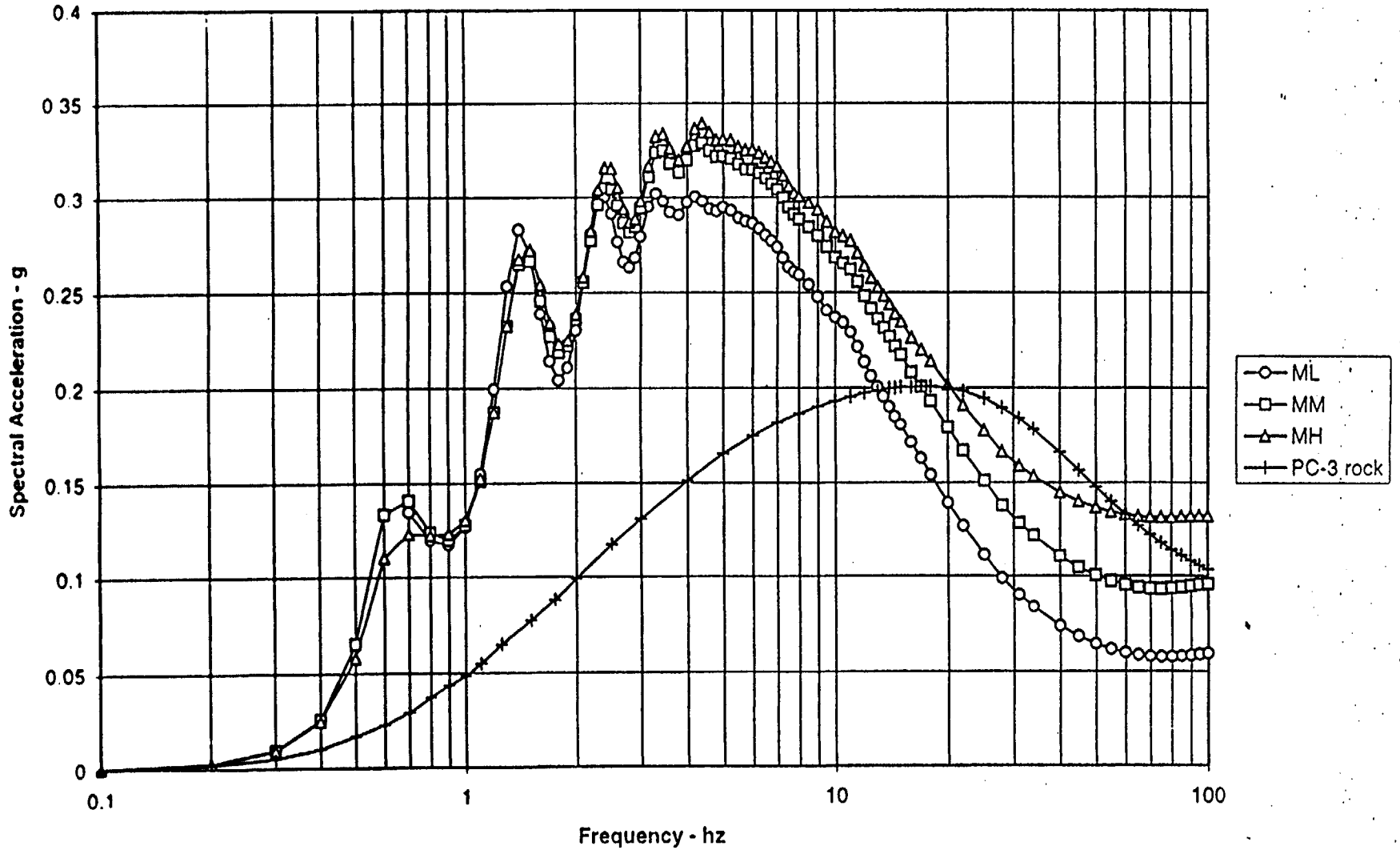

Figure 9.2(a) - Performance Category 3 5% damped soil response spectra from 1-2.5 Hz mean based scaling of broadened bedrock UHS (PC-3 rock). Response shown using low (ML), medium (MM), and high (MH) magnitude scaling. Soil category 2 over crystalline bedrock.

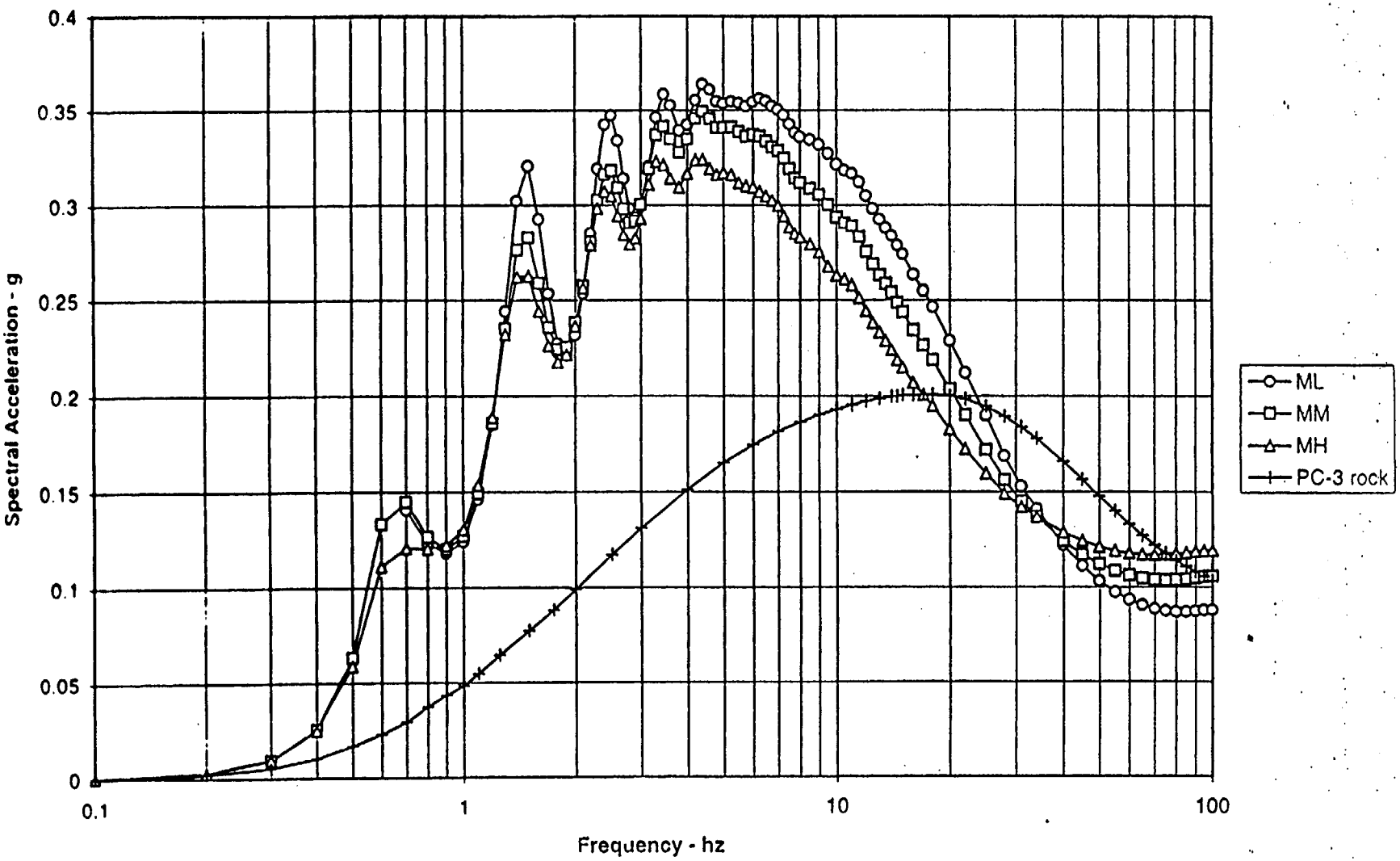

Figure 9.2(b) - Performance Category 3 5% damped soil response spectra from 5-10 Hz mean based scaling of broadened bedrock UHS (PC-3 rock). Response shown using low (ML), medium (MM), and high (MH) magnitude scaling. Soil category 2 over crystalline bedrock.

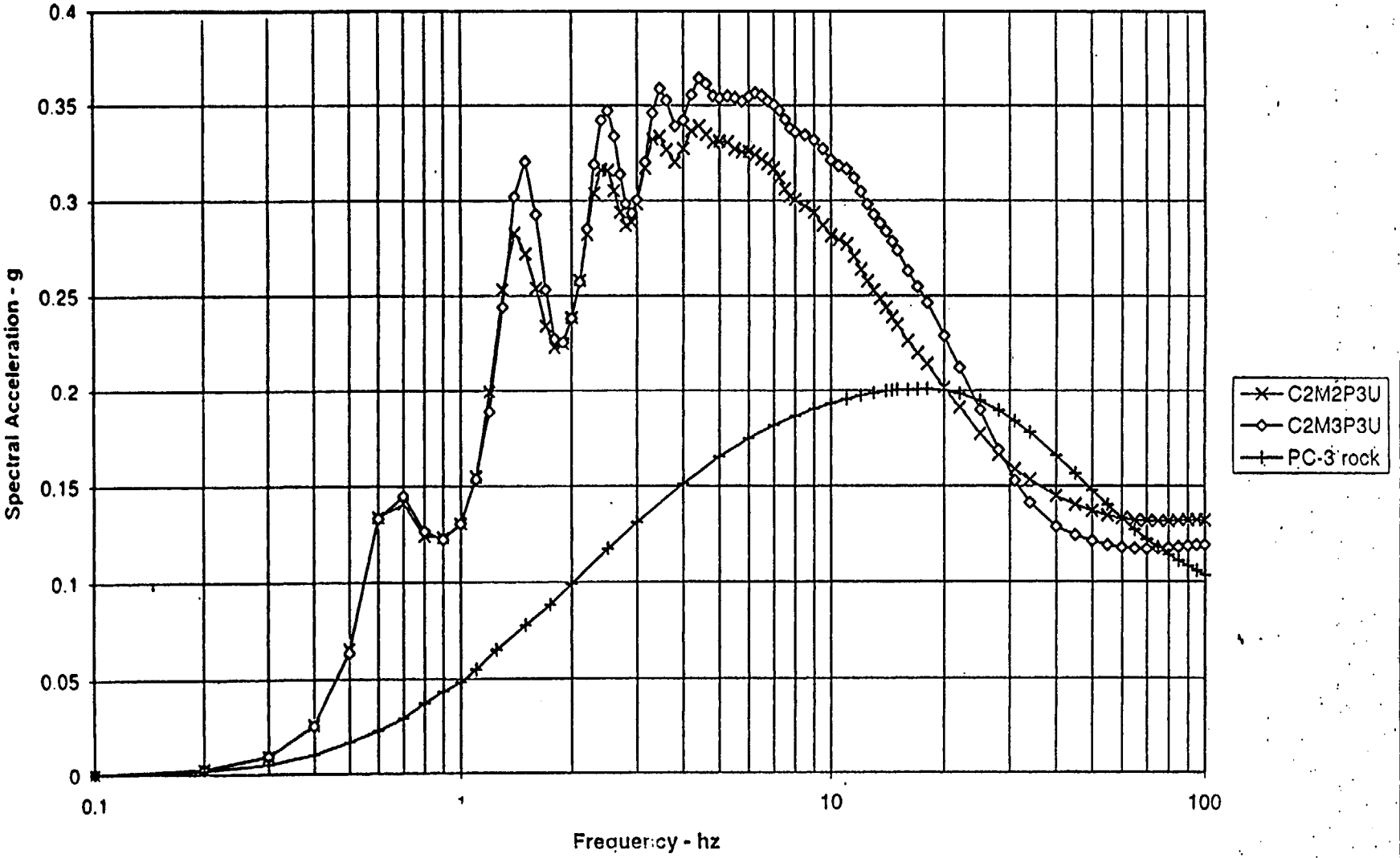

Figure 9.2(c) - Enveloping of Performance Category 3 5% damped soil response spectra from 1-2.5 Hz (C2M2P3U) and 5-10 Hz (C2M3P3U) mean based scaling of broadened bedrock UHS (PC-3 rock). Envelopes of low, medium, and high magnitude scaled spectra are shown. Soil category 2 over crystalline bedrock.

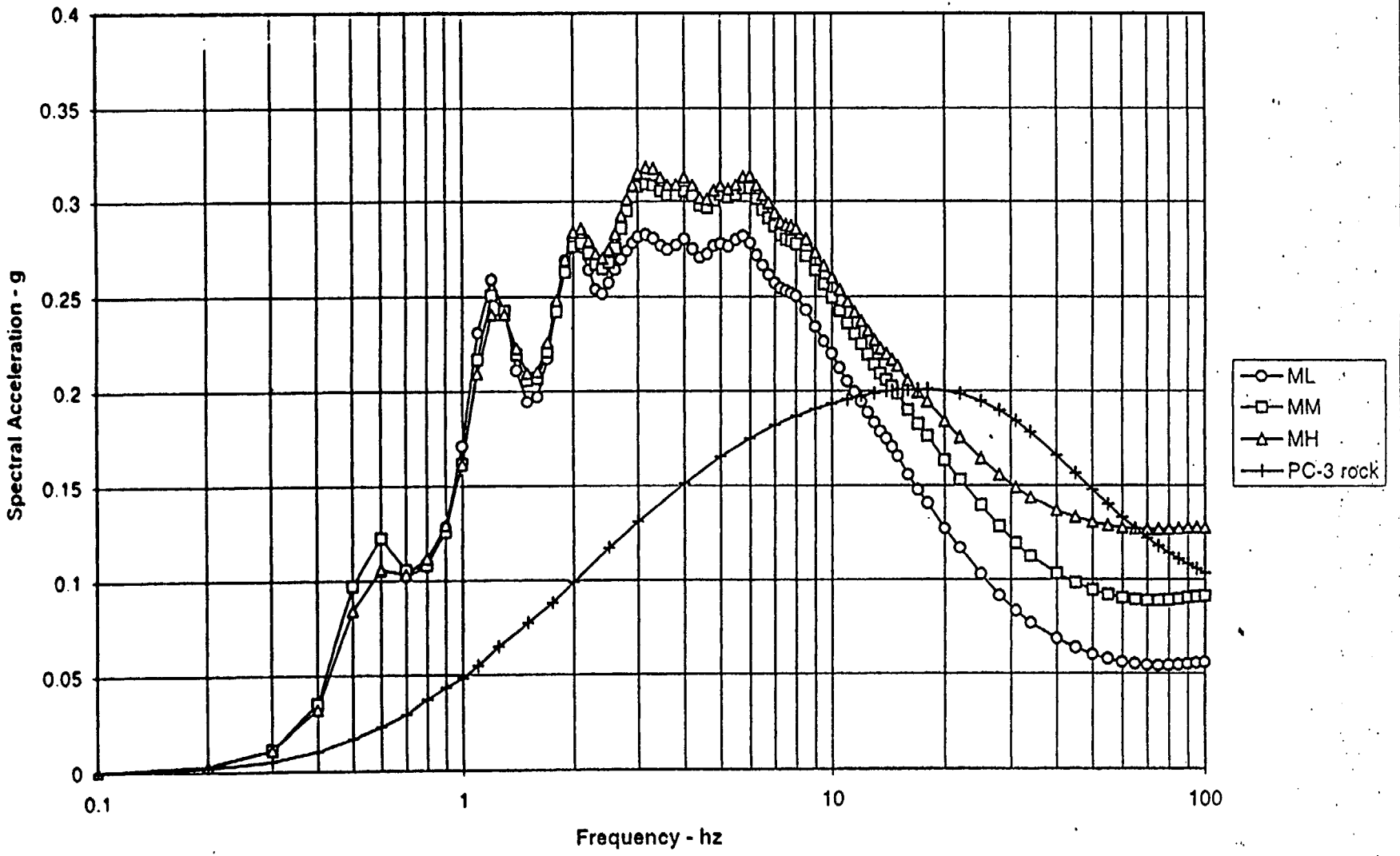

Figure 9.3(a) - Performance Category 3 5% damped soil response spectra from 1-2.5 Hz mean based scaling of broadened bedrock UHS (PC-3 rock). Response shown using low (ML), medium (MM), and high (MH) magnitude scaling. Soil category 3 (1000-1200 ft) over crystalline bedrock.

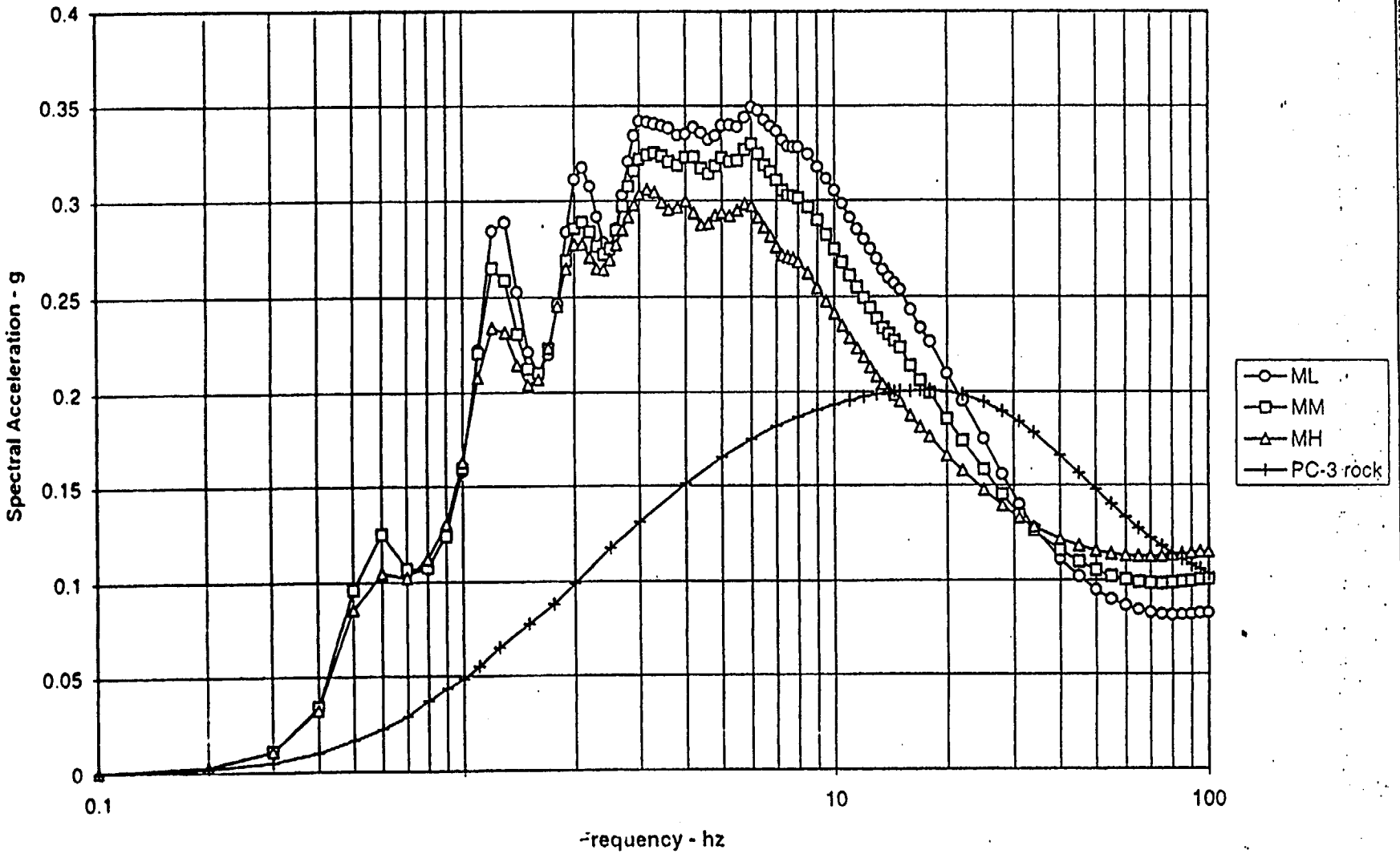

Figure 9.3(b) - Performance Category . 5% ed soil response spectra from 5-10 Hz mean based scaling of broadened bedrock UHS (PC-3 rock). Response shown using low (ML), medium (MM), and high (MH) magnitude scaling. Soil category 3 over crystalline bedrock.

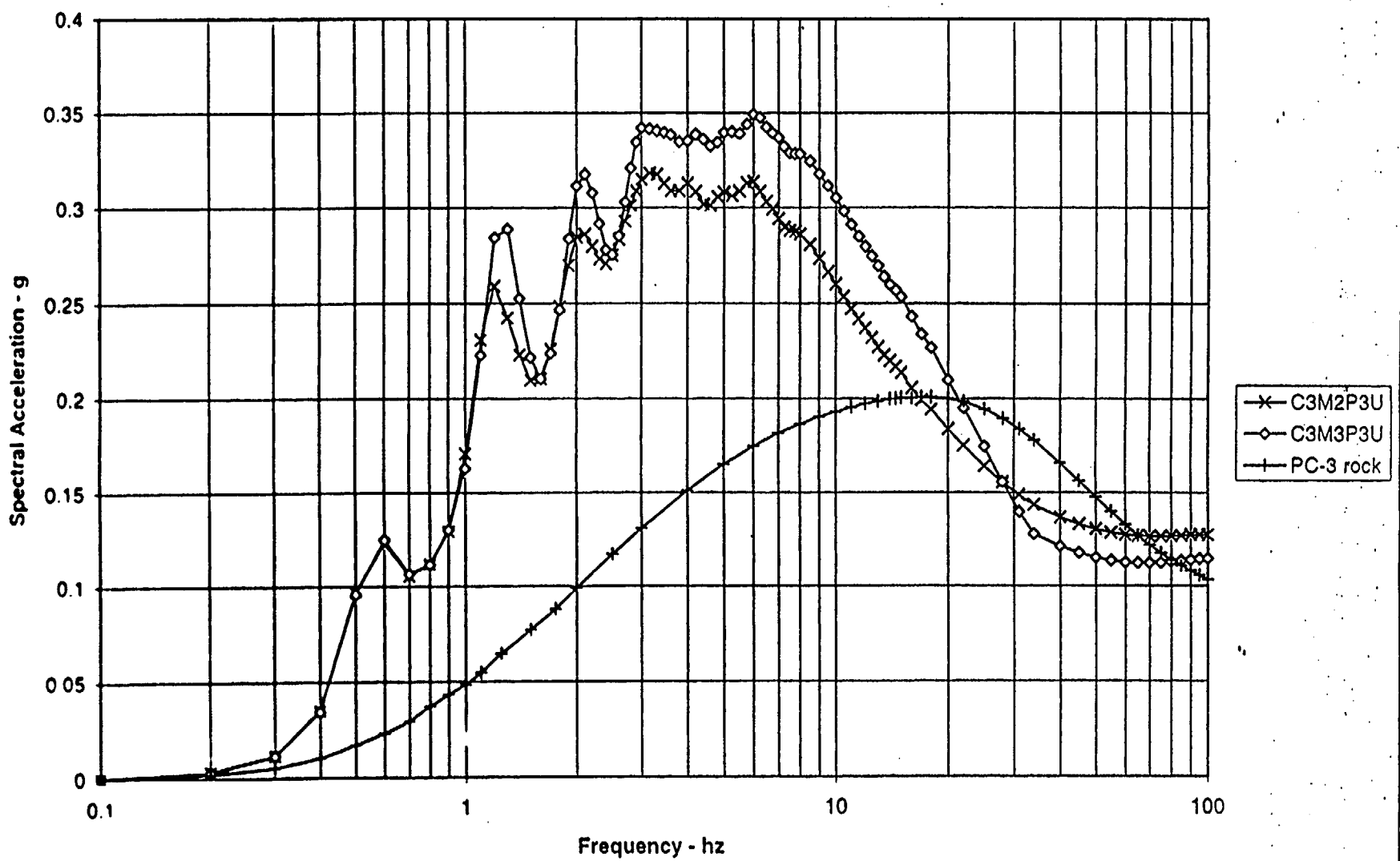

Figure 9 3(c) - Enveloping of Performance Category 3 5% damped soil response spectra from 1-2.5 Hz (C3M2P3U) and 5-10 Hz (C3M3P3U) mean based scaling of broadened bedrock UHS (PC-3 rock). Envelopes of low, medium, and high magnitude scaled spectra are shown. Soil category 3 over crystalline bedrock.

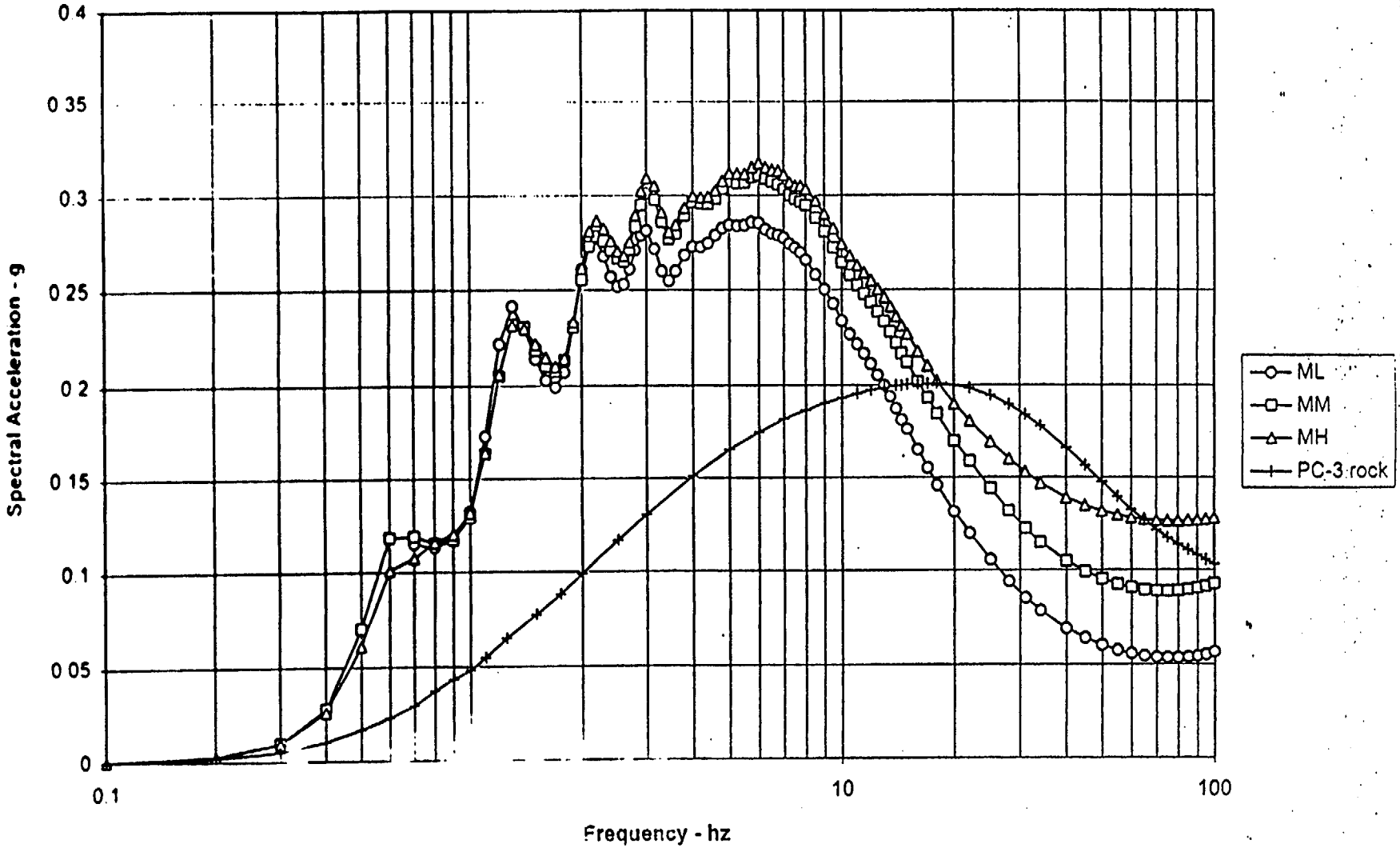

Figure 9.4(a) - Performance Category 5% c... ed soil response spectra from 1-2.5 Hz mean based scaling of broadened bedrock UHS (PC-3 rock). Response sh..wn f... ow (ML), medium (MM), and high (MH) magnitude scaling. Soil category 1 over Triassic bedrock.

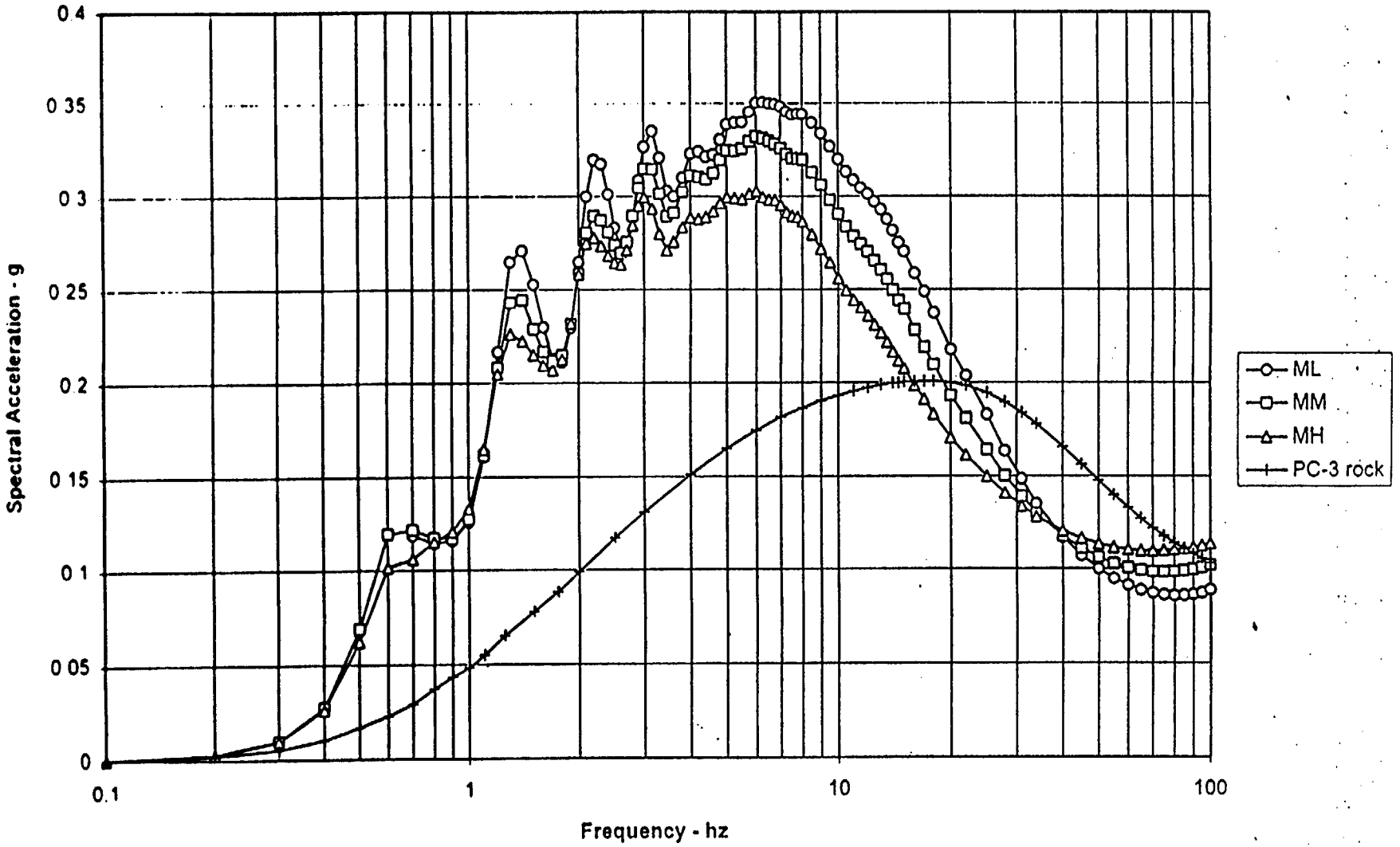

Figure 9.4(b) - Performance Category 3 5% damped soil response spectra from 5-10 Hz mean based scaling of broadened bedrock UHS (PC-3 rock). Response shown using low (ML), medium (MM), and high (MH) magnitude scaling. Soil category 1 over Triassic bedrock.

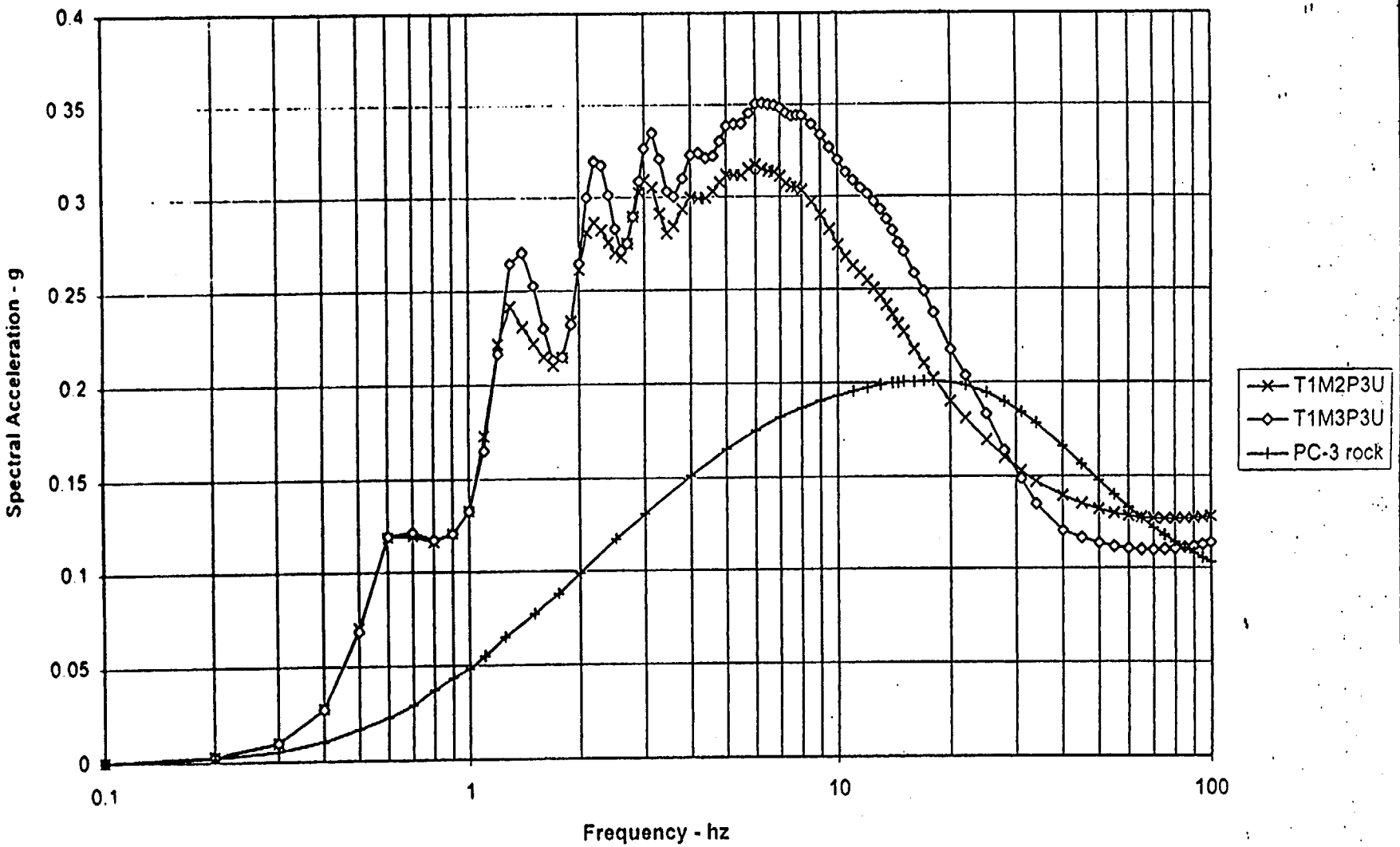

Figure 9.4(c) - Enveloping of Performance Category 3 5% damped soil response spectra from 1-2.5 Hz (T1M2P3U) and 5-10 Hz (T1M3P3U) mean based scaling of broadened bedrock UHS (PC-3 rock). Envelopes of low, medium, and high magnitude scaled spectra are shown. Soil category 1 over Triassic bedrock.

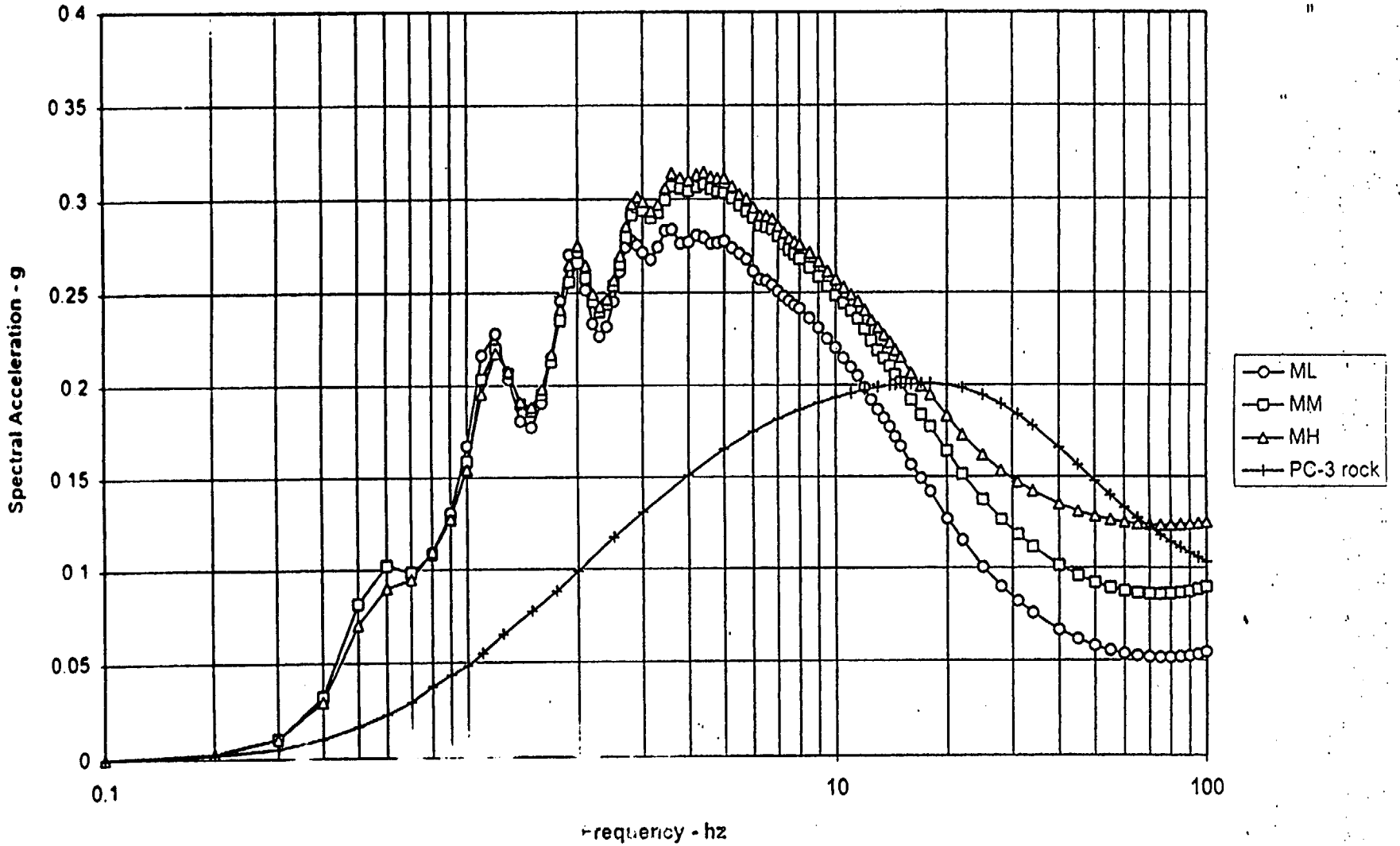

Figure 9.5(a) - Performance Category - SRS ... ed soil response spectra from 1-2.5 Hz mean based scaling of broadened bedrock UHS (PC-3 rock). Response shown u... ow (M...), medium (MM), and high (MH) magnitude scaling. Soil category 2 over Triassic bedrock.

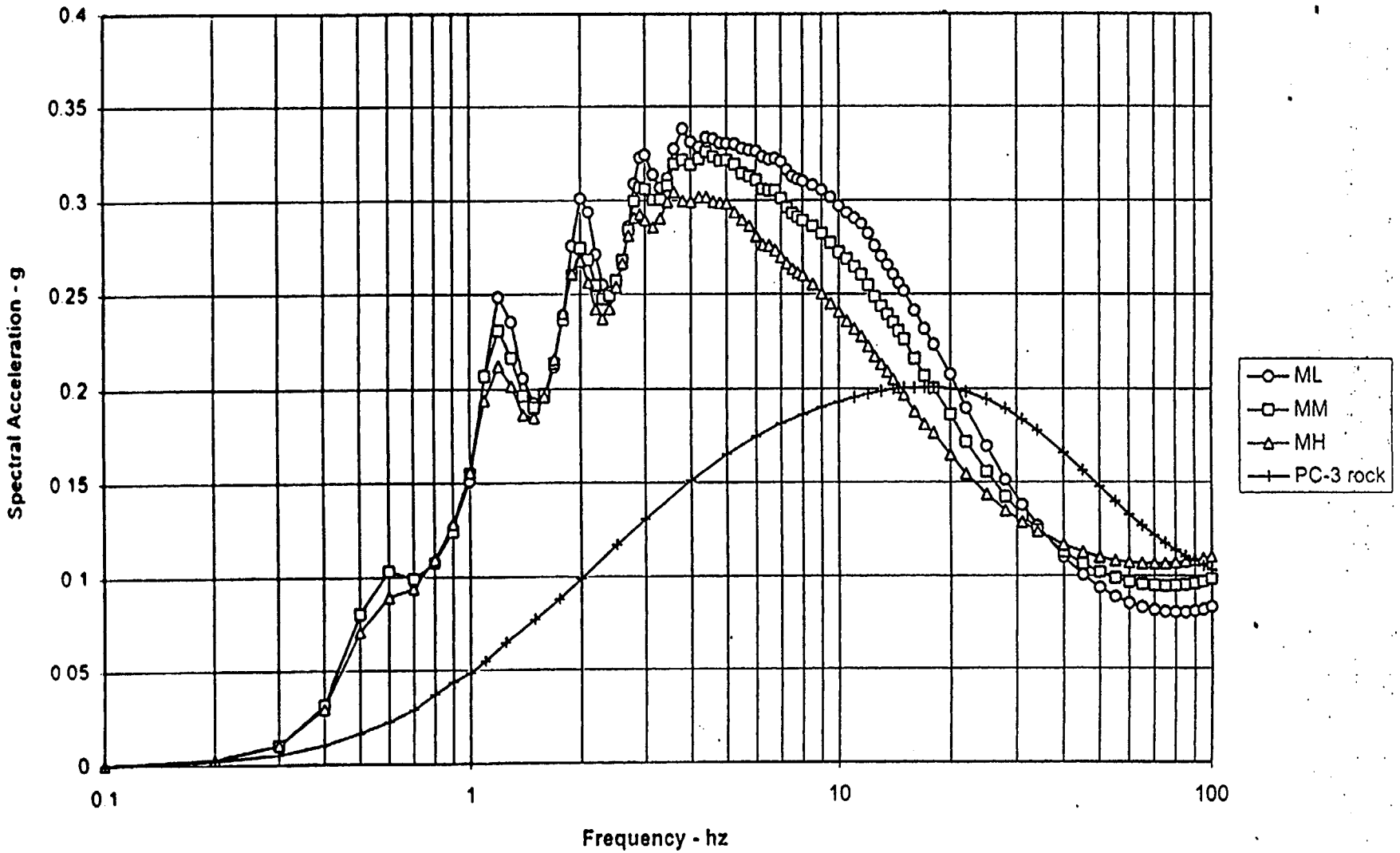

Figure 9.5(b) - Performance Category 3 5% damped soil response spectra from 5-10 Hz mean based scaling of broadened bedrock UHS (PC-3 rock). Response shown using low (ML), medium (MM), and high (MH) magnitude scaling. Soil category 2 over Triassic bedrock.

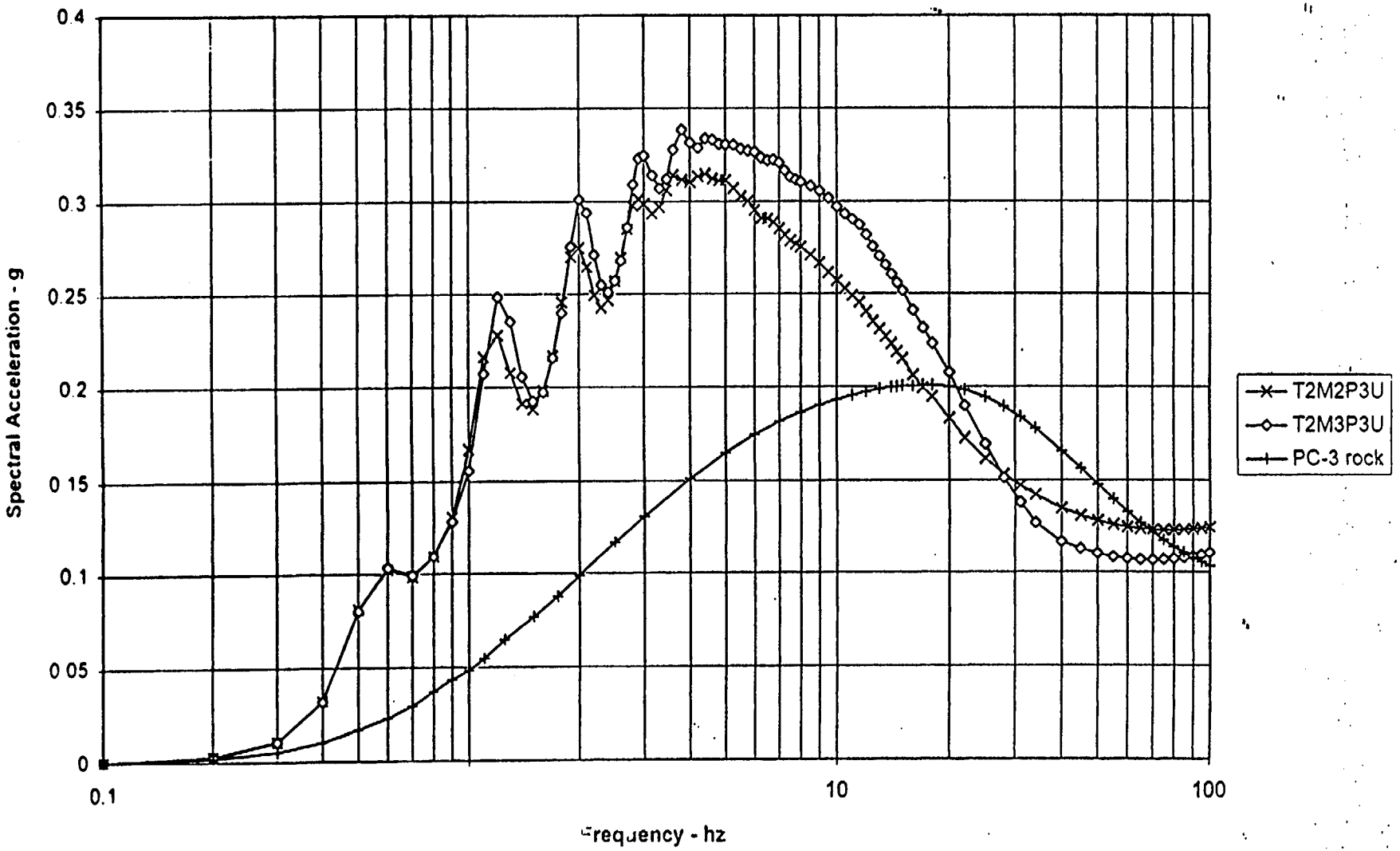

Figure 9.5(c) - Enveloping of Performance C ory 3 5 damped soil response spectra from 1-2.5 Hz (T2M2P3U) and 5-10 Hz (T2M3P3U) mean based scaling of br ed be ock UHS (PC-3 rock). Envelopes of low, medium, and high magnitude scaled spectra are shown. Soil category 2 over Triassic bedrock.

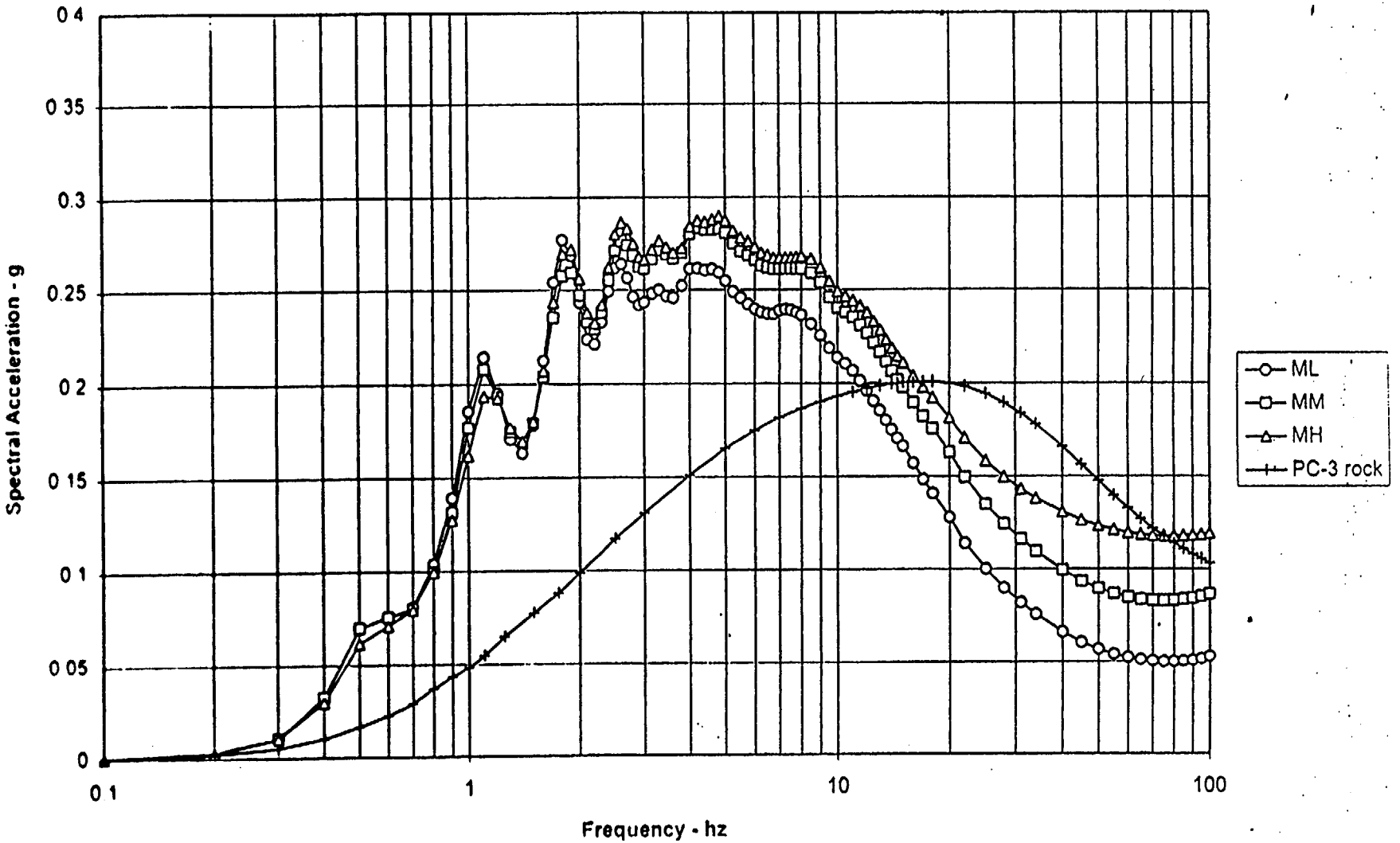

Figure 9.6(a) - Performance Category 3 5% damped soil response spectra from 1-2.5 Hz mean based scaling of broadened bedrock UHS (PC-3 rock). Response shown using low (ML), medium (MM), and high (MH) magnitude scaling. Soil category 3 over Triassic bedrock.

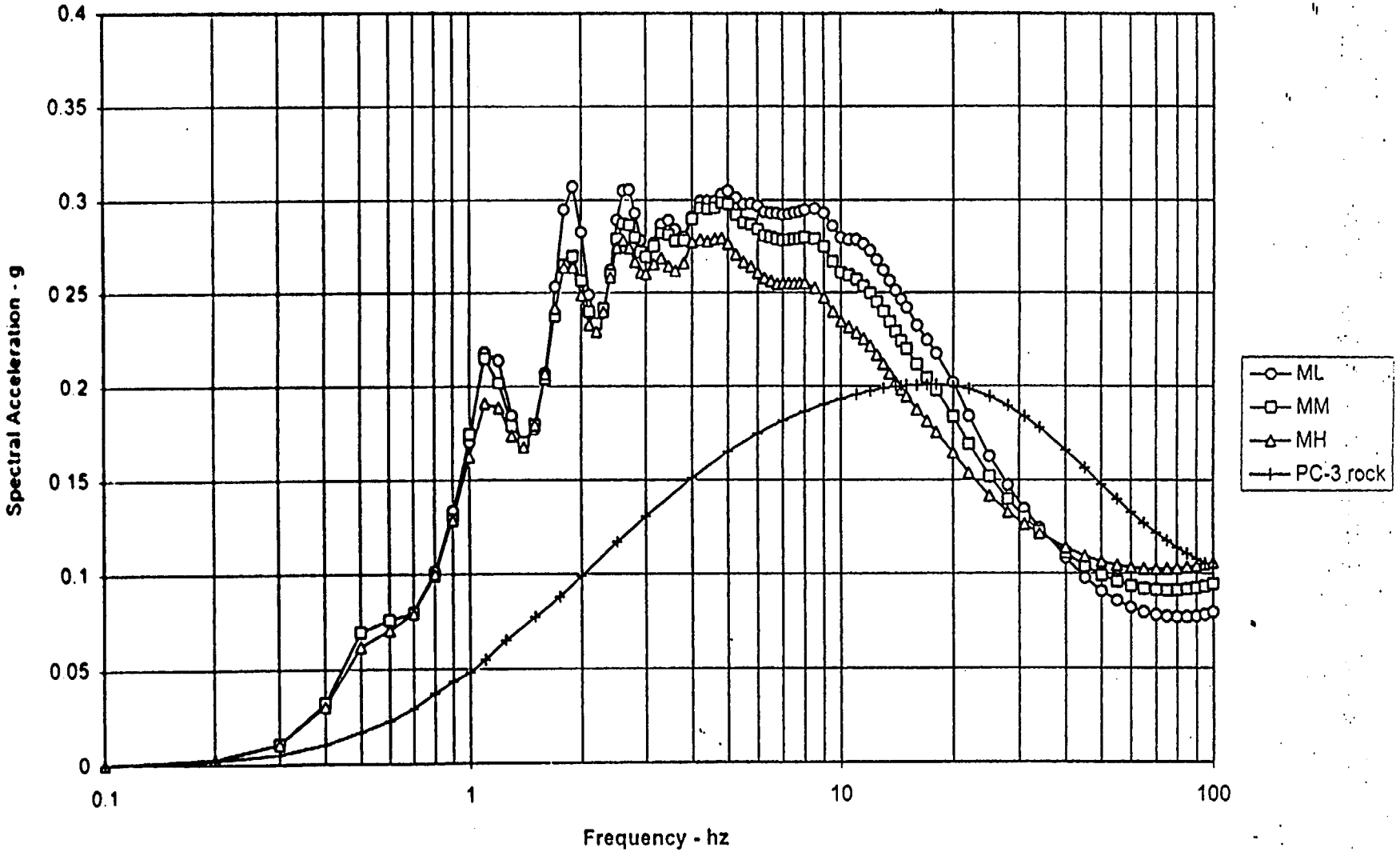

Figure 9.6(b) - Performance Category 3 5% damped soil response spectra from 5-10 Hz mean based scaling of broadened bedrock UHS (PC-3 rock). Response shown using low (ML), medium (MM), and high (MH) magnitude scaling. Soil category 3 over Triassic bedrock.

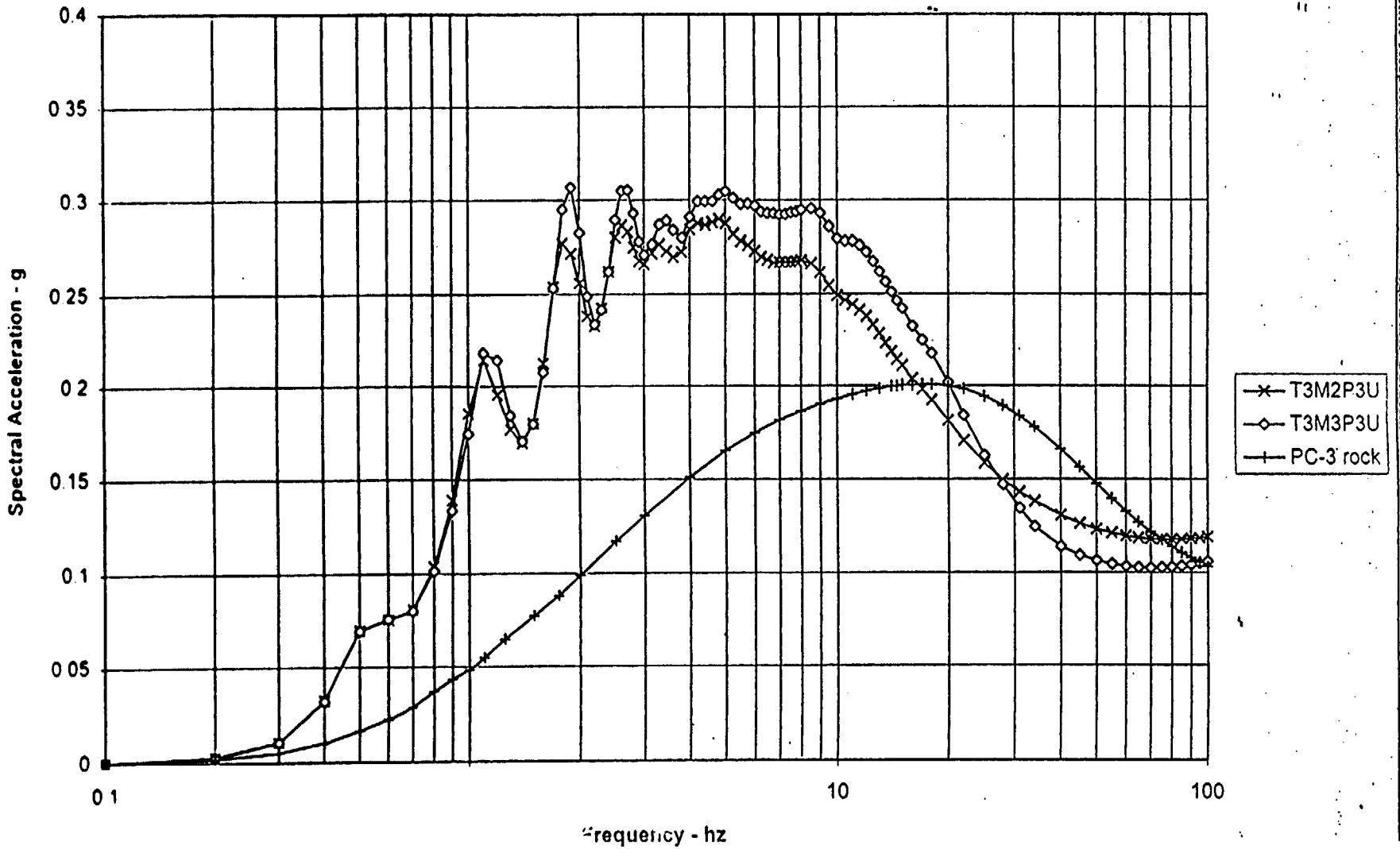

Figure 9.6(c) - Enveloping of Performance Category 3 5% damped soil response spectra from 1-2.5 Hz (T3M2P3U) and 5-10 Hz (T3M3P3U) mean based scaling of broad-banded bedrock UHS (PC-3 rock). Envelopes of low, medium, and high magnitude scaled spectra are shown. Soil category 3 over Triassic bedrock.

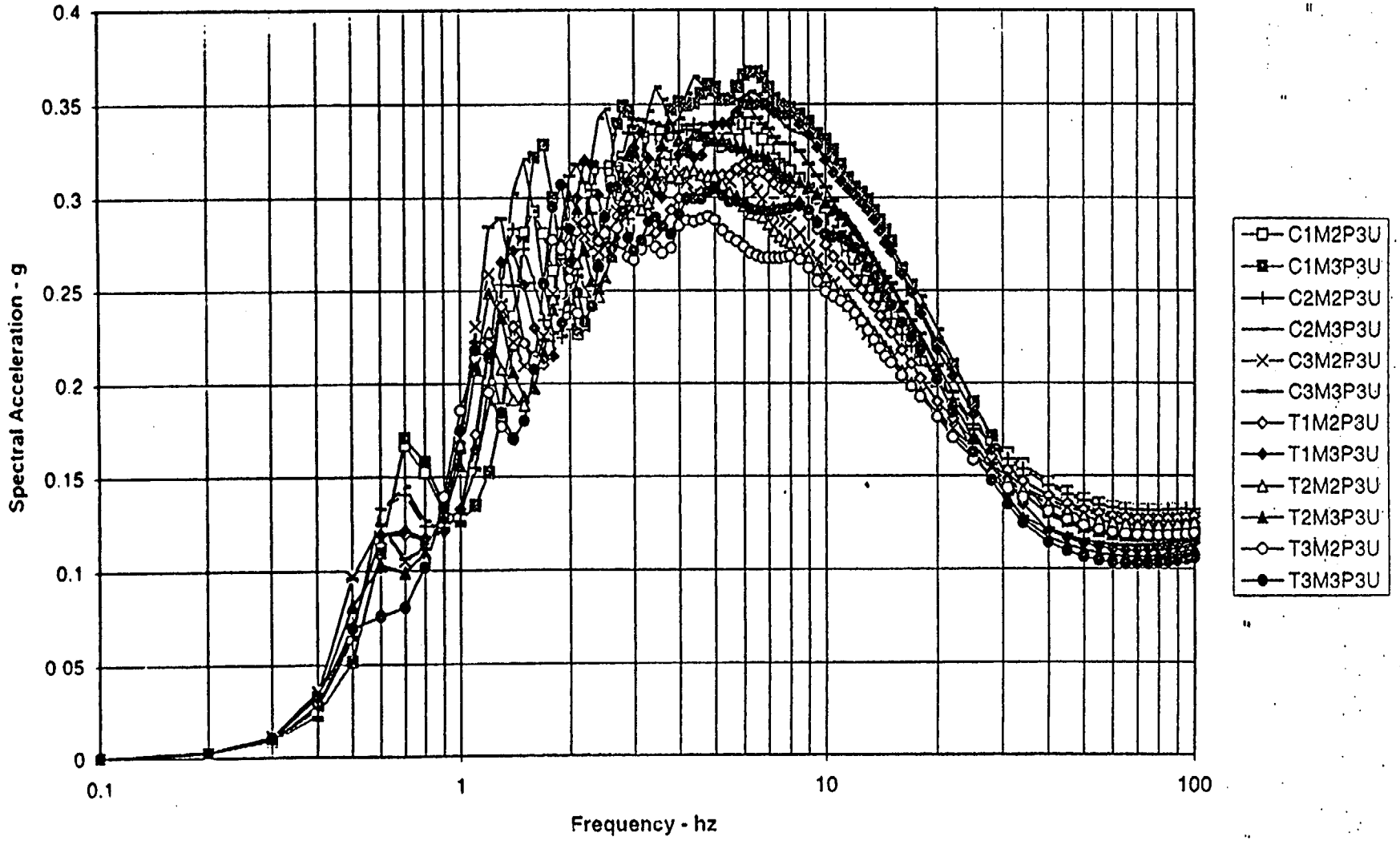

Figure 9.7 - All envelopes of Performance Category 3 5% damped soil response spectra from 1-2.5 Hz and 5-10 Hz mean based scaling of broadened bedrock UHS (PC-3 rock). All soil column categories (600-1500 ft) and both types of bedrock (crystalline and Triassic) are included.

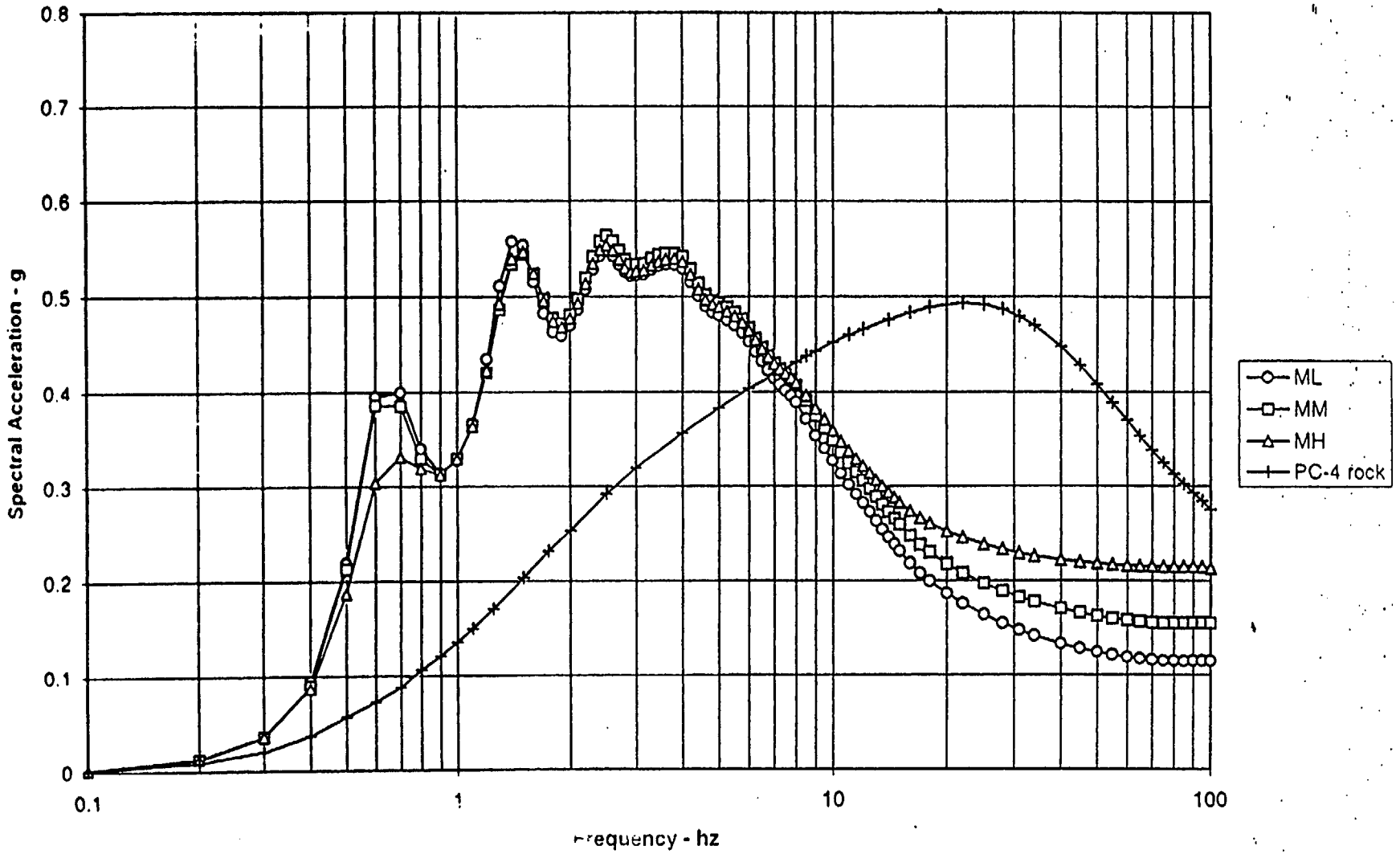

Figure 9.8(a) - Performance Category 4 5% damped soil response spectra from 1-2.5 Hz mean based scaling of broadened bedrock UHS (PC-4 rock). Response shown using low (ML), medium (MM), and high (MH) magnitude scaling. Soil category 1 (600-800 ft) over crystalline bedrock.

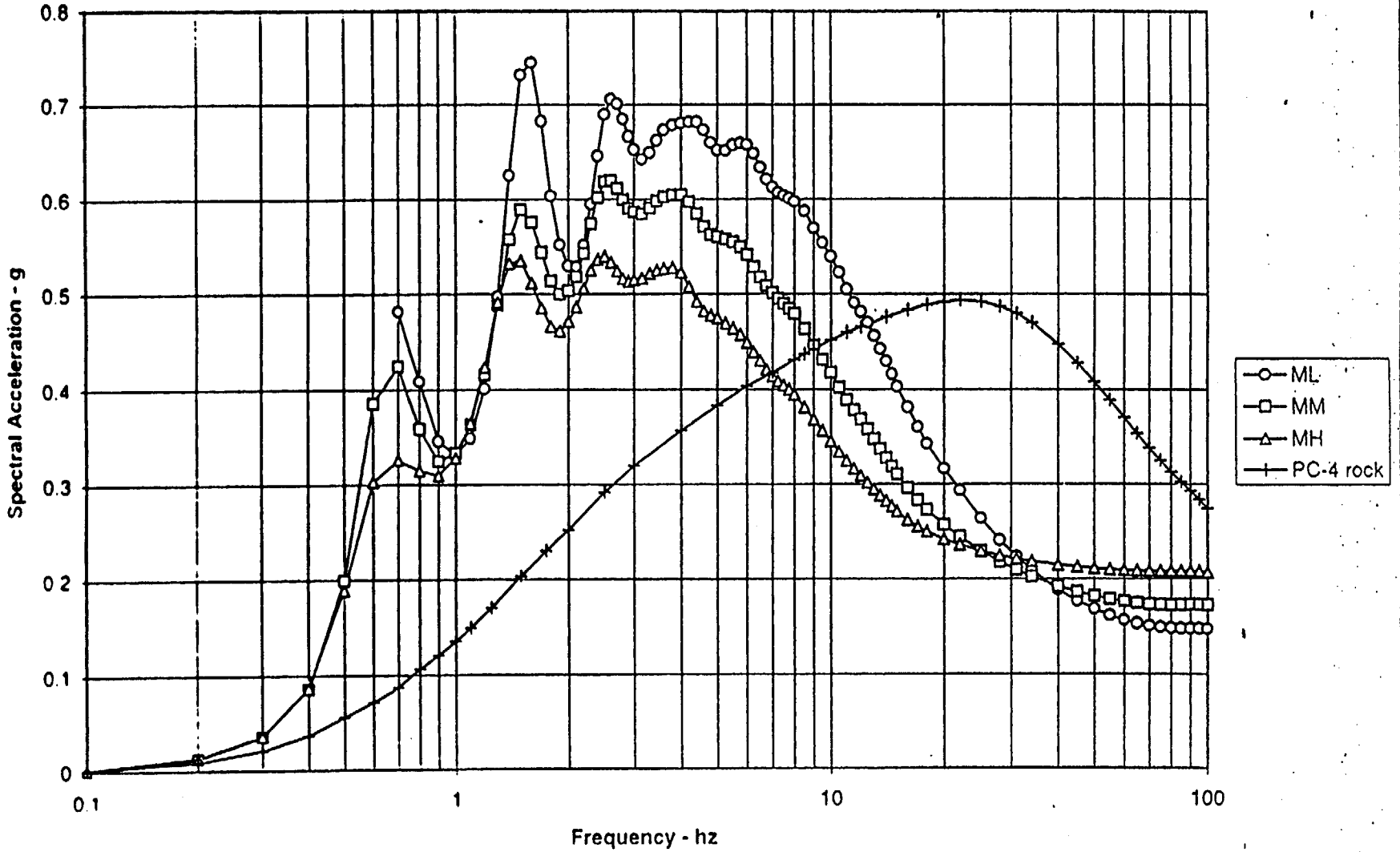

Figure 9 8(b) - Performance Category 4 5% damped soil response spectra from 5-10 Hz mean based scaling of broadened bedrock UHS (PC-4 rock). Response shown using low (ML), medium (MM), and high (MH) magnitude scaling. Soil category 1 over crystalline bedrock.

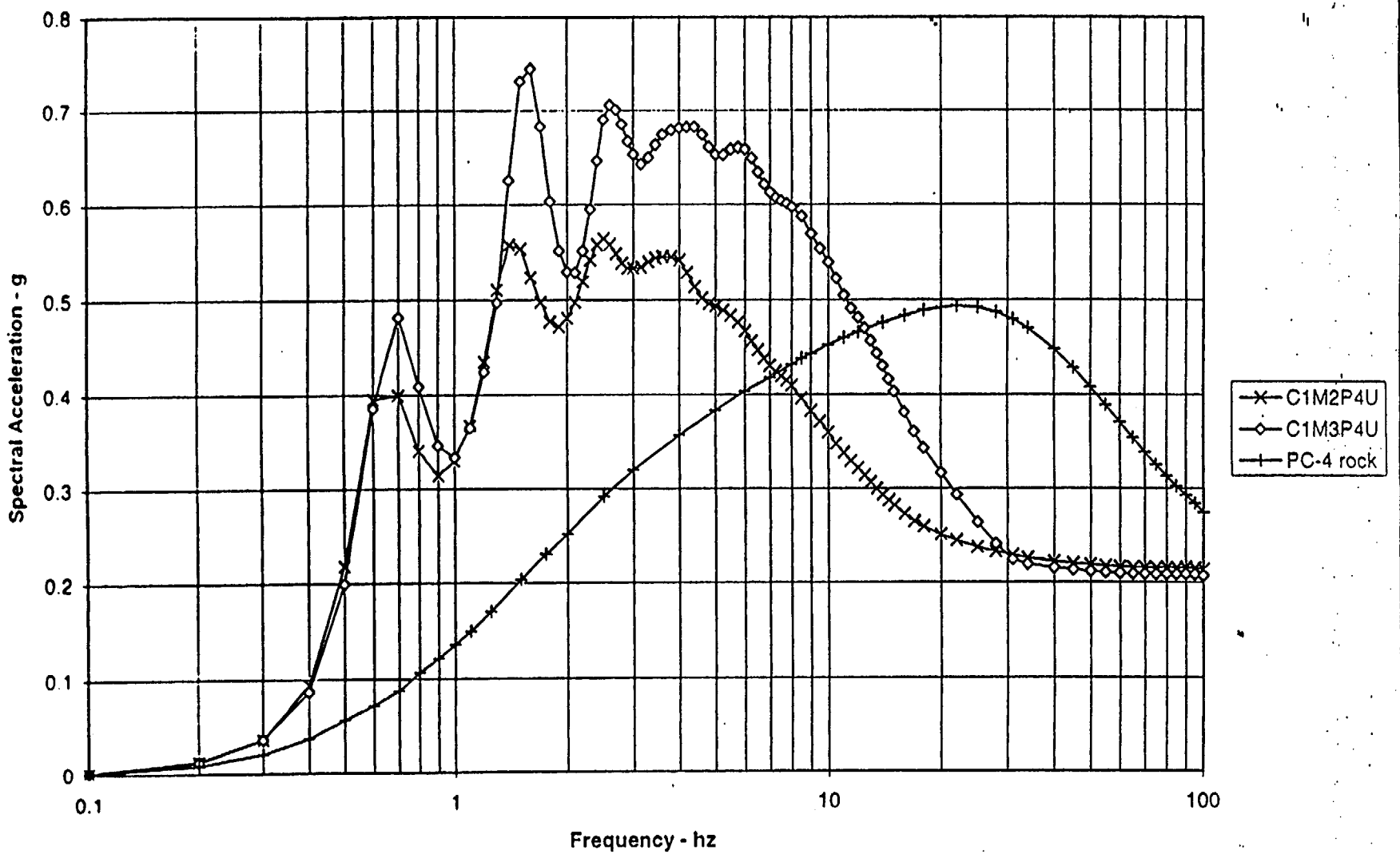

Figure 9.8(c) - Enveloping of Performance Category 4 5% damped soil response spectra from 1-2.5 Hz (C1M2P4U) and 5-10 Hz (C1M3P4U) mean based scaling of broadened bedrock UHS (PC-4 rock). Envelopes of low, medium, and high magnitude scaled spectra are shown. Soil category I over crystalline bedrock.

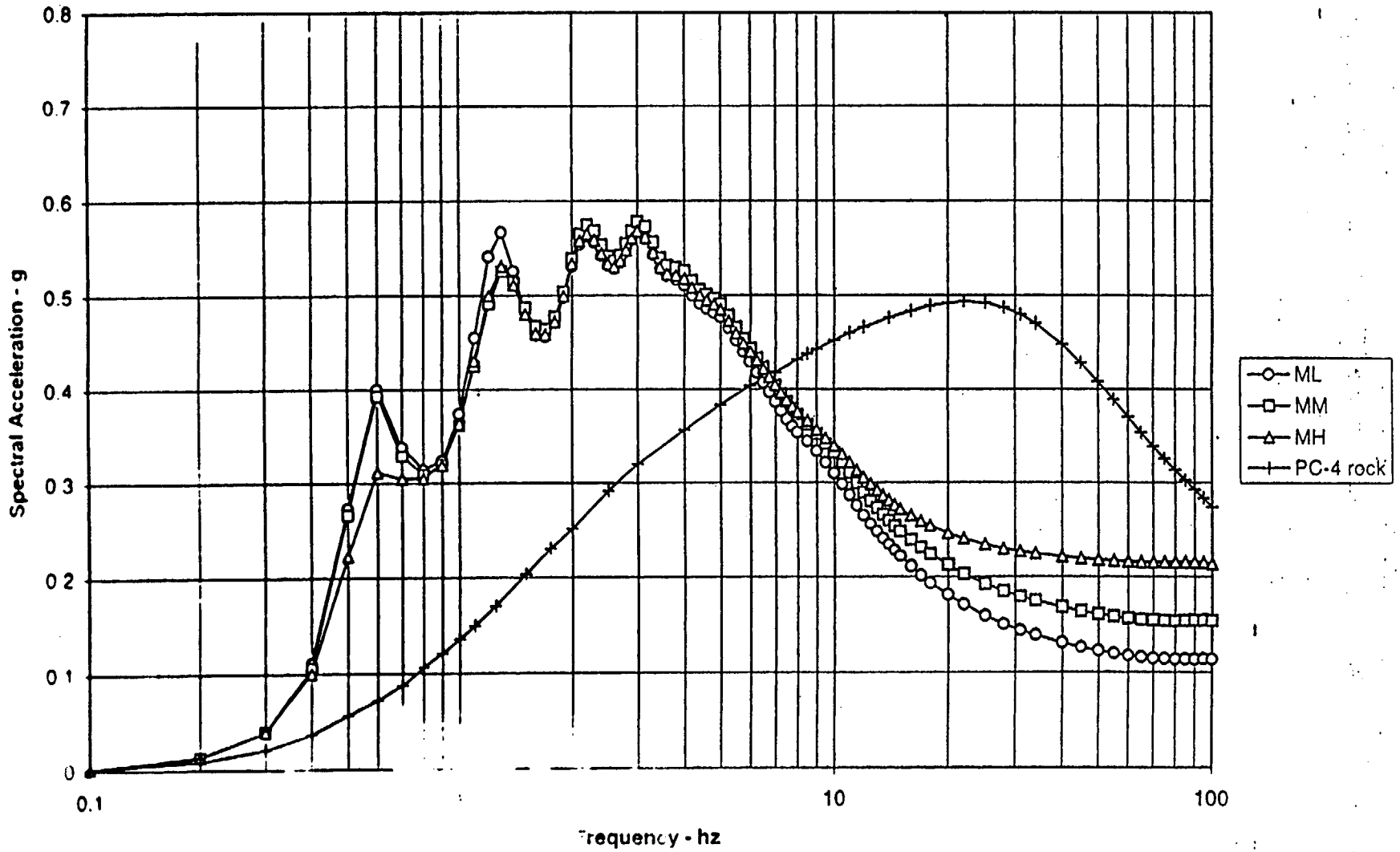

Figure 9.9(a) - Performance Category 5% d... ...o soil response spectra from 1-2.5 Hz mean based scaling of broadened bedrock UHS (PC-4 rock). Response shown using low (ML), medium (MM), and high (MH) magnitude scaling. Soil category 2 over crystalline bedrock.

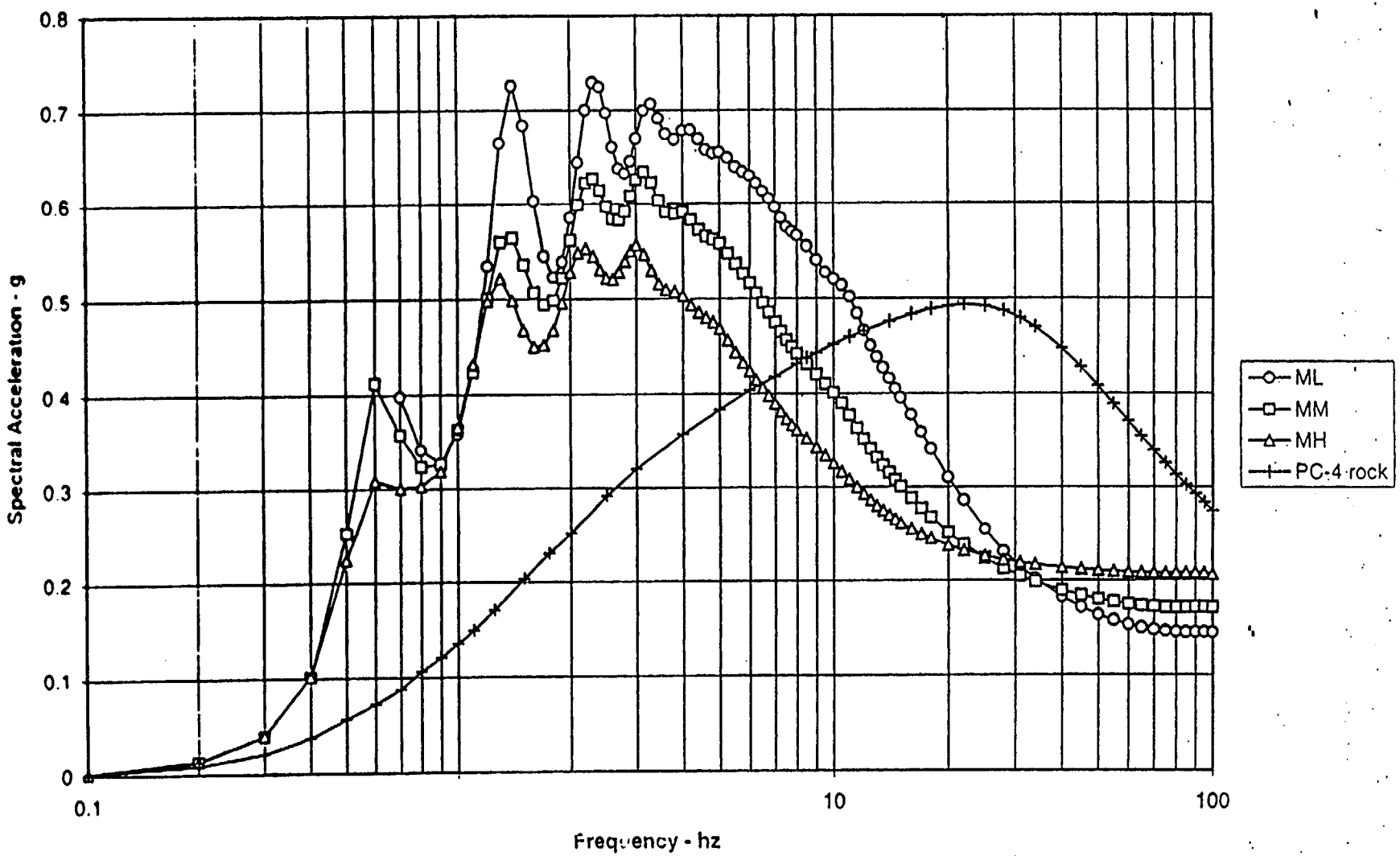

Figure 9.9(b) - Performance Category 4 5% damped soil response spectra from 5-10 Hz mean based scaling of broadened bedrock UHS (PC-4 rock). Response shown using low (ML), medium (MM), and high (MH) magnitude scaling. Soil category 2 over crystalline bedrock.

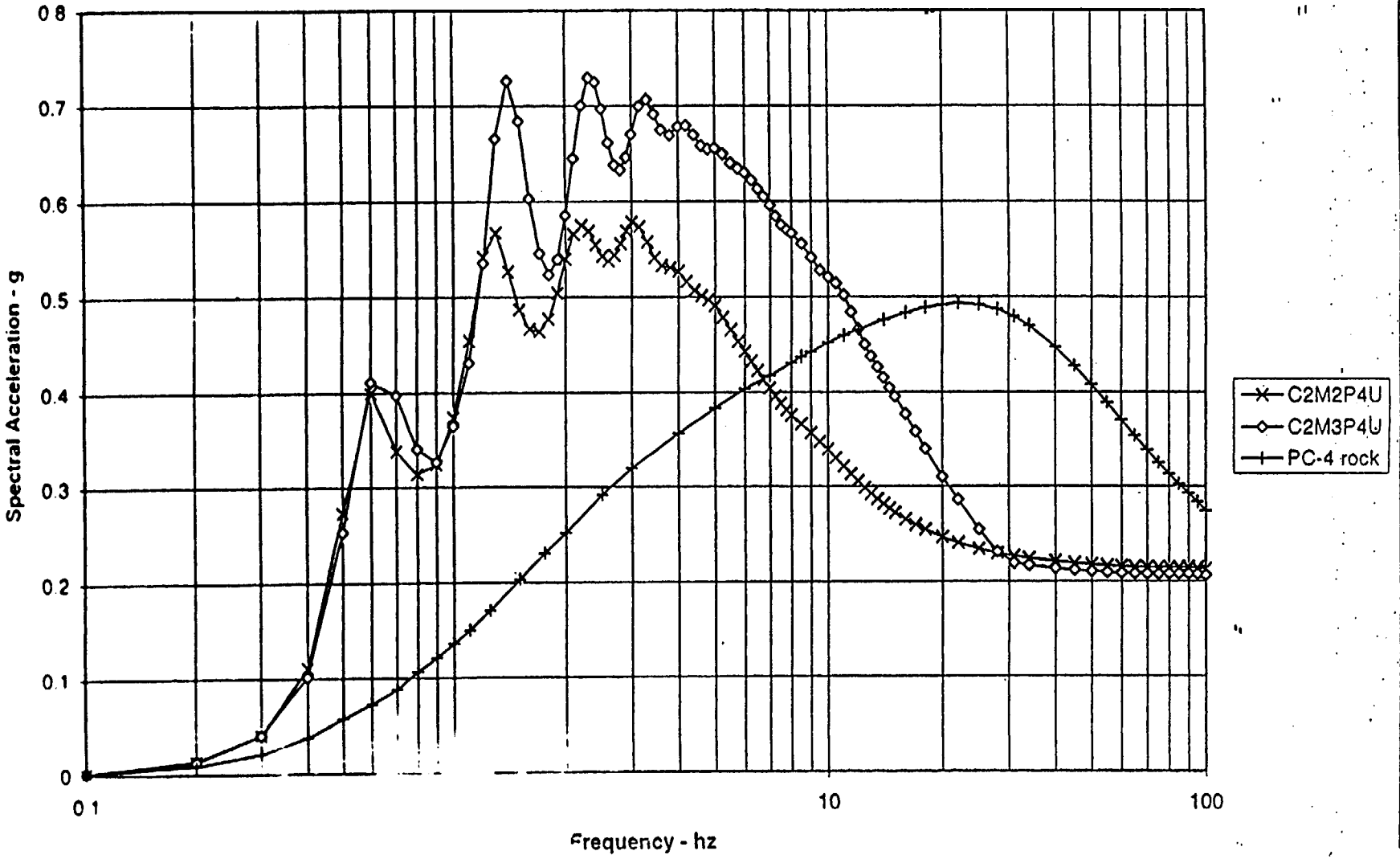

Figure 9.9(c) - Enveloping of Performance Goal 4 5% damped soil response spectra from 1-2.5 Hz (C2M2P4U) and 5-10 Hz (C2M3P4U) mean based scaling of bedrock UHS (PC-4 rock). Envelopes of low, medium, and high magnitude scaled spectra are shown. Soil category 2 over crystalline bedrock.

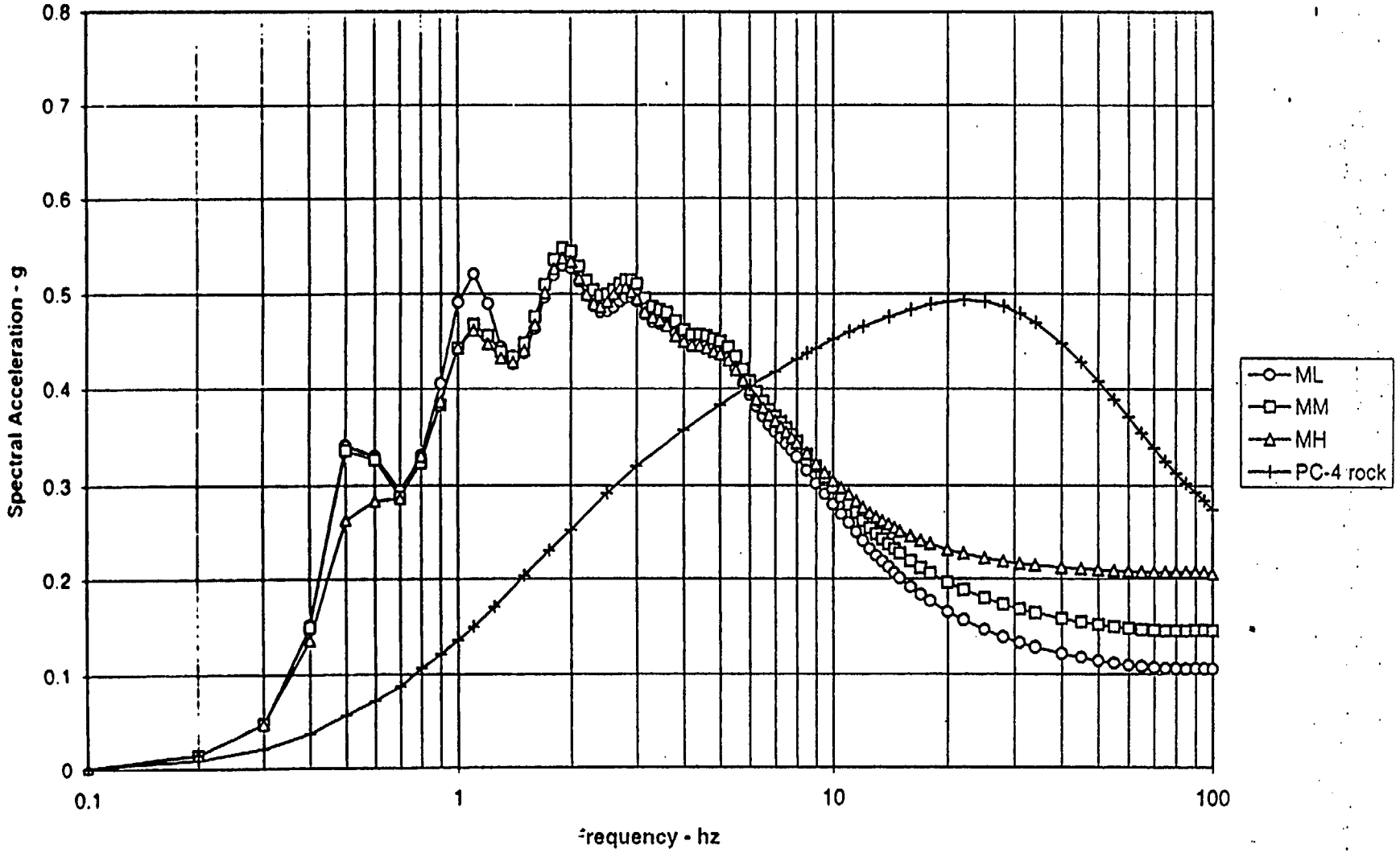

Figure 9.10(a) - Performance Category 4 5% damped soil response spectra from 1-2.5 Hz mean based scaling of broadened bedrock UHS (PC-4 rock). Response shown using low (ML), medium (MM), and high (MH) magnitude scaling. Soil category 3 (1000-1200 ft) over crystalline bedrock.

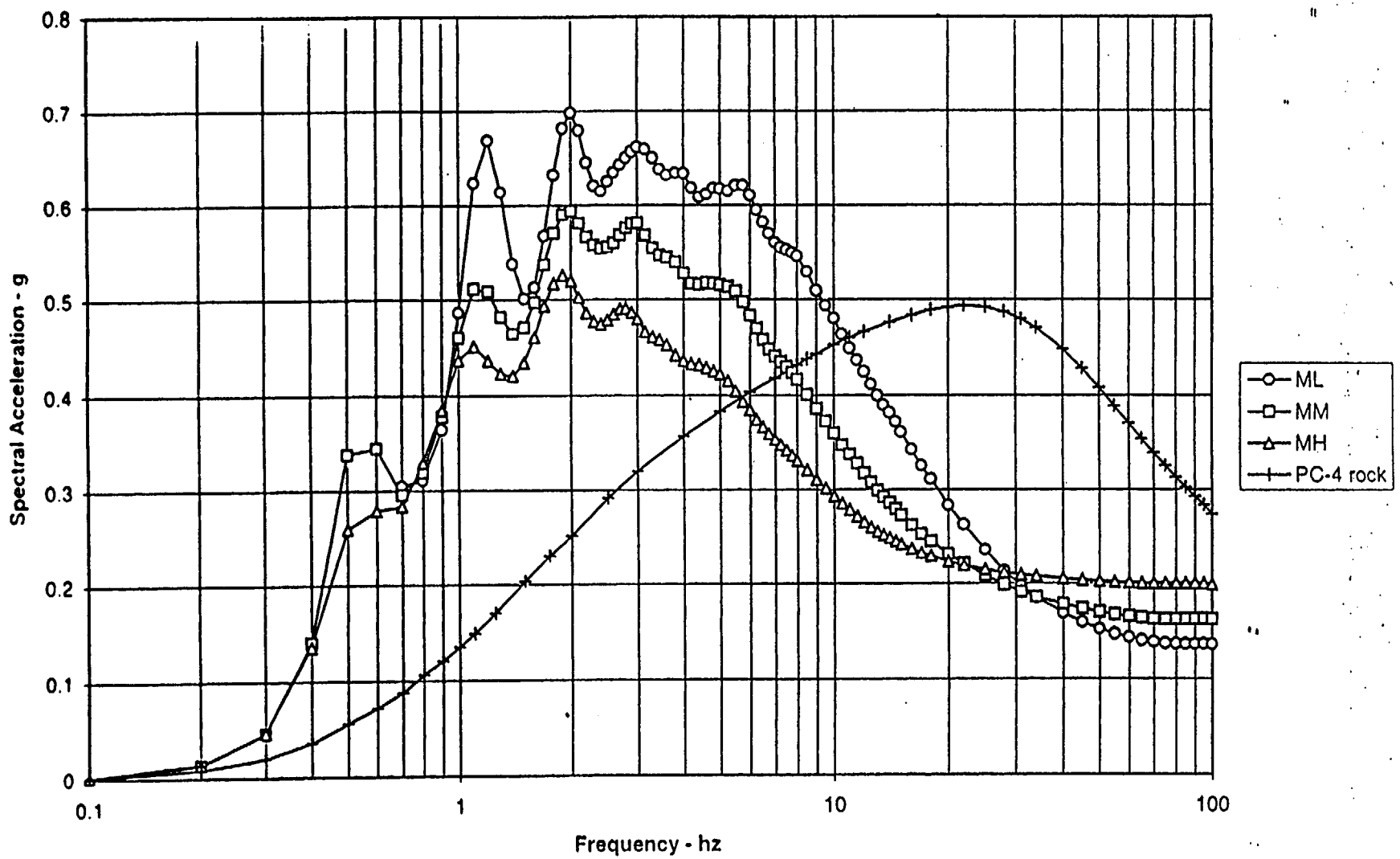

Figure 9.10(b) - Performance Category 4 5% damped soil response spectra from 5-10 Hz mean based scaling of broadened bedrock UHS (PC-4 rock). Response shown using low (ML), medium (MM), and high (MH) magnitude scaling. Soil category 3 over crystalline bedrock.

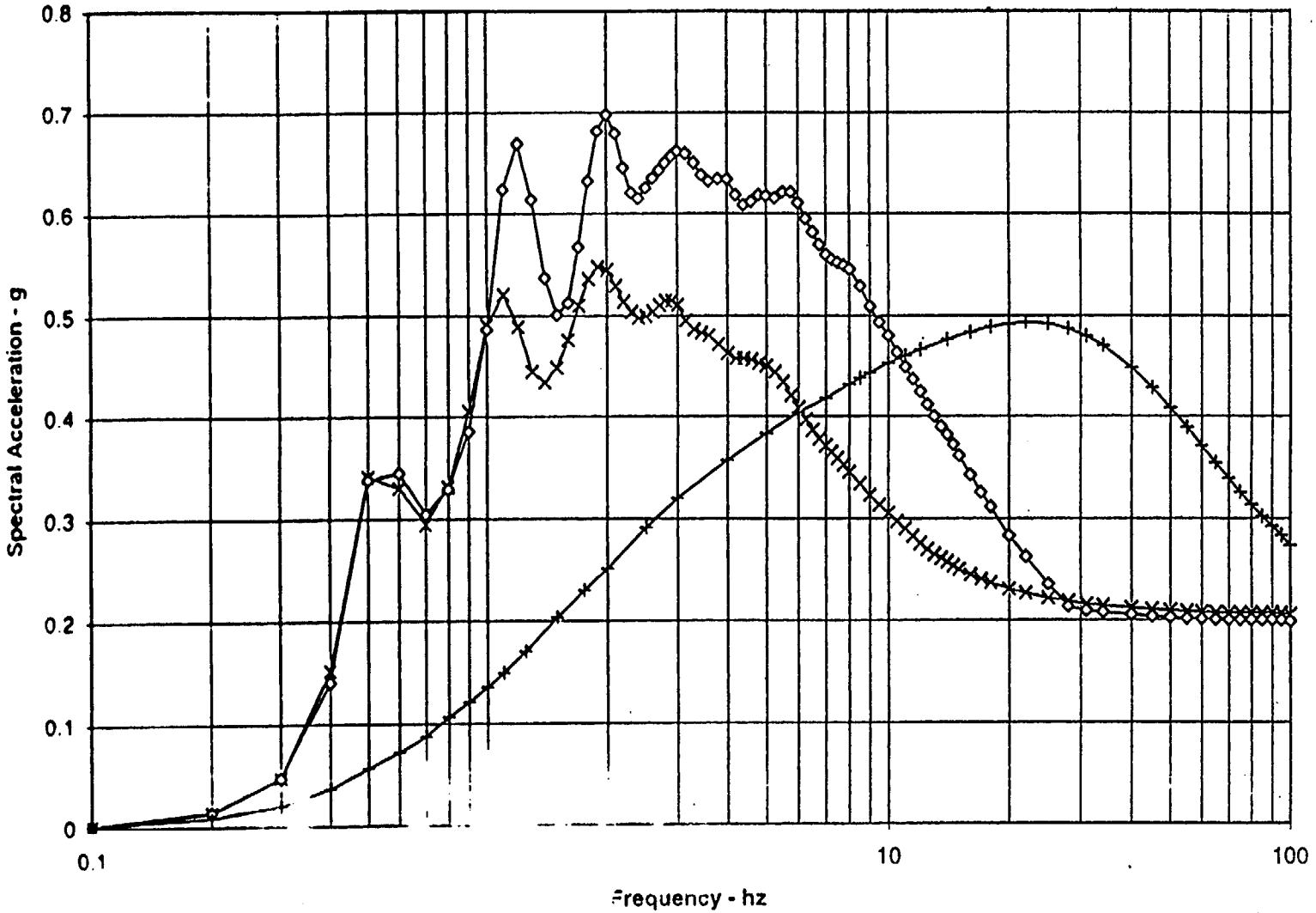

Figure 9.10(c) - Enveloping of Performance ... 4.5% damped soil response spectra from 1-2.5 Hz (C3M2P4U) and 5-10 Hz (C3M3P4U) mean based scaling of broadened bedrock UHS (PC-4 rock). Envelopes of low, medium, and high magnitude scaled spectra are shown. Soil category 3 over crystalline bedrock.

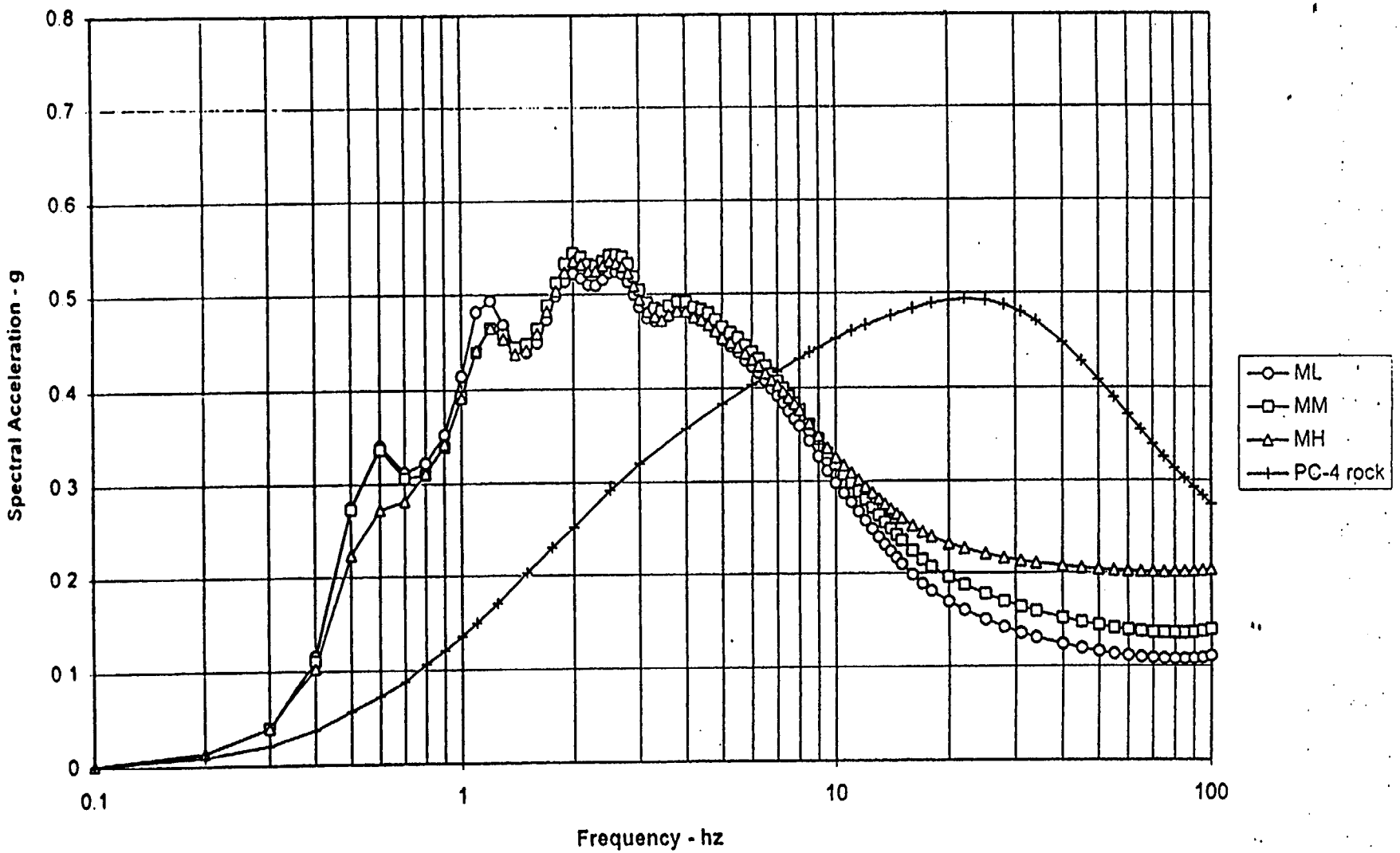

Figure 9.11(a) - Performance Category 4 5% damped soil response spectra from 1-2.5 Hz mean based scaling of broadened bedrock UHS (PC-4 rock). Response shown using low (ML), medium (MM), and high (MH) magnitude scaling. Soil category 1 (900-1100 ft) over Triassic bedrock.

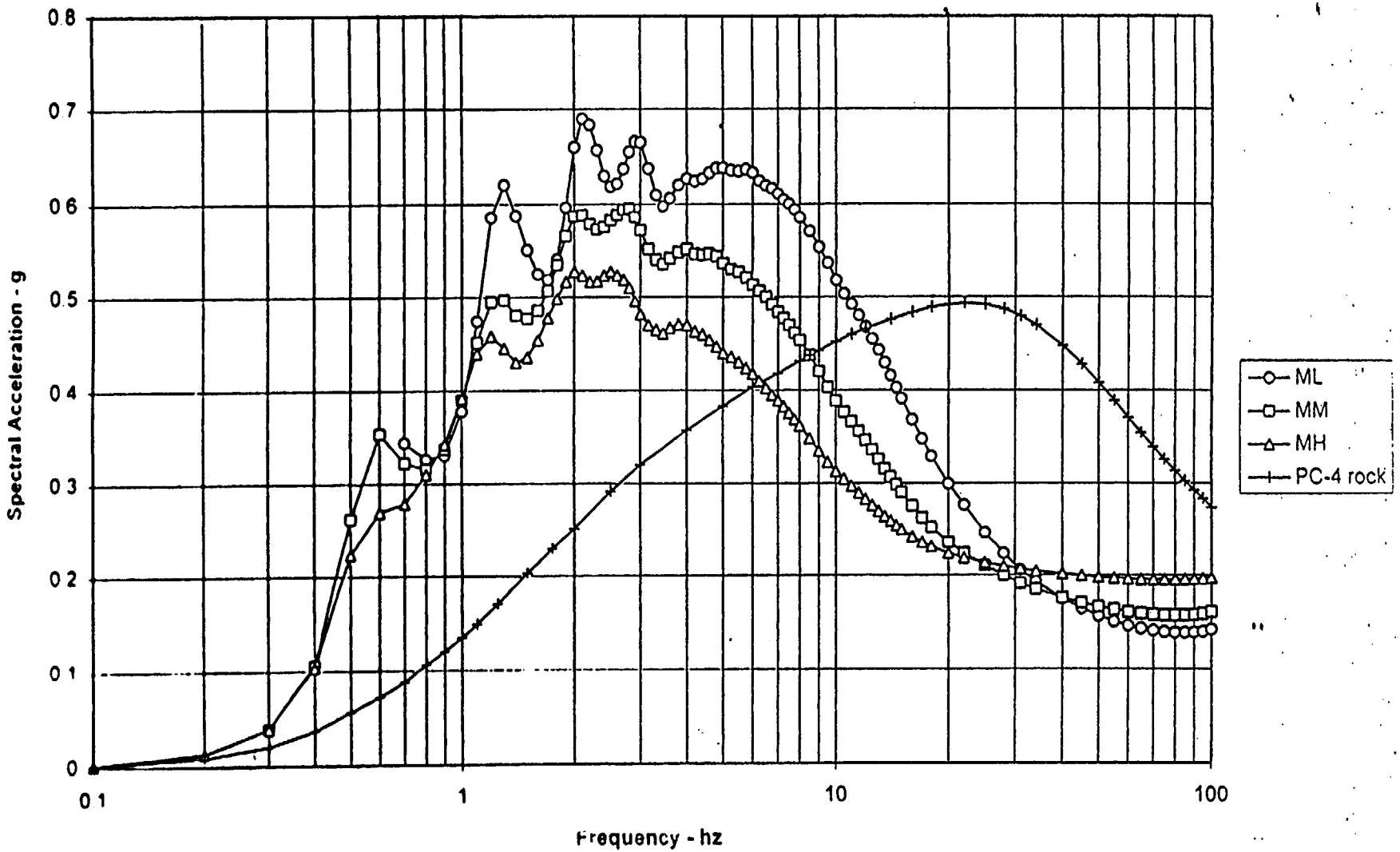

Figure 9.11(b) - Performance Category 4 5% damped soil response spectra from 5-10 Hz mean based scaling of broadened bedrock UHS (PC-4 rock). Response shown using low (ML), medium (MM), and high (MH) magnitude scaling. Soil category 1 over Triassic bedrock.

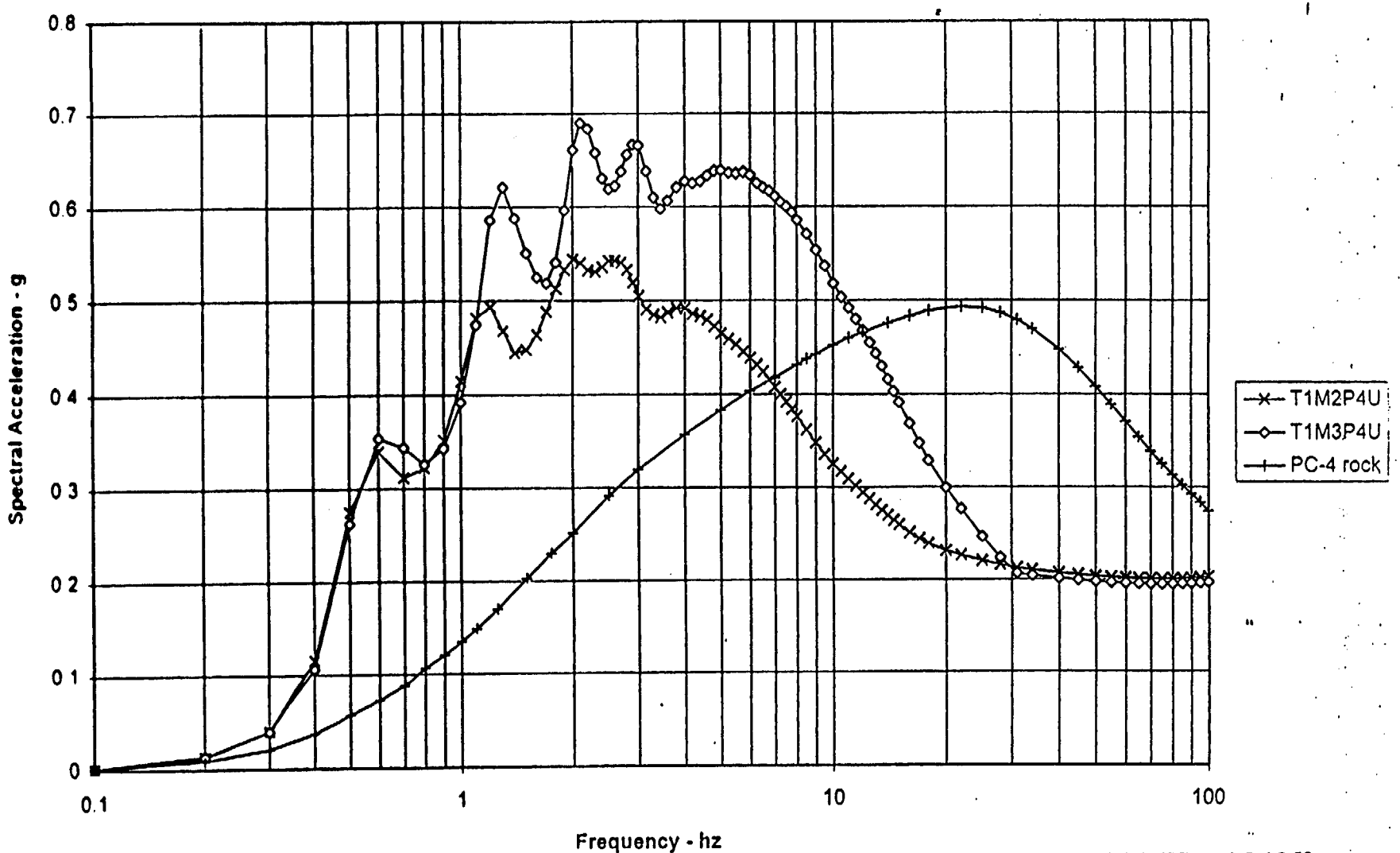

Figure 9.11(c) - Enveloping of Performance Category 4 5% damped soil response spectra from 1-2.5 Hz (T1M2P4U) and 5-10 Hz (T1M3P4U) mean based scaling of broadened bedrock UHS (PC-4 rock). Envelopes of low, medium, and high magnitude scaled spectra are shown. Soil category 1 over Triassic bedrock.

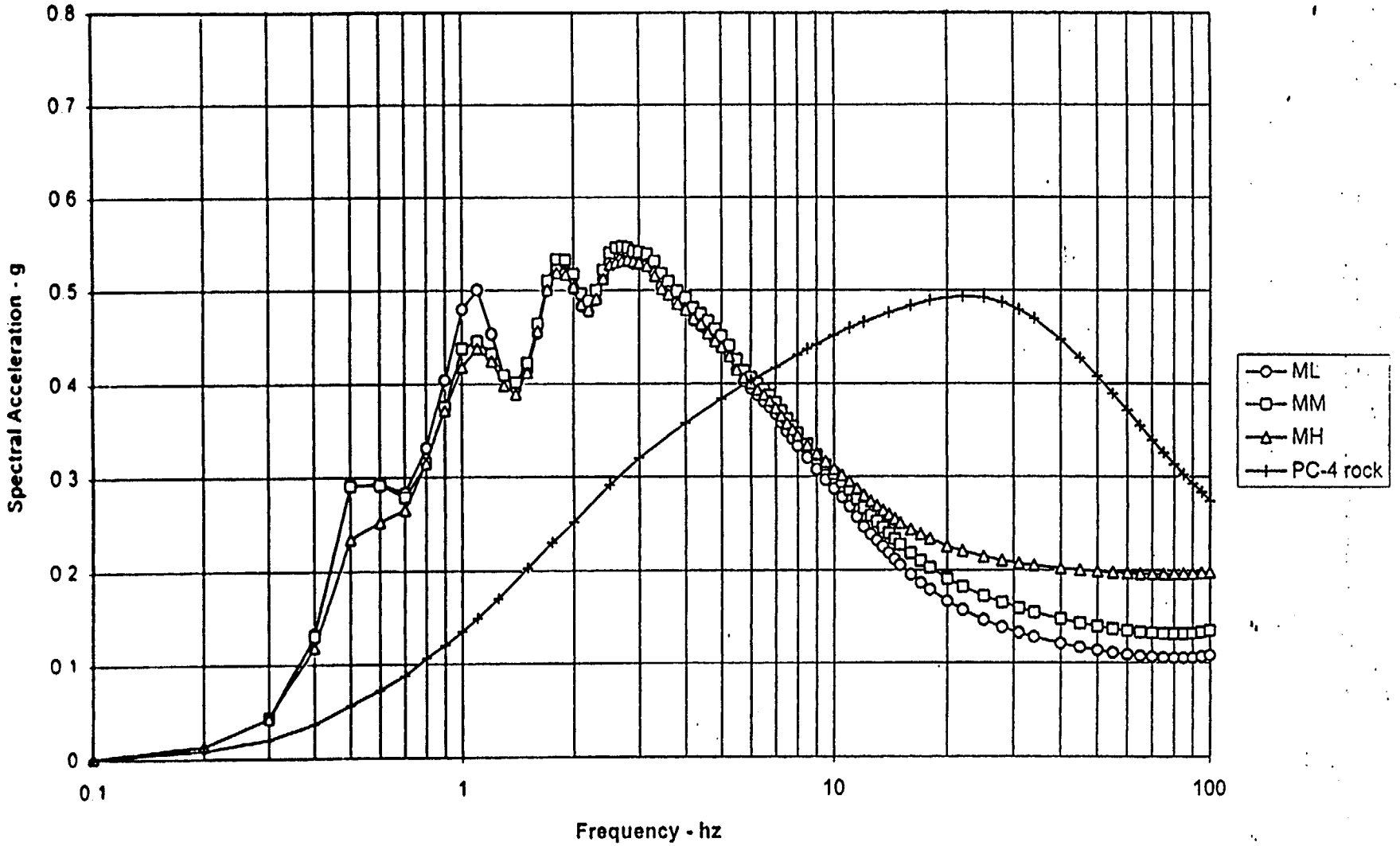

Figure 9.12(a) - Performance Category 4 5% damped soil response spectra from 1-2.5 Hz mean based scaling of broadened bedrock UHS (PC-4 rock). Response shown using low (ML), medium (MM), and high (MH) magnitude scaling. Soil category 2 (1100-1300 ft) over Triassic bedrock.

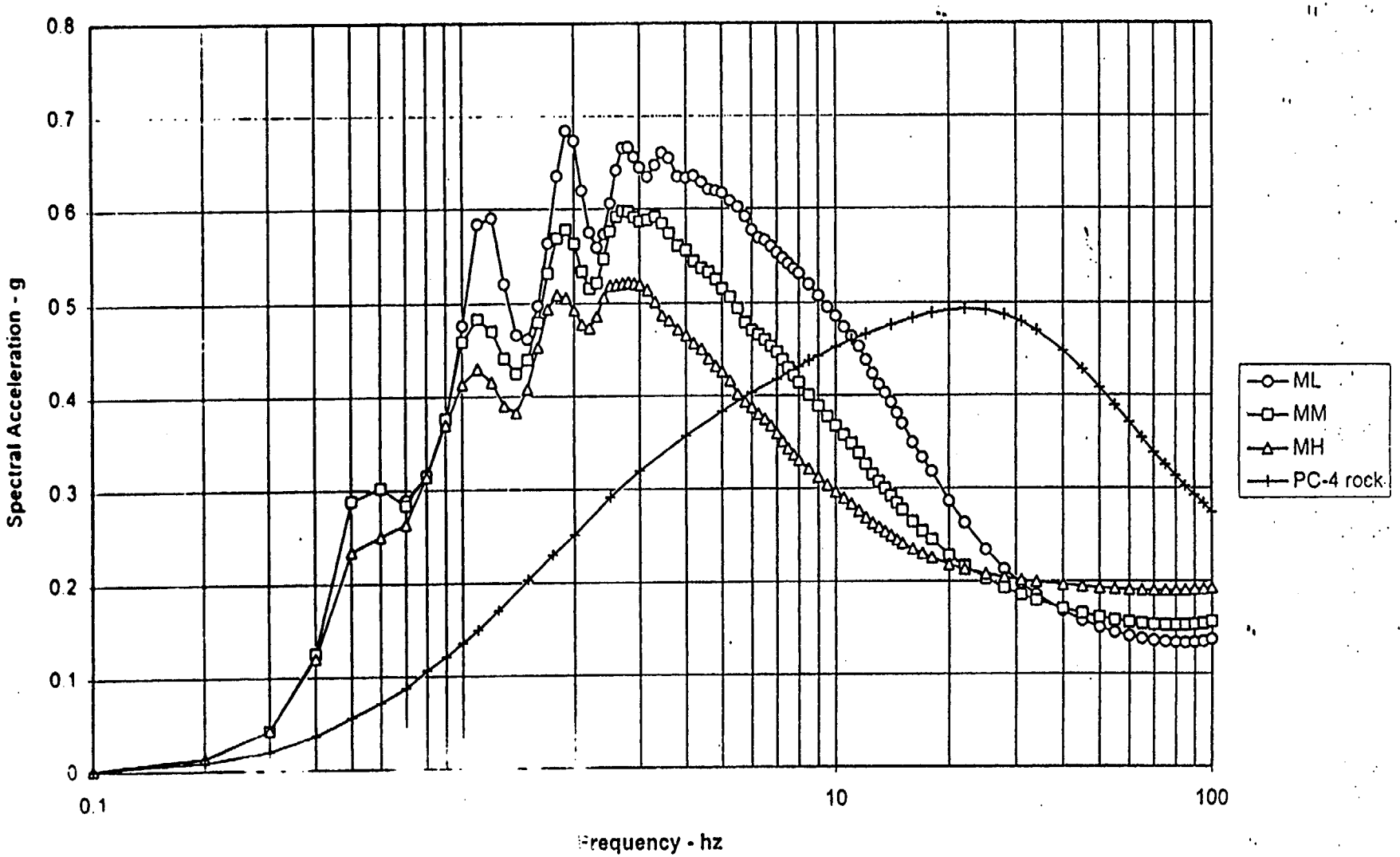

Figure 9.12(b) - Performance Category 4 5% damped soil response spectra from 5-10 Hz mean based scaling of broadened bedrock UHS (PC-4 rock). Response shown using low (ML), medium (MM), and high (MH) magnitude scaling. Soil category 2 over Triassic bedrock.

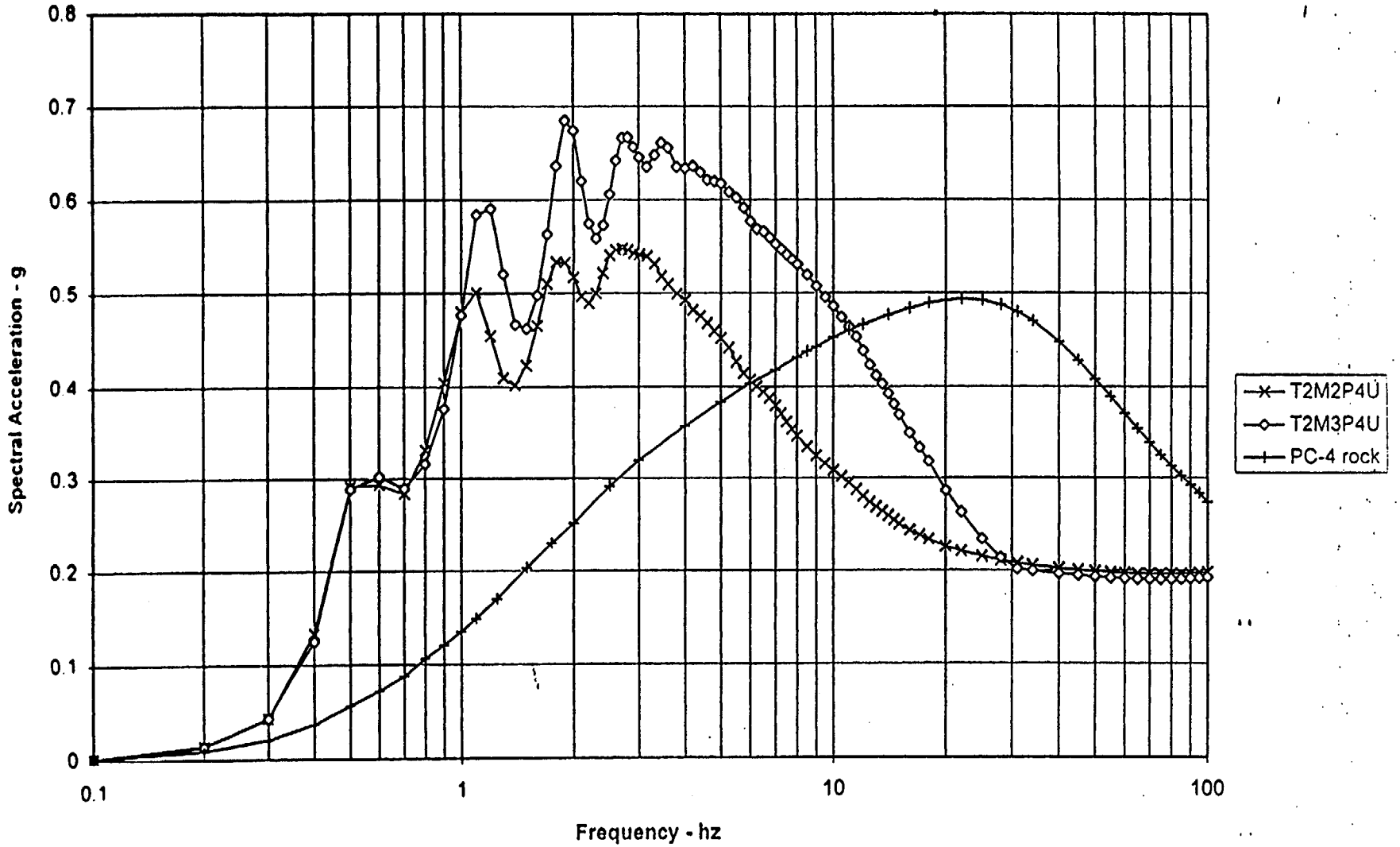

Figure 9.12(c) - Enveloping of Performance Category 4 5% damped soil response spectra from 1-2.5 Hz (T2M2P4U) and 5-10 Hz (T2M3P4U) mean based scaling of broadened bedrock UHS (PC-4 rock). Envelopes of low, medium, and high magnitude scaled spectra are shown. Soil category 2 over Triassic bedrock.

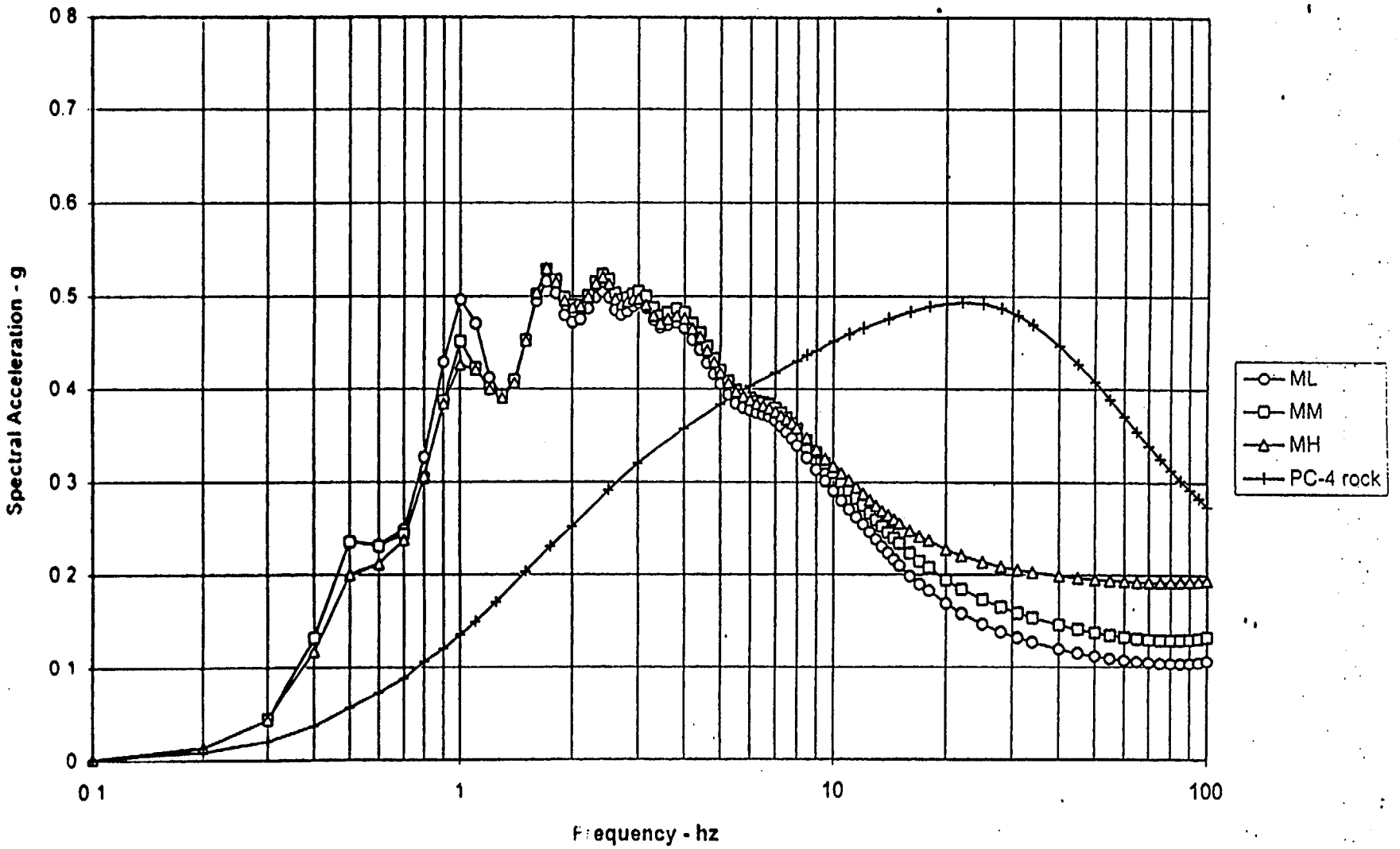

Figure 9.13(a) - Performance Category 4 5% damped soil response spectra from 1-2.5 Hz mean based scaling of broadened bedrock UHS (PC-4 rock). Response shown using low (ML), medium (MM), and high (MH) magnitude scaling. Soil category 3 (1300-1500 ft) over Triassic bedrock.

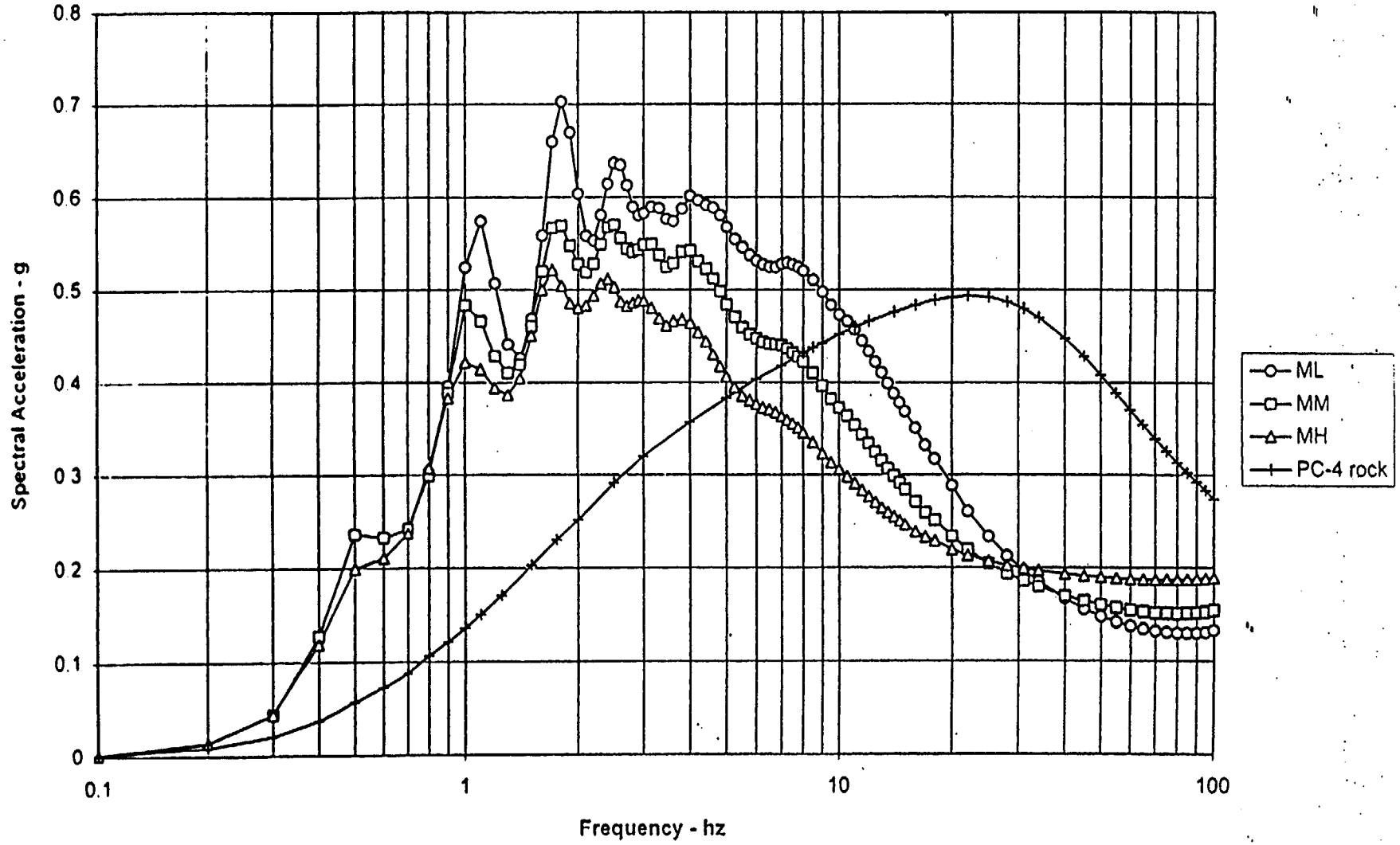

Figure 9.13(b) - Performance Category 4 5% damped soil response spectra from 5-10 Hz mean based scaling of broadened bedrock UHS (PC-4 rock). Response shown using low (ML), medium (MM), and high (MH) magnitude scaling. Soil category 3 over Triassic bedrock.

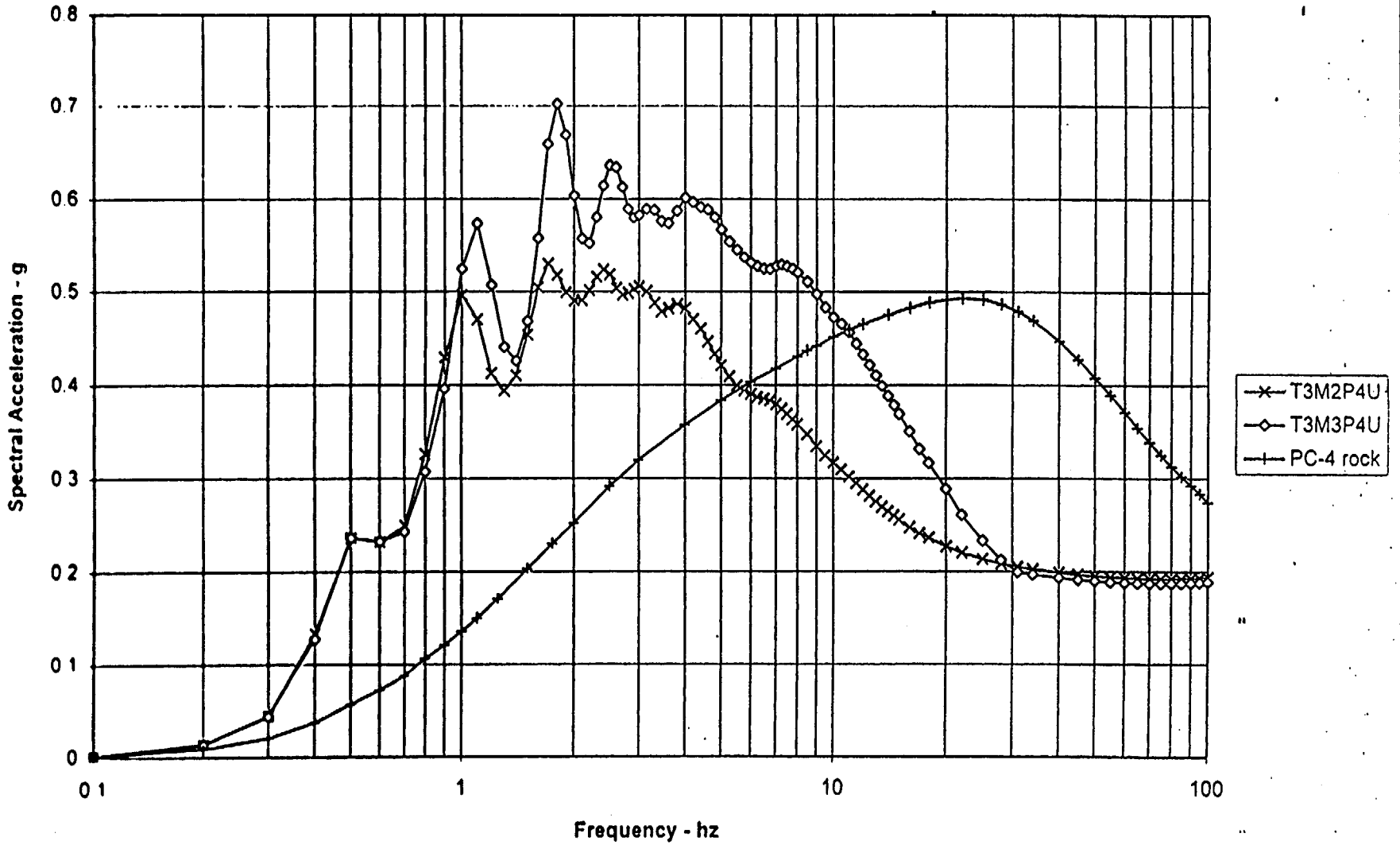

Figure 9.13(c) - Enveloping of Performance Category 4 5% damped soil response spectra from 1-2.5 Hz (T3M2P4U) and 5-10 Hz (T3M3P4U) mean based scaling of broadened bedrock UHS (PC-4 rock). Envelopes of low, medium, and high magnitude scaled spectra are shown. Soil category 3 over Triassic bedrock.

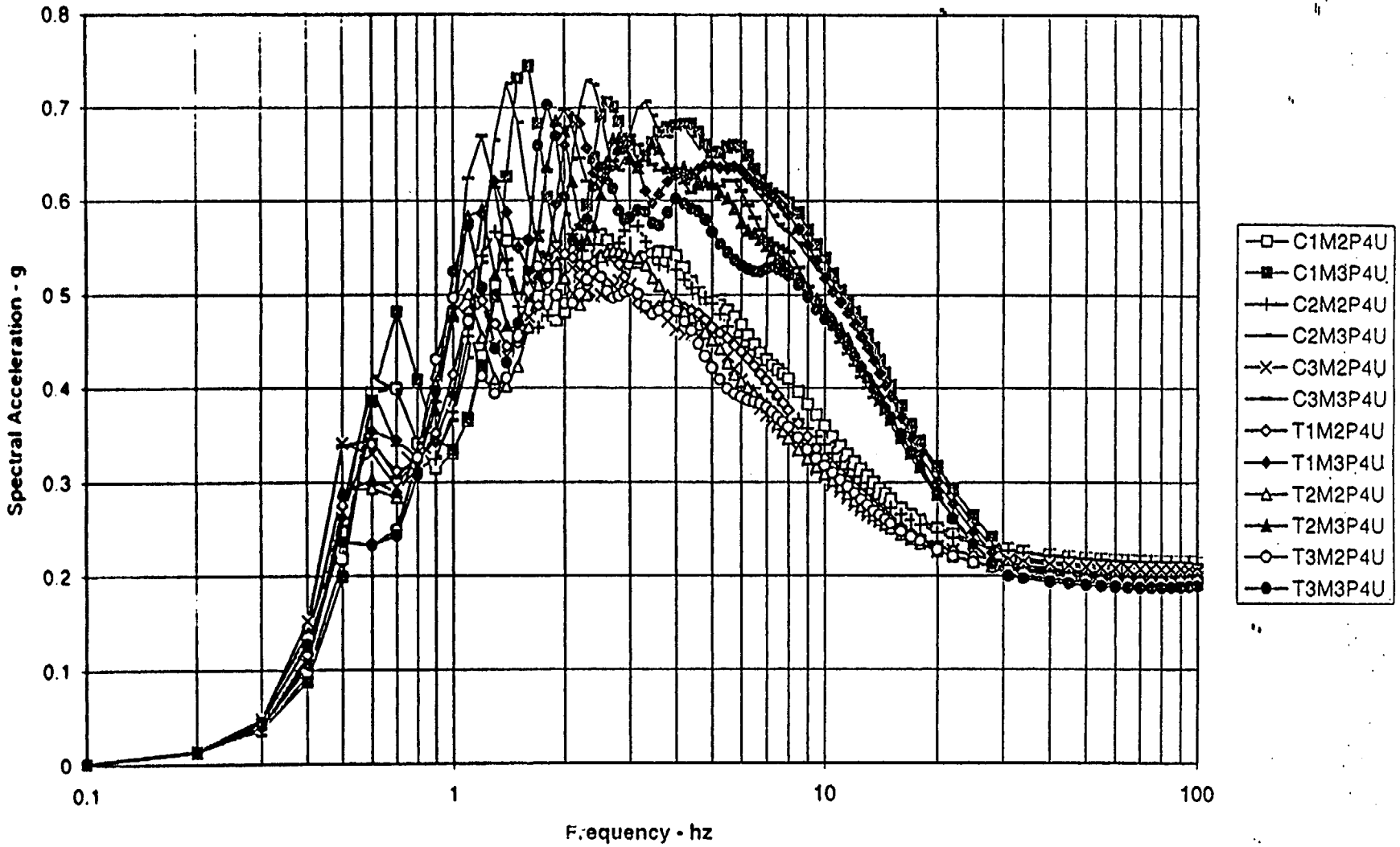

Figure 9.14 - All envelopes of Performance Category 4 5% damped soil response spectra from 1-2.5 Hz and 5-10 Hz mean based scaling of broadened bedrock UHS (PC rock). All soil categories (600-1500 ft) and both types of bedrock (crystalline and Triassic).

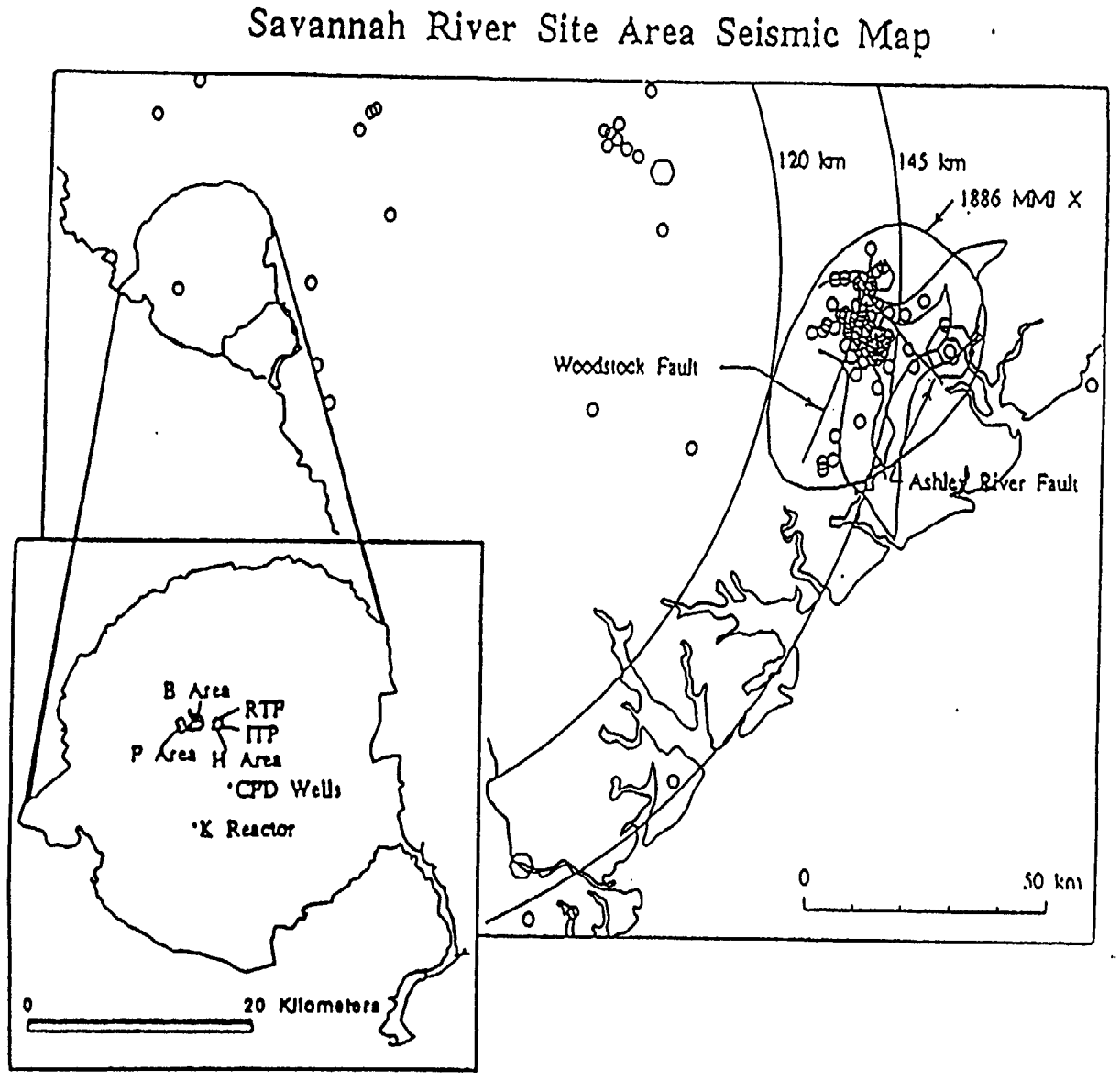

Figure 10.1 - Charleston earthquake distance from SRS. Radii shown are measured from site center. Dark irregular lines are the isoseismals for the Charleston earthquake taken from Dutton (1890).

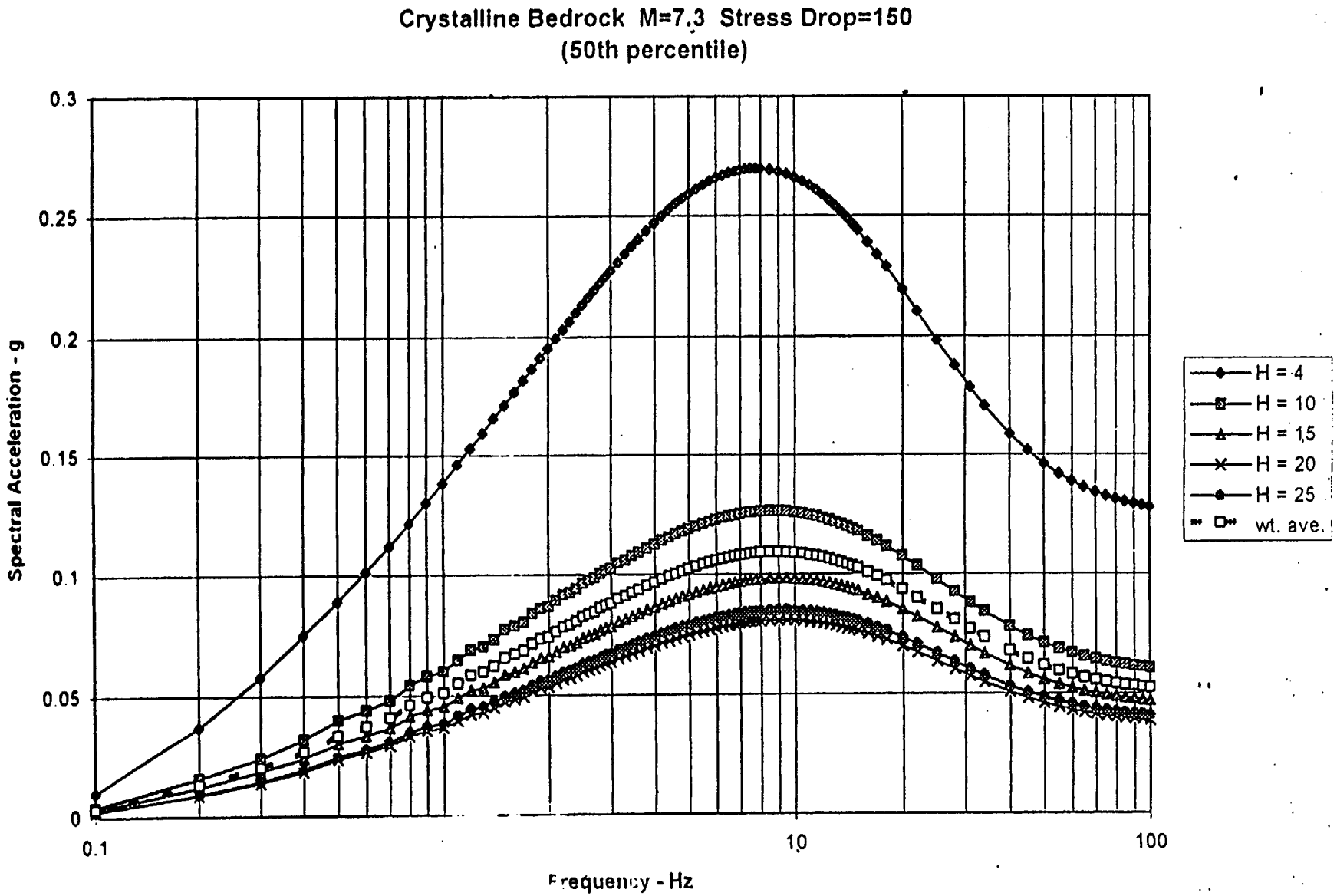

Figure 10.2 - Point-source RVT 5% damped response spectra for Mw 7.3, $\Delta\sigma$ = 150 bars, and R = 120 km. Comparison shown of point-source depths of 4, 10, 15, 20, and 25 km. Weighted average based on vertical distribution of southeastern U.S. hypocenters.

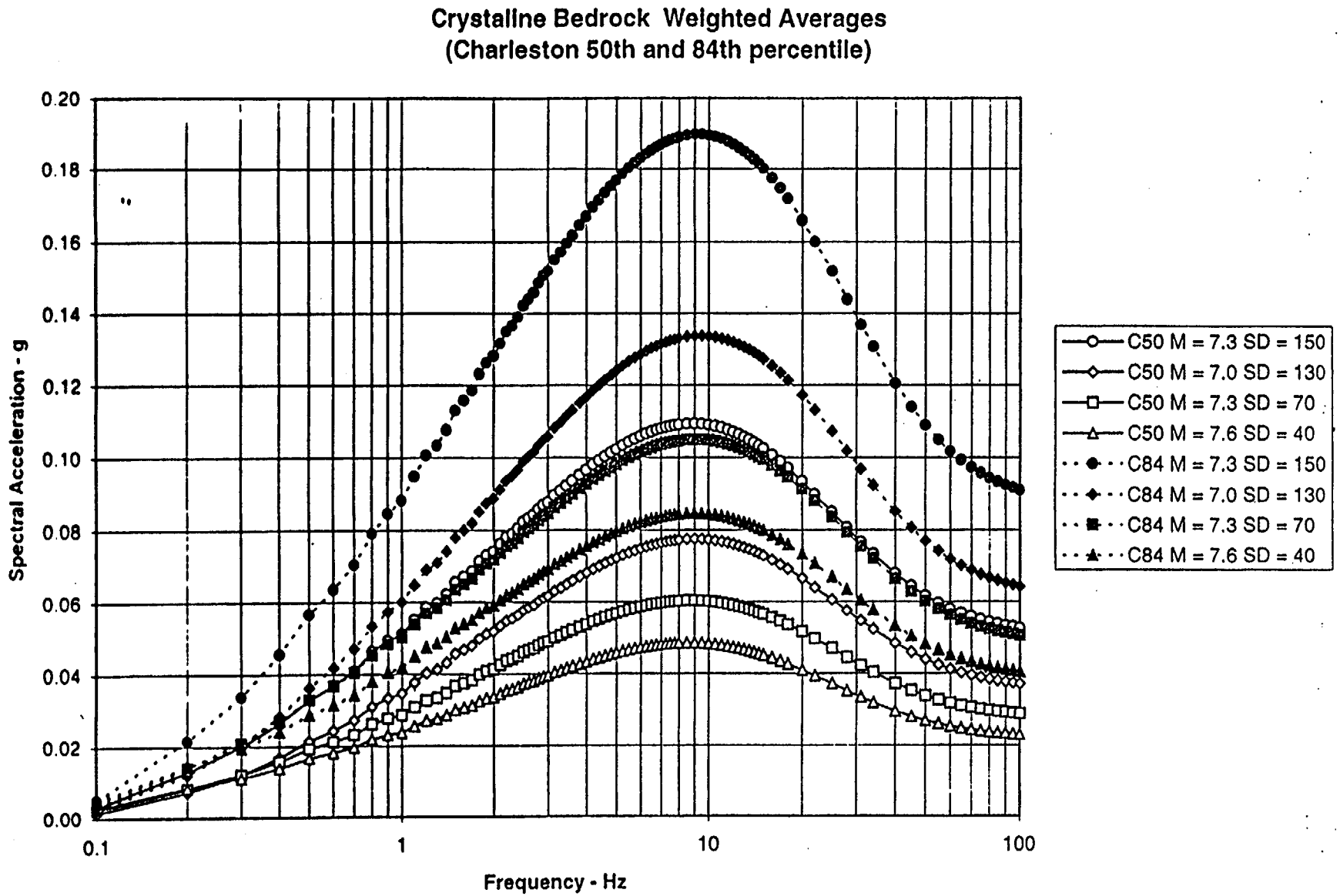

Figure 10.3 - Charleston median and 84th percentile point-source RVT 5% damped bedrock response spectra for the suite of magnitudes and stress-drops considered in this study (Mw 7.3, $\Delta\sigma$ = 150 bars, Mw 7.3, $\Delta\sigma$ = 70 bars, Mw 7.6, $\Delta\sigma$ = 40 bars, Mw 7.0, $\Delta\sigma$ = 130 bars).

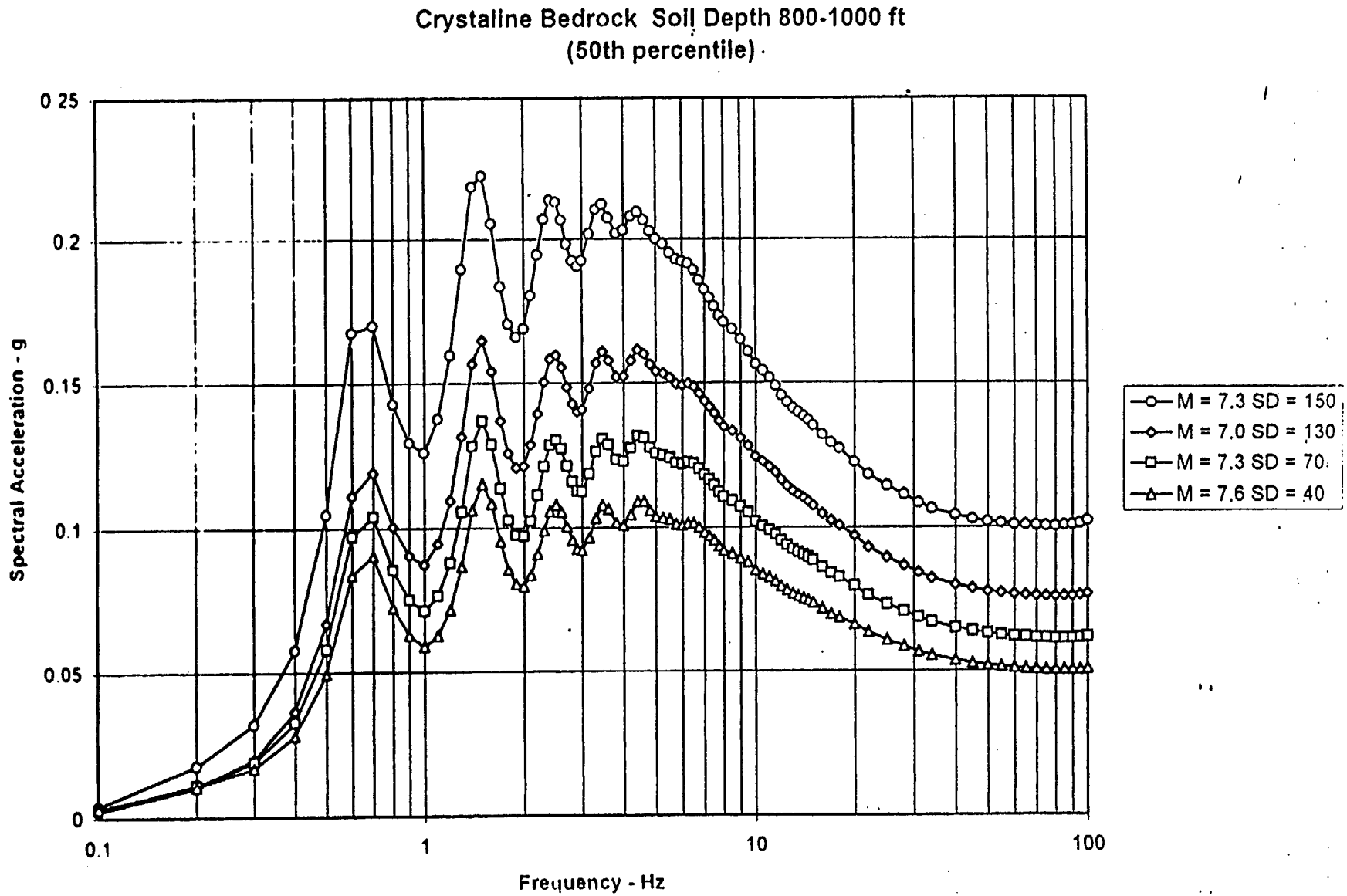

Figure 10.4 - Charleston median 5% damped soil response spectra for the suite of magnitudes and stress-drops considered in this study. Soil depth range is 800-1000 ft over crystalline rock.

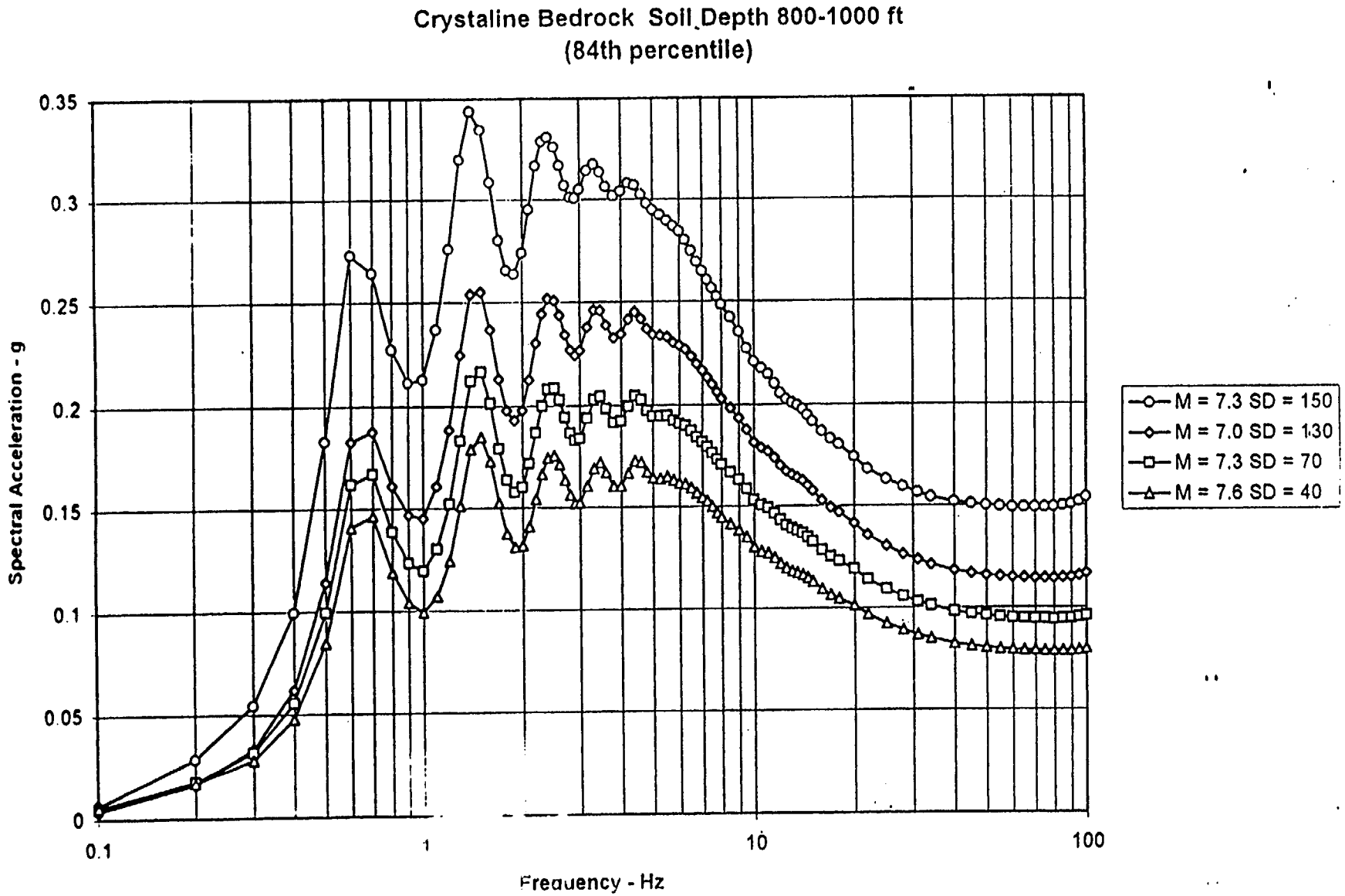

Figure 10.5 - Charleston 84th percentile 5% damped soil response spectra for the suite of magnitudes and stress-drops considered in this study. Soil depth range is 800-1000 ft over crystalline rock.

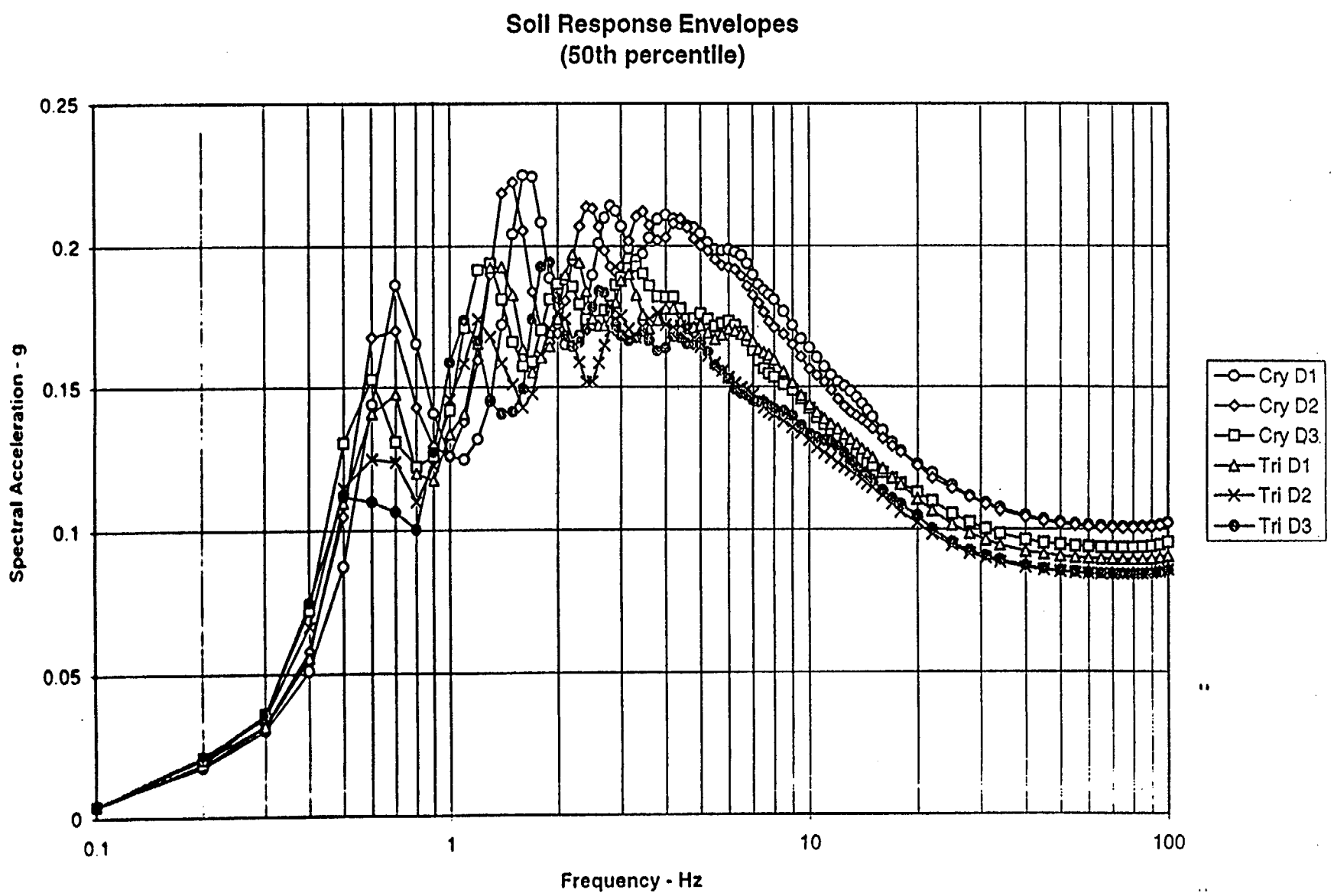

Figure 10 6 - Charleston (Mw 7.3, $\Delta\sigma$ = 150 bars) median 5% damped soil response spectra for all soil categories (D1= 600-800 ft, etc.) and bedrock types (Cry = crystalline, etc.).

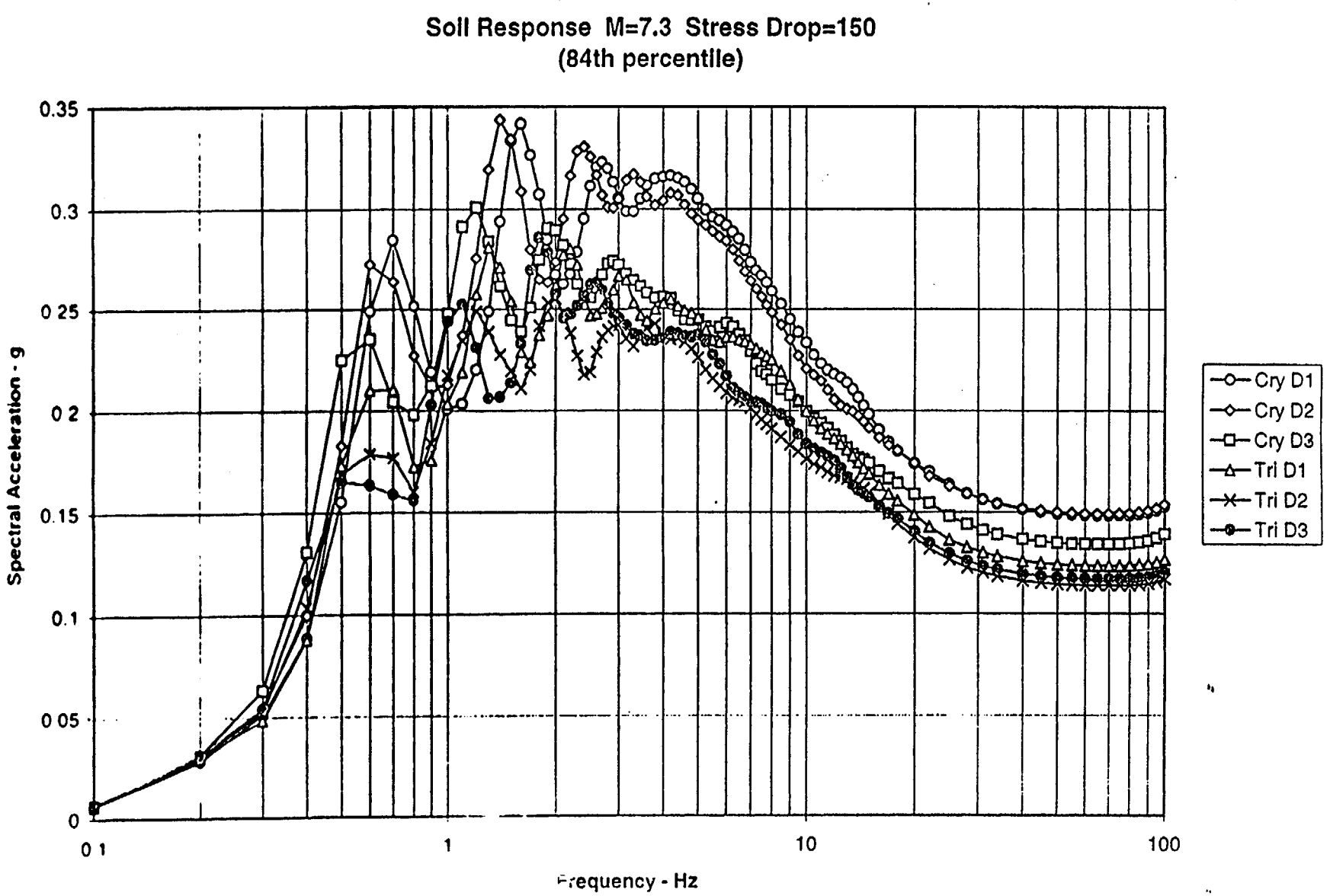

Figure 10.7 - Charleston (Mw 7.3, $\Delta\sigma$ = 150 bars) 84th percentile 5% damped soil response spectra for all soil categories (D1= 600-800 ft, etc.) and bedrock types (Cry = crystalline, etc.).

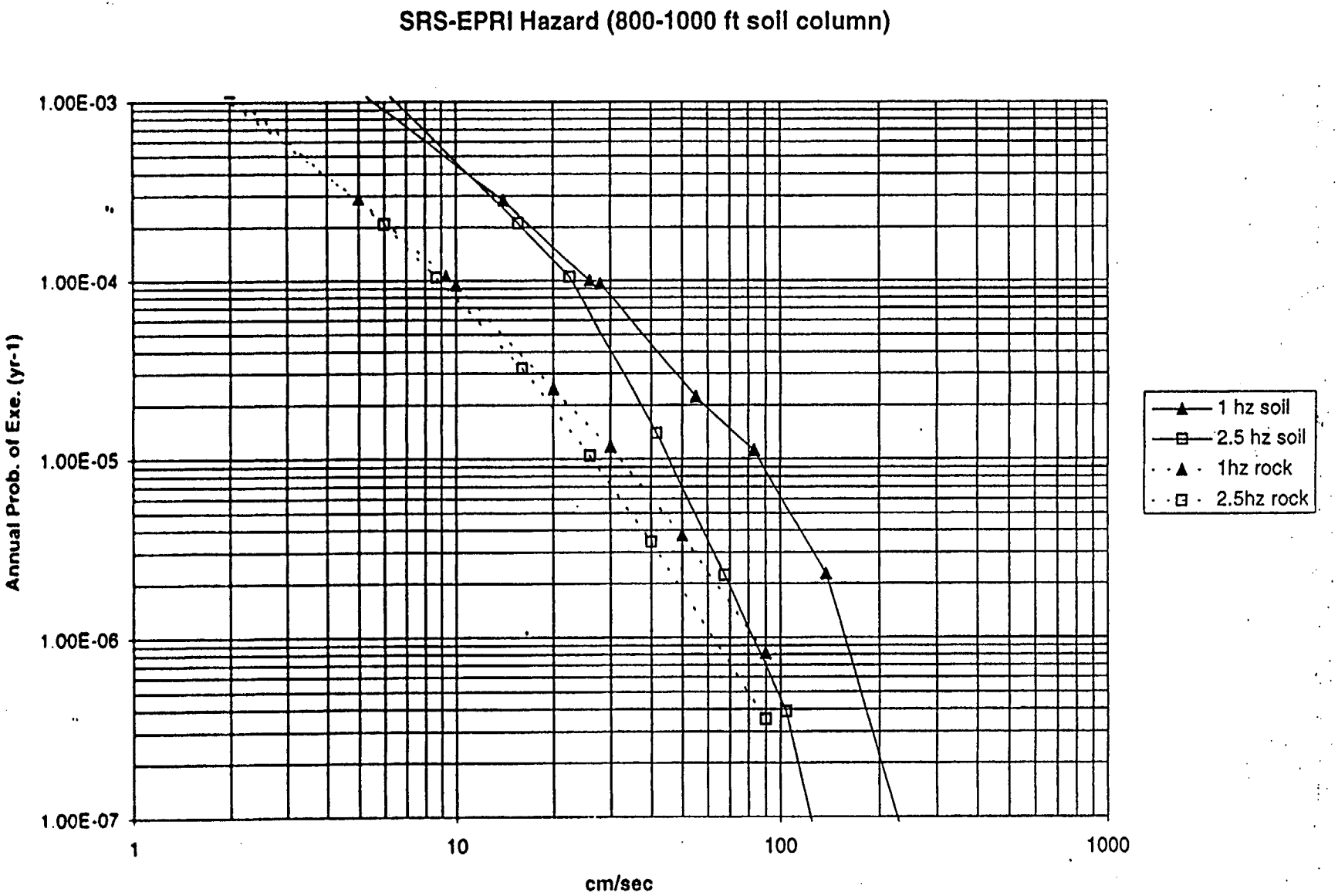

Figure 11.1 - EPRI annual probability of exceedence vs. 5% damped spectral velocity for SRS bedrock (dashed lines for both 1 and 2.5 Hz). Computed soil hazard results for soil category 2 (800-1000 ft) over crystalline bedrock (solid lines for both 1 and 2.5 Hz).

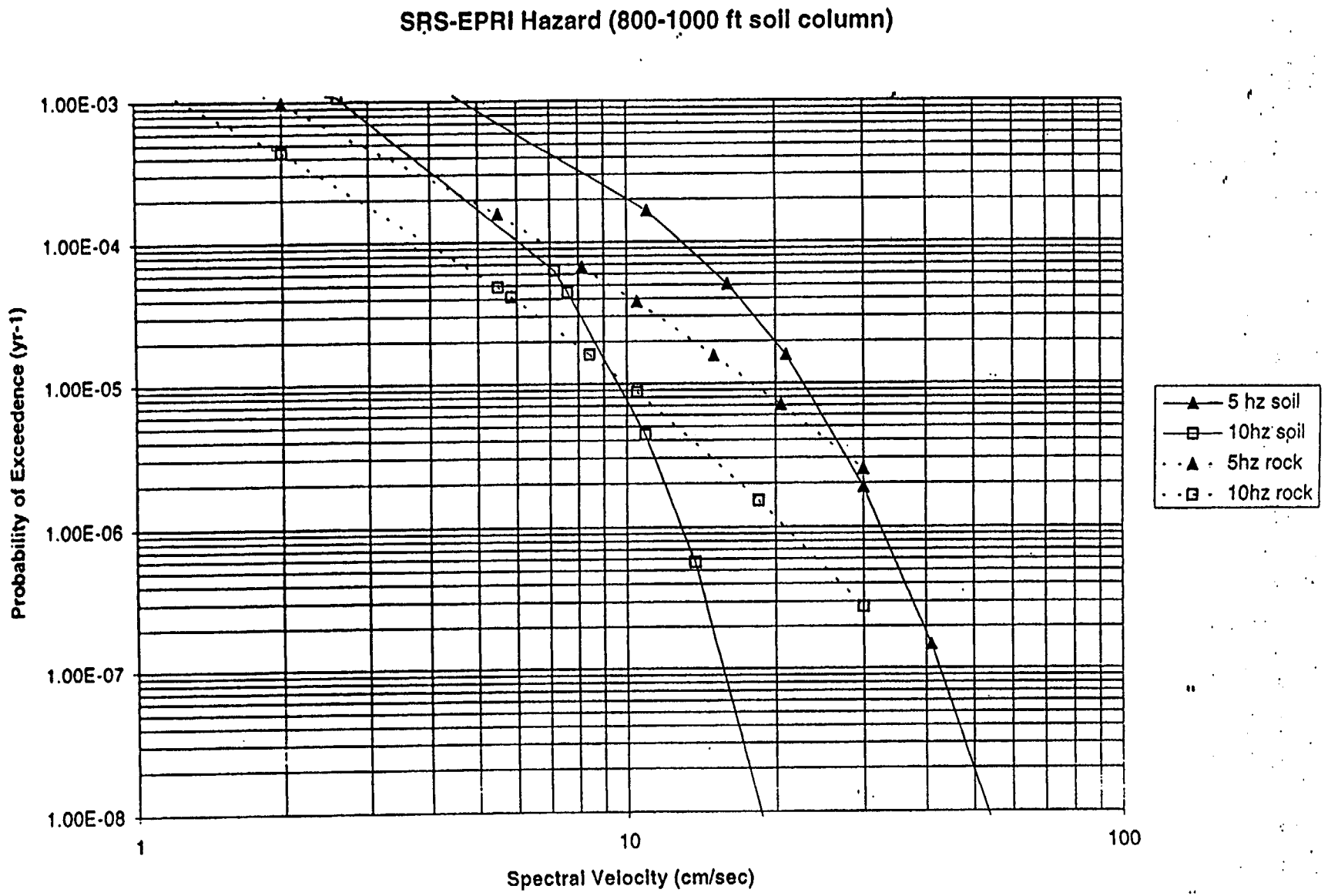

Figure 11.2 - EPRI annual probability of exceedence vs. 5% damped spectral velocity for SRS bedrock (dashed lines for both 5 and 10 Hz). Computed soil hazard results for soil category 2 (800-1000 ft) over crystalline bedrock (solid lines for both 5 and 10 Hz).

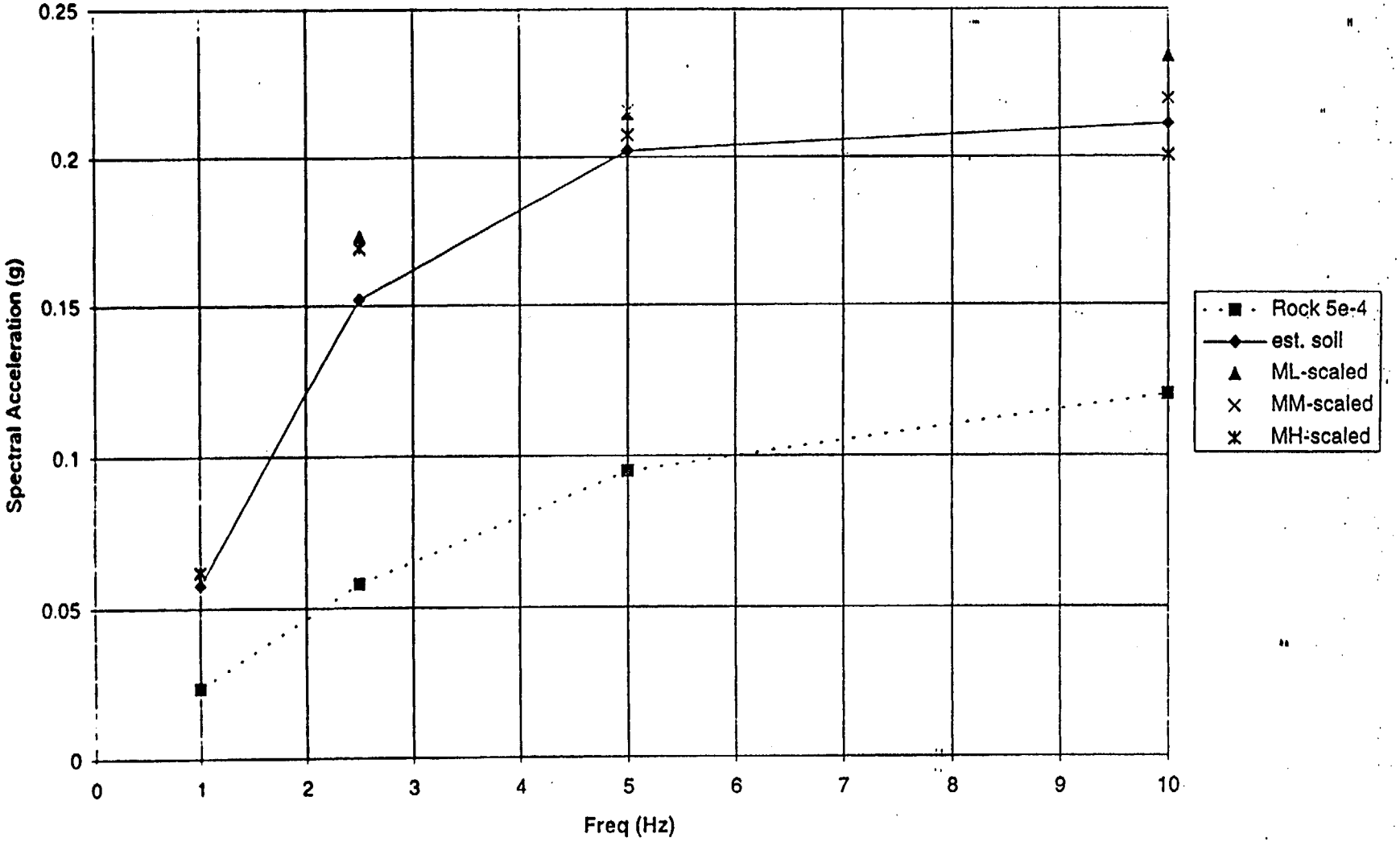

Figure 11.3 - EPRI bedrock UHS for annual probability of exceedance of 5×10^{-4} (dashed line) and the computed soil UHS (solid line) for the 800-1000 ft soil column overlying crystalline rock. The UHS were obtained by linear interpolation of the soil hazard curves (Figures 11.1 and 11.2). Values of the mean-based scaling of the bedrock UHS (Methodology of Section 9) are shown as unconnected symbols (ML-, MM-, and MH-scaled).

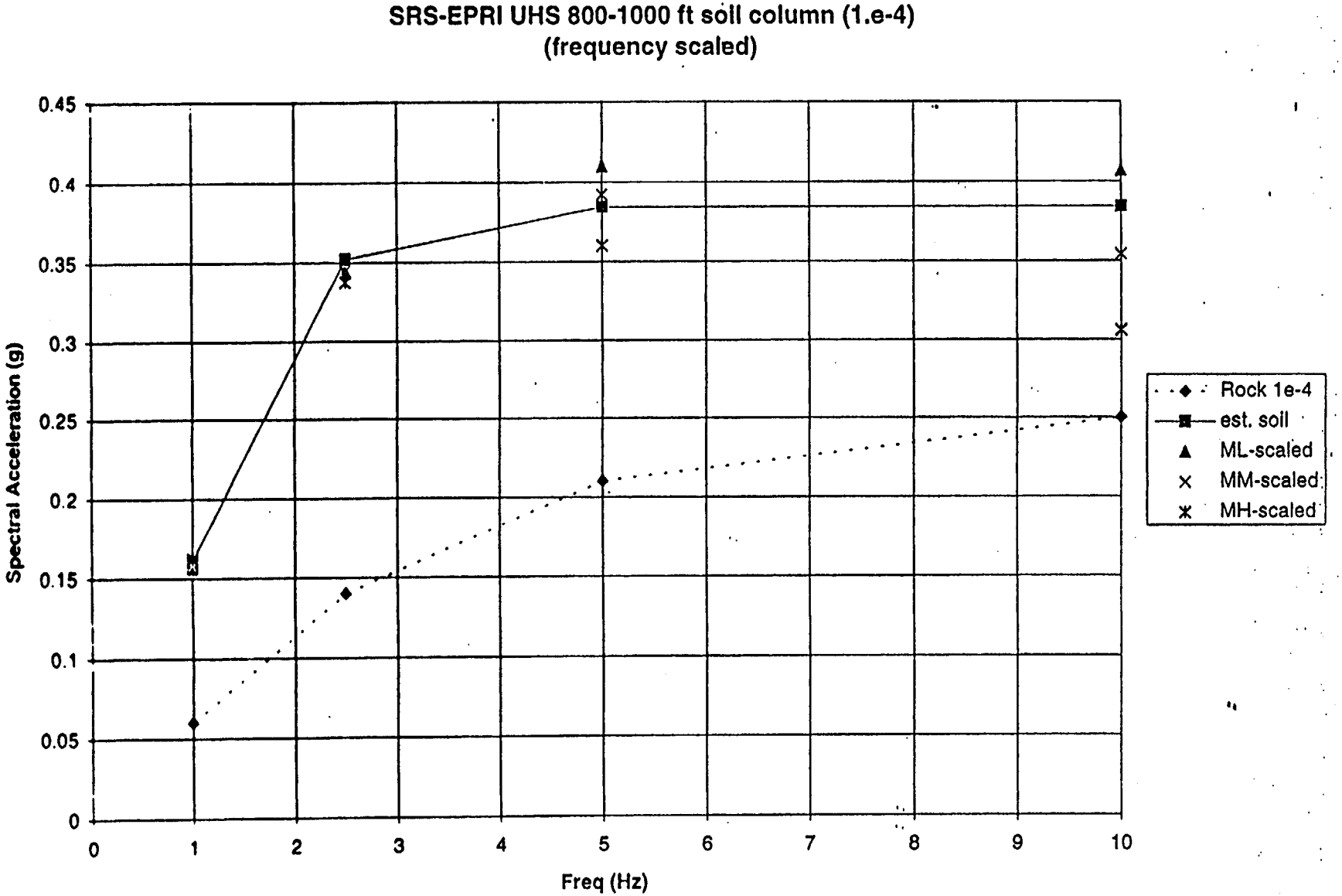

Figure 11.4 - EPRI bedrock UHS for annual probability of exceedance of $1x10^{-4}$ (dashed line) and the computed soil UHS (solid line) for soil category 2 (800-1000 ft) overlying crystalline rock. The UHS were obtained by linear interpolation of the soil hazard curves (Figures 11.1 and 11.2). Values of the mean-based scaling of the bedrock UHS (Methodology of Section 9) are shown as unconnected symbols (ML-, MM-, and MH-scaled).

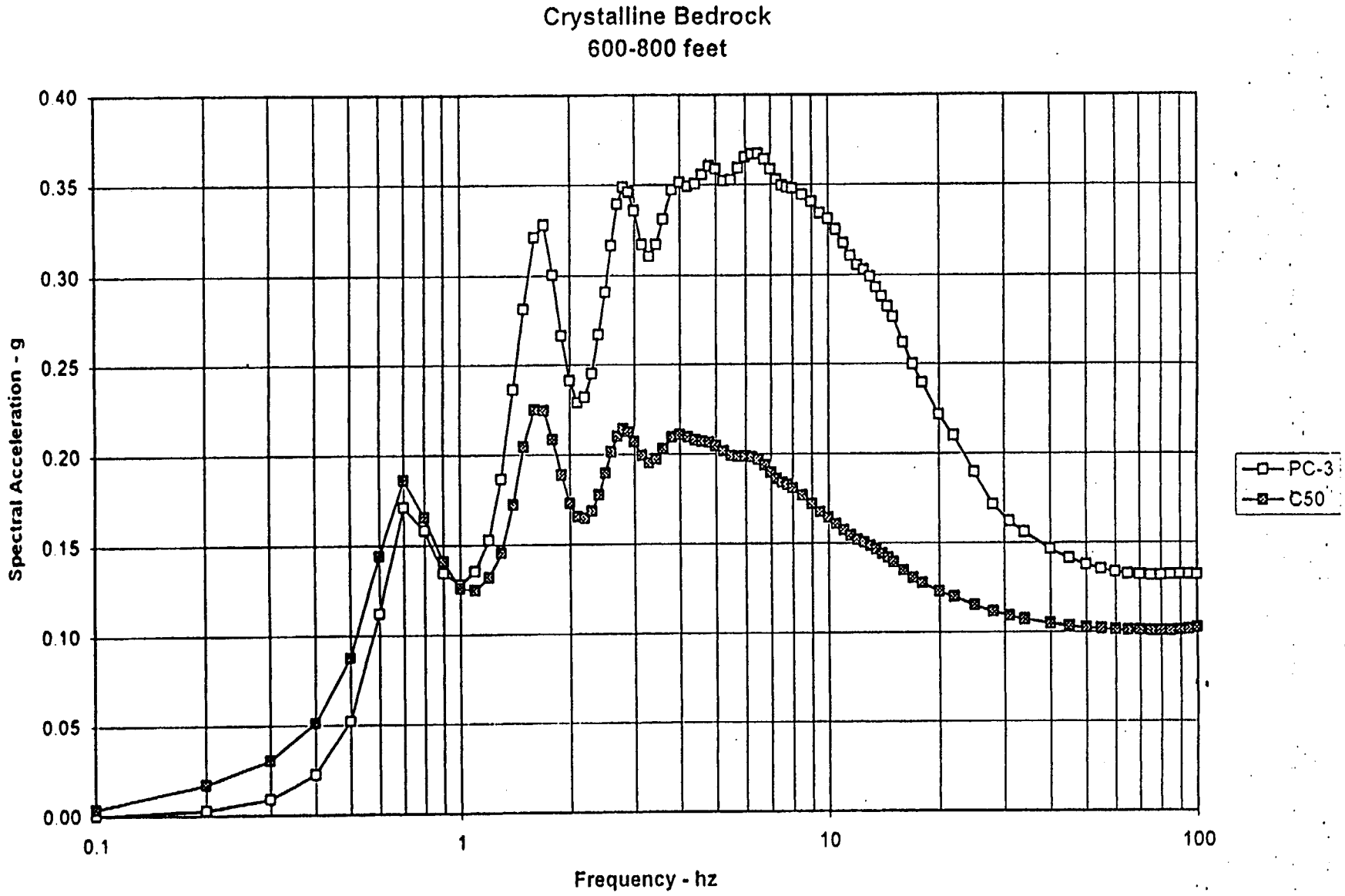

Figure 13.1 - Comparison of envelope of mean UHS Performance Category 3 soil response spectra to Charleston 50th percentile deterministic response spectrum for crystalline bedrock, soil category 1 (600-800 ft) 5% damping.

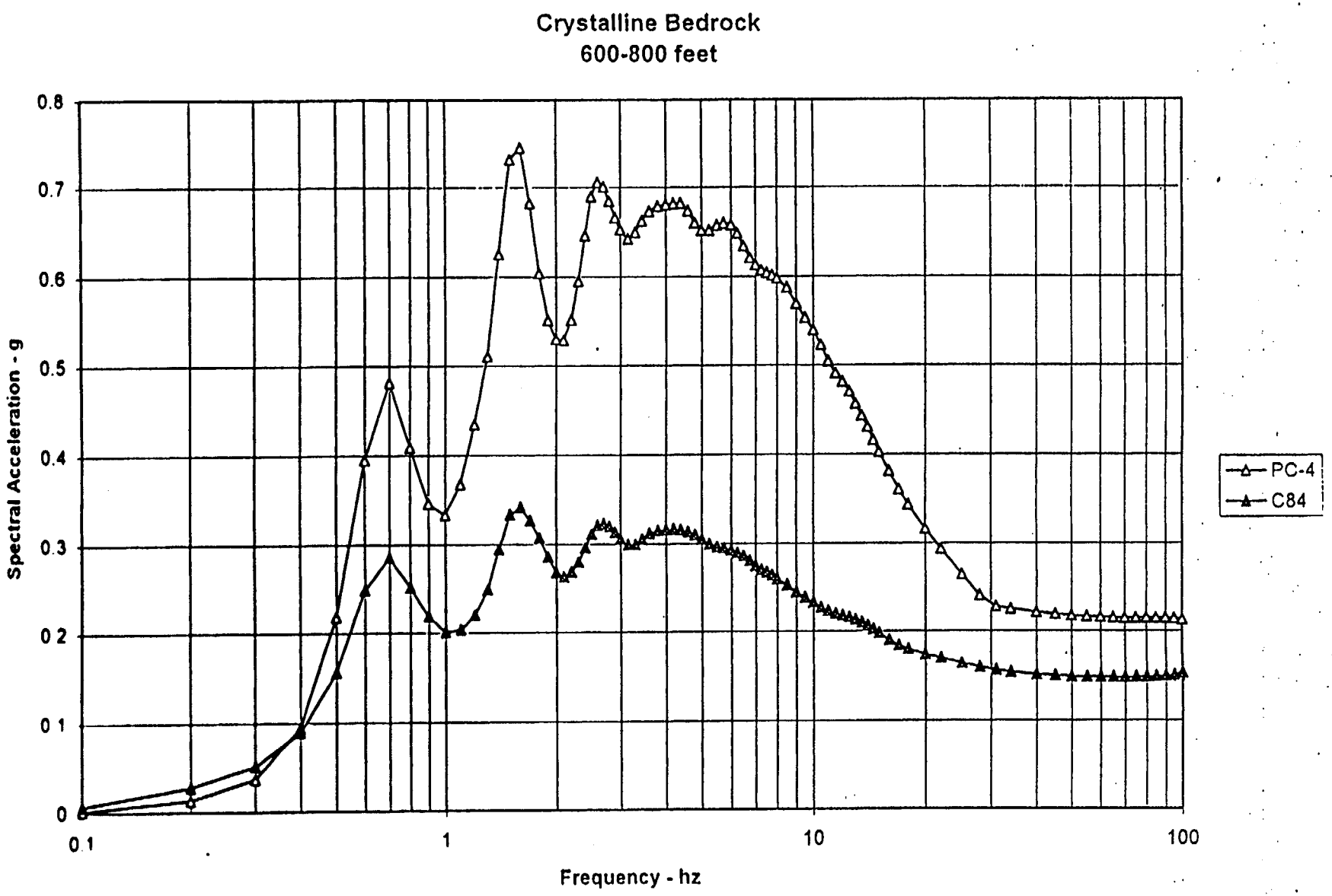

Figure 13 2 - Comparison of envelope of mean UHS Performance Category 4 soil response spectra to Charleston 84th percentile deterministic response spectrum for crystalline bedrock, soil category 1 (600-800 ft) 5% damping.

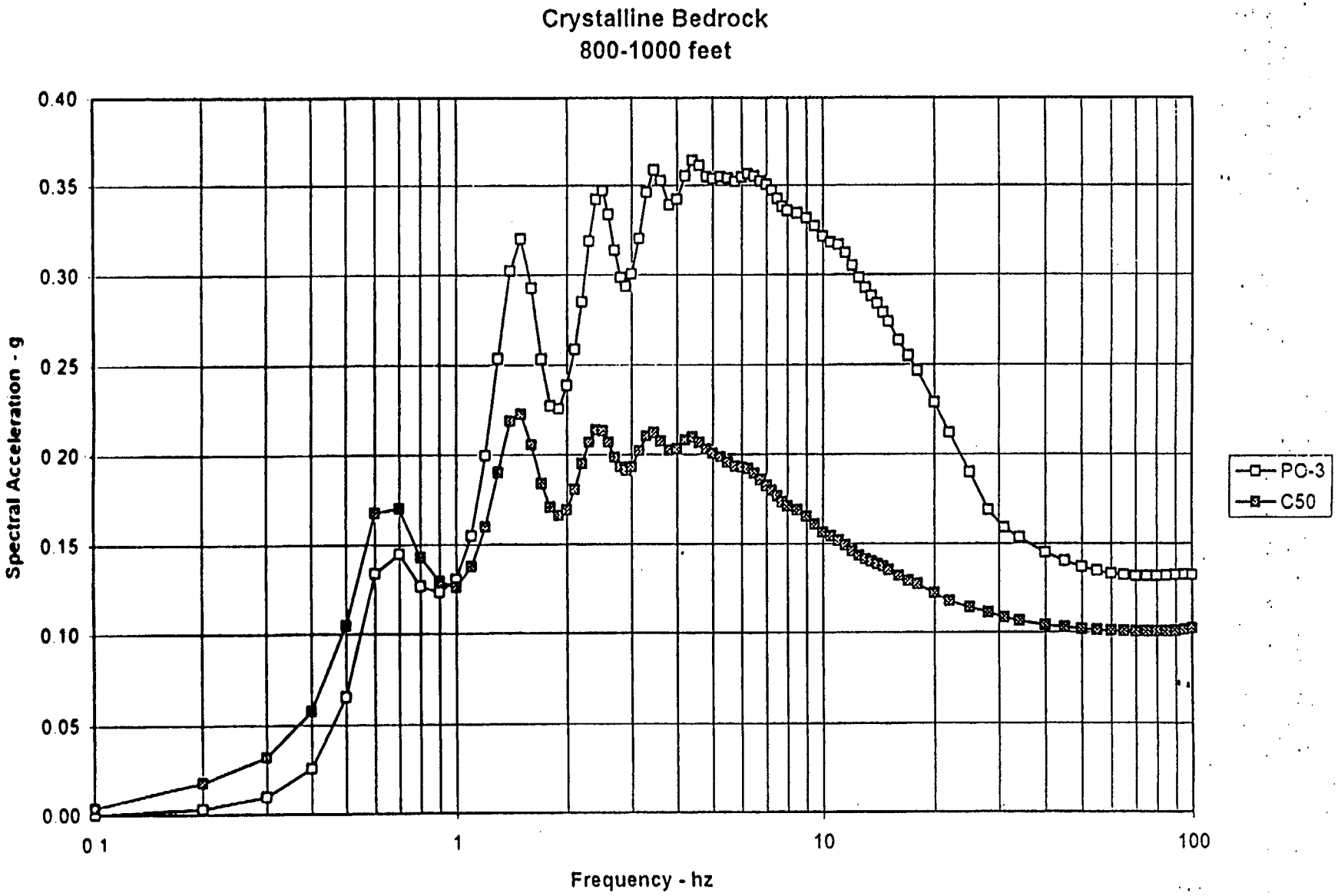

Figure 13.3 - Comparison of envelope of mean UHS Performance Category 3 soil response spectra to Charleston 50th percentile deterministic response spectrum for crystalline bedrock, soil category 2 (800-1000 ft) 5% damping.

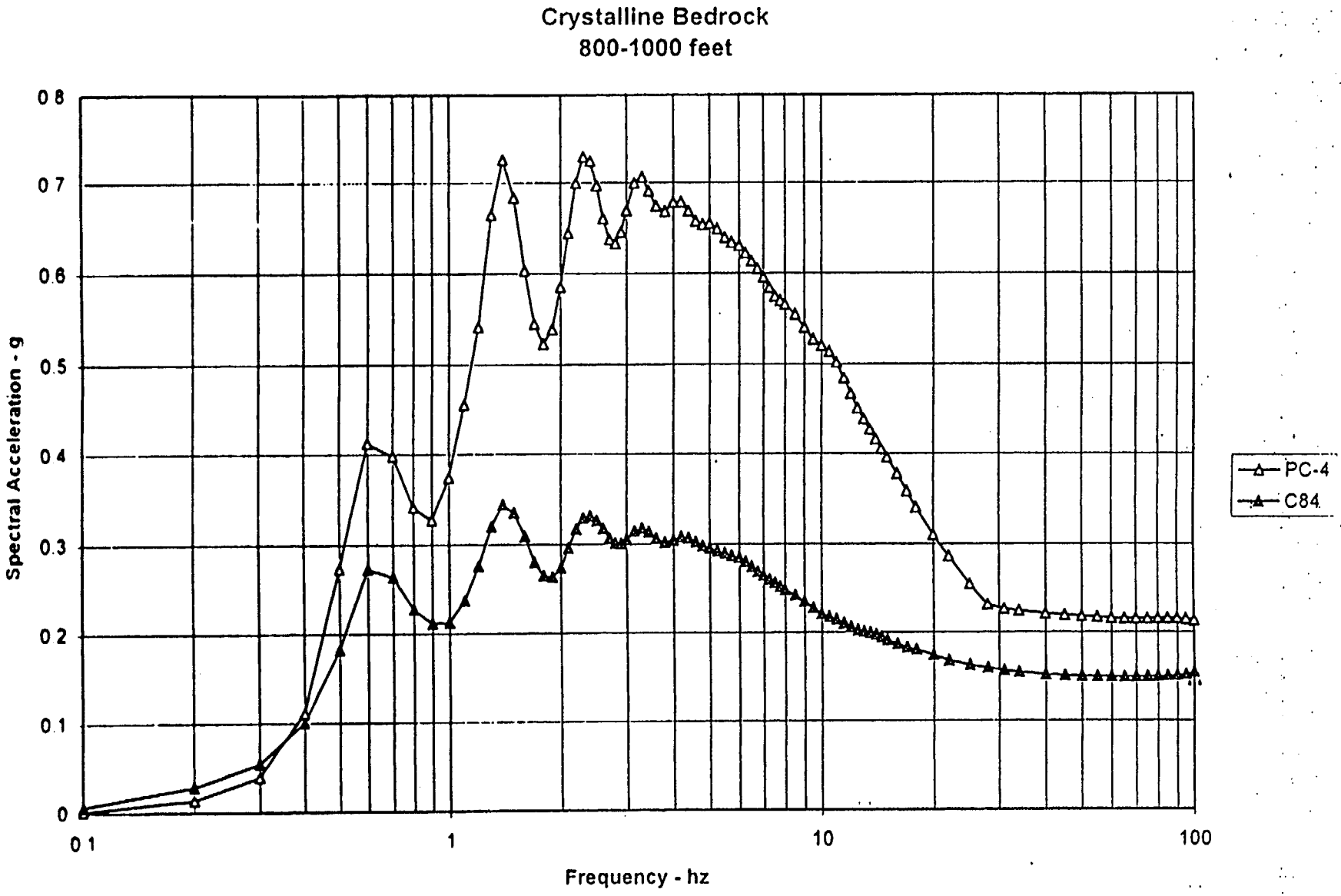

Figure 13 4 - Comparison of envelope of mean UHS Performance Category 4 soil response spectra to Charleston 84th percentile deterministic response spectrum for crystalline bedrock, soil category 2 (800-1000 ft) 5% damping.

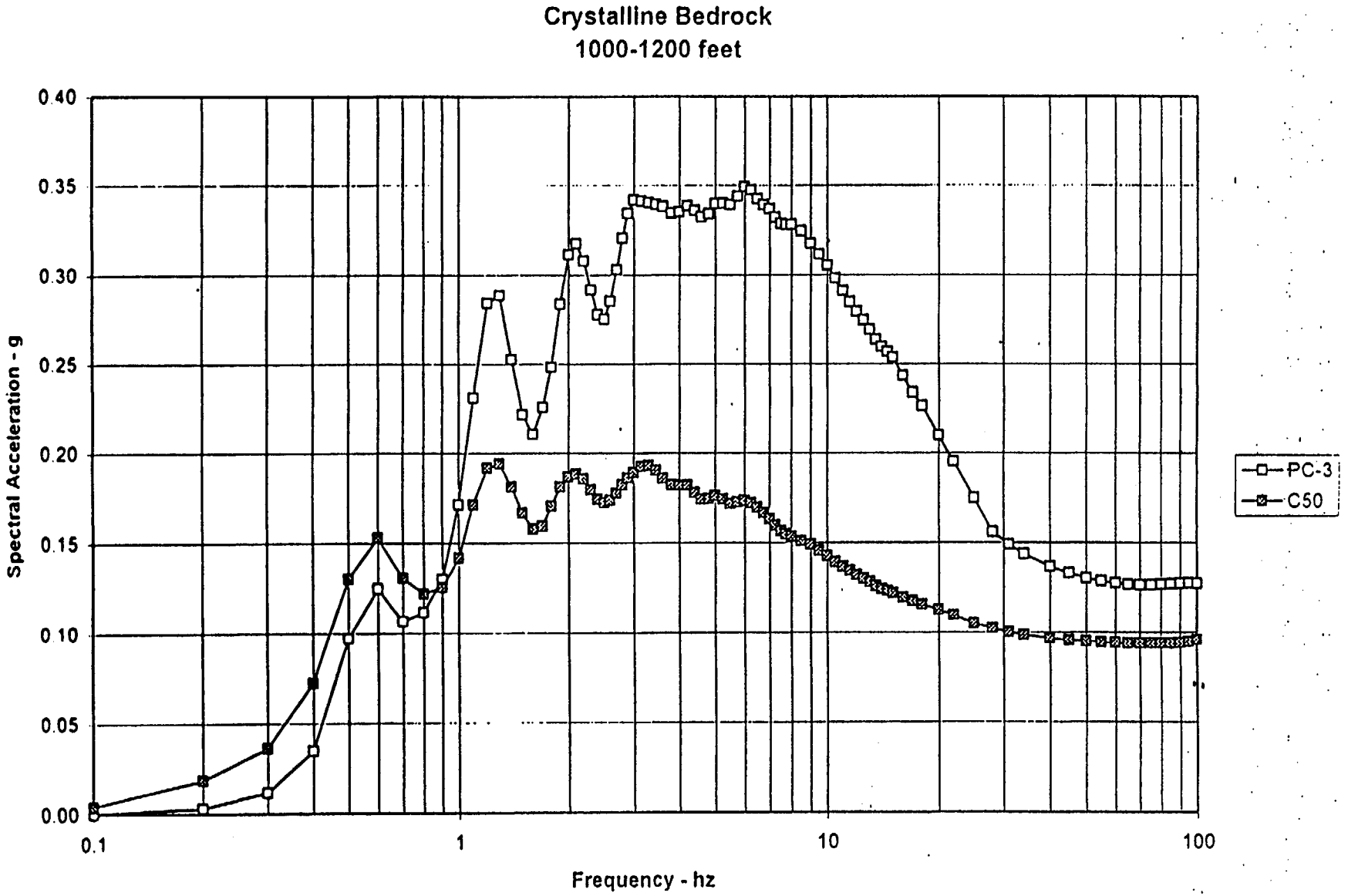

Figure 13.5 - Comparison of envelope of mean UHS Performance Category 3 soil response spectra to Charleston 50th percentile deterministic response spectrum for crystalline bedrock, soil category 3 (1000-1200 ft) 5% damping.

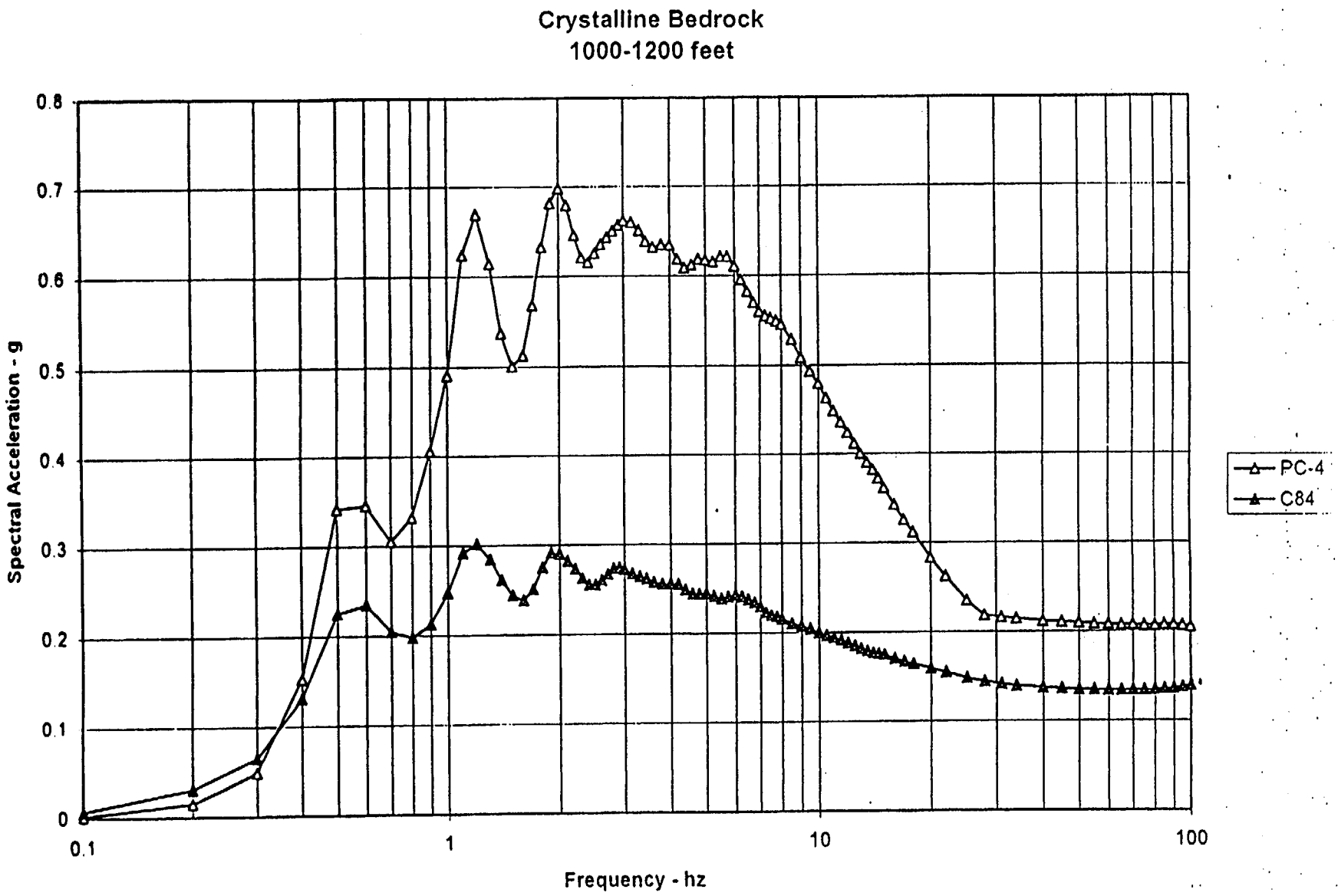

Figure 13.6 - Comparison of envelope of mean UHS Performance Category 4 soil response spectra to Charleston 84th percentile deterministic response spectrum for crystalline bedrock, soil category 3 (1000-1200 ft) 5% damping.

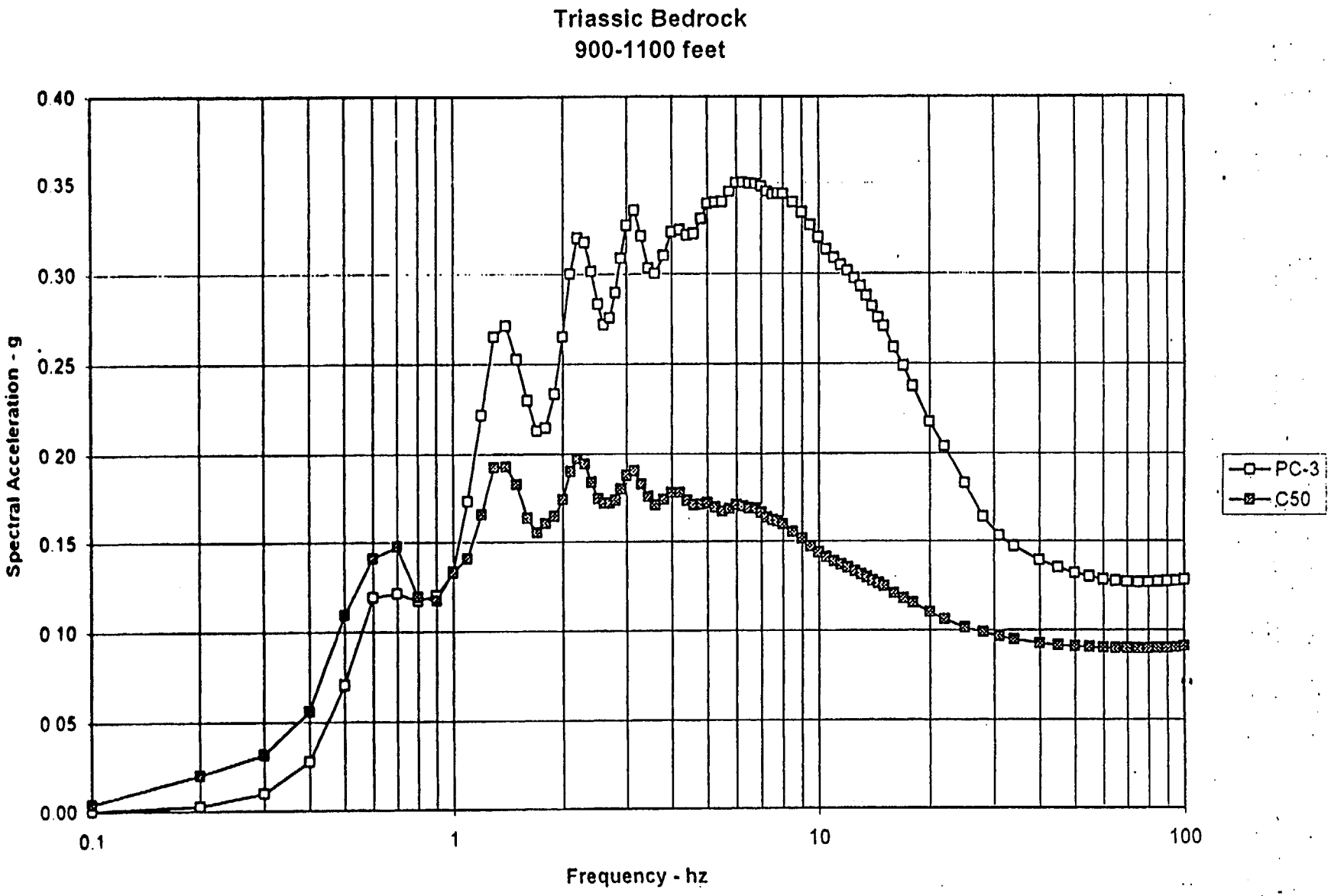

Figure 13.7 - Comparison of envelope of mean UHS Performance Category 3 soil response spectra to Charleston 50th percentile deterministic response spectrum for Triassic bedrock, soil category 1 (900-1100 ft) 5% damping.

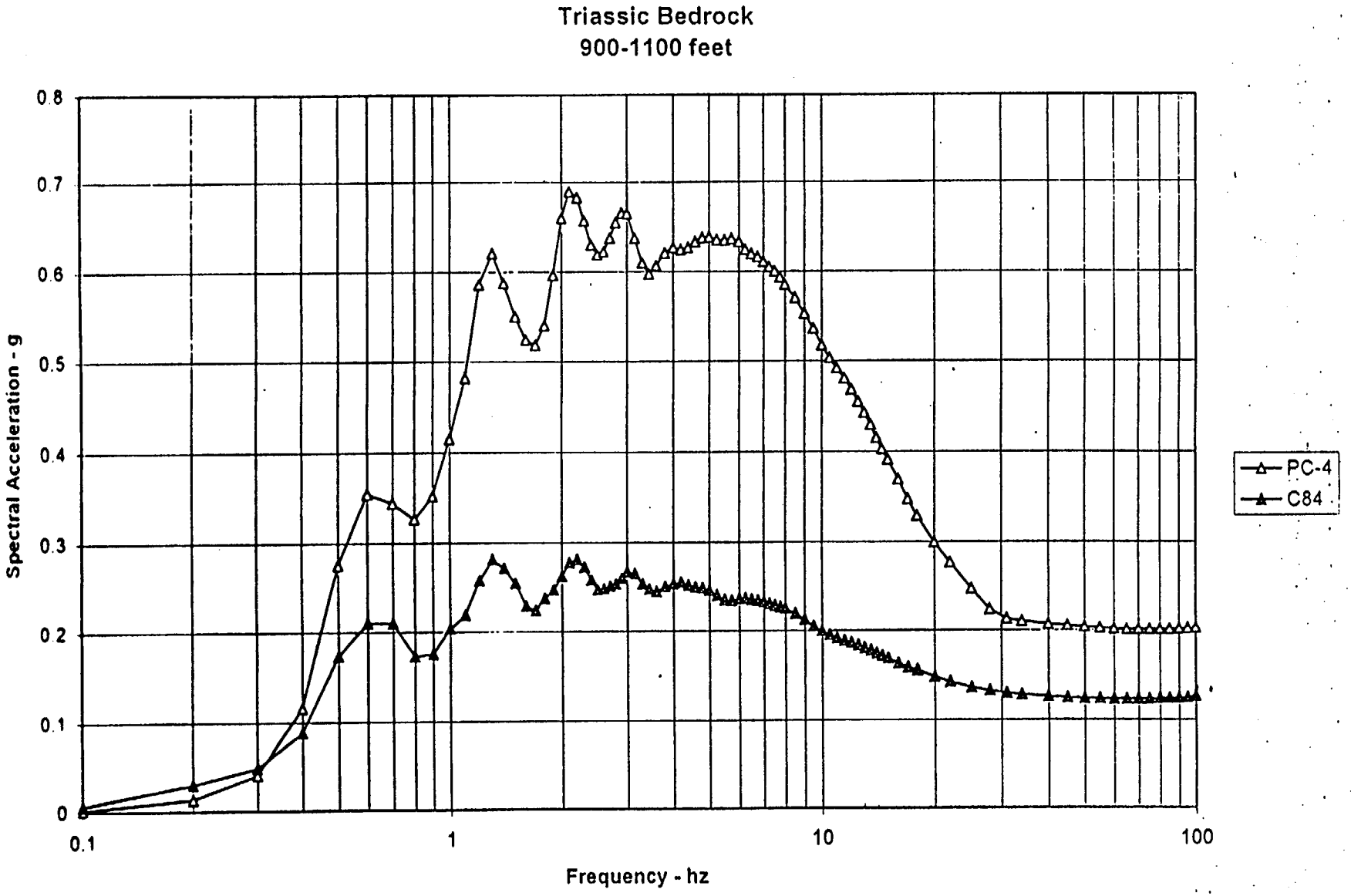

Figure 13.8 - Comparison of envelope of mean UHS Performance Category 4 soil response spectra to Charleston 84th percentile deterministic response spectrum for Triassic bedrock, soil category 1 (900-1100 ft) 5% damping.

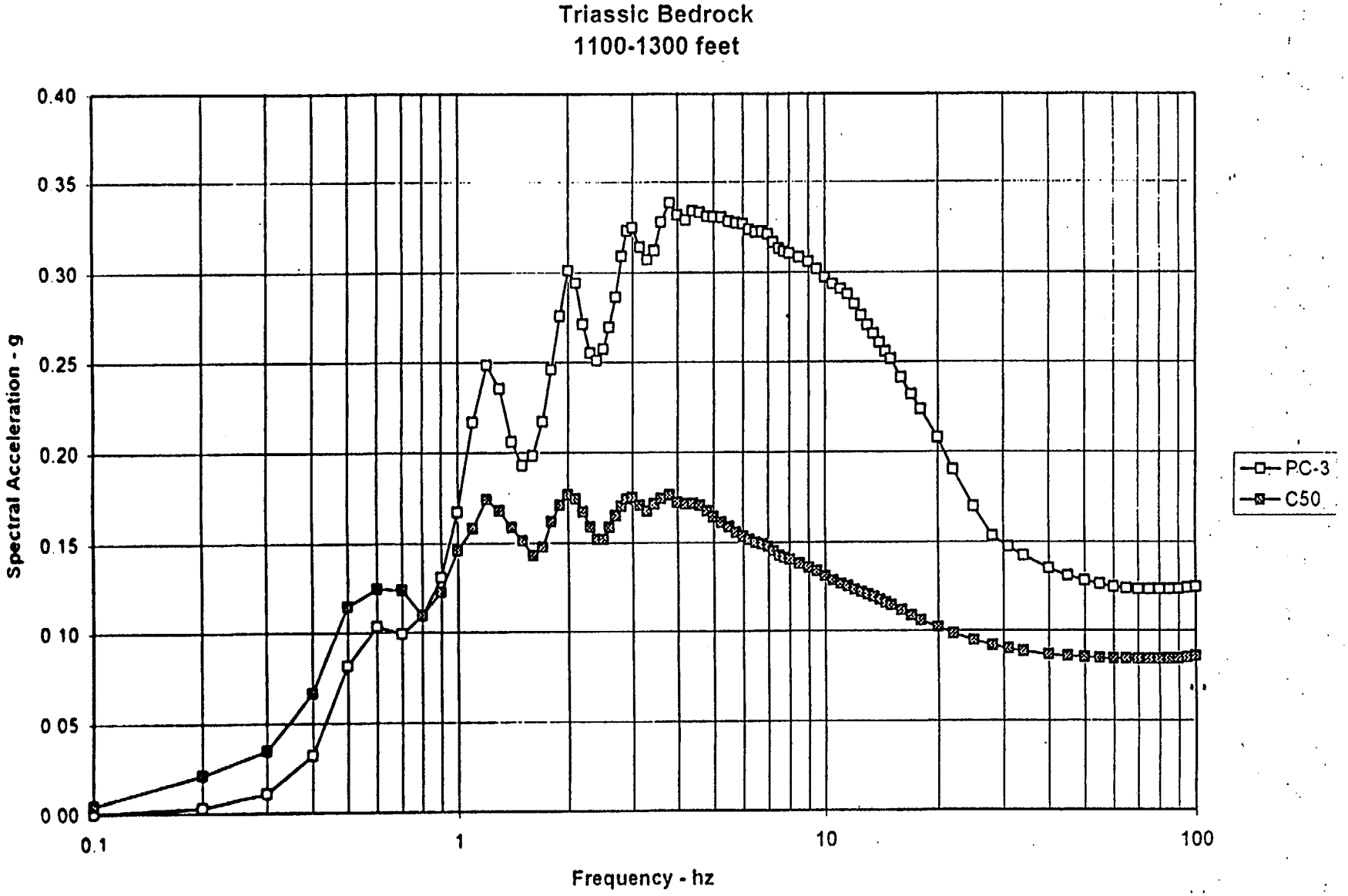

Figure 13 9 - Comparison of envelope of mean UHS Performance Category 3 soil response spectra to Charleston 50th percentile deterministic response spectrum for Triassic bedrock, soil category 2 (1100-1300 ft) 5% damping.

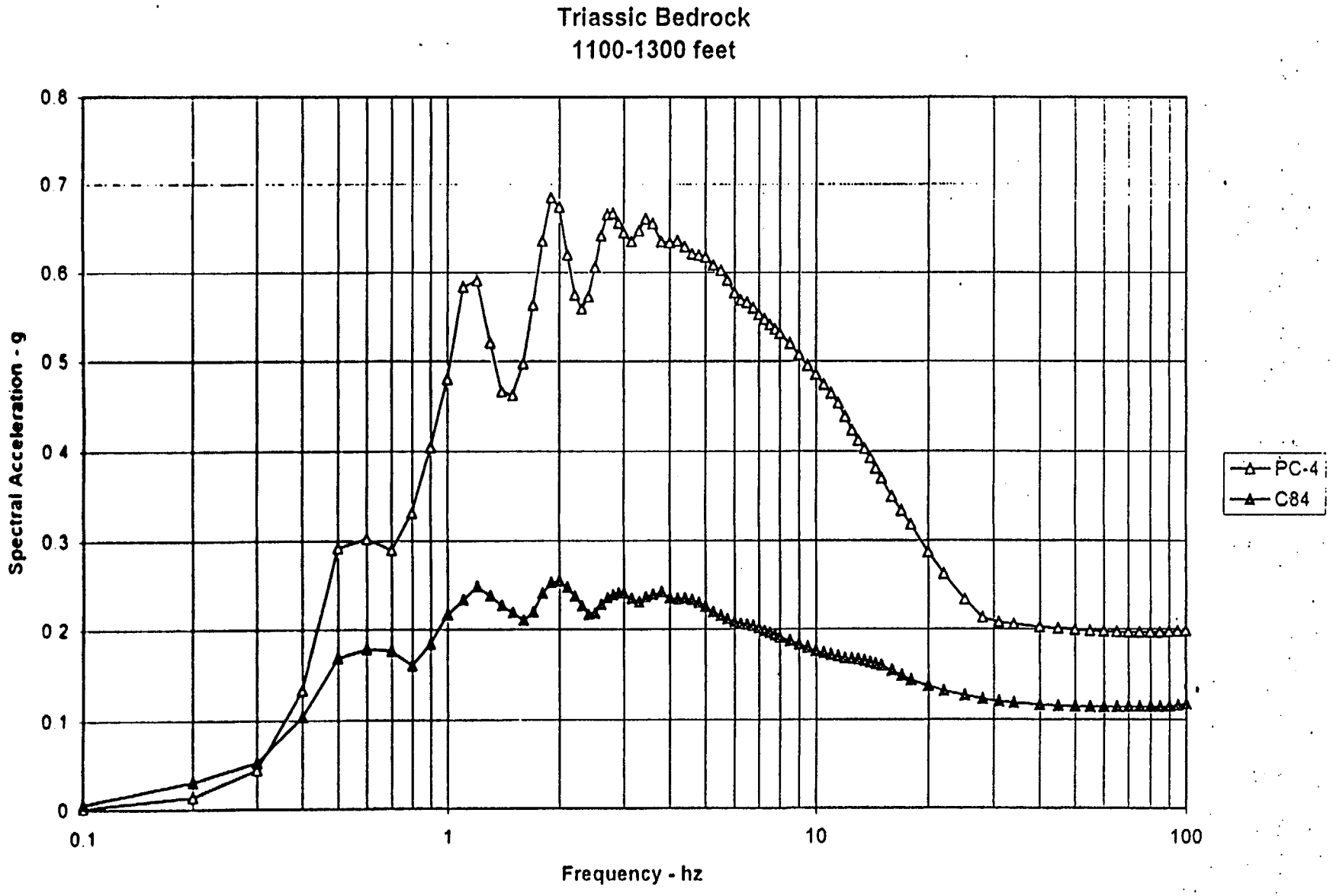

Figure 13 10 - Comparison of envelope of mean UHS Performance Category 4 soil response spectra to Charleston 84th percentile deterministic response spectrum for Triassic bedrock, soil category 2 (1100-1300 ft) 5% damping.

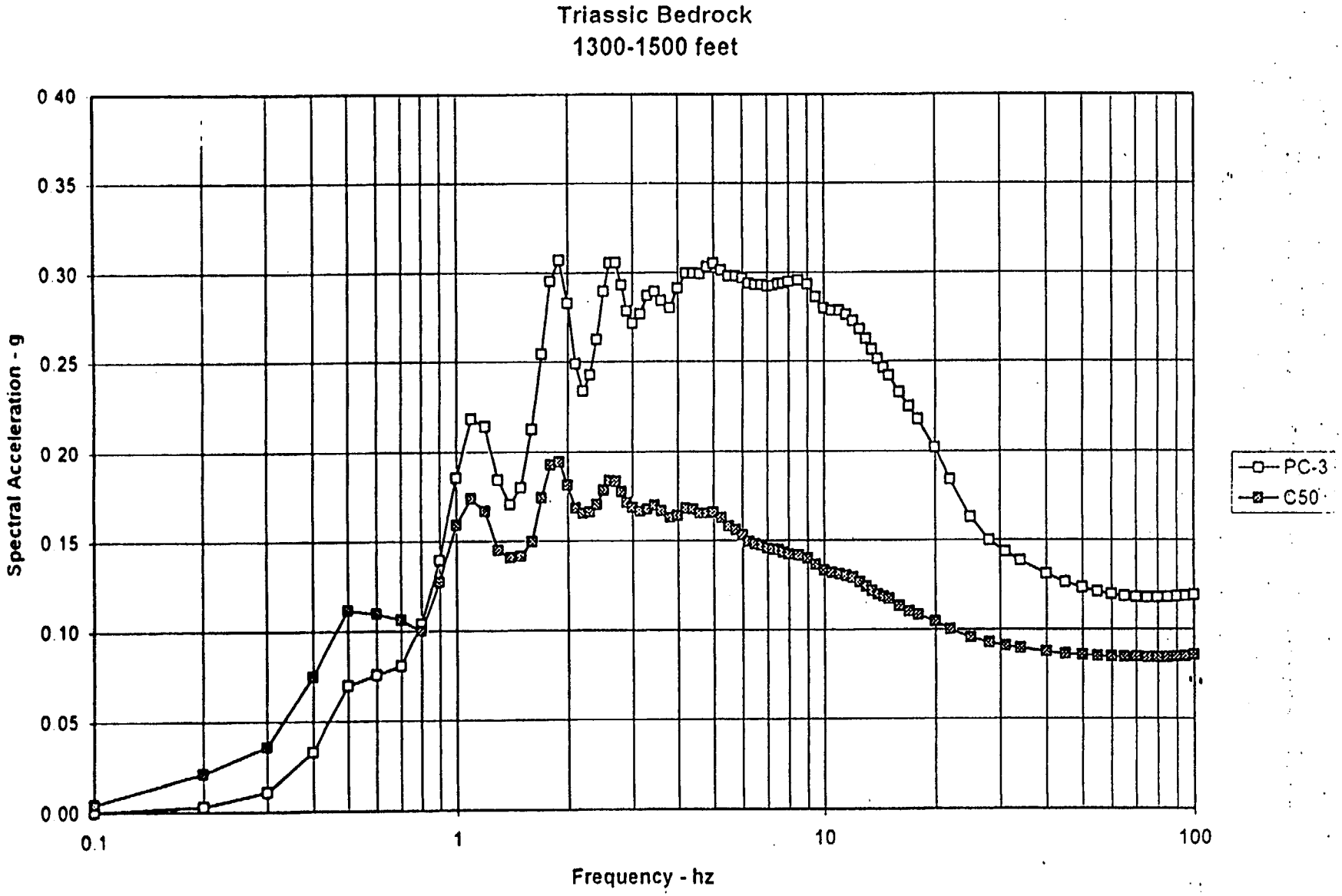

Figure 13.11 - Comparison of envelope of mean UHS Performance Category 3 soil response spectra to Charleston 50th percentile deterministic response spectrum for Triassic bedrock, soil category 3 (1300-1500 ft) 5% damping.

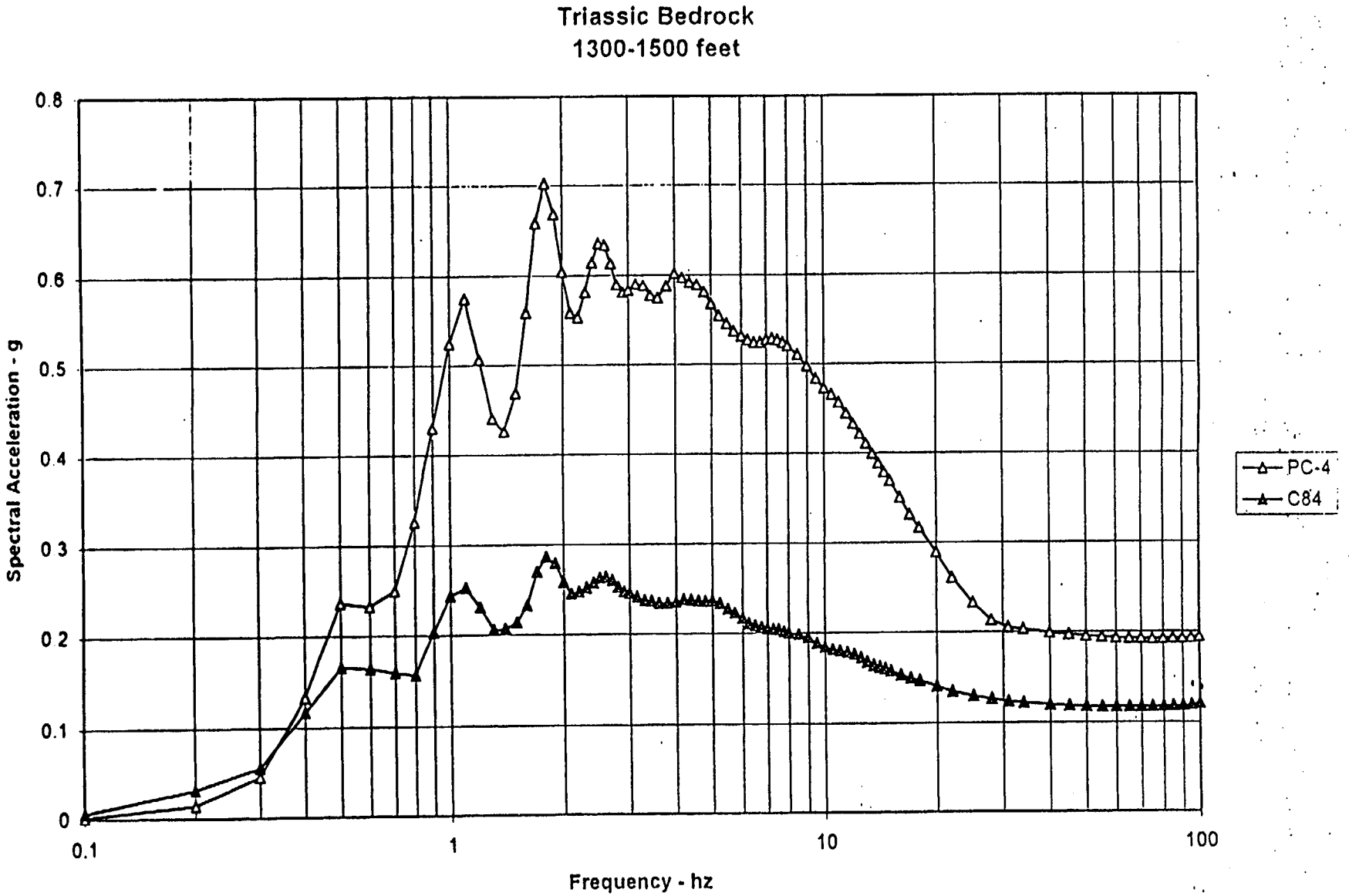

Figure 13.12 - Comparison of envelope of mean UHS Performance Category 4 soil response spectra to Charleston 84th percentile deterministic response spectrum for Triassic bedrock, soil category 3 (1300-1500 ft) 5% damping.

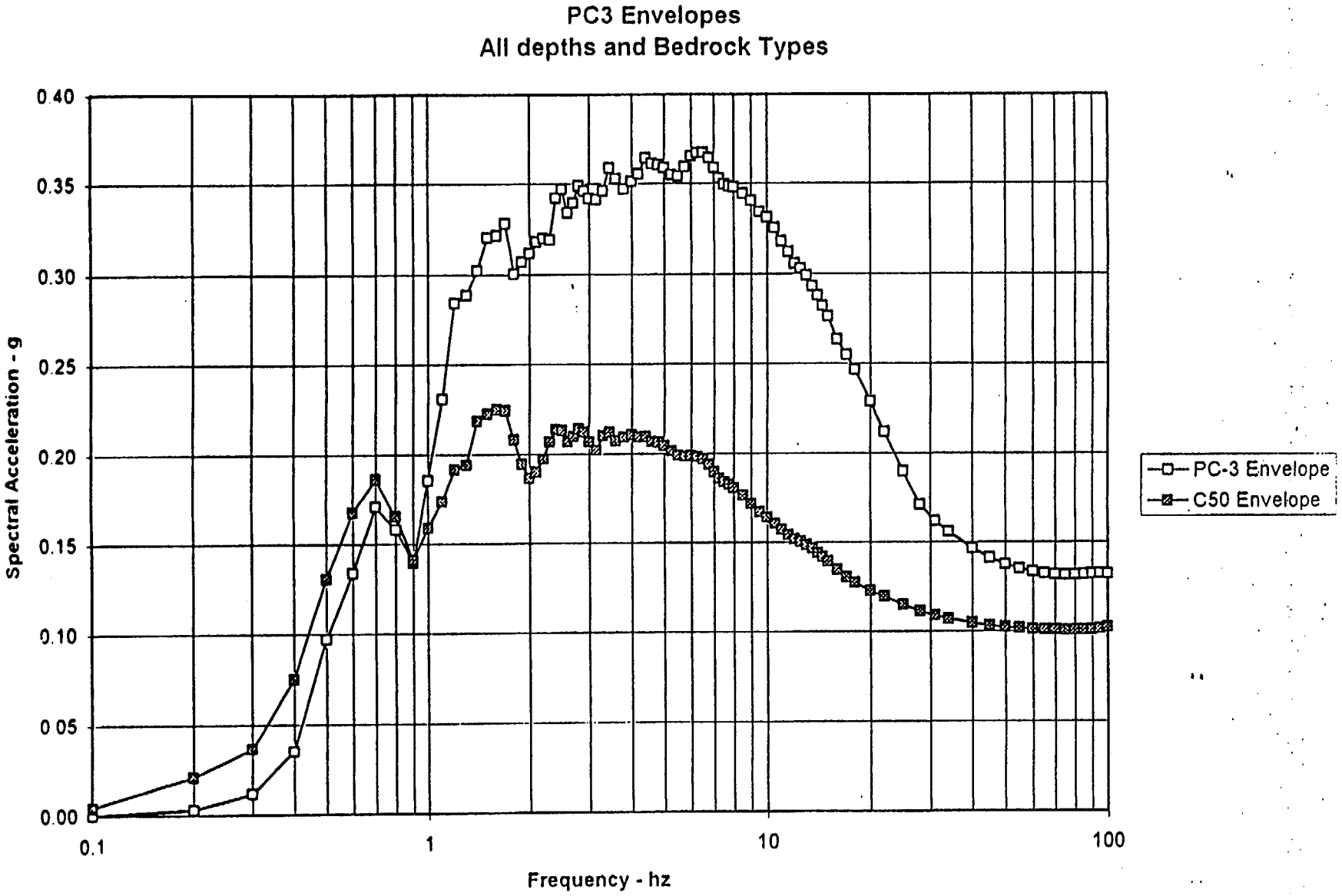

Figure 13.13 - Comparison of envelope of mean UHS Performance Category 3 soil response spectra to Charleston 50th percentile deterministic response spectrum for all soil categories and both bedrock types 5% damping.

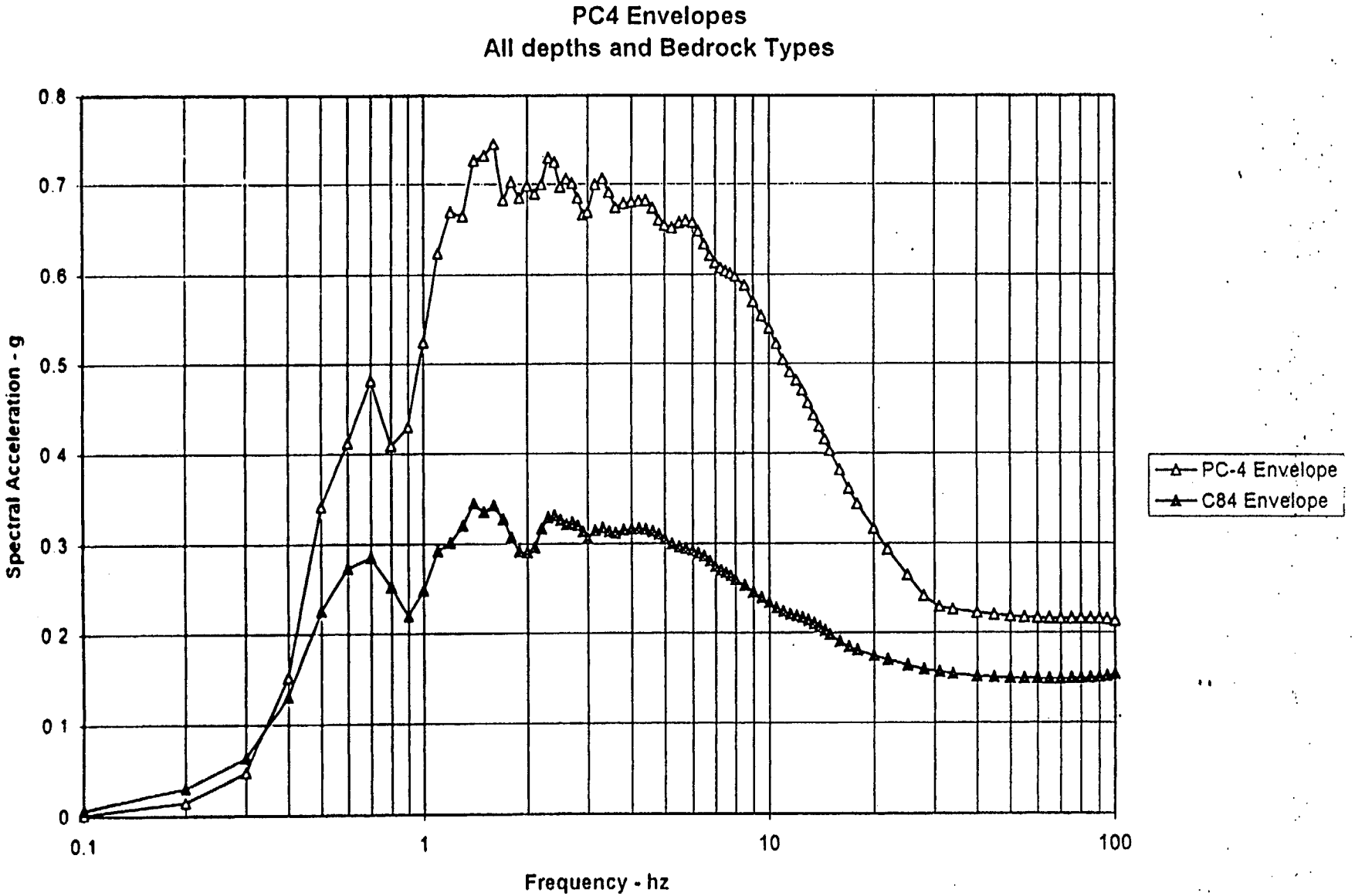

Figure 13 14 - Comparison of envelope of mean UHS Performance Category 4 soil response spectra to Charleston 84th percentile deterministic response spectrum for all soil categories and both bedrock types 5% damping.

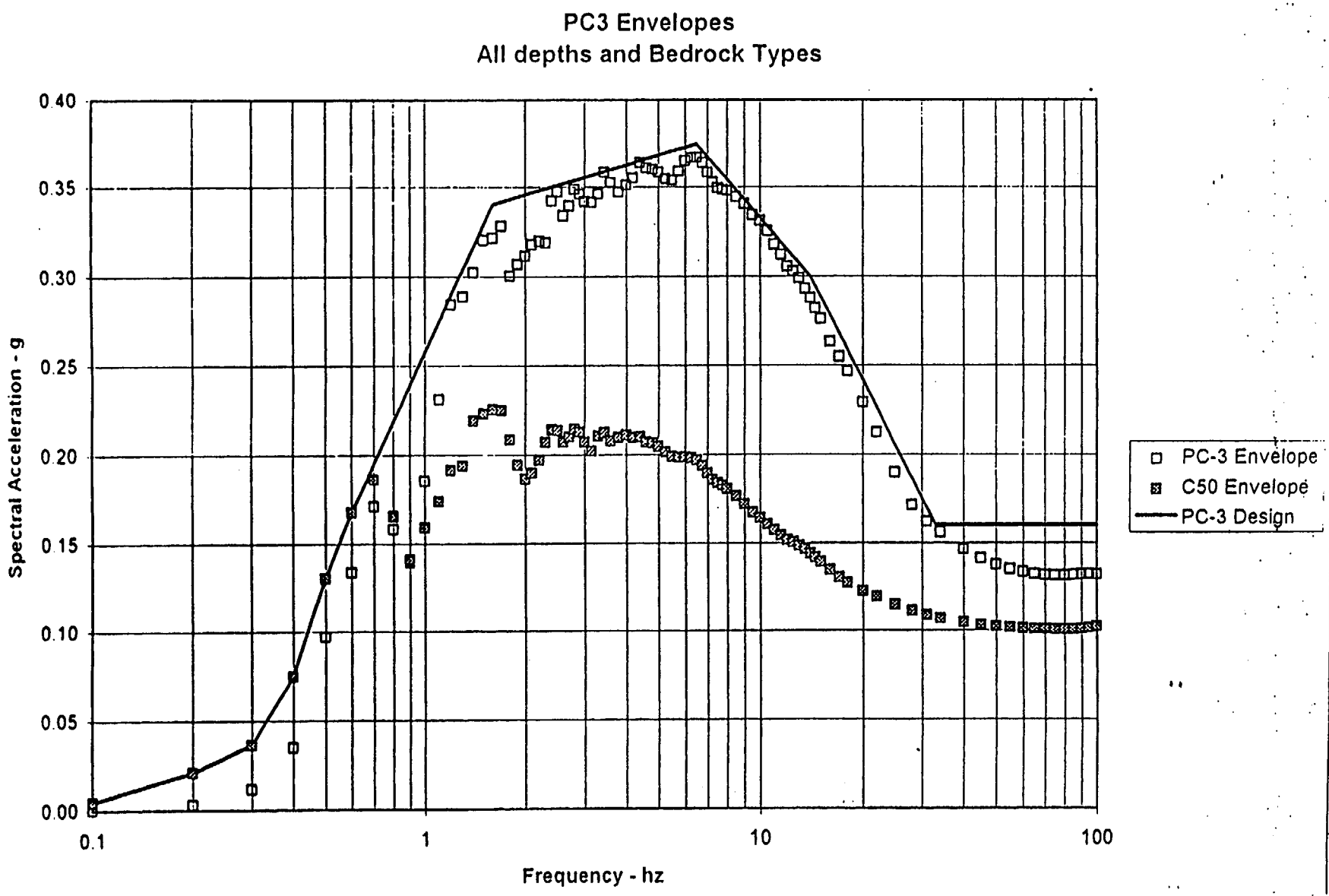

Figure 13.15 - PC3 design basis envelope of mean scaled UHS and Charleston deterministic response spectrum for all soil categories and both bedrock types 5% damping.

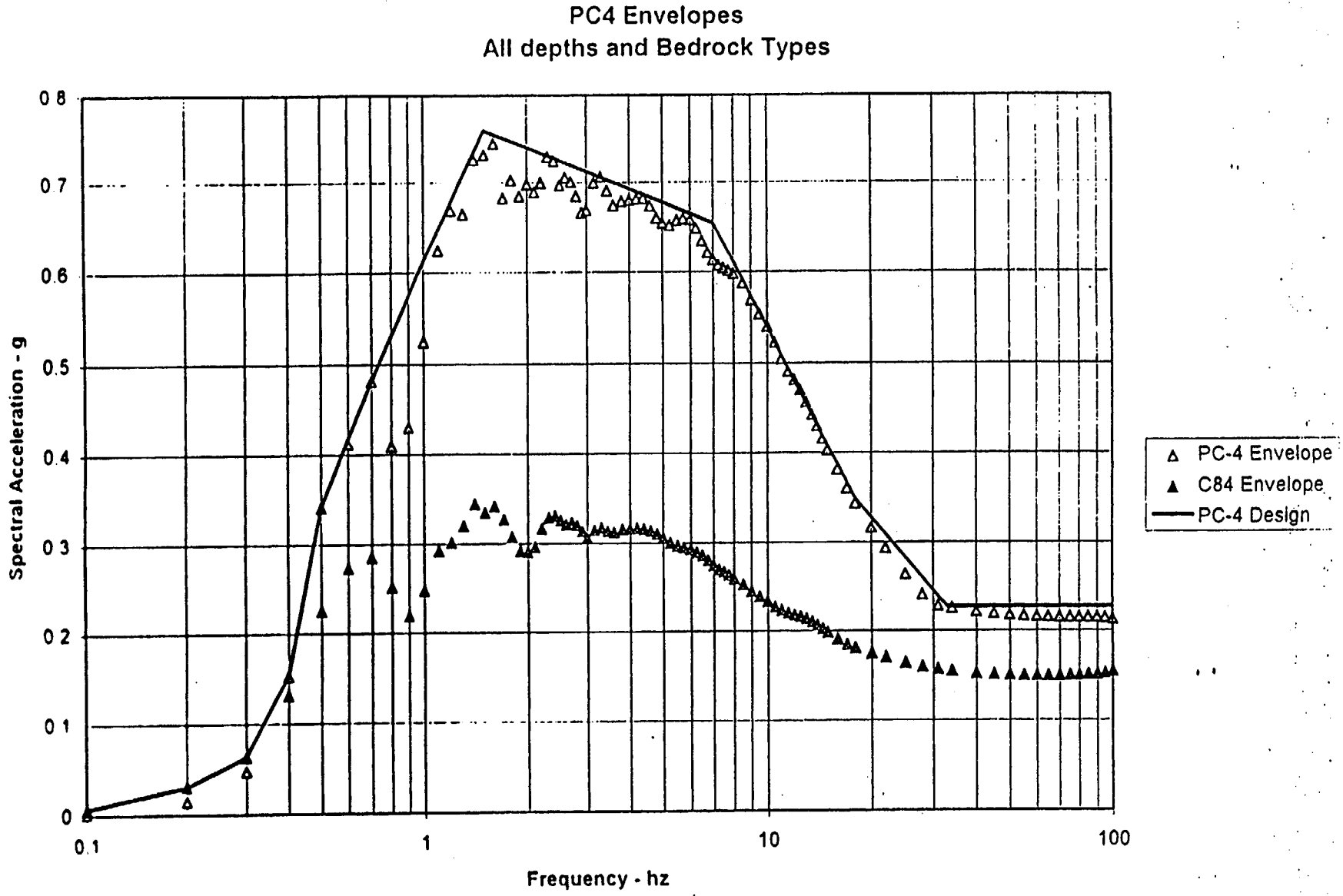

Figure 13 16 - PC4 design basis envelope of mean scaled UHS and Charleston deterministic response spectrum for all soil categories and both bedrock types 5% damping.

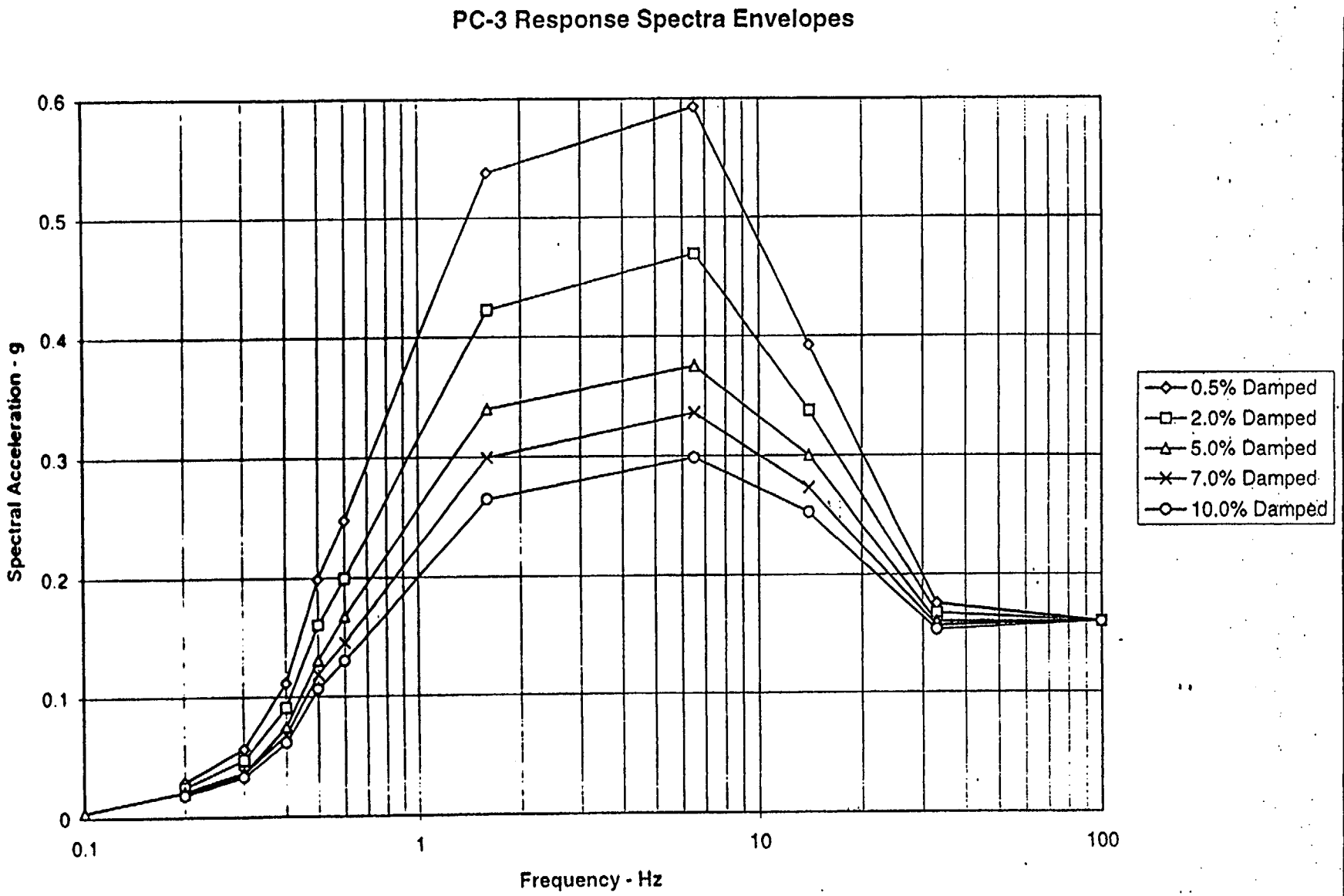

Figure 13.17 - PC3 design basis envelope spectra for oscillator dampings of 0.5, 2.0, 5.0, 7.0, and 10.0% damping.

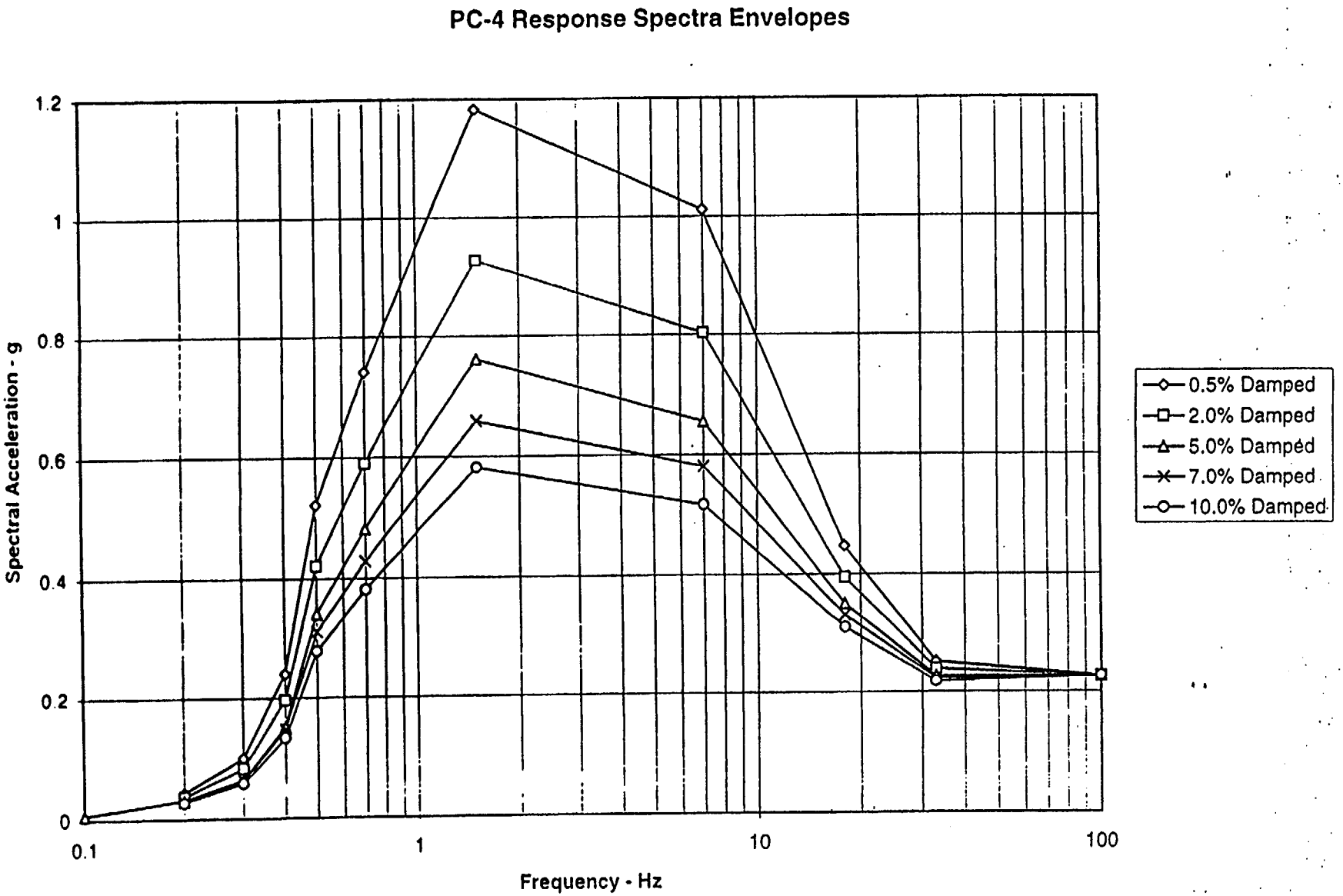

Figure 13.18 - PC4 design basis envelope spectra for oscillator dampings of 0.5, 2.0, 5.0, 7.0, and 10.0% damping.

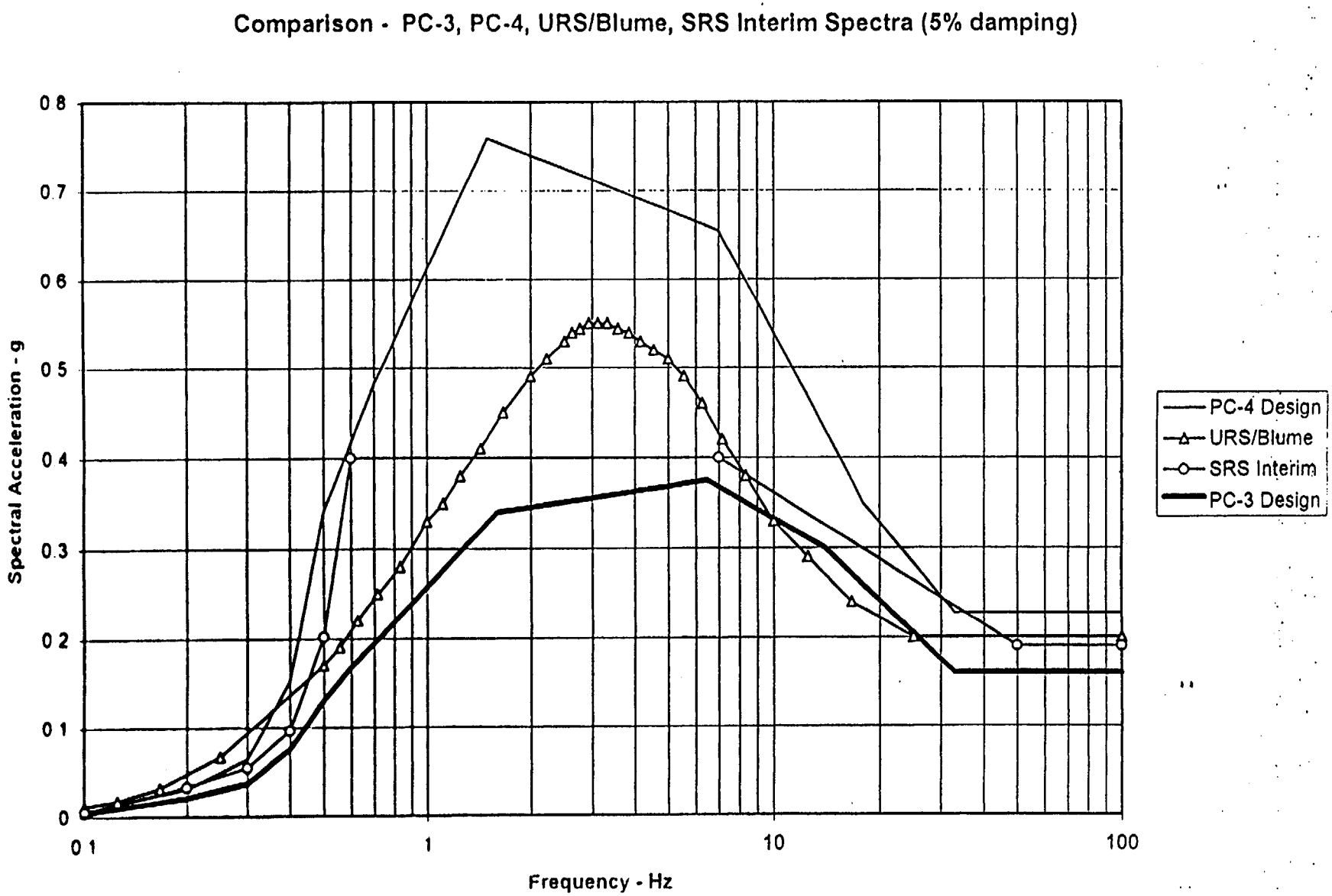

Figure 13 19 - PC3 and PC4 5% damped design basis envelope spectral shape comparison to URS/Blume (1982) and SRS Interim Spectra

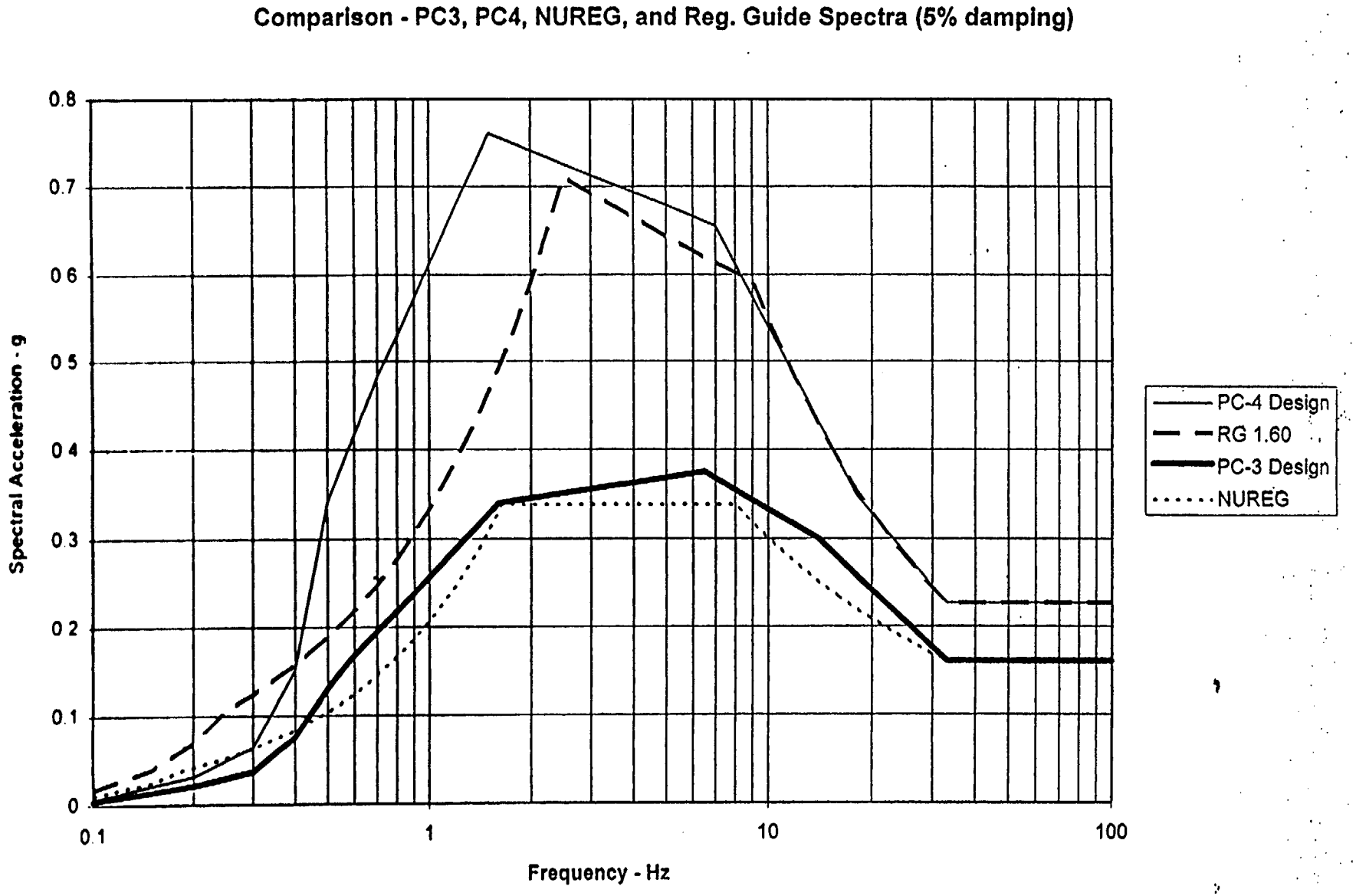

Figure 13.20 - PC3 and PC4 5% damped design basis envelope spectral shape comparison to NUREG and Regulatory Guide Spectra.

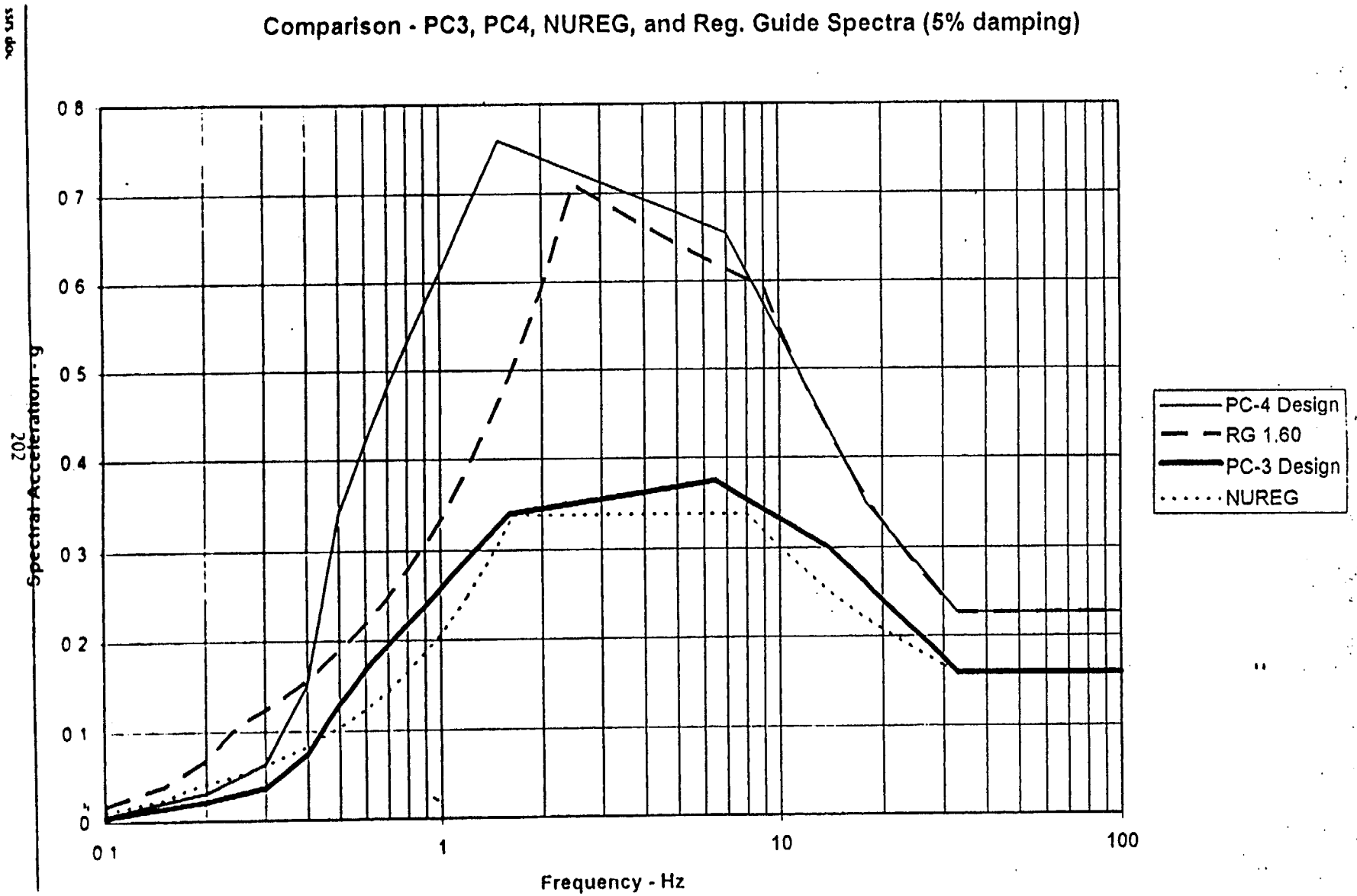

Figure 13 20 - PC3 and PC4 5% damped design basis envelope spectral shape comparison to NUREG and Regulatory Guide Spectra.

Appendix A

PROBABILISTIC MODELS OF SHEAR-WAVE VELOCITY PROFILES AT THE SAVANNAH RIVER SITE AIKEN, SOUTH CAROLINA

Prepared by

Gabriel R. Toro

Risk Engineering, Inc.

4155 Darley Avenue, Suite A

Boulder, CO 80303

for

Pacific Engineering and Analysis

311 Pomona Avenue

El Cerrito, CA 94530

April 4, 1997

CONTENTS

ABSTRACT

A probabilistic model is constructed for the variation of shear-wave velocity in soil sites in the Savannah River Site (SRS), for the purpose of calculating site-amplification factors and their uncertainty at sites in SRS. The data used for constructing and calibrating the model consists of 176 profiles. The probabilistic model is based on earlier work by Risk Engineering, Inc. (EPRI, 1993; Toro et al., 1994, Toro, 1995). This model consists of three parts, as follows: (1) a model that describes the random stratigraphy at the site, (2) a median site-velocity profile, and (3) a model that describes the deviations of the velocity in each layer from the median and its correlation with the velocity in the layer above.

The probabilistic model is used to simulate artificial velocity profiles. This is done for generic sites and for sites in a specific cluster. The simulations for a specific cluster use both parameters of the generic model and the actual measurements obtained in that cluster. This is important if the number of measured profiles in the cluster is not sufficient for the determination of a new set of model parameters for the cluster.

1. INTRODUCTION

This report presents a model for the probabilistic characterization of the shear-wave velocity profiles at soil sites and applies it to develop a generic model for SRS using available shear-wave velocity profile data. This model can be used to generate a suite of artificial velocity profiles for an arbitrary site in SRS. These artificial profiles can then be used to calculate the median and uncertainty of ground-motion amplification at that site (see Roblee et al., 1995). An extended version of the probabilistic model can be used to generate artificial profiles for an SRS site within a cluster in which some velocity profiles are available.

The model utilized here is essentially the same used in Toro (1995), and on earlier work by the author (Toro et al., 1994; see also Appendix 6A of EPRI, 1993). This study utilized a more homogeneous data set, both in terms of the smaller geographic region considered and in

terms of the higher quality of the velocity-profile data. As a result, there is less variation between profiles. In addition to estimating model parameters for the SRS data set, it was necessary to modify the model in order to accommodate the characteristics observed in the data. The most important of these modifications are as follows: (1) the introduction of a depth-dependent standard deviation, (2) the use of weighting in the likelihood function to avoid dominance by a single cluster, and (3) the use of a renewal model to represent the distribution of layer thickness.

Section 2 of this report presents a summary of the data used for this study and the site categorizations employed. Section 3 describes the probabilistic models of layering and velocity, the procedure used to derive model parameters for the entire SRS dataset (and for cluster H, which can be treated as a distinct data set due to its large size). Section 4 describes an extension of the above model to situations where one wishes to simulate profiles for a cluster where some site-specific velocity data are available (but those data are not sufficient for calculating a new set of cluster-specific model parameters), and the application of this model to clusters A and F. We refer to the model in Section 3 as the generic model, and to the model in Section 4 (where correlation between profiles in the same cluster is considered) as the site-specific model.

2. DATA

The velocity data set used in this study was provided by Dr. Richard Lee of Westinghouse Savannah River Company (WSRC) through Pacific Engineering and Analysis and subjected to extensive scrutiny in order to remove spurious and duplicate data. The dataset consists of 176 interpreted shear-wave velocity profiles, with locations shown in Figure 1. Most of these profiles were obtained from suspension-logger data (low-pass filtered at 70 Hz) or from profiles interpreted by ARA (a consultant to WSRC). The profile data come from nine geographic clusters, associated with various facilities at SRS (see Figure 1), with cluster H containing more than half of the profiles. This uneven distribution of profiles among

cluster necessitated the introduction of a weighting scheme, which will be described in Section 3.

Table 2 lists the shear-wave velocity profiles considered in this study, together with their coordinates and depths. Most of the profiles do not begin at the surface and only ten of them extend to depths greater than 75 m, as shown in more detail in Table 2.

A few of these profiles extend into bedrock. The bedrock portion of these profiles was truncated, using information provided by WSRC, so that all velocities in the data set apply to soil.

3. GENERIC MODEL: DATA ANALYSIS, MODEL FITTING, AND RESULTS

Figures 2 and 3 show the median[1] ± logarithmic σ and the logarithmic σ (± the standard error of estimation in the logarithmic σ) as a function of depth, as calculated from all profiles (without any weighting). Figures 4 through 21 show similar results for the individual clusters[2]. These figures show lower values of the logarithmic σ than earlier results, due to the more homogeneous nature of this data set. In addition, the logarithmic σ is not constant, having its highest value near the surface.

Another difference with observations from typical profiles (e.g., EPRI, 1993; Toro, 1995) is that the median profiles do not show a velocity gradient near the surface. In many SRS

[1]What we actually show is the geometric mean (sometimes called logarithmic mean), not the median. Because the distribution of velocities is approximately lognormal, the geometric mean is approximately equal to the median.

[2]Figures 8, 9, 13, 16, 17, and 19 show erratic behavior at the bottom of the dataset. This is the result of having only one or two profiles near the bottom and is not statistically significant.

profiles, the weathered soils near the surface have higher velocities than soils beneath them. Variations in this weathering are also responsible for the higher σ near the surface.

3.1 Elements of Probabilistic Model

The probabilistic model to characterize these profiles attempts to capture the main features observed in interpreted soil velocity profiles; namely, random layering, velocities with the observed depth-dependent σ, and correlated velocities. Figure 22 illustrates the various elements of the soil-profile model. The layering model describes the thicknesses of the layers (or the location of layer boundaries). The velocity model describes the velocity at the mid-point of each layer and its relationship to the velocity in other layers.

Bedrock is represented separately from the soil layers in the simulations, having its own distribution of velocity and depth.

The general structure of this probabilistic model, as illustrated in Figure 22, is the same used in Toro (1995). The parameter values, detailed model parameterization, and details of the analysis procedure are different as a result of differences in the dataset.

3.2 Layering Model

Regarding the layering, we note that layers tend to be thinner near the surface and thicker at depth (see Figures 1 through 4 and 13). A simple probabilistic model to characterize the layering is a Poisson process with depth-dependent rate (i.e., a non-homogeneous Poisson process; see Parzen, 1962). In this model, the mean layer thickness is depth-dependent, but the thickness of layer i is probabilistically independent of the thickness of layer $i-1$. In a Poisson model with constant rate, the layer thicknesses follow an exponential distribution. Because we utilize a depth-dependent rate, the distribution of layer thickness is no longer exponential, but this causes no problems in the analysis or in the generation of artificial profiles.

We adopt a modified power-law model to characterize the depth-dependent rate of layer boundaries, i.e.,

$$\lambda(h)=c_3[h+c_1]^{-c_2} \quad (1)$$

where λ is the rate of layer boundaries (m^{-1}) and h denotes depth in meters. The Poisson model is chosen because it is the simplest possible model for the location of discrete events. The power-law functional form is chosen for the variation of λ because this functional form is often used to represent the variation of shear-wave velocity with depth.

Coefficients c_1 through c_3 in Equation 1 are estimated from the entire SRS dataset, using the method of maximum likelihood (Benjamin and Cornell, 1971). The following result is obtained for the entire SRS data set:

$$\lambda(h)=4.588[h+163]^{-0.675} \quad (2)$$

Figure 23 compares the rate function in Equation 2 to the observed rate of layer boundaries[3] (or transition rate). The observed rates (thin line) are shown as running averages over a 10 m window (i.e., the quantity shown for a depth of 50 m is the number of layer boundaries between 45 and 55 m, divided by the number of profiles that contain data at a depth of 50 m). This figure shows a good agreement between the data and the fitted model, although a model with constant λ for the first 30 m and Equation 1 for greater depths would have provided a better fit.

[3]It is useful to think of the rate of layer boundaries as the reciprocal of the mean layer thickness. This is strictly applicable only if the rate varies slowly.

One may interpret the rate λ(h) as the reciprocal of the mean layer thickness for a given depth. According to this, Equation 2 indicates mean layer thicknesses of approximately 6 m near the surface and of approximately 15 m for a depth of 300 m.

Although a statistical goodness-of-fit test for the EPRI data set (Toro et al., 1994) indicated no significant deviation from the assumption of a Poisson process, an examination of the normalized layer thicknesses shows some deviations from Poisson in the SRS data set. For this purpose, we introduce the normalized layer thickness for layer i (between depths h_i and h_{i+1}), which we define as

$$\begin{aligned} \tau_i &= \int_{h_i}^{h_{i+1}} \lambda(h)\,dh \\ &\approx (h_{i+1}-h_i)\lambda\left(\frac{h_{i+1}+h_i}{2}\right) \\ &\approx \frac{(h_{i+1}-h_i)}{\bar{T}\left(\frac{h_{i+1}+h_i}{2}\right)} \end{aligned} \qquad (3)$$

where $\bar{T}(h)=[\lambda(h)]^{-1}$ represents average layer thickness. Figure 24 shows a histogram of normalized layer thickness. The observed distribution has a coefficient of variation (COV) of 0.7 and has its mode at approximately 0.5. In contrast the exponential distribution associated with the Poisson process would have a COV of unity and would have its mode at zero. Figure 24 also shows the shapes of the exponential (with a mean of 1) and gamma (with a mean of 1 and a COV of 0.71) distributions, for the sake of comparison. Both the exponential and gamma models will be used in the simulations.

3.3 Velocity Model

As shown in Figure 22, the velocity model operates on the velocities at the layer midpoints. One can think of these velocities, for a given profile, as a sequence of velocity values (i.e.,

V_1, V_2, V_3, ...V_n). The velocity model defines the probability distribution of ln[V_i], and its correlation with the ln-velocities in adjacent layers. More precisely, the model operates with the normalized quantity

$$Z_i = \frac{\ln(V_i) - \ln[V_{median}(h_i)]}{\sigma_{\ln V}} \tag{4}$$

where the standard deviation σ_{lnV} is treated as a function of depth. As a result of the normalization in Equation 4, Z_i has a mean of zero and a standard deviation of unity.

Normal probability plots in Toro et al. (1994) indicate that Z_i is well approximated by a normal distribution (or, equivalently, that V_i is well approximated by a log-normal distribution).

We characterize the lognormal distribution of velocities and the correlation among layers by means of a first-order auto-regressive model, so that the conditional distribution of Z in layer i (given the values of Z in layers 1, 2, ... i-1) is normal with mean and standard deviation given by

$$\text{mean}(Z_i|Z_1,Z_2,...Z_{i-1}) = \text{mean}(Z_i|Z_{i-1}) = \rho Z_{i-1} \tag{5}$$

$$\sigma(Z_i|Z_1,Z_2,...Z_{i-1}) = \sigma(Z_i|Z_{i-1}) = \sqrt{1-\rho^2} \tag{6}$$

where ρ is the serial auto-correlation coefficient of Z.

Equations 5 and 6 exhibit the so-called Markov property, because the conditional distribution of Z_i depend only on Z_{i-1} and not on $Z_1, Z_2, ...Z_{i-2}$. The Markov property applies only if ρ is constant, but we will assume that it applies even though we will make ρ a function of depth.

We use the method of maximum likelihood to estimate model parameters. This formulation may be thought of as an extension of the regression procedure used by Toro et al. (1994). The log-likelihood function for profile j, which contains n layers with normalized velocities $z_1, z_2, \ldots z_n$, is given by

$$\ln L_j = \ln[f_{Z_1}(z_1)] + \sum_{i=2}^{n} \ln[f_Z(z_i | z_{i-1})] \tag{7}$$

where

$$f_Z(z_1) = \frac{1}{\sqrt{2\pi}} \exp\left[-\frac{1}{2} z_1^2\right] \tag{8}$$

is the probability distribution of Z for the top layer of the profile and

$$f_Z(z_i | z_{i-1}) = \frac{1}{\sqrt{2\pi(1-\rho^2)}} \exp\left[-\frac{1}{2}\left(\frac{z_i - \rho z_{i-1}}{\sqrt{1-\rho^2}}\right)^2\right] \tag{9}$$

is the conditional probability of Z in layer i given the value of Z in the layer above. We introduce weights in Equation 7, so that profiles from one cluster do not dominate the calculations. The resulting log-likelihood function is given by

$$\ln L_j = w_1 \ln[f_{Z_1}(z_1)] + \sum_{i=2}^{n} w_i \ln[f_Z(z_i | z_{i-1})] \tag{10}$$

where the weight w_i depends both on the number of profiles in the cluster and on the homogeneity of velocities in that cluster. This weight is given by the expression:

$$w_i = \frac{1}{1 + (n_{ik} - 1)\rho_{hk}} \tag{11}$$

where n_{ik} is the number of profiles in cluster k (the cluster containing profile j; only those profiles that have data at the depth of layer i are counted in n_{ik}) and ρ_{hk} is the horizontal correlation between profiles in the cluster. This choice of weights is designed to minimize

the standard error of estimation of the median profile. The values of ρ_{hk} for the calculation of weights were obtained by fitting a model with constant $\sigma_{\ln V}$ to the entire dataset and to the data from each individual cluster. The resulting values are shown in Table 3. Test calculations using equal weights and weights of n_{ik}^{-1} lead to small differences in the median profile.

The total log-likelihood function for all m profiles in the data set is the sum of the log-likelihood functions of the profiles, i.e.,

$$\ln L = \sum_{j=1}^{m} \ln L_j \tag{12}$$

Toro (1995) uses a different form of the likelihood function, which allows for the possibility that some of the velocity data represent bedrock. This is not required in this study because all data used in this study correspond to soil.

The value of the likelihood function (given the data) depends on the median velocity, the standard deviation $\sigma_{\ln V_i}$, and the layer correlation coefficient ρ, all of which as treated as functions of depth. The variation of the median velocity with depth is represented as piecewise linear in terms of the median velocities at several control depths and is made smooth by applying a penalty function. The variation of $\sigma_{\ln V_i}$ with depth is represented as constant between 0, piecewise linear between 5 and 200 m (with control depths at 5, 15, 50, 100, and 200 m), and constant at greater depths. The variation of ρ with depth is represented by the function

$$\rho(h) = \begin{cases} \rho_{200}\left[\dfrac{h+h_0}{200+h_0}\right]^b & \text{for } h \le 200 \\ \rho_{200} & \text{for } h > 200 \end{cases} \qquad (13)$$

where ρ_{200}, h_0, and b are parameters to be determined. Toro (1995) uses a more complicated correlation model, where, in addition to being depth-dependent, the correlation between thin layers is higher than the correlation between thick layers. The SRS data set does not require the presence of those terms.

The maximum-likelihood estimation procedure solves for the median velocity at the velocity control depths, values $\sigma_{\ln V}$ at the σ control depths. and parameters ρ_{200}, h_0, and b. Table 4 lists the estimated parameter values. Table 5 and Figure 25 show the median velocity versus depth values obtained as part of the estimation process. These median velocities differ somewhat from those calculated from the raw profiles (e.g., Figure 2) in because of the smoothing. The median velocities extend to a depth where fewer than five profiles are available in the corresponding category. Data at greater depths were not used in the calculations. Figure 26 shows the variation of $\sigma_{\ln V}$ and ρ as a function of depth.

Because cluster H has a sufficiently large number of profiles to obtain stable estimates of the above model parameters (at least at depths of 70 m or less), we apply the same analysis procedure to this cluster (clusters A and F will be treated differently in Section 4). Because only one profile in cluster H extends beyond 70 m, we added the data from deep profiles in other clusters to the data from cluster H[4]. We could have given higher weight to the one profile from cluster H. This would have a small effect because all deep profiles are quite similar as shown by the low $\sigma_{\ln V}$ at depth (see Figure 26). Tables 4 and 5, and Figures 27 and 28 show the parameters obtained. Comparing these Figures to Figures 24 and 25, we

[4] These deep profiles from other clusters were truncated at the shallowest layer boundary deeper than 70 m, so that the data for h< 70 m come entirely from cluster H.

note a small difference in the median profiles and that σ_{lnV} is slightly lower for cluster H than for the generic model.

3.4 Simulation Results

Figures 29 and 30 show samples of artificial profiles generated using the model and parameters developed here for generic SRS conditions. Figure 29 uses the exponential distribution of normalized thickness (non-homogeneous Poisson) and Figure 30 uses the Gamma distribution with a COV of 0.71 (see Figure 24). In the generation of artificial profiles, the truncation of ln-velocities and residuals at $\pm 2\sigma$ (see Toro et al., 1994) is still used although it may no longer be necessary. The profiles in Figure 30 look more realistic because they do not exhibit very thin or very thick layers, but those on Figure 29 appear adequate. Both types of profiles yield similar results in site-response calculations, but fewer profiles are required to obtain stable results for the exponential distribution of normalized thickness (W. Silva, personal communication, 1996). Therefore, the exponential distribution is preferable for the sake of computational efficiency. Figure 31 shows the logarithmic median$\pm\sigma_{lnV}$ profile calculated from 50 simulated profiles and figure 32 shows the corresponding $\sigma_{lnV} \pm$ its standard error of estimation.

Figures 33 through 35 show similar results obtained for cluster H. Comparison of the median$\pm\sigma_{lnV}$ and $\sigma_{lnV} \pm$ standard error plots to those obtained above for the generic model shows only minor differences. We will return to this issue in the conclusions.

4. SITE-SPECIFIC MODEL

4.1 Introduction

A site-specific velocity model could be developed by collecting site-specific profile data and repeating the analysis procedure followed in Section 3 above. This approach is generally not

practical because it requires a large number of site-specific profiles. The procedure developed here uses the site-specific velocity measurements and stratigraphy to modify the generic model. The relative weights given to the site-specific data and to the generic parameters depend on the amount of data and its (profile-to-profile) variability. If the correlation between two profiles in the same cluster depends on the horizontal distance between the borings, then profiles closer to the target site are given more weight in modifying the generic results.

The site-specific model is based on the idea that if one applies the model in Section 3 to a narrow class of sites (assuming there are sufficient data to obtain stable results), one would obtain a lower $\sigma_{\ln V}$ (and usually a different median profile) than for the broader class of sites. This is exemplified by comparing the generic-SRS results obtained here to the broader nationwide results obtained in Toro (1995). The lower value of $\sigma_{\ln V}$ obtained in this study arises because there are some characteristics in common among the profiles in the narrow class, which are not shared with all other profiles in the broader class. Therefore, there is less variability among the profiles in the narrow class. This lower variability, relative to the variability in the broader class of profiles, may be interpreted as positive correlation among the profiles in the narrow class. In this analysis, the narrow class corresponds to a cluster of sites with distances of a few hundred to a thousand meters.

The information provided by the measured profiles at the cluster is treated as additional information, which is combined with the information contained in the generic model to produce a site-specific model. Because there is correlation between sites in the cluster, the cluster-specific data are more relevant than the generic data. The advantage of not discarding the generic data is that we obtain more stable results in cases where the number of available cluster-specific profiles is small.

The key to applying the site-specific model is the horizontal (more precisely, profile-to-profile) correlation between profiles in the same cluster and its possible dependence on distance. Toro (1995) investigated the spatial correlation of shear-wave velocity in clusters

from SRS and California, and concluded that the correlation between profiles in a cluster is roughly independent of distance for the range of distances found in these clusters. As a result, this study will assume that the correlation between profiles in a cluster is independent of distance. Obviously, the correlation between profiles will depend on distance for distances that are much longer or much shorter than the range of distances in these clusters and this assumption will not be valid in other situations.

Section 4.2 presents the formulation for a site-specific velocity model, which includes horizontal correlation, vertical correlation, and the generic model (an early version of this model was presented in Appendix 6A of EPRI,1993). Section 4.3 presents a preliminary site-specific model for the stratigraphy. Section 4.4 presents the simulation of site-specific profiles for the A and H clusters in SRS.

4.2 Site-Specific Velocity Model

Consider a cluster of sites that exhibits inter-cluster correlation (i.e., where the within-cluster variance is smaller than or equal to the generic variance) and assume that we have computed the within-cluster variance $\sigma^2_{\ln V,\ \text{cluster k}}$ and the generic (or site-wide) variance $\sigma^2_{\ln V,\ \text{generic}}$. From these variances, we can calculate the horizontal within-cluster correlation function $\rho_h = 1 - \sigma^2_{\ln V,\ \text{cluster k}} / \sigma^2_{\ln V,\ \text{generic}}$ (we use the subscript h to emphasize that this quantity represents horizontal correlation). This model provides information about the horizontal correlation between the ln-velocities of the various profiles, at a given depth.

Let $Z_{0,j}$ denote the normalized ln-velocity (see eq. 4) at location 0 (the location at which we wish to generate an artificial profile) and at depth h_j. Let $Z_{i,j}$, i=1,n be the normalized ln-velocities at depth h_j in the n profiles measured in the cluster. We do not know $Z_{0,j}$, but we know $Z_{i,j}$, i=1,n. We also know that the random vector $Z_j=[Z_{0,j},Z_{1j},Z_{2j},...Z_{nj}]^T$ follows a multi-normal distribution with mean zero and with an autocorrelation matrix that is given in terms of ρ_h. This correlation matrix may be written as

$$R_{Z_j} = \begin{bmatrix} 1 & R_{0,i}^T \\ R_{0,i} & R_{i,i} \end{bmatrix} \quad (14)$$

where $R_{i,i}$ is the n×n correlation matrix of the cluster ln-velocities and $R_{0,i}$ is an n×1 column vector containing the correlations between Z_0 and the clustered ln-velocities. In the case considered here, where ρ_h is independent of distance, all diagonal terms are 1 and all off-diagonal terms are equal to ρ_h.

In addition, the generic velocity model specifies the vertical correlation (within a profile) between the ln-velocity of a layer and that of the layer immediately above (i.e., the correlation between $Z_{0,j}$ and $Z_{0,j-1}$, where the latter is also assumed to be known if we are generating artificial velocities from the top to the bottom of the profile. This correlation is given by equation 7 (we will call this correlation ρ_v).

The normalized ln-velocities at depth h_{j-1} (i.e., $Z_{j-1}=[Z_{0,j-1},Z_{1,j-1},Z_{2,j-1},...Z_{n,j-1}]^T$) also have the correlation matrix given by equation 14.

We have no information, however, about the correlation between the values of Z in two different profiles and at different depths (all we know is that this correlation cannot be zero). A reasonable assumptions is that the correlation between the ln-velocity at depth j in one profile and depth j-1 in another profile is given by $\rho_v \times \rho_h$ (this assumption is analogous to a Markov assumption). Thus, one can construct the joint covariance matrix of the Z's at depths j and j-1 in terms of the quantities in eq. 14 and of ρ_v [5]. Using this correlation matrix, one can determine the conditional distribution of $Z_{0,j}$ (the only unknown quantity), given the

[5]This formulation should also include correlation between $Z_{0,j}$ and $Z_{i,j+1}$ (C.A. Cornell, personal communication). It is anticipated that this additional correlation has little effect on the results.

values of the other quantities, using the properties of the multi-normal distribution[6]. In the special case where the horizontal correlation is independent of distance (horizontal equicorrelation), one obtains the following expression for the conditional mean of ln $V_{0,i}$:

$$\ln V_{0j,\text{cond.median}} = \frac{n\rho_h}{1+(n-1)\rho_h}\overline{\ln V}_j + \left[1-\frac{n\rho_h}{1+(n-1)\rho_h}\right]\ln V_{j,\text{median}} + \rho_v\left(\ln V_{0,j-1}-\ln V_{j-1,\text{median}}\right)\frac{\sigma_{\ln Vj}}{\sigma_{\ln Vj-1}} - \frac{n\rho_h\rho_v}{1+(n-1)\rho_h}\left(\overline{\ln V}_{j-1}-\ln V_{j-1,\text{median}}\right)\frac{\sigma_{\ln Vj}}{\sigma_{\ln Vj-1}} \quad (15)$$

where n is the number of profiles in the cluster (at depth h_j), ρ_h is the correlation between profiles in the clusters, $\overline{\ln V}_j$ and $\overline{\ln V}_{j-1}$ are the mean ln-velocities from all profiles in the cluster at depths h_j and h_{j-1}, and $V_{0,j-1}$ is the (previously calculated) artificial velocity in the layer above. The quantity

$$\frac{n\rho_h}{1+(n-1)\rho_h} \quad (16)$$

in the first term represents the weight given to the site-specific mean ln-velocity [illegible] approaches 1 (and the weight given to the generic data in the second term approaches 0) when $n\rho_h >> 1$. For instance, the weight one would give to the site-specific data in the H site at shallow and moderate depths (n=79, ρ_h=0.33) would be 0.97. The third term represents vertical correlation between adjacent layers in the same profile (coming from the generic model). The final term (which has a lower weight than the first and third terms) is required because the correlation between ln-velocities at different depths and in different profiles

[6]This process is equivalent to linear regression or to the determination of weights in geostatistical "Kriging."

cannot be zero. In the case where the horizontal correlation depends on distance, one would obtain a similar expression in terms of weighted averages of the ln-velocities in the cluster at depths h_j and h_{j-1}.

Similarly, one obtains the following expression for the conditional variance of ln $V_{0,i}$:

$$\sigma^2_{\ln V_{0,j},\,\text{cond.}} = \sigma^2_{\ln V,j}(1-\rho_v^2)\left(1-\rho_h^2\frac{n}{1+(n-1)\rho_h}\right) \tag{17}$$

The equation above indicates that the conditional variance is reduced by both the vertical correlation and the horizontal correlation. The reduction factor for horizontal correlation is $(1-\rho_h^2)$ for n=1 and $(1-\rho_h)$ for $n\rho_h>>1$.

This site-specific model is not applicable to cases where the cluster variance is greater than the generic variance. The current implementation of the simulation code assumes $\rho_h=0$ in these cases, thereby ignoring the site-specific data and using the generic model alone.

4.3 Site-specific Layering Model

If the profiles in a cluster tend to have layer boundaries concentrated at certain depths, one would like the artificial profiles to also have layer boundaries concentrated at those depths. On the other hand, one should not preclude all artificial profiles from having layer boundaries at depths different from those occurring in the observed profiles, especially if the number of site-specific profiles is small. In a manner analogous to that used for the velocity data, one can construct a rate function $\lambda(h)$ that is a combination of the generic rate function in Equation 2 and the observed rate of layer boundaries in the site-specific profiles. The resulting expression for the rate of layer boundaries between depths h_1 and h_2 is given by

$$\Lambda(h_1,h_2) = \frac{m\int_{h_1}^{h_2}\lambda(t)dt + N(h_1,h_2)}{m+n} \tag{18}$$

where m is the "equivalent number of site-specific profiles" represented by the generic data, $N(h_1,h_2)$ is the number of observed layer boundaries between depths h_1 and h_2 in the cluster data, and n is the number of site-specific profiles that extend down to depth h_2 or greater. We do not have a quantitative procedure to estimate m, but visual examination of simulation results indicates that a value m=1 is appropriate. Note that if n is large, equation 18 will be dominated by the depth-wise distribution of layer boundaries in the cluster data. The calculation of layer boundaries in the artificial profiles uses Equation 18 may be done with either the Poisson (i.e., exponential normalized thickness) or the renewal (i.e., non-exponential normalized thickness) assumption.

One of the benefits of using this site-specific model for the simulation of the layering (as opposed to the generic model) is that the median of the artificial profiles is closer to the site-specific median when n is large and the site-specific median profile has sharp changes in velocity. If one uses the generic layering model, the median of the artificial profiles tends to be smooth, even if the cluster median has sharp changes in velocity.

4.4 Examples of Artificial Site-Specific Profiles

Figures 36 through 41 show artificial profiles for clusters A and F of SRS, as well as the respective medians and standard deviations calculated from 100 artificial profiles. We see that the median profile for cluster A (from simulations) is intermediate between the observed median from cluster-A data (Figure 4) and the median velocity of the generic model (Figure 25). The standard deviation between 10 and 30 m depth (Figure 38) is lower than the generic standard deviation in Figure 26, because the data from cluster A have a low standard deviation at these depths.

Results for cluster F also show the stabilizing effect of this approach. Figure 8 shows that the median velocity calculated for this cluster is very high near 55 m. These high velocities come from only four profiles (many other profiles terminate at shallower depths). The effect of these higher velocities is moderated by the combination with the generic median profile.

5. SUMMARY AND CONCLUSIONS

The generic model developed in this study for Savannah River Site (SRS) shear-wave velocity profiles differs from models developed in earlier studies for broader (nationwide) data sets in the following three main aspects: (1) the median profile for SRS shows less of a gradient at depths shallower than 30 m, and (2) the standard deviation of ln[Velocity] is lower for the SRS dataset than for the nationwide dataset (except in the top 10 m, where the standard deviations are comparable), and (3) the standard deviation of ln[Velocity] is treated as a function of depth in this study.

Other differences with the earlier the models in earlier studies (i.e., Toro et al., 1994; Toro, 1995) include the introduction of weights in order to keep one cluster from dominating the results, and the use of a Gamma distribution (with a 71% coefficient of variation) for normalized layer thickness as an alternative to the exponential distribution implicit in the non-homogeneous Poisson model. Differences between the two distributions of normalized thickness do not lead to large differences in the simulated profiles, and the Poisson model is still considered adequate.

The profiles in cluster H are analyzed using the same approach, obtaining a model of the same form as the generic-SRS model discussed above, but with slightly different parameters. The median profile for cluster H differs little from the generic-SRS median profile and the standard deviation is moderately smaller than that obtained for the generic-SRS data.

The smaller number of profiles in clusters A and F necessitate a different approach, where we combine the generic-SRS model with the profiles in each specific cluster. The resulting model utilizes the local velocity information but is more robust than a model that would use that information alone. The resulting median profile is a linear combination of the site-specific and generic median and the resulting standard deviation is lower than the generic standard deviation but higher than the cluster standard deviation.

Comparison of the medians and standard deviations of simulated profiles corresponding to the generic model and to clusters A, F, and H (Figures 42 and 43) shows small differences in the median profiles and moderate differences in σ vs. depth. Therefore, it is appropriate to use the generic SRS model for these three clusters.

These observations suggest that, in the case of SRS, the important benefit in reducing the uncertainty of site amplification is achieved in going from the nationwide velocity model to the generic-SRS velocity model. The benefits obtained in going from the generic-SRS model to cluster-scale models are small. This conclusion is applicable to SRS (and to clusters A, F, and H) and may not be valid in general.

6. ACKNOWLEDGMENTS

This work has benefited from discussions with Walt Silva, Richard Lee, Matt Maryak, Carl Costantino, Carl Stepp, S.C. Wu, John Schneider, I. Idriss, and others. Allin Cornell and Carl Stepp reviewed an early draft of this report and made valuable suggestions. The soil-profile database used in this study was developed by Pacific Engineering and Analysis.

7. REFERENCES

Benjamin, J. R., and C. A. Cornell (1971). *Probability, Statistics and Decisions for Civil Engineers*. McGraw Hill, New York.

Parzen, E. (1962). *Stochastic Processes*. Holden Day.

Electric Power Research Institute (1993). *Guidelines for Determining Design Basis Ground Motions, Vol. I: Early Site Permit Demonstration Program*, Palo Alto, CA, November.

Roblee, C. J., W.J. Silva, G.R. Toro, and N.A. Abrahamson, (1996). "Variability in Site-Specific Seismic Ground-Motion Design Predictions," *Uncertainty in the Geologic Environment: From Theory to Practice,* ASCE.

Silva, W. J., et al. (1994). "Generic Soil Amplification Factors for Application to Ground Motion in Eastern North America," submitted to Earthquake Spectra.

Toro, G. R., S. C. Wu, and W. J. Silva (1994). "Probabilistic Models of Shear-Wave Velocity Profiles," submitted to Earthquake Spectra.

Toro, G. R. (1995). *Probabilistic Models of Site Velocity Profiles for Generic and site-Specific Ground-Motion Amplification Studies*, report to Brookhaven National Laboratory, second draft, November 17.

Table 1. Velocity Profiles Used in this Study

Area	Prof. No.	Name	Lat.	Lon.	Min. Depth (m)	Max. Depth (m)
A	1505	ACPT-1	33.344	81.739	2.74	38.10
A	1506	ACPT-2	33.344	81.738	2.74	37.49
A	1507	ACPT-4	33.344	81.737	2.74	36.27
A	1508	ACPT-7	33.346	81.738	2.74	36.27
A	1509	ACPT-8	33.345	81.739	2.74	37.19
CFD	1537	CFD-18	33.240	81.632	2.71	310.90
CFD	1538	CFD-1	33.238	81.630	0.91	292.61
F	1388	F-SEP-C2	33.288	81.678	7.62	52.43
F	1389	F-SEP-C3	33.288	81.675	2.74	35.36
F	1390	F-SEP-C4	33.287	81.676	2.74	33.53
F	1391	F-SEP-C5	33.287	81.676	3.05	34.75
F	1392	F-SEP-C6	33.288	81.676	4.57	54.56
F	1393	F-SEP-C7	33.289	81.676	3.05	51.51
F	1394	F-SEP-C8	33.286	81.678	4.88	36.88
F	1395	F-SEP-C9	33.288	81.679	3.05	46.03
F	1396	F-SEP-C10	33.290	81.678	3.05	46.03
F	1397	F-SEP-C11	33.289	81.677	3.05	52.43
F	1398	F-SEP-C12	33.288	81.679	3.05	54.25
F	1399	F-SEP-C13	33.289	81.678	2.74	52.12
F	1400	F-SEP-C14	33.287	81.679	3.05	46.94
F	1401	F-SEP-C15A	33.287	81.677	3.05	48.77
F	1402	F-SEP-C16	33.287	81.674	3.05	47.85
F	1403	F-SEP-C17	33.288	81.678	4.57	55.47
F	1404	F-SEP-C1	33.288	81.680	3.05	48.46
F	1407	F-TNK-C3	33.282	81.678	3.05	48.77
F	1409	F-TNK-C5	33.283	81.679	3.05	26.82
F	1410	F-TNK-C6	33.282	81.676	3.35	50.60
F	1412	F-TNK-C8	33.283	81.678	3.05	24.99
F	1413	F-TNK-C9	33.282	81.676	5.79	41.76
F	1414	F-TNK-C10	33.282	81.677	3.05	38.41
F	1415	F-TNK-C11	33.283	81.676	3.05	36.88
F	1416	F-TNK-C12	33.284	81.676	3.35	45.11
F	1417	F-TNK-C13	33.275	81.669	3.05	40.54
F	1419	F-TNK-C15	33.283	81.677	3.05	24.08
F	1420	F-TNK-C16	33.281	81.678	3.05	38.71
F	1421	F-TNK-C17	33.284	81.678	3.05	40.23
F	1511	235F-CPT1	33.291	81.676	3.66	46.33
F	1512	235F-CPT2	33.290	81.676	3.66	44.50
F	1513	235F-CPT3	33.291	81.676	3.66	49.99
F	1514	235F-CPT5	33.291	81.676	3.66	47.24
F	1539	F-51	33.289	81.676	3.05	35.66
GCB2	1649	GCB-2, interp	33.322	81.720	43.01	194.49
H	1422	htf-c18	33.284	81.639	3.05	34.14
H	1424	cpt-05	33.285	81.639	2.77	61.27
H	1425	cpt-06	33.285	81.639	2.80	44.50
H	1426	cpt-07	33.285	81.640	2.68	60.35*
H	1427	cpt-10	33.285	81.640	5.91	42.37

Table 1. Velocity Profiles Used in this Study (continued)

Area	Prof. No.	Name	Lat.	Lon.	Min. Depth (m)	Max. Depth (m)
H	1428	cpt-11	33.285	81.639	15.24	60.96
H	1430	cpt-16	33.284	81.640	2.62	33.53
H	1431	cpt-18	33.284	81.639	2.84	53.04
H	1432	cpt-20	33.285	81.638	10.15	32.92
H	1433	cpt-20.1	33.285	81.638	21.73	33.83
H	1434	cpt-20.2	33.285	81.638	3.69	30.21
H	1435	cpt-23	33.286	81.639	4.15	33.22
H	1436	cpt-25	33.286	81.639	2.80	44.50
H	1437	cpt-26	33.285	81.639	2.77	47.55
H	1438	cpt-28.2	33.285	81.638	2.56	37.19
H	1439	cpt-29	33.285	81.640	6.52	60.96
H	1440	cpt-30	33.285	81.639	2.90	62.79
H	1441	cpt-31	33.284	81.640	11.00	41.15
H	1442	H-CYN-C01	33.290	81.641	3.05	41.45
H	1443	H-CYN-C02	33.289	81.643	6.71	44.20
H	1445	H-CYN-C04	33.299	81.651	3.05	54.25
H	1446	H-CYN-C05	33.288	81.641	4.88	49.68
H	1447	H-CYN-C06	33.290	81.643	3.05	51.51
H	1448	H-CYN-C07	33.290	81.639	3.05	46.03
H	1449	H-CYN-C08	33.290	81.638	3.05	45.11
H	1450	H-CYN-C09	33.291	81.642	3.96	57.00
H	1451	H-CYN-C10	33.289	81.640	2.74	58.22
H	1452	H-CYN-C12	33.287	81.639	2.74	57.30
H	1453	H-CYN-C13	33.287	81.641	2.74	58.22
H	1454	HTF-C05	33.286	81.640	3.05	60.66
H	1455	HTF-C06	33.286	81.640	5.79	61.57
H	1456	HTF-C07	33.285	81.640	3.05	65.53
H	1457	HTF-C08	33.286	81.641	5.79	56.08
H	1458	HTF-C09	33.285	81.641	3.05	57.00
H	1459	HTF-C10	33.285	81.645	3.96	12.19
H	1460	HTF-C11	33.285	81.644	7.50	12.07
H	1461	HTF-C12	33.285	81.646	3.05	12.19
H	1462	HTF-C13	33.284	81.645	3.96	44.20
H	1463	HTF-C14	33.284	81.642	4.88	45.11
H	1464	HTF-C15	33.284	81.641	4.88	46.94
H	1465	HTF-C16	33.285	81.641	5.79	43.28
H	1466	HTF-C17	33.286	81.642	4.88	31.39
H	1467	H244-C01	33.286	81.645	3.69	53.34
H	1468	H244-C02	33.286	81.645	2.77	49.07
H	1469	HCPT-32	33.285	81.643	2.74	57.91
H	1470	HCPT-34	33.284	81.643	3.72	57.61
H	1471	HCPT-37	33.285	81.644	2.68	57.61
H	1472	HCPT-38	33.284	81.643	4.69	58.52
H	1477	RHLWE-C1	33.285	81.645	0.00	50.29
H	1478	RHLWE-C5	33.285	81.645	0.00	50.29
H	1479	RHLWE-C10	33.285	81.645	0.00	50.29
H	1480	RHLWE-C12	33.285	81.645	2.74	54.86

Table 1. Velocity Profiles Used in this Study (continued)

Area	Prof. No.	Name	Lat.	Lon.	Min. Depth (m)	Max. Depth (m)
H	1481	H-NWT-C1	33.284	81.643	8.23	39.32
H	1482	H-NWT-C2	33.284	81.643	10.97	47.55
H	1483	H-NWT-C3	33.284	81.642	3.66	52.12
H	1484	H-NWT-C4	33.284	81.643	3.66	53.04
H	1485	HMMC-B02	33.284	81.644	3.05	53.34
H	1487	HMMC-C02	33.284	81.644	3.05	30.79
H	1488	HCIFC06A	33.291	81.639	2.74	25.15
H	1489	HCIFC06B	33.291	81.639	2.74	53.34
H	1490	HCIFC07	33.291	81.639	3.05	54.25
H	1491	HCIFC08	33.291	81.640	4.27	36.88
H	1492	HCIFC09	33.291	81.640	2.74	47.85
H	1493	HCIFC10	33.291	81.640	2.74	43.28
H	1494	HLWFC01	33.286	81.638	4.57	54.25
H	1495	HLWFC02	33.286	81.638	2.44	53.34
H	1496	HLWFC04	33.287	81.638	2.74	47.55
H	1540	B3 &B10	33.290	81.646	1.52	60.35
H	1541	B10 & B11	33.290	81.646	1.52	60.35
H	1542	B1 & B8	33.289	81.646	1.52	60.35
H	1543	B8 & B9	33.289	81.646	1.52	60.35
H	1545	SCPT-01	33.285	81.640	3.66	55.79
H	1547	SCPT-14	33.284	81.640	3.68	48.45
H	1589	SCPTU-1	33.290	81.646	5.33	49.53
H	1591	SCPTU7	33.290	81.647	3.81	48.46
H	1592	SCPTU-11	33.289	81.647	5.03	49.99
H	1608	RTFCPT04	33.290	81.646	3.69	50.35
H	1611	RTFCPT15	33.289	81.646	3.68	50.30
H	1615	MMP-2A-SB (R1-R2)	33.284	81.644	1.00	289.00
K	1318	P-25	33.211	81.657	0.00	121.92
K	1544	P-25B &P-25TB	33.211	81.657	0.00	94.49
K	1550	K-1012	33.212	81.666	4.60	57.90
K	1551	K-1008	33.211	81.664	3.00	57.60
K	1552	K-1003	33.213	81.663	3.00	57.90
K	1561	KC-2	33.213	81.663	2.30	37.30
K	1562	KC-RT3	33.213	81.663	2.30	36.60
K	1565	KC-9	33.212	81.662	2.29	37.34
K	1566	KC-10	33.211	81.663	2.29	41.68
K	1567	KC-15	33.213	81.664	2.29	49.71
K	1568	KC-18	33.213	81.664	2.33	28.19
K	1569	KC-20	33.211	81.663	2.29	38.86
K	1570	KR-1	33.210	81.665	3.90	30.97
K	1571	KR-2A	33.211	81.664	3.87	26.73
K	1572	KR-3	33.211	81.664	3.81	29.75
K	1573	KR-5	33.211	81.666	3.81	23.56
K	1574	KR-6	33.211	81.666	5.33	38.86
K	1576	KR-9	33.212	81.664	3.93	38.89
K	1577	KR-12B	33.212	81.666	6.86	22.49
K	1616	MMP-3-SB (R1-R2)	33.211	81.657	1.00	313.00

Table 1. Velocity Profiles Used in this Study (continued)

Area	Prof. No.	Name	Lat.	Lon.	Min. Depth (m)	Max. Depth (m)
L	1515	LREC-C01	33.210	81.627	3.96	29.57
L	1517	LREC-C03	33.214	81.624	3.05	34.14
L	1518	LREC-C04	33.210	81.625	3.05	49.68
L	1519	LREC-C05	33.212	81.626	3.05	48.77
L	1520	LREC-C06	33.211	81.624	3.05	52.43
L	1521	LREC-C07	33.211	81.624	3.05	46.03
L	1522	LREC-C08	33.210	81.624	3.05	51.51
L	1523	LREC-C11	33.211	81.623	3.05	7.62
L	1524	LREC-C12	33.210	81.622	3.05	50.60
L	1525	LREC-C13	33.210	81.623	3.96	5.79
L	1526	LREC-C14	33.210	81.623	3.05	48.46
L	1527	LREC-C16	33.210	81.621	3.05	43.28
L	1528	LREC-C17	33.213	81.622	3.05	37.80
L	1529	LREC-C20	33.210	81.621	3.05	44.20
L	1530	LREC-C21	33.214	81.624	3.05	47.85
L	1531	LREC-C22	33.210	81.621	3.05	44.20
L	1532	LREC-C23	33.209	81.621	2.74	43.28
L	1533	LREC-C24	33.209	81.621	3.05	49.68
L	1578	L205 AND L206	33.212	81.626	3.05	51.82
MMP4	1510	MMP-4C	33.338	81.708	3.66	39.93
MMP4	1617	MMP-4-SB (R1-R2)	33.338	81.708	1.00	221.00
NPR	1347	NPR M12A-17	33.253	81.638	0.00	78.94
NPR	1348	NPR M12A-18	33.252	81.637	0.00	42.98
NPR	1349	NPR M12A-19	33.253	81.637	0.00	63.09
NPR	1351	NPR M12A-21	33.253	81.637	0.00	70.41
NPR	1352	NPR M12A-22	33.253	81.636	0.00	79.55
NPR	1353	NPR M12A-25	33.254	81.637	0.00	53.04
NPR	1354	NPR M12A-26	33.251	81.638	0.00	41.15
NPR	1355	NPR M12A-27	33.253	81.639	0.00	44.81
NPR	1356	NPR M12A-28	33.254	81.636	0.00	66.75
NPR	1357	NPR M12A-29	33.252	81.636	0.00	59.44
NPR	1358	NPR M12A-30	33.252	81.635	0.00	64.92
NPR	1553	AFR-E24	33.257	81.627	3.00	91.40
NPR	1554	AFR-E25	33.258	81.628	1.50	91.40
NPR	1555	AFR-E26	33.259	81.630	1.50	91.40

Table 2. Summary of Deeper Profiles

Profiles Deeper Than 75m

Area	Prof. No.	Name	Lat.	Lon.	Max. Depth (m)
CFD	1537	CFD-18	33.240	81.632	310.90
CFD	1538	CFD-1	33.238	81.630	292.61
GCB2	1649	GCB-2, interp	33.322	81.720	194.49
H	1615	MMP-2A-SB (R1-R2)	33.284	81.644	289.00
K	1318	P-25	33.211	81.657	121.92
K	1544	P-25B &P-25TB	33.211	81.657	94.49
K	1616	MMP-3-SB (R1-R2)	33.211	81.657	313.00
MMP4	1617	MMP-4-SB (R1-R2)	33.338	81.708	221.00
NPR	1347	NPR M12A-17	33.253	81.638	78.94
NPR	1352	NPR M12A-22	33.253	81.636	79.55
NPR	1553	AFR-E24	33.257	81.627	91.40
NPR	1554	AFR-E25	33.258	81.628	91.40
NPR	1555	AFR-E26	33.259	81.630	91.40

Profiles Deeper Than 100m

Area	Prof. No.	Name	Lat.	Lon.	Max. Depth (m)
CFD	1537	CFD-18	33.240	81.632	310.90
CFD	1538	CFD-1	33.238	81.630	292.61
GCB2	1649	GCB-2, interp	33.322	81.720	194.49
H	1615	MMP-2A-SB (R1-R2)	33.284	81.644	289.00
K	1318	P-25	33.211	81.657	121.92
K	1616	MMP-3-SB (R1-R2)	33.211	81.657	313.00
MMP4	1617	MMP-4-SB (R1-R2)	33.338	81.708	221.00

Profiles Deeper Than 200m

Area	Prof. No.	Name	Lat.	Lon.	Max. Depth (m)
CFD	1537	CFD-18	33.240	81.632	310.90
CFD	1538	CFD-1	33.238	81.630	292.61
H	1615	MMP-2A-SB (R1-R2)	33.284	81.644	289.00
K	1616	MMP-3-SB (R1-R2)	33.211	81.657	313.00
MMP4	1617	MMP-4-SB (R1-R2)	33.338	81.708	221.00

Table 3. Horizontal Correlation Coefficients used in the Calculation of Weights

Cluster (k)	ρ_{hk}	Number of Profiles
A	0.54	5
CFD	0.00	2
F	0.00	34
GCB2	-	1
H	0.33	79
K	0.29	20
L	0.00	19
MMP4	0.00	2
NPR	0.51	14

Table 4. Parameters of Velocity Model

Parameter	Model	
	Generic	Cluster H
Sigma(0-5m)	0.33	0.26
Sigma(15m)	0.17	0.15
Sigma(50m)	0.21	0.17
Sigma(100m)	0.10	0.10
Sigma(>200m)	0.14	0.12
Rho(200)	0.687	0.667
ho	20	20
b	0.509	0.639

Table 5. Median Velocity Model (m/sec)

Depth (m)	Model	
	Generic	Cluster H
0.00	366	351
0.20	366	350
0.23	366	350
0.26	366	350
0.30	366	350
0.35	366	350
0.40	366	351
0.46	367	351
0.53	367	352
0.61	368	352
0.70	368	353
0.81	369	354
0.93	371	355
1.07	372	356
1.23	374	357
1.42	376	359
1.63	379	360
1.87	381	361
2.15	384	362
2.48	385	363
2.85	386	363
3.27	386	364
3.76	386	364
4.33	386	365
4.98	388	365
5.73	390	365
6.58	387	365
7.57	379	365
8.71	369	360
10.01	359	356
11.52	351	355
13.24	349	355
15.23	347	350
17.51	343	347
20.14	337	351
23.16	340	356
26.64	338	356
30.63	340	356
35.22	347	354
40.51	359	356
46.58	372	369
53.57	394	392
61.61	422	421
70.85	453	459
81.48	490	493
93.70	526	522
107.75	569	574
123.92	608	609
142.50	658	653
163.88	722	721
188.46	797	799
216.73	860	864
249.24	919	914

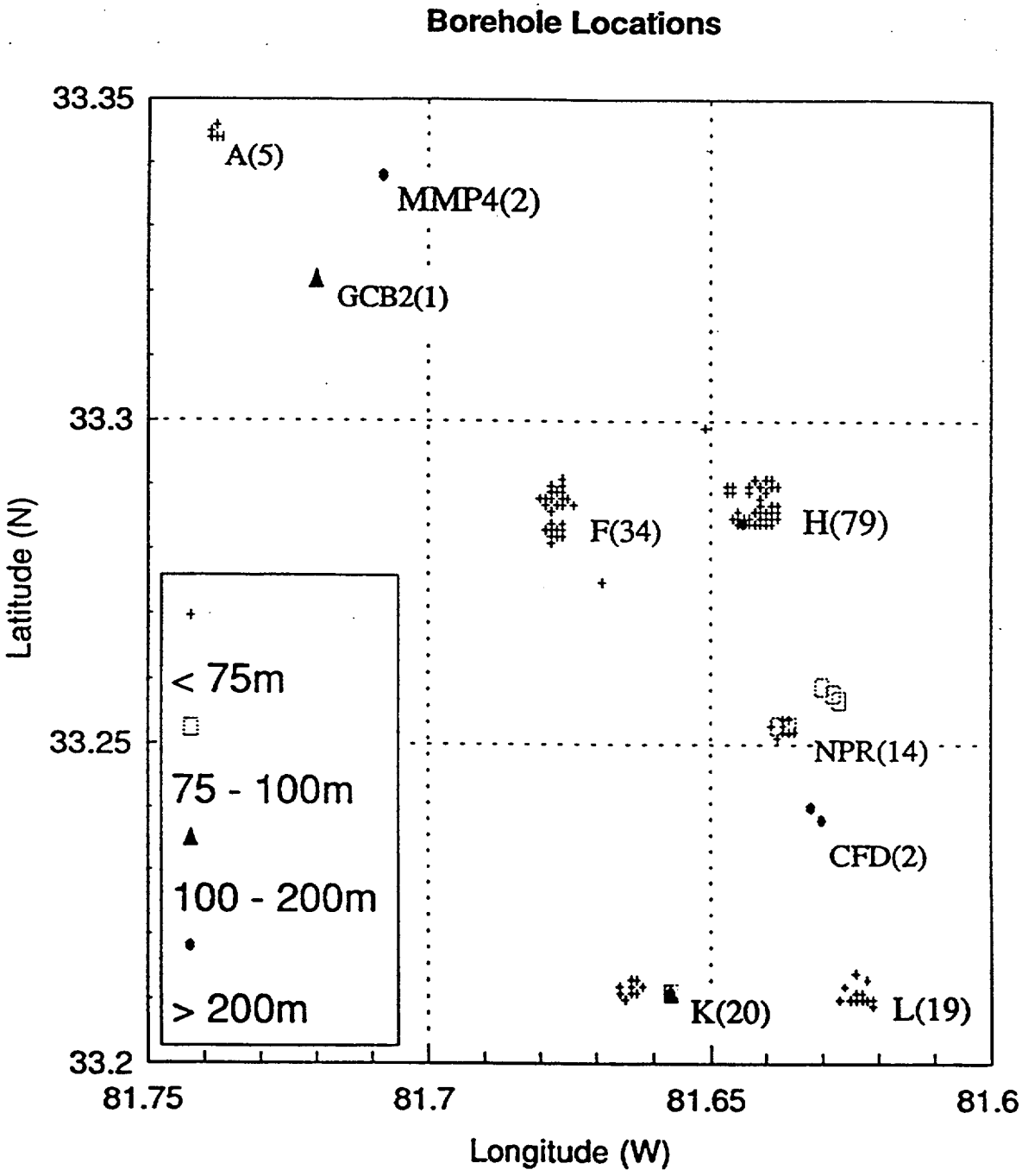

Figure 1. Location of SRS velocity-profile clusters analyzed in this study. Numbers in parentheses indicate the number of profiles in each cluster

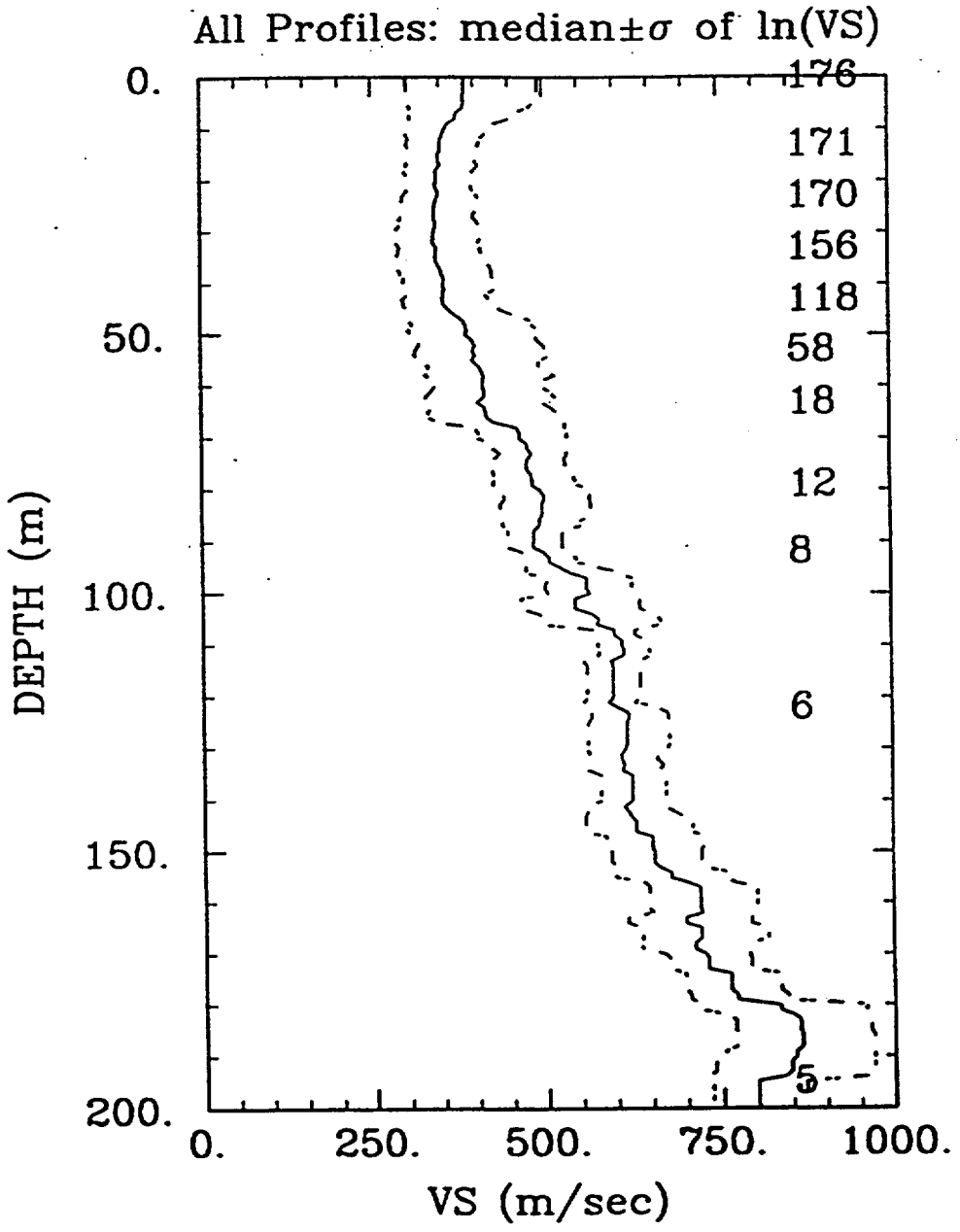

Figure 2. Summary statistics for all SRS velocity-profile data: median profile and variability. Solid line, median profile; dashed line, median ± logarithmic standard deviation. The numbers on the right side of the frame indicate the numbers of profiles at that depth or greater.

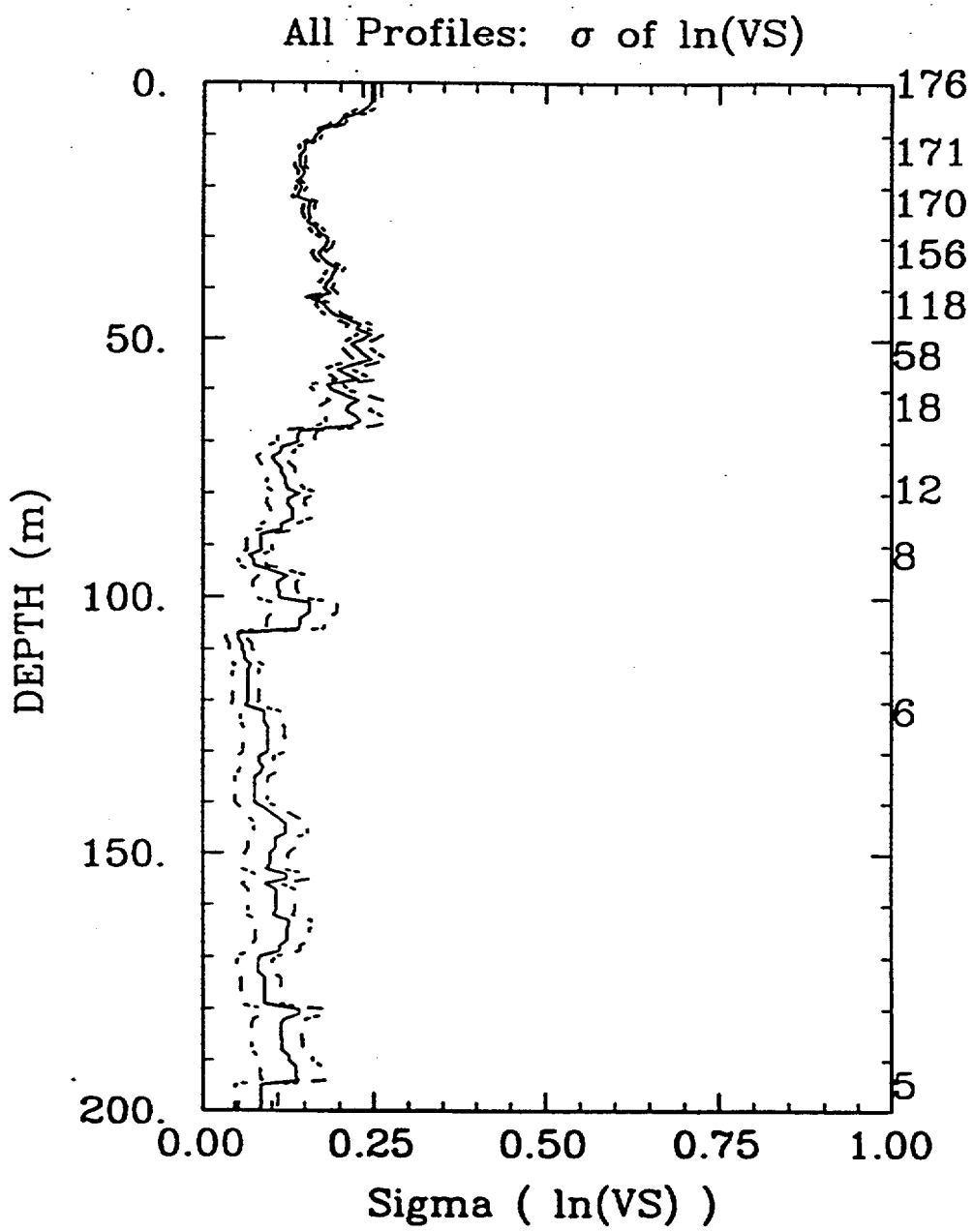

Figure 3. Summary statistics for all SRS velocity-profile data: σ_{lnV} vs. depth. Solid line, best estimate; dashed line, best estimate ± standard error of estimation. The numbers on the right side of the frame indicate the numbers of profiles at that depth or greater.

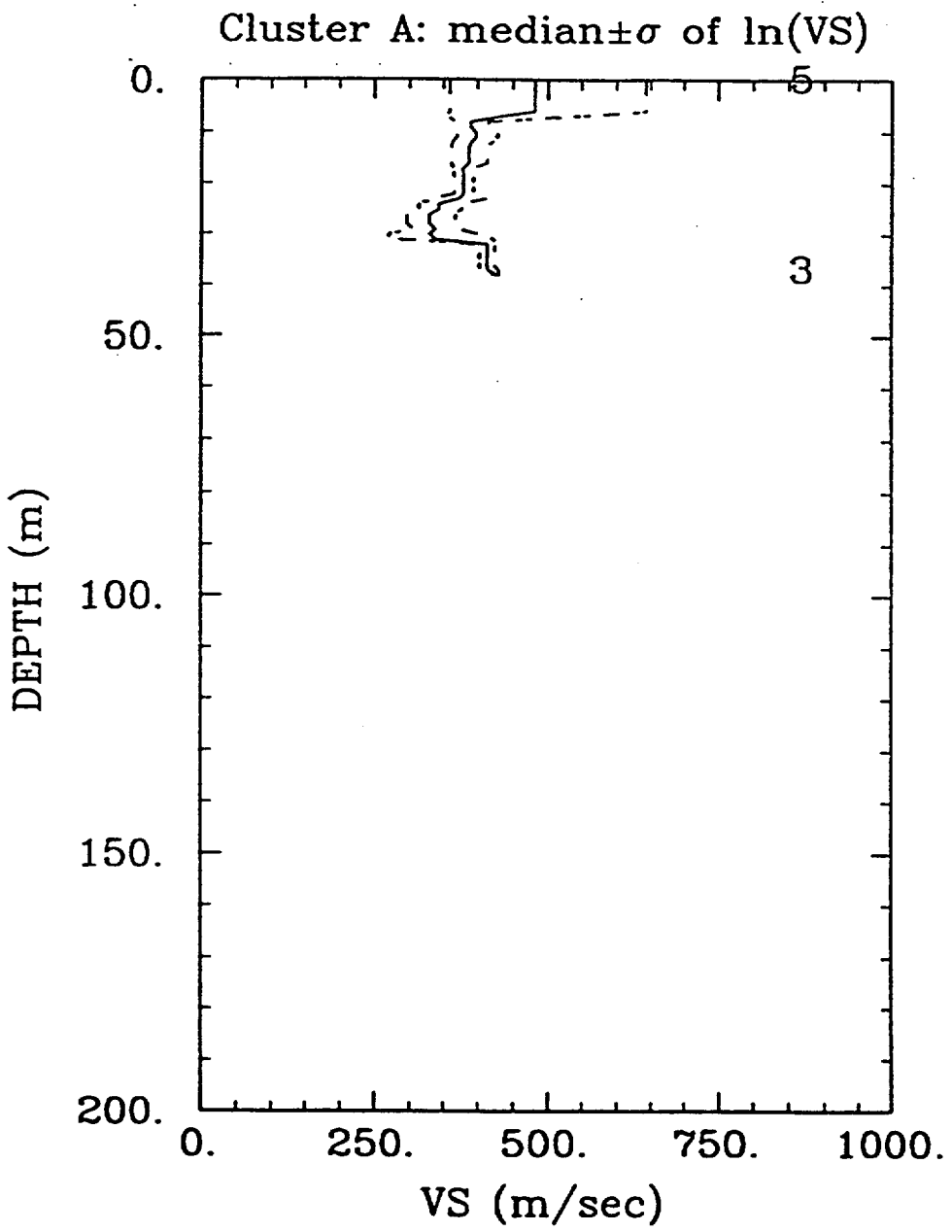

Figure 4. Summary statistics for data from cluster A: median profile and variability. Solid line, median profile; dashed line, median ± logarithmic standard deviation.

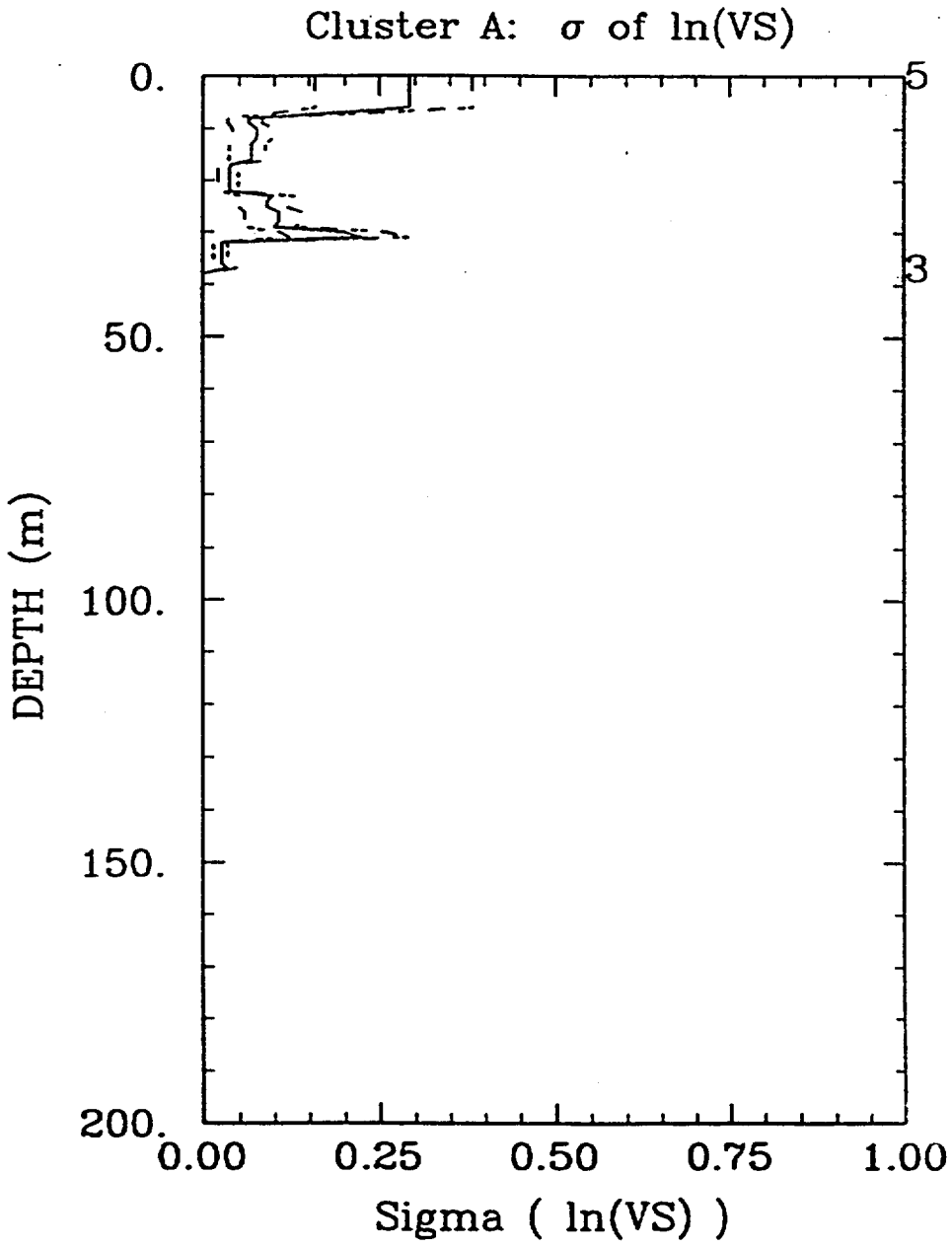

Figure 5. Summary statistics for data from cluster A: σ_{lnV} vs. depth. Solid line, best estimate; dashed line, best estimate ± standard error of estimation.

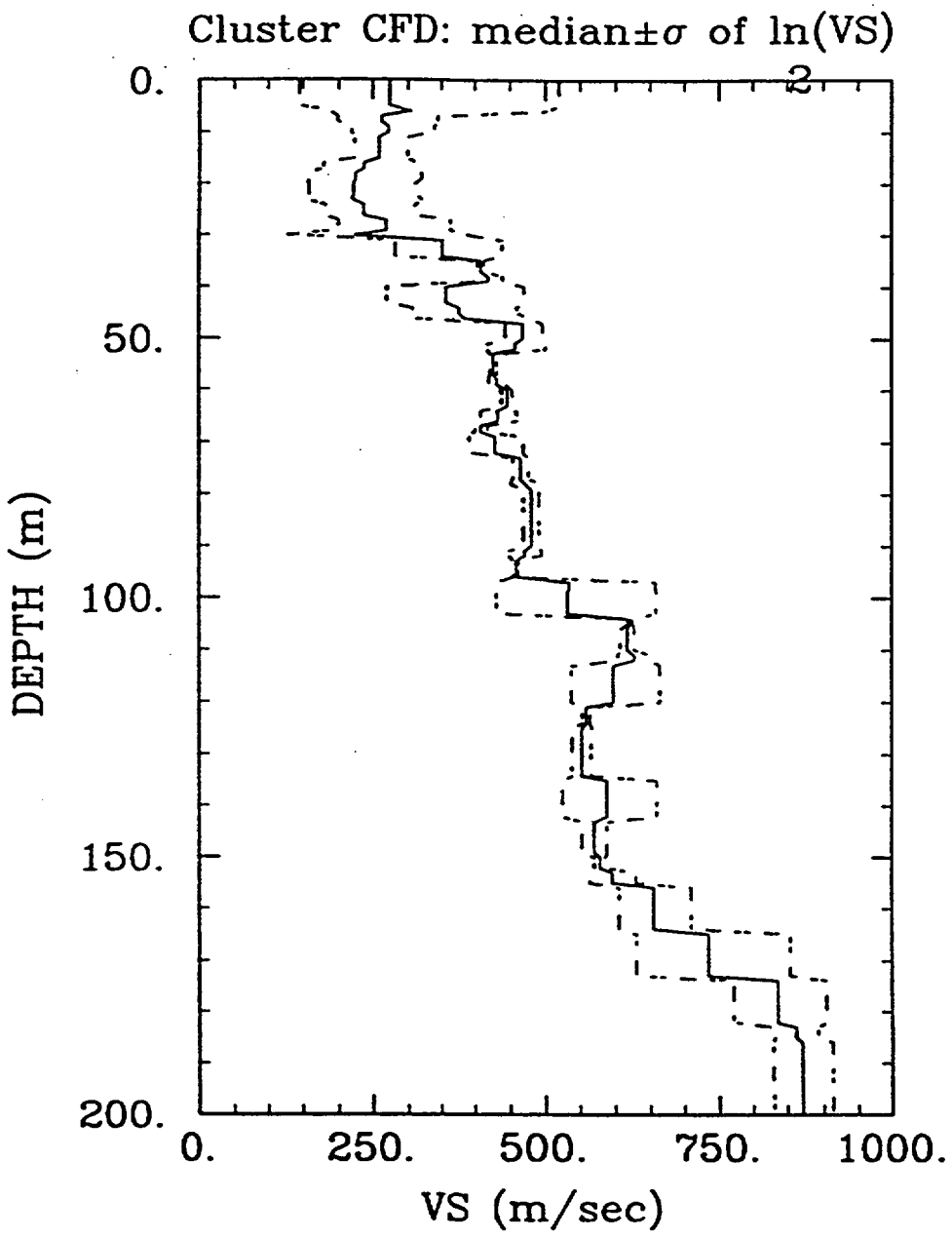

Figure 6. Summary statistics for data from cluster CFD: median profile and variability. Solid line, median profile; dashed line, median ± logarithmic standard deviation.

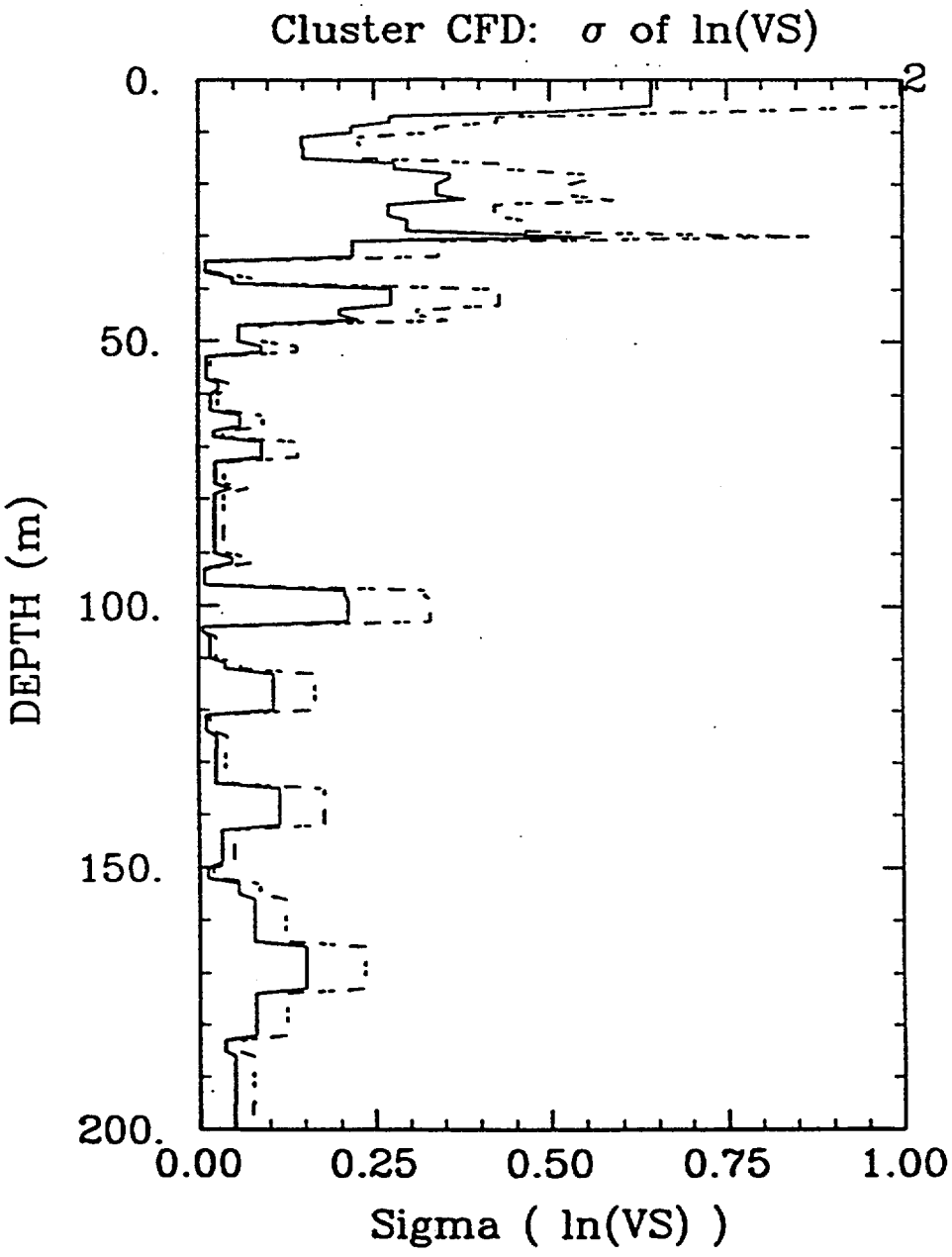

Figure 7. Summary statistics for data from cluster CFD: σ_{lnV} vs. depth. Solid line, best estimate; dashed line, best estimate ± standard error of estimation.

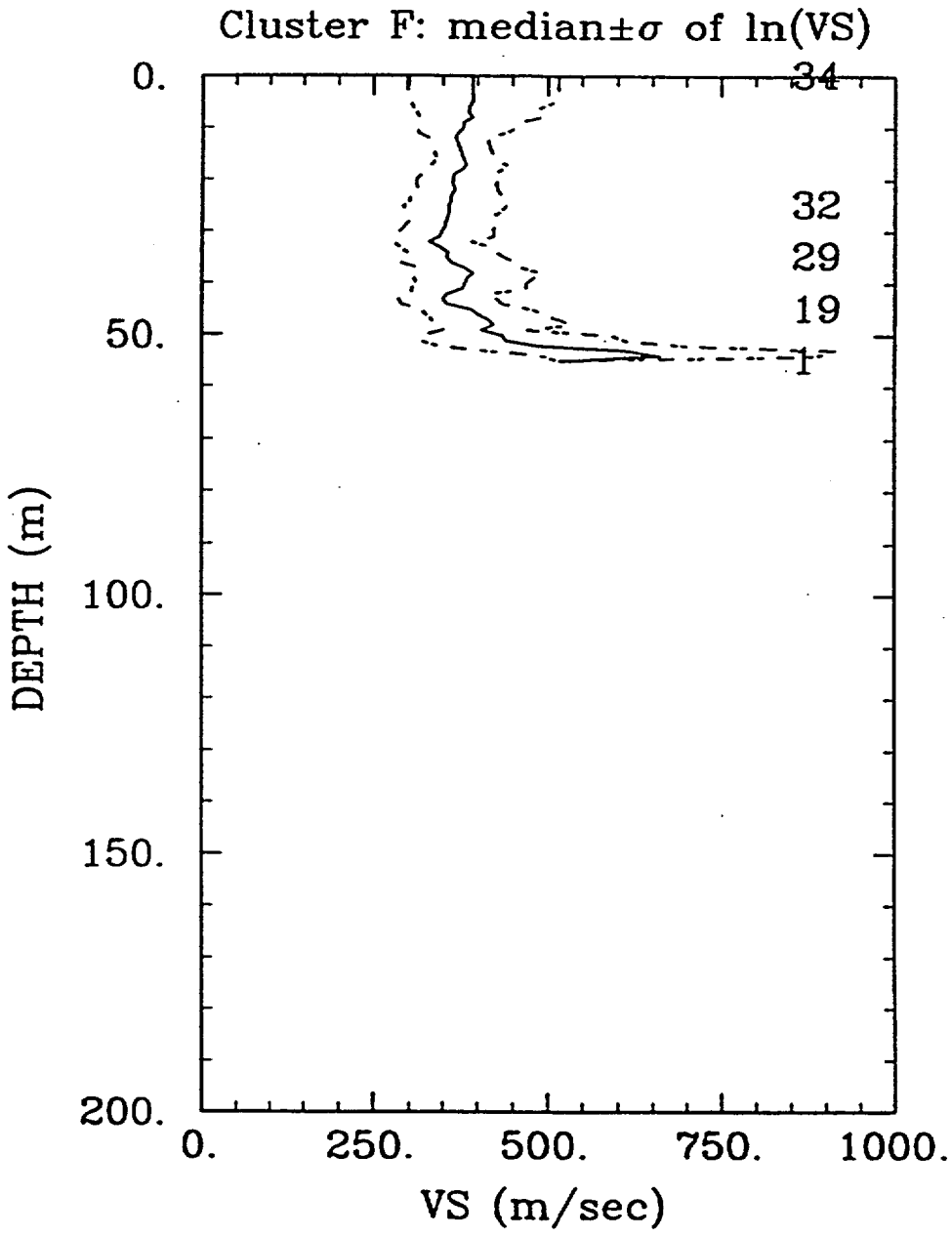

Figure 8. Summary statistics for data from cluster F: median profile and variability. Solid line, median profile; dashed line, median ± logarithmic standard deviation.

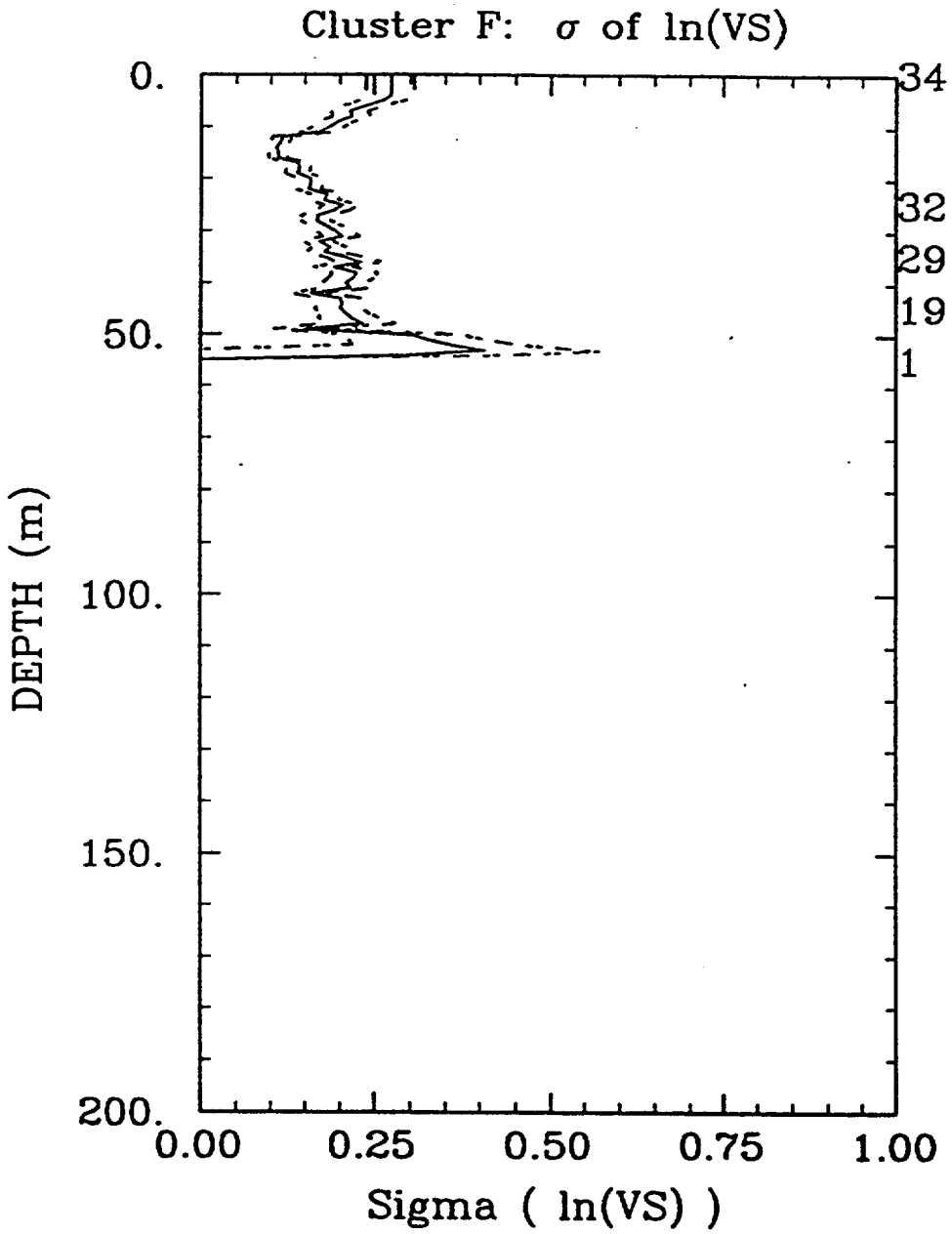

Figure 9. Summary statistics for data from cluster F: σ_{lnV} vs. depth. Solid line, best estimate; dashed line, best estimate ± standard error of estimation.

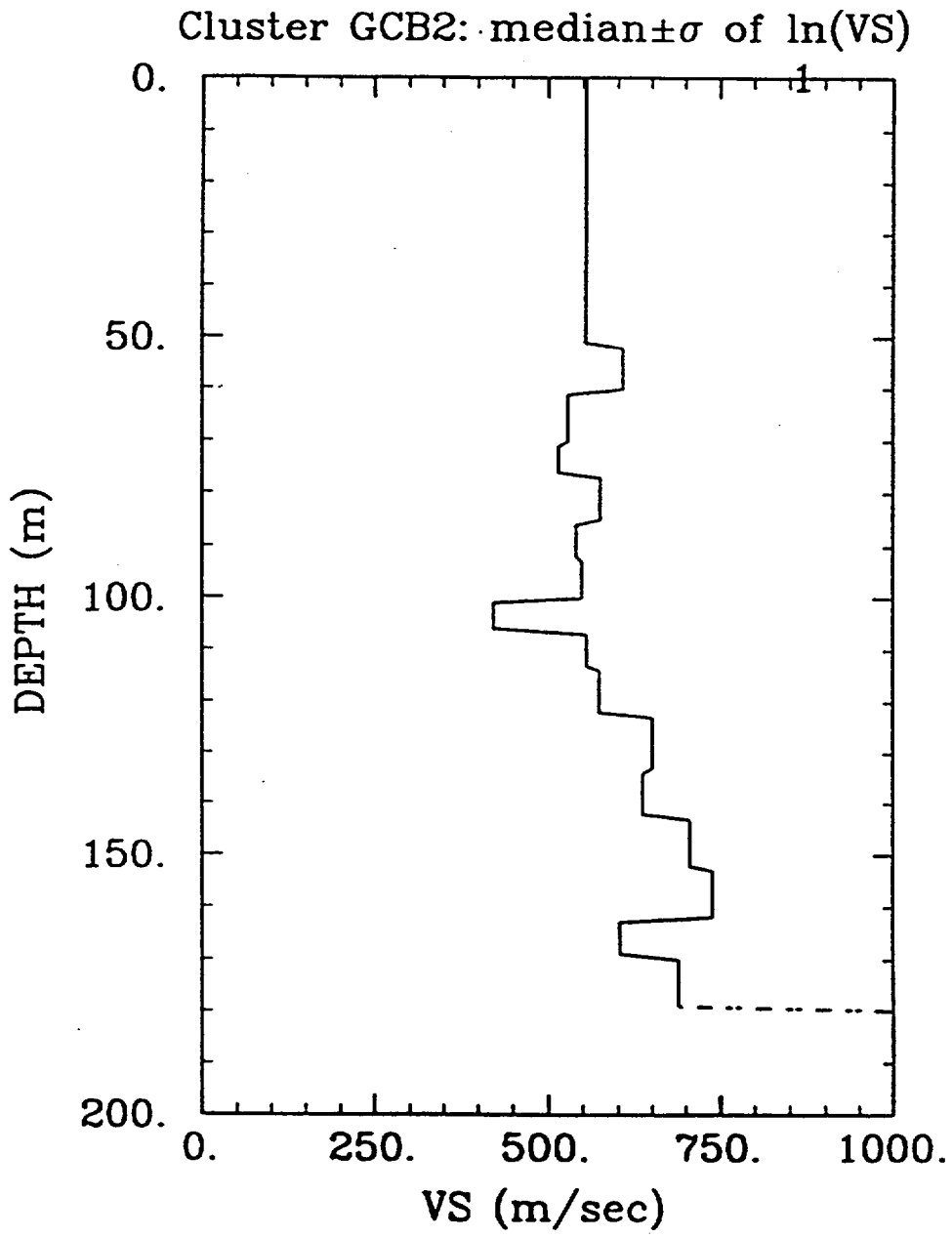

Figure 10. Summary statistics for data from cluster GCB2: median profile and variability. Solid line, median profile; dashed line, median ± logarithmic standard deviation.

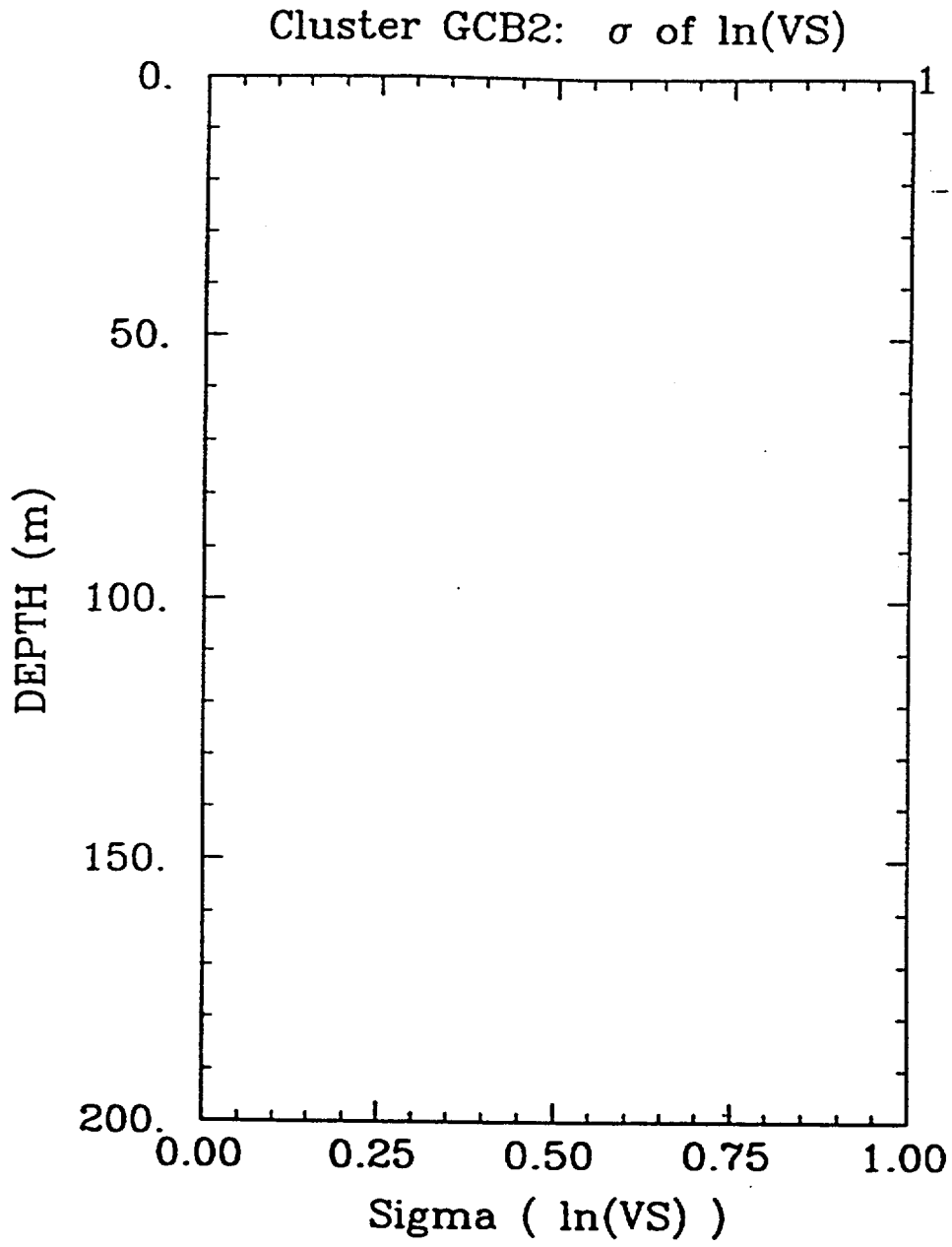

Figure 11. Summary statistics for data from cluster GCB2: σ_{lnV} vs. depth. Solid line, best estimate; dashed line, best estimate ± standard error of estimation. Note: no value of the standard deviation is shown because this quantity cannot be computed using one profile.

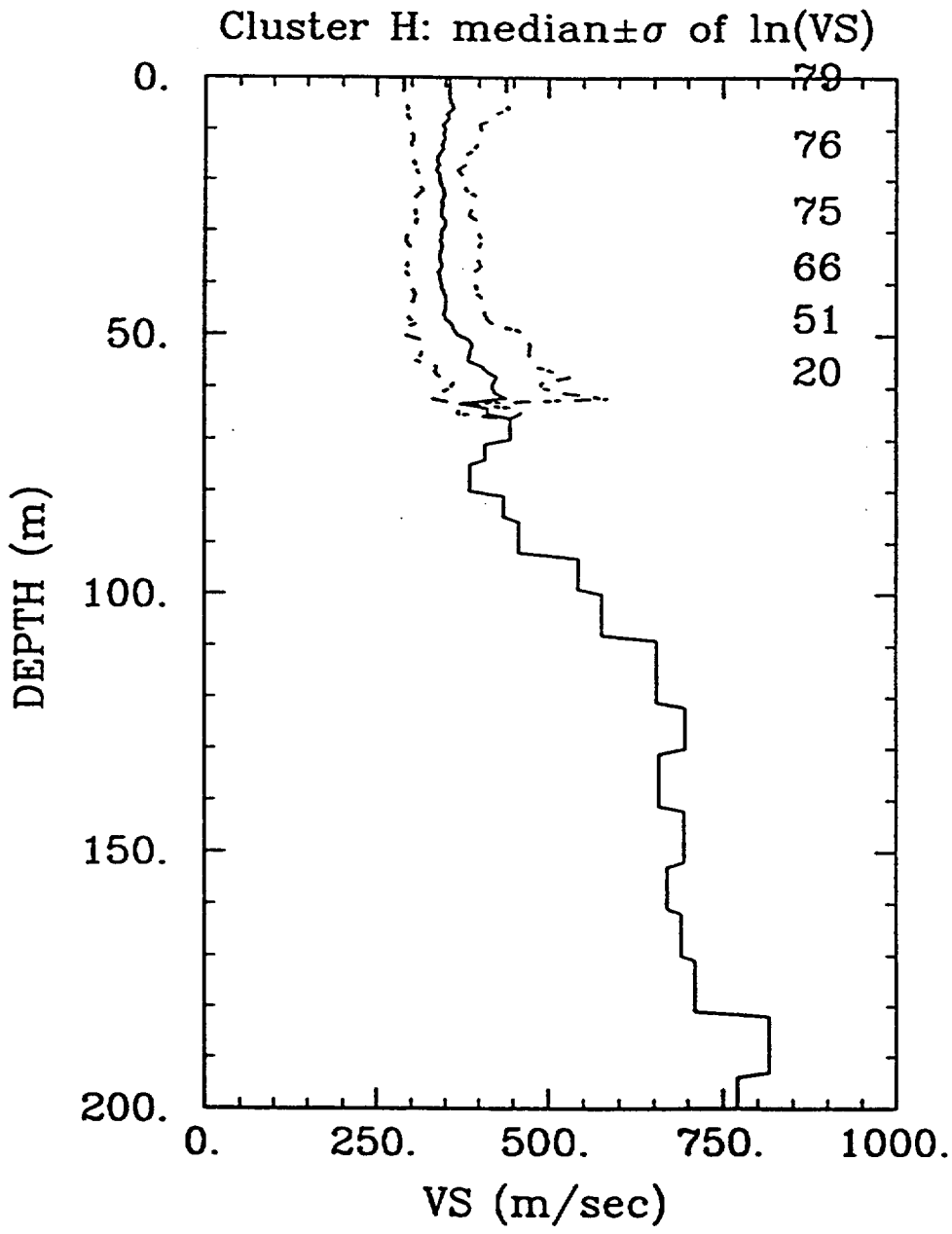

Figure 12. Summary statistics for data from cluster H: median profile and variability. Solid line, median profile; dashed line, median ± logarithmic standard deviation.

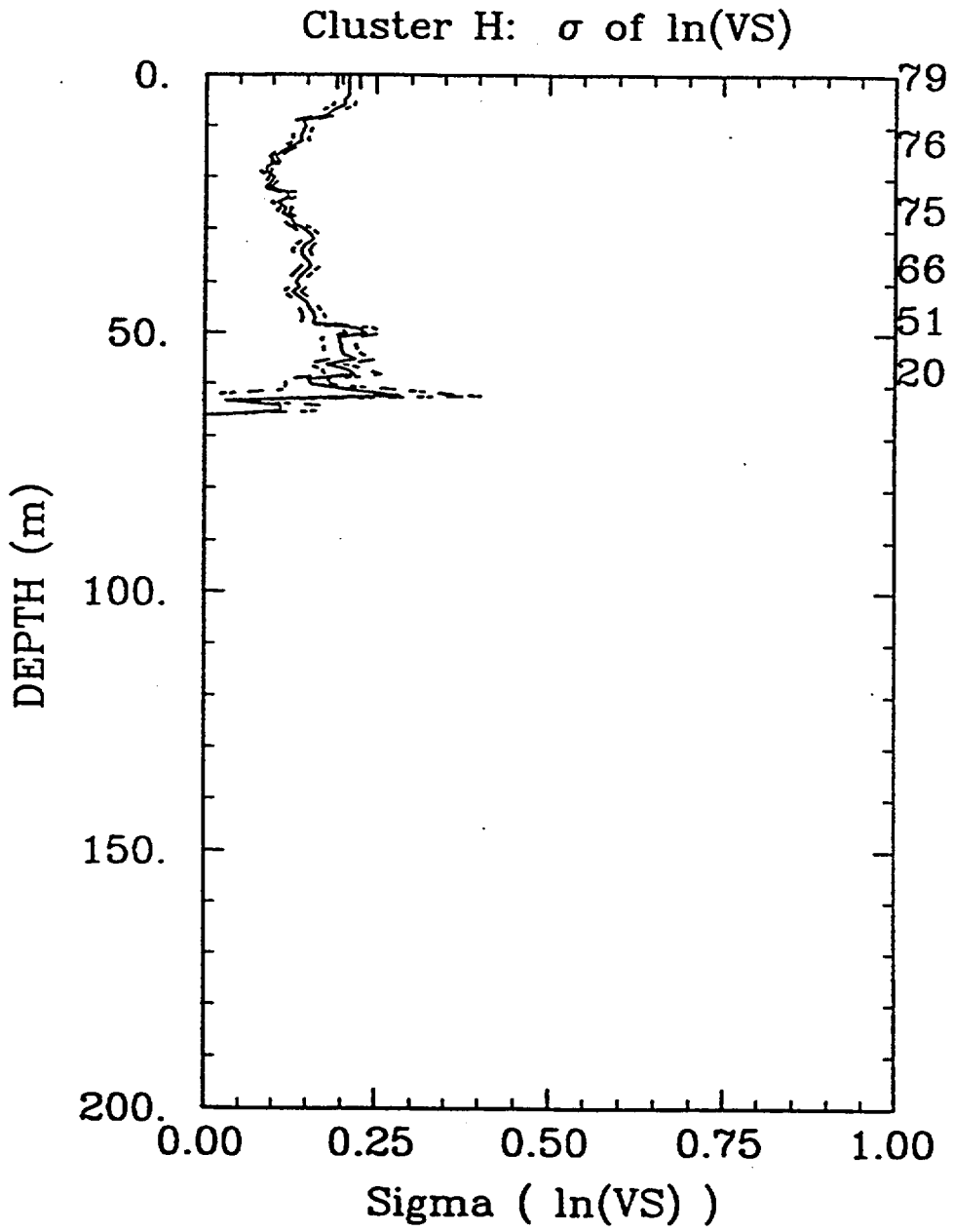

Figure 13. Summary statistics for data from cluster H: σ_{lnV} vs. depth. Solid line, best estimate; dashed line, best estimate ± standard error of estimation.

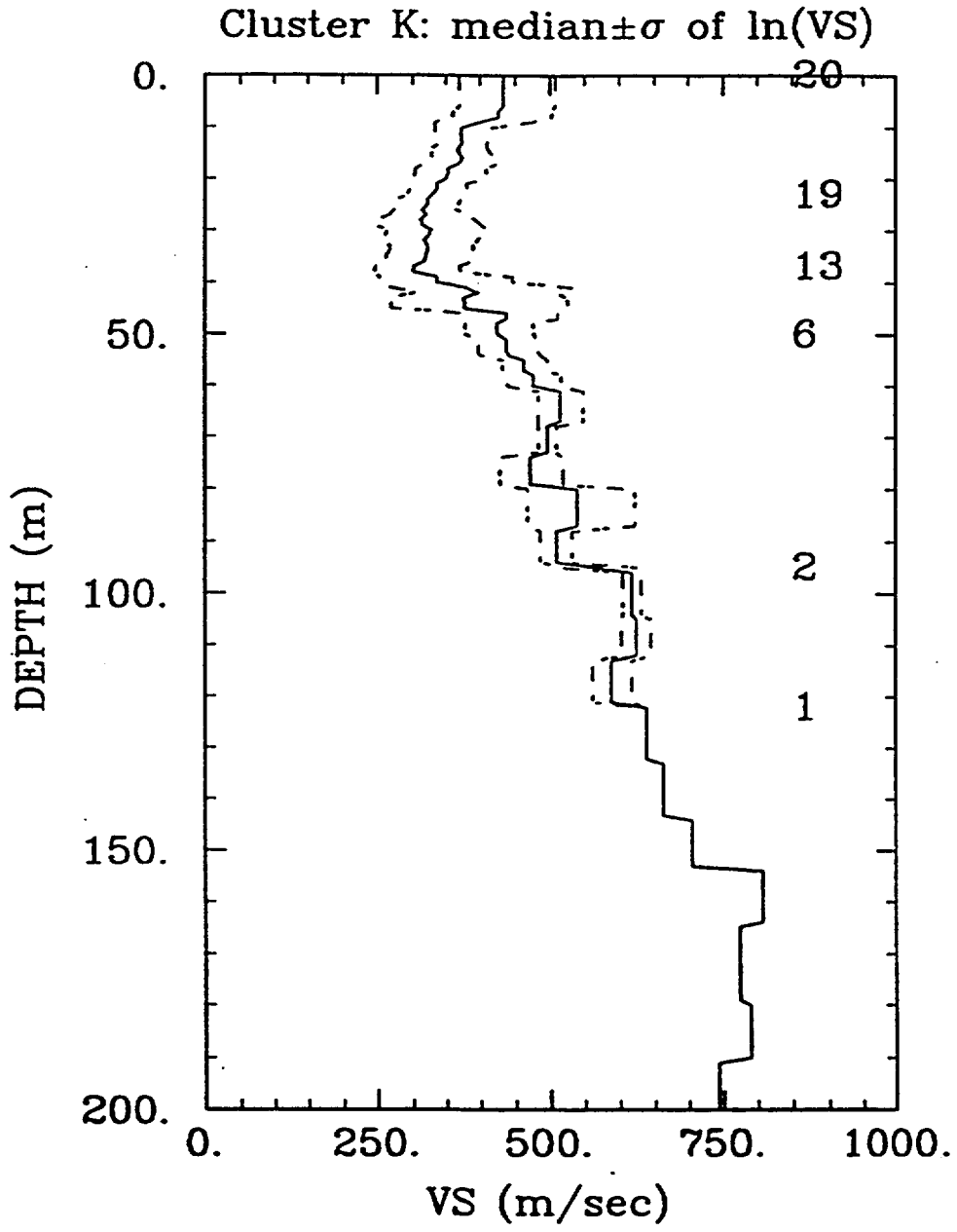

Figure 14. Summary statistics for data from cluster K: median profile and variability. Solid line, median profile; dashed line, median ± logarithmic standard deviation.

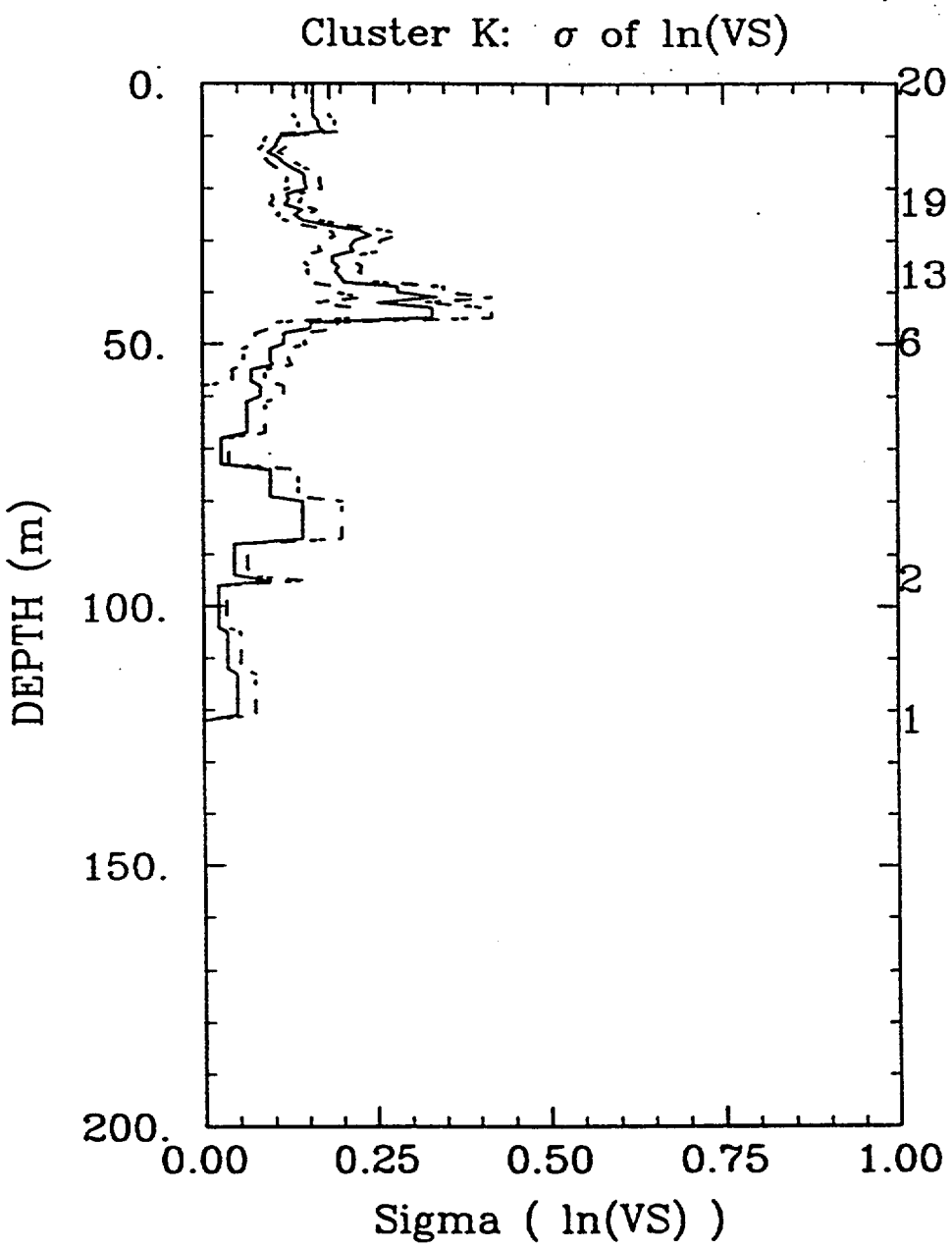

Figure 15. Summary statistics for data from cluster K: σ_{lnV} vs. depth. Solid line, best estimate; dashed line, best estimate ± standard error of estimation.

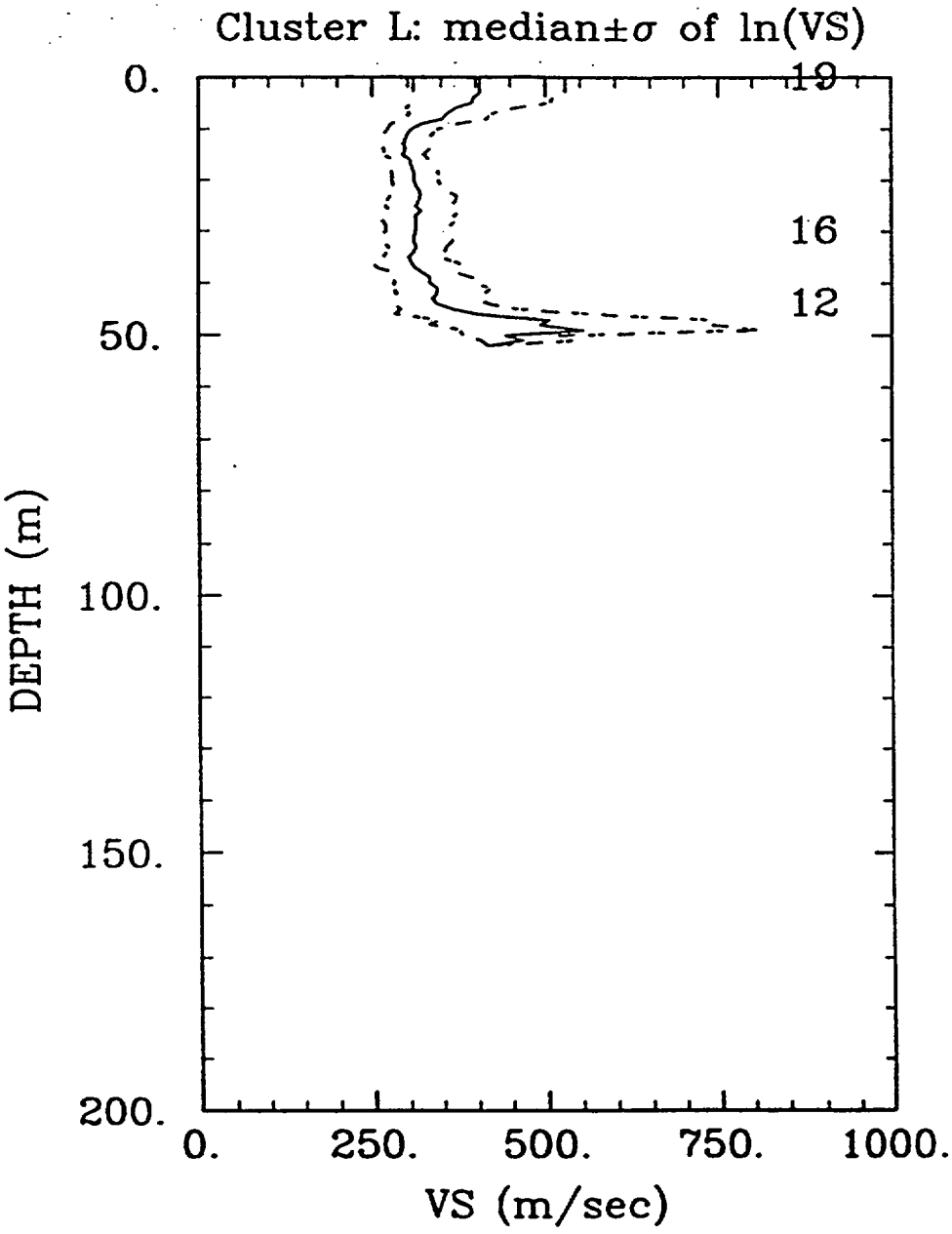

Figure 16. Summary statistics for data from cluster L: median profile and variability. Solid line, median profile; dashed line, median ± logarithmic standard deviation

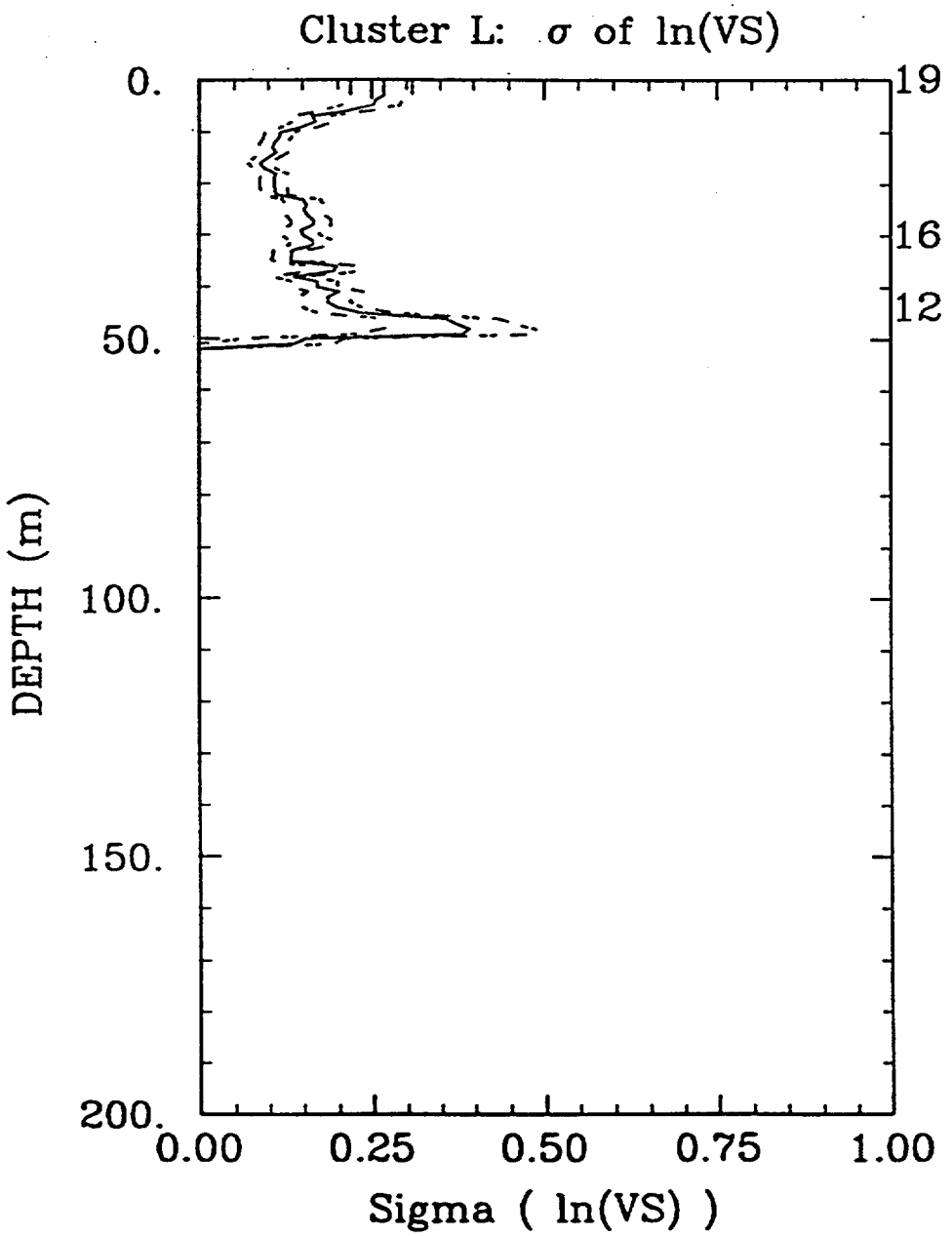

Figure 17. Summary statistics for data from cluster L: σ_{lnV} vs. depth. Solid line, best estimate; dashed line, best estimate ± standard error of estimation.

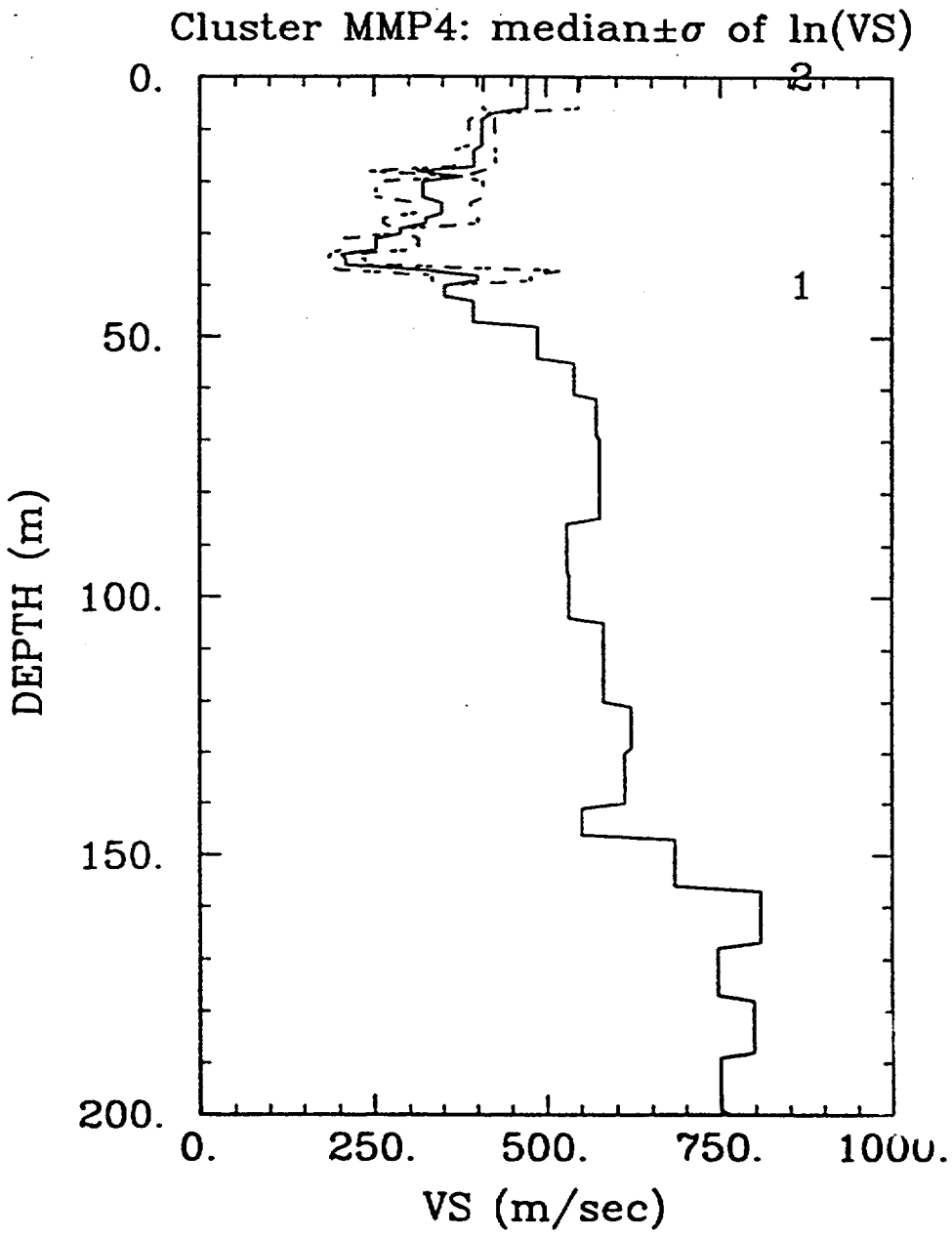

Figure 18. Summary statistics for data from cluster MMP4: median profile and variability. Solid line, median profile; dashed line, median ± logarithmic standard deviation.

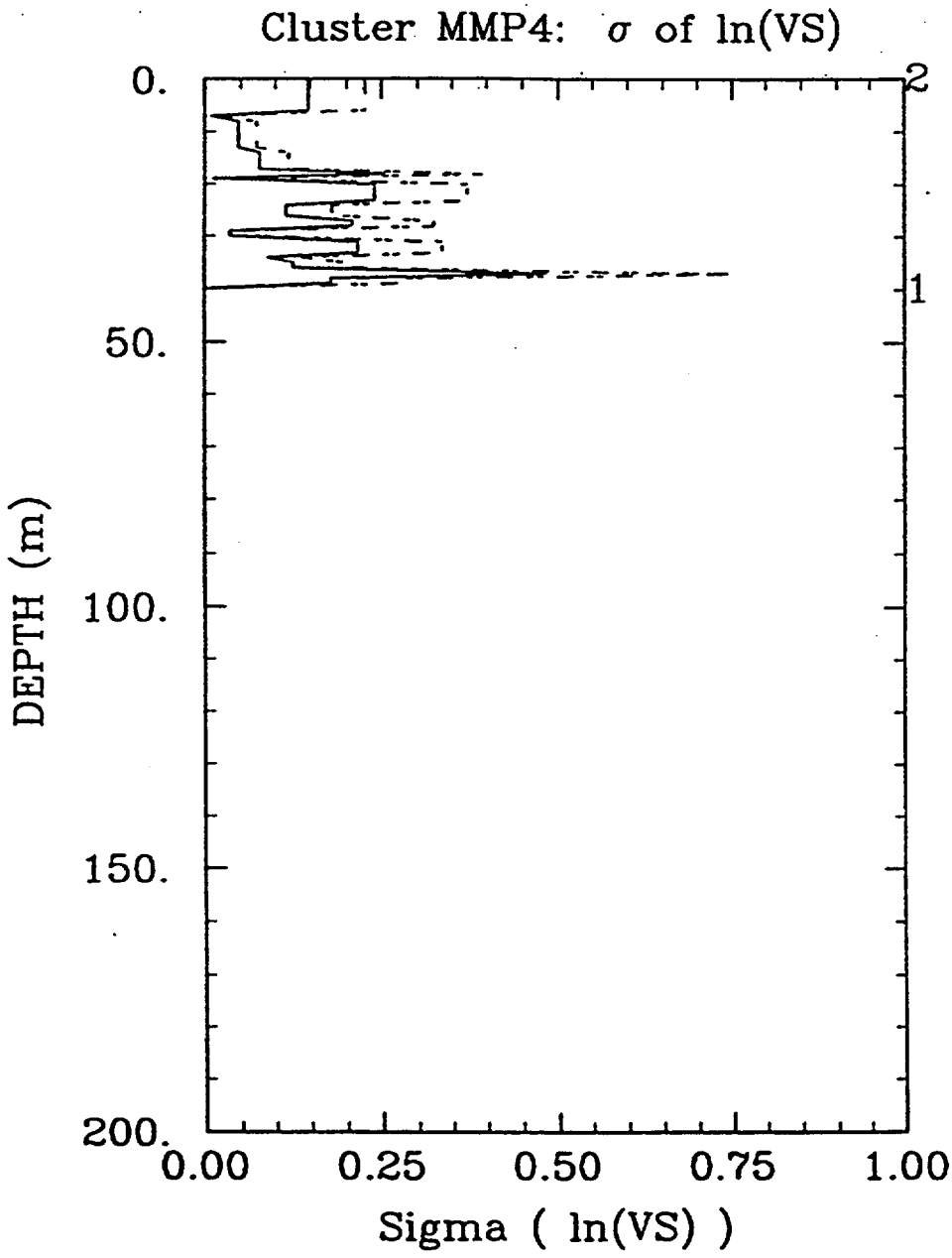

Figure 19. Summary statistics for data from cluster MMP4: σ_{lnV} vs. depth. Solid line, best estimate; dashed line, best estimate ± standard error of estimation.

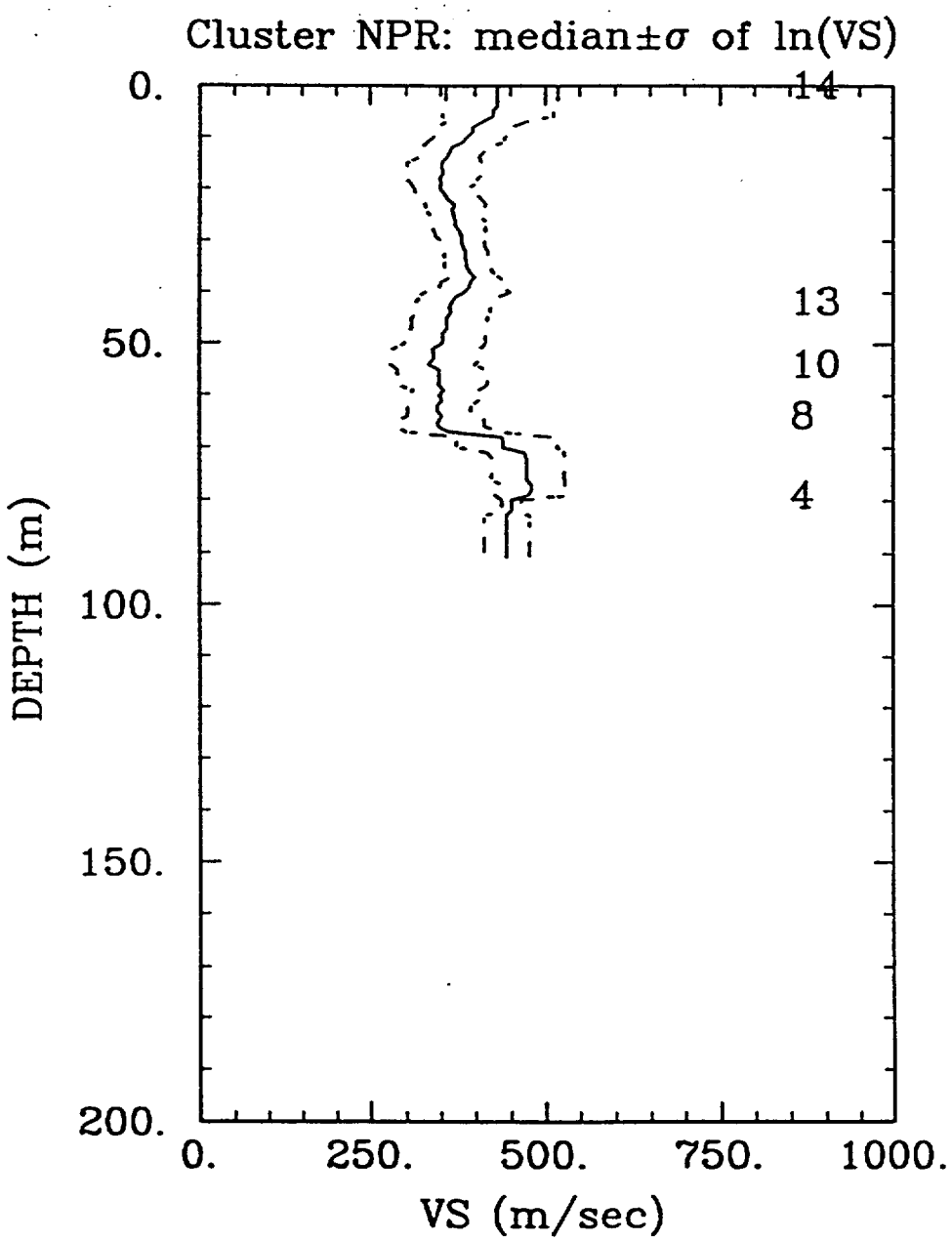

Figure 20. Summary statistics for data from cluster NPR: median profile and variability. Solid line, median profile; dashed line, median ± logarithmic standard deviation.

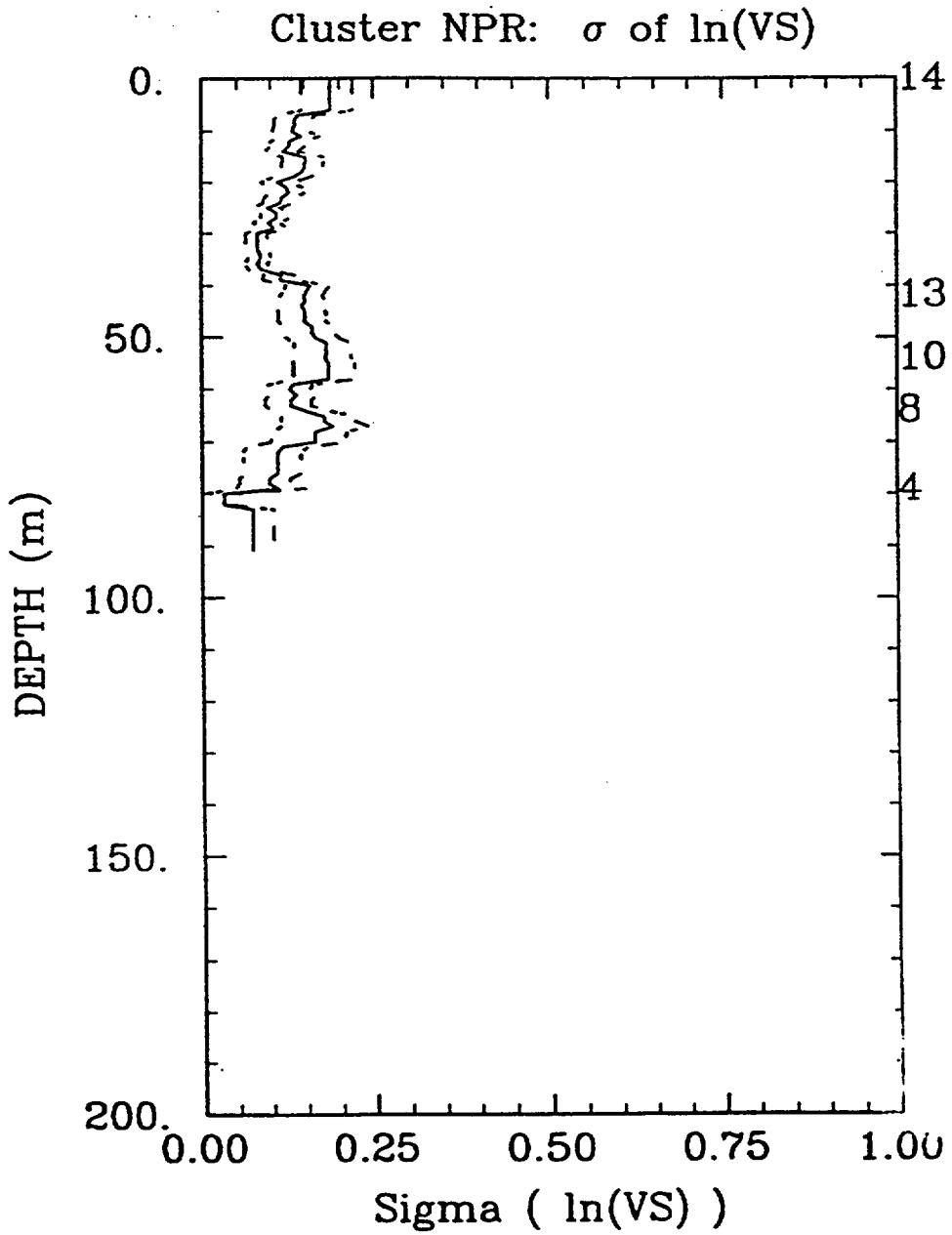

Figure 21. Summary statistics for data from cluster NPR: $\sigma_{Ln\,V}$ ... depth. Solid line, best estimate; dashed line, best estimate ± standard error of estimation.

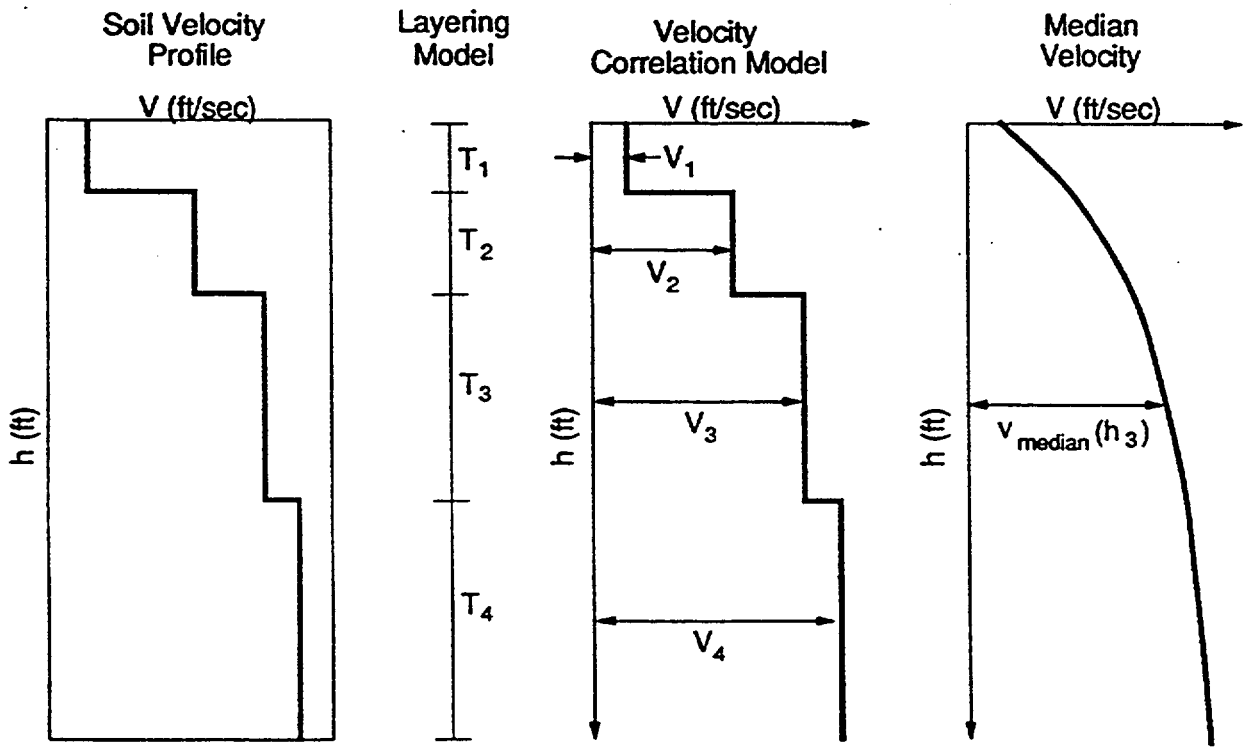

Figure 22. Schematic representation of the three elements of the probabilistic model of velocity profiles.

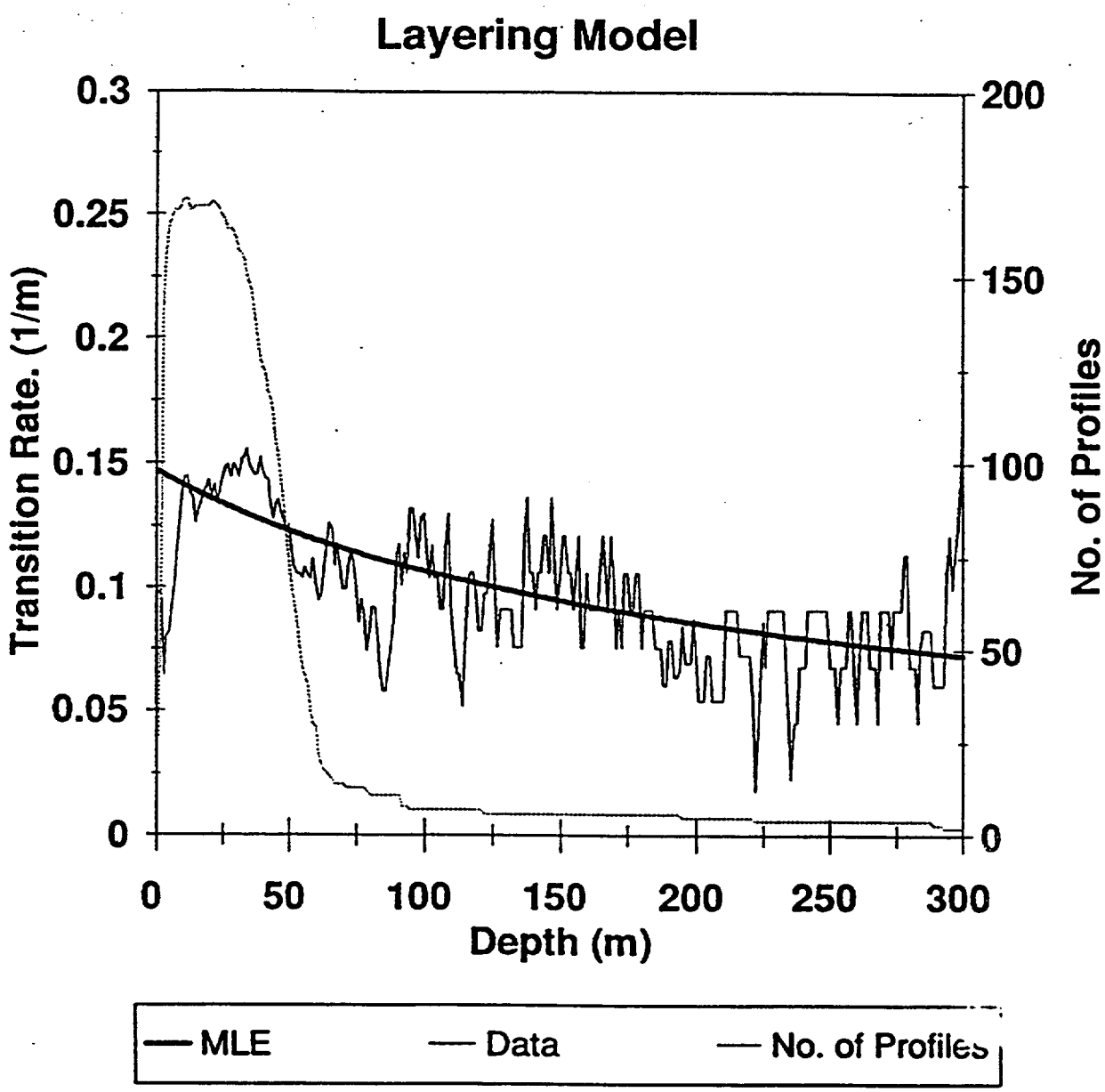

Figure 23. Probabilistic model of layer thickness. Thin jagged lines, transition rate of layer boundaries; thin smooth curve, maximum-likelihood model for transition rate $\lambda(h)$, dashed line, number of profiles at this depth (scale given in right Y axis).

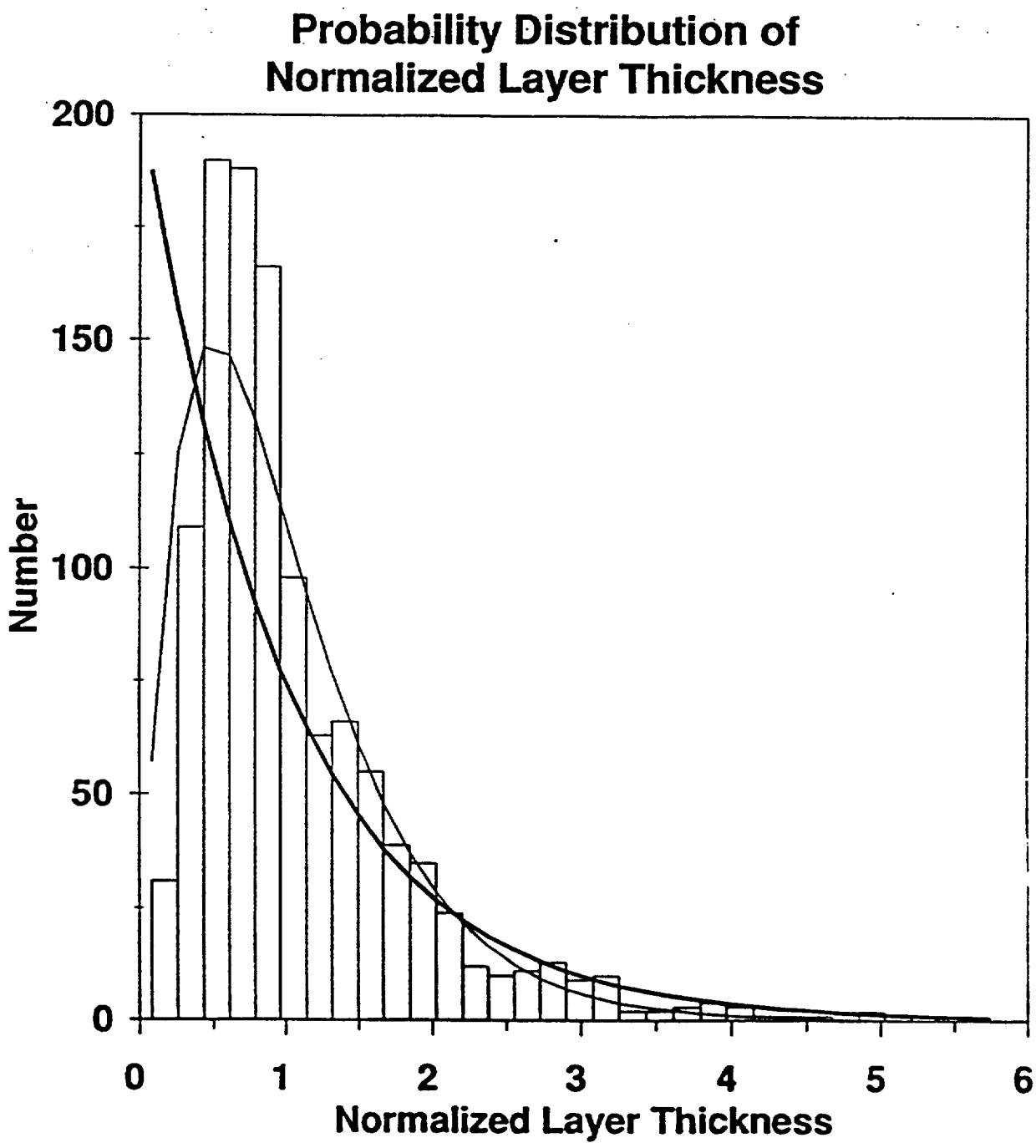

Figure 24. Observed distribution of normalized layer thickness τ (histogram). Thick line, exponential distribution; thin line, gamma distribution with COV of 0.71.

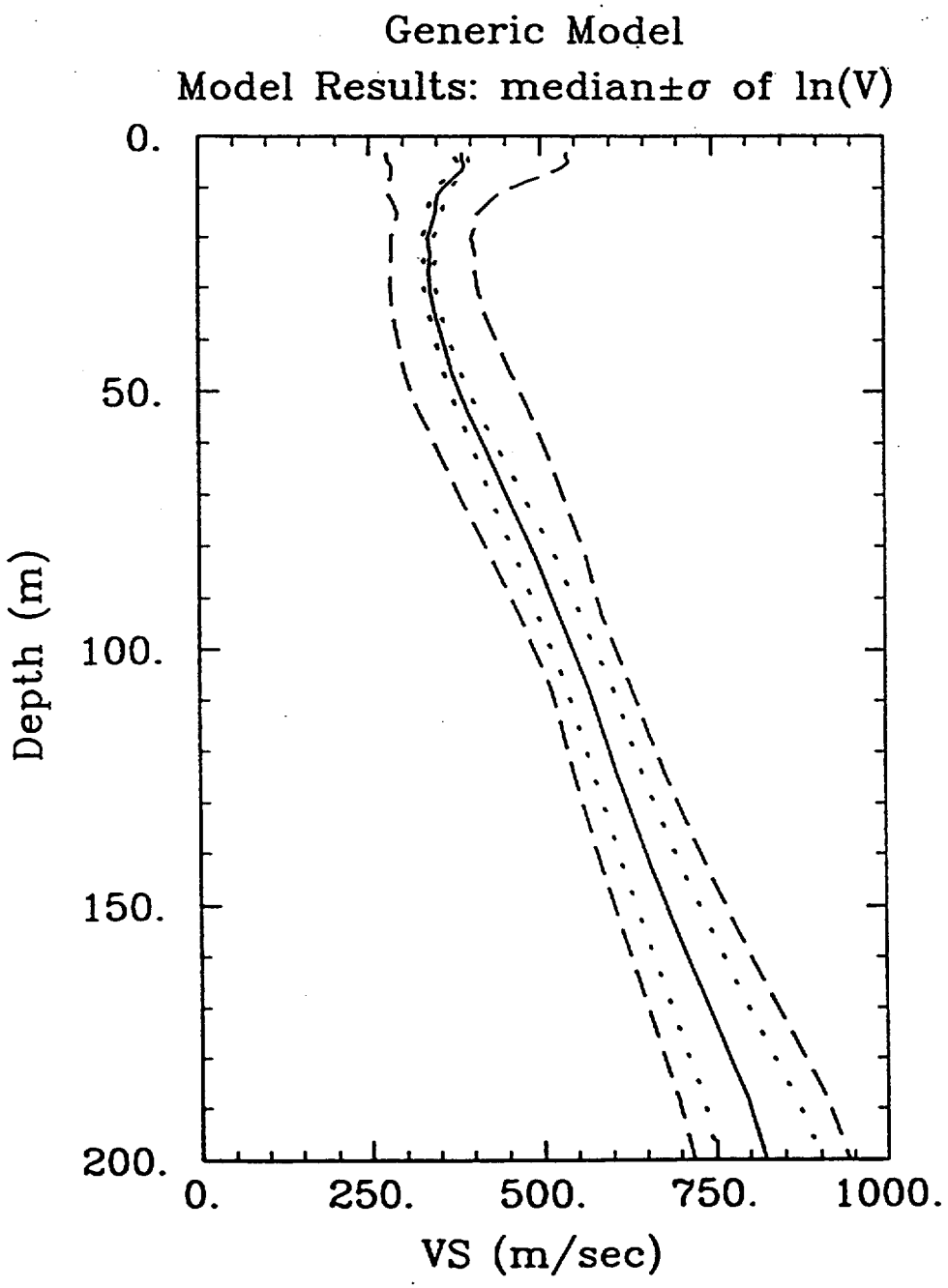

Figure 25. Generic SRS shear-wave velocity model: median profile and variability. Solid line, median profile; dashed line, median ± logarithmic standard deviation; dotted line, median ± standard error of estimation.

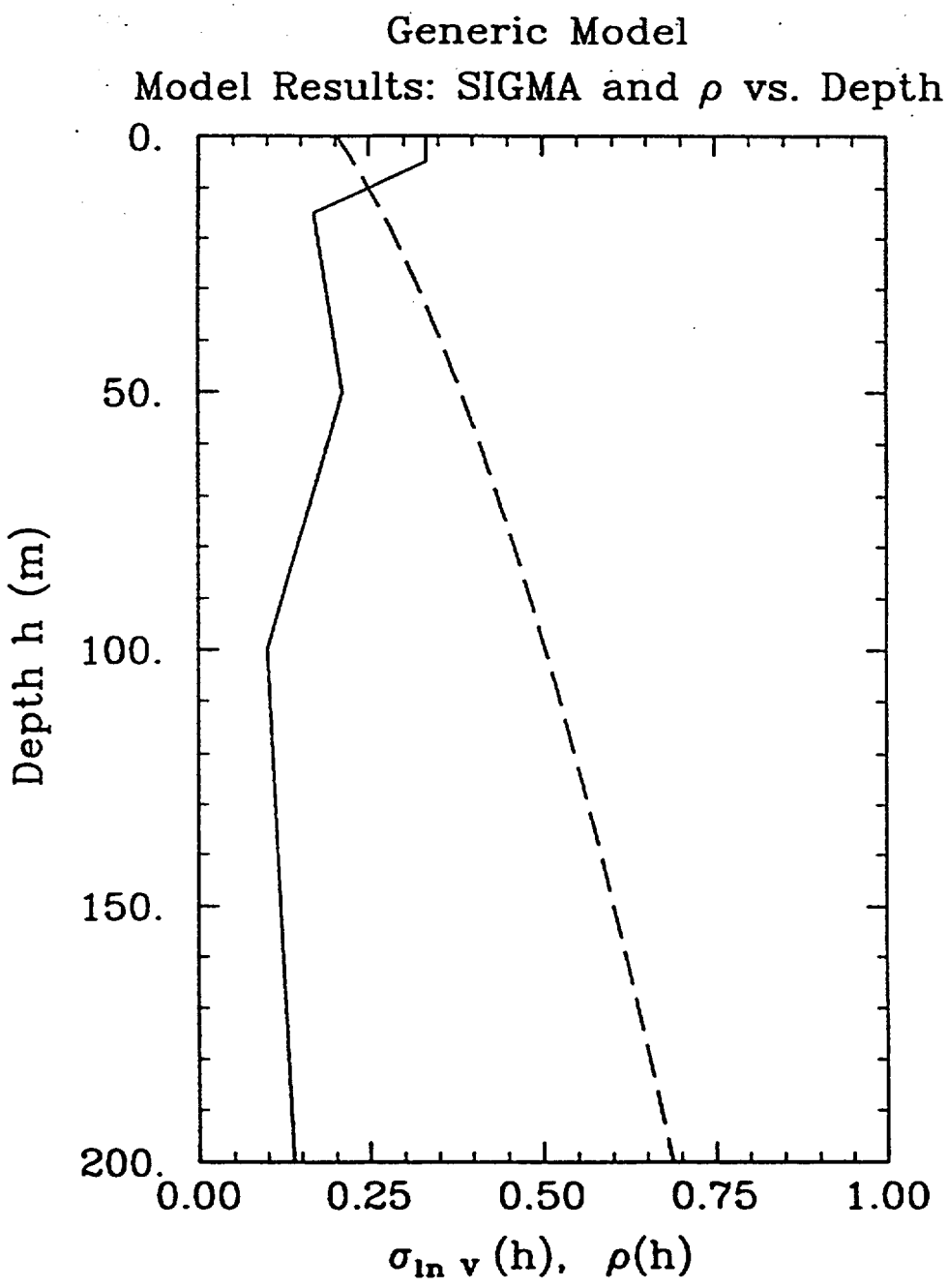

Figure 26. Generic SRS shear-wave velocity model: standard deviation σ_{lnV} and correlation coefficient $\rho(h)$ vs. depth. Solid line, standard deviation; dashed line, correlation coefficient.

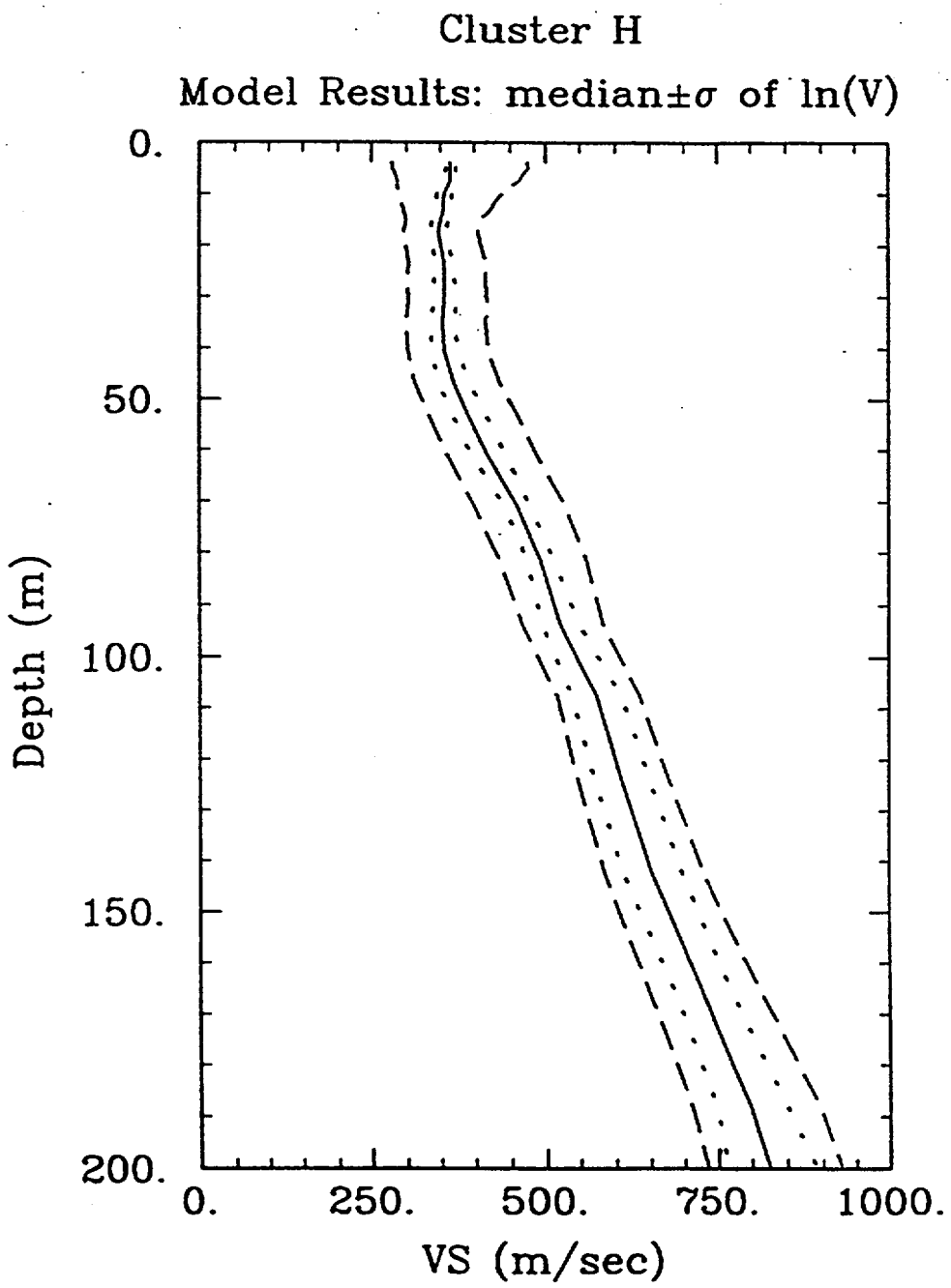

Figure 27. Shear-wave velocity model for cluster H: median profile and variability. Solid line, median profile; dashed line, median ± logarithmic standard deviation; dotted line, median ± standard error of estimation.

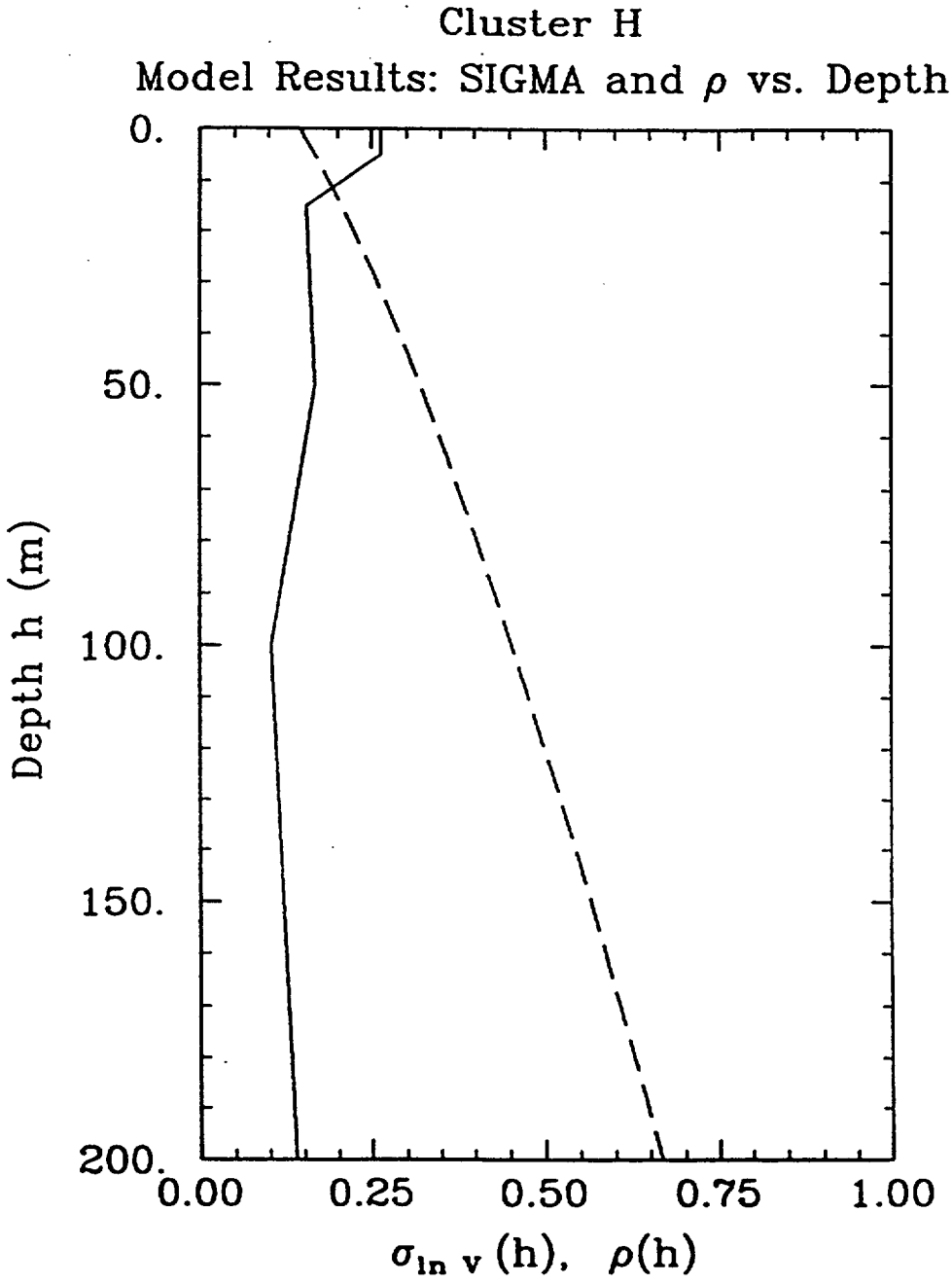

Figure 28. Shear-wave velocity model for cluster H: standard deviation σ_{lnV} and correlation coefficient $\rho(h)$ vs. depth. Solid line, standard deviation; dashed line, correlation coefficient.

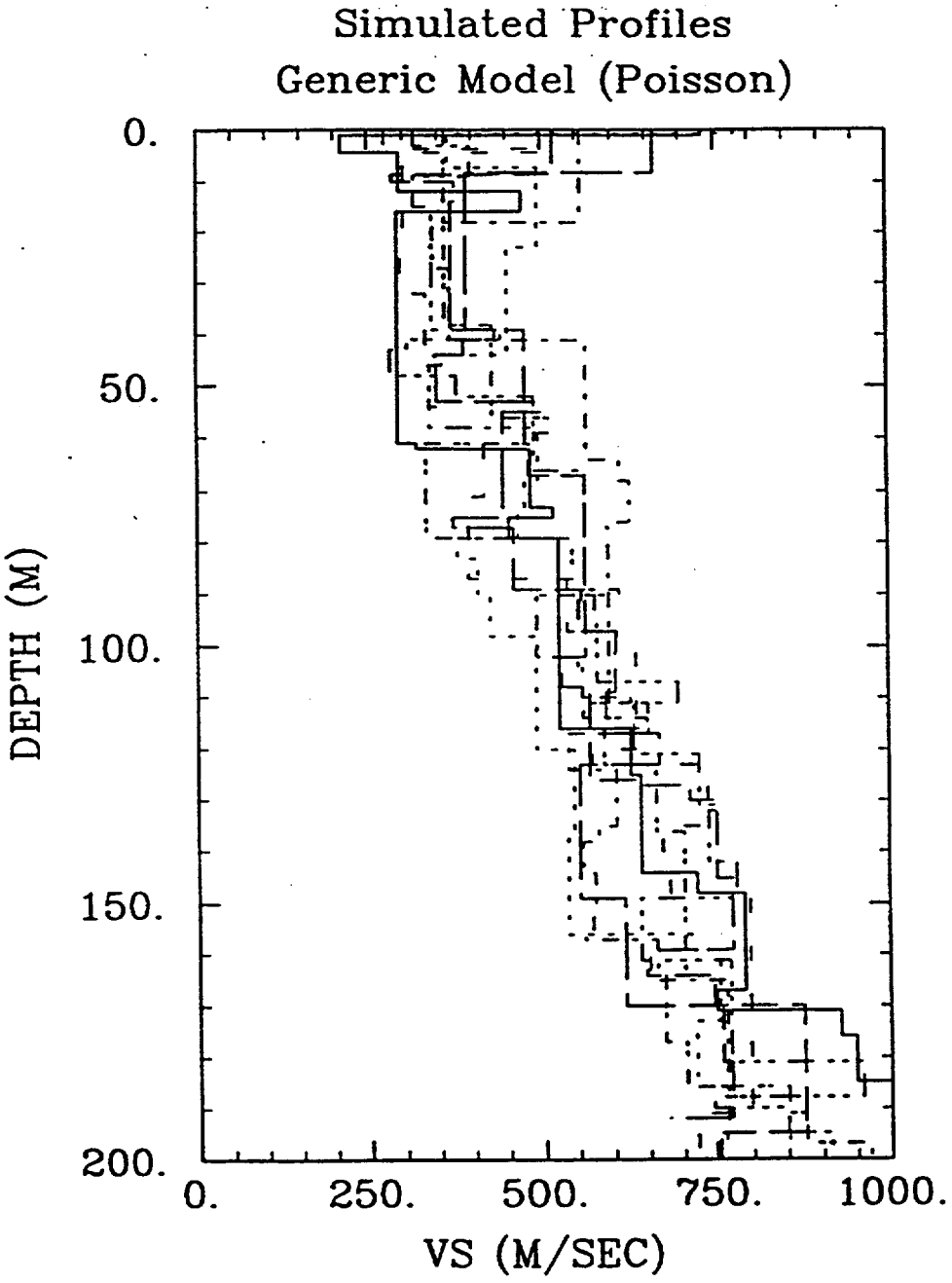

Figure 29. Velocity profiles simulated with the generic SRS shear-wave velocity model, non-homogeneous Poisson layering model.

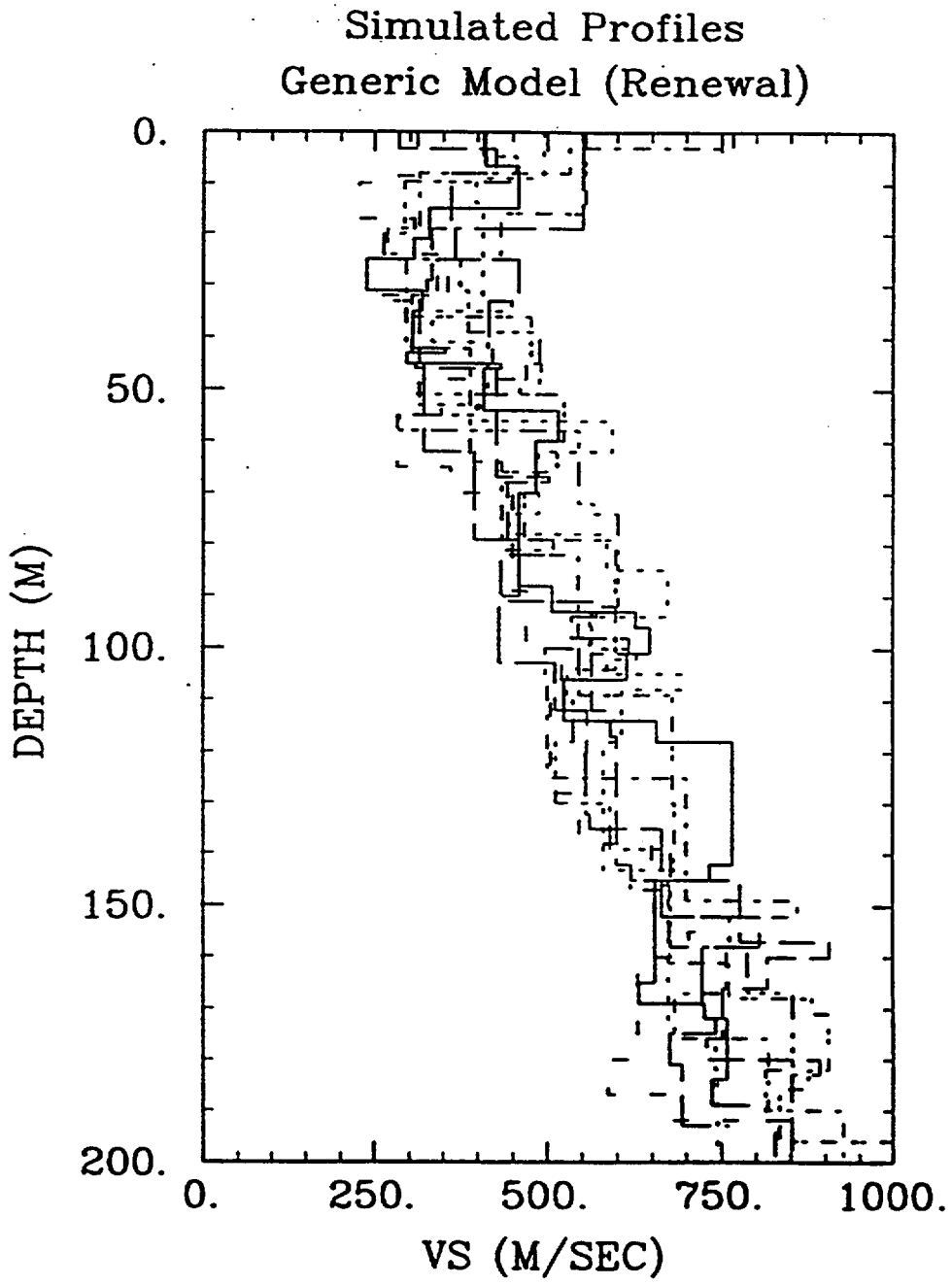

Figure 30. Velocity profiles simulated with the generic SRS shear-wave velocity model, non-homogeneous renewal layering model.

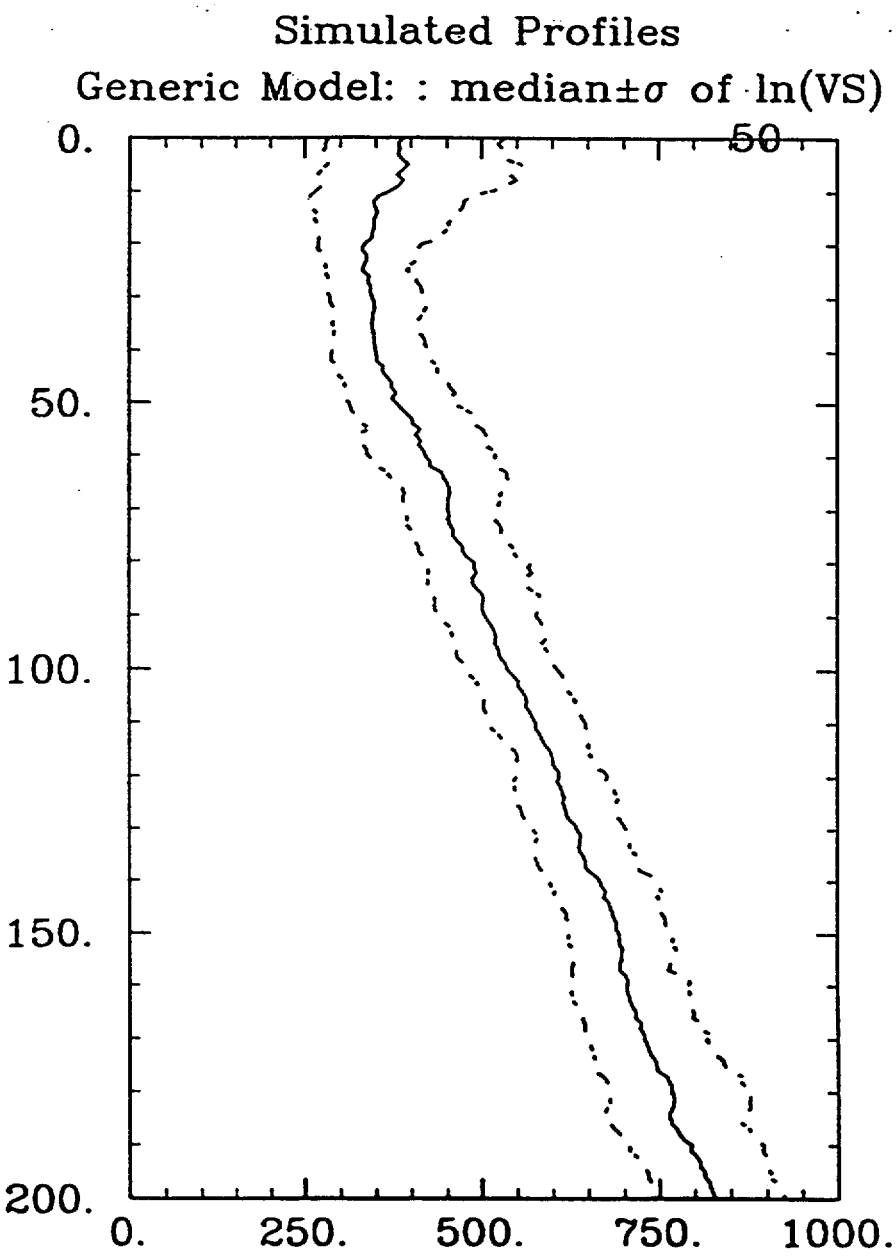

Figure 31. Summary statistics for 50 artificial profiles simulated with the generic SRS velocity model: median profile and variability. Solid line, median profile; dashed line, median ± logarithmic standard deviation.

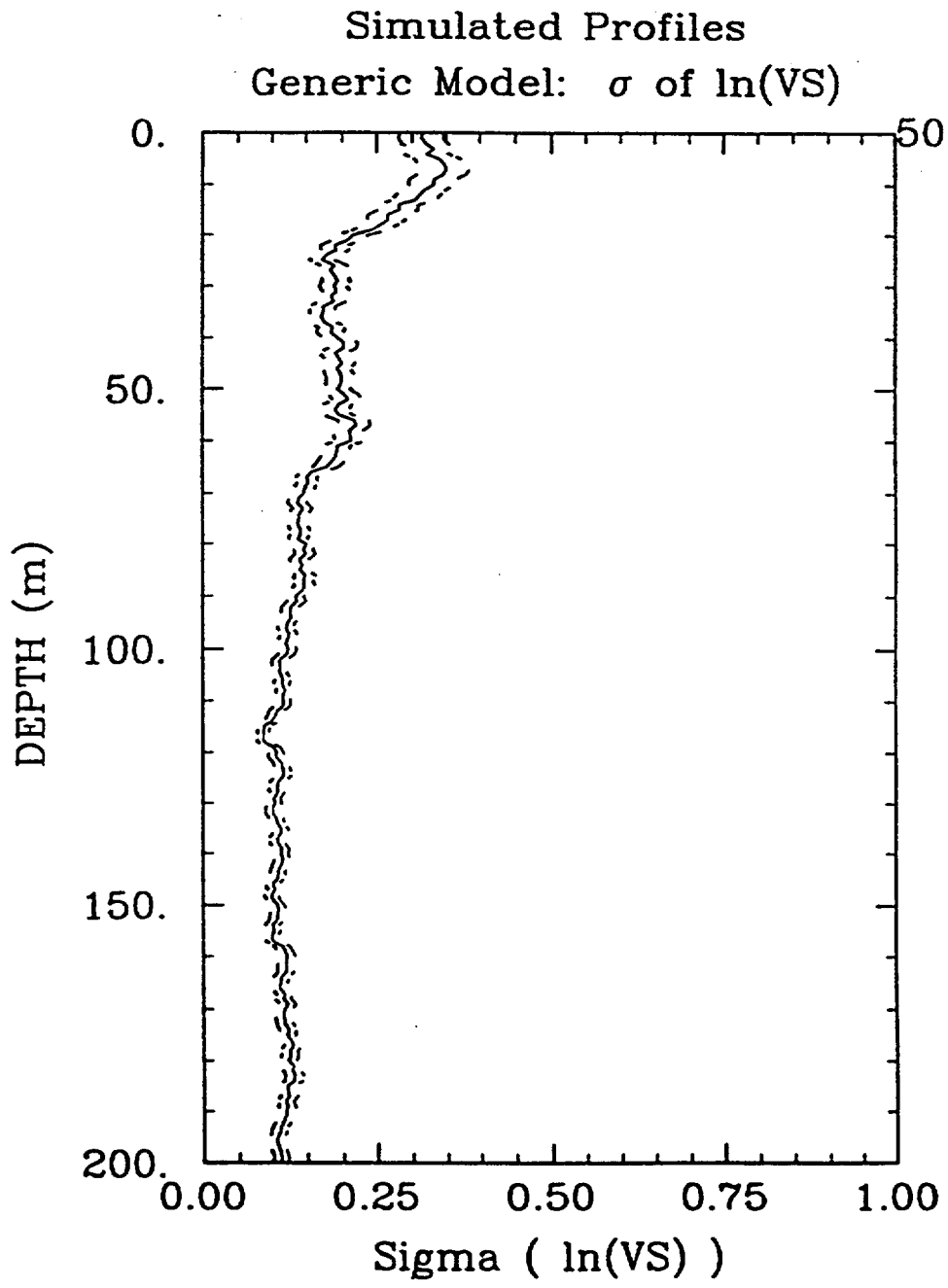

Figure 32. Summary statistics for 50 artificial profiles simulated with the generic SRS velocity model: σ_{lnV} vs. depth. Solid line, best estimate; dashed line, best estimate $\pm$ standard error of estimation.

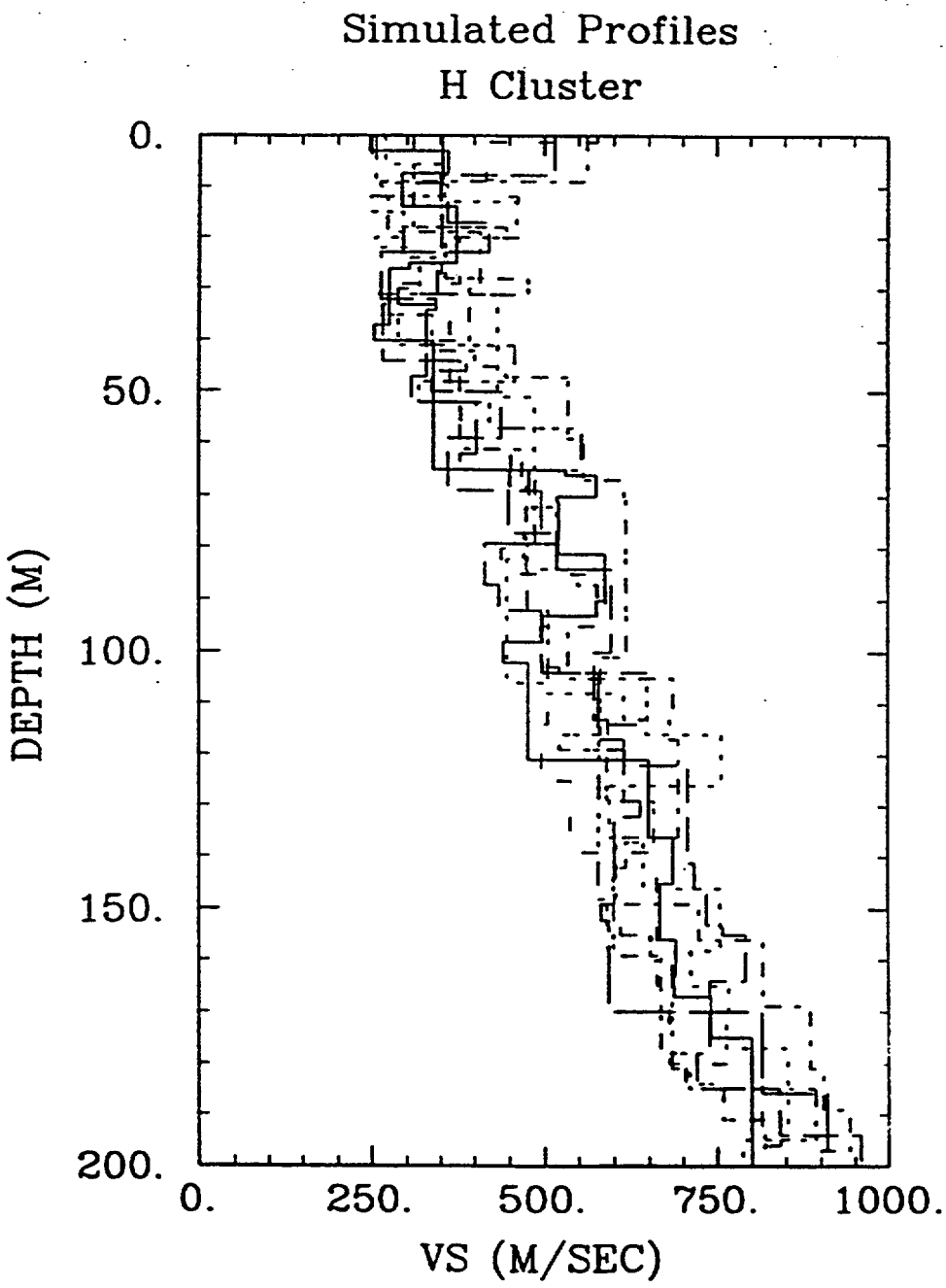

Figure 33. Velocity profiles simulated with the shear-wave velocity model for cluster H, non-homogeneous renewal layering model.

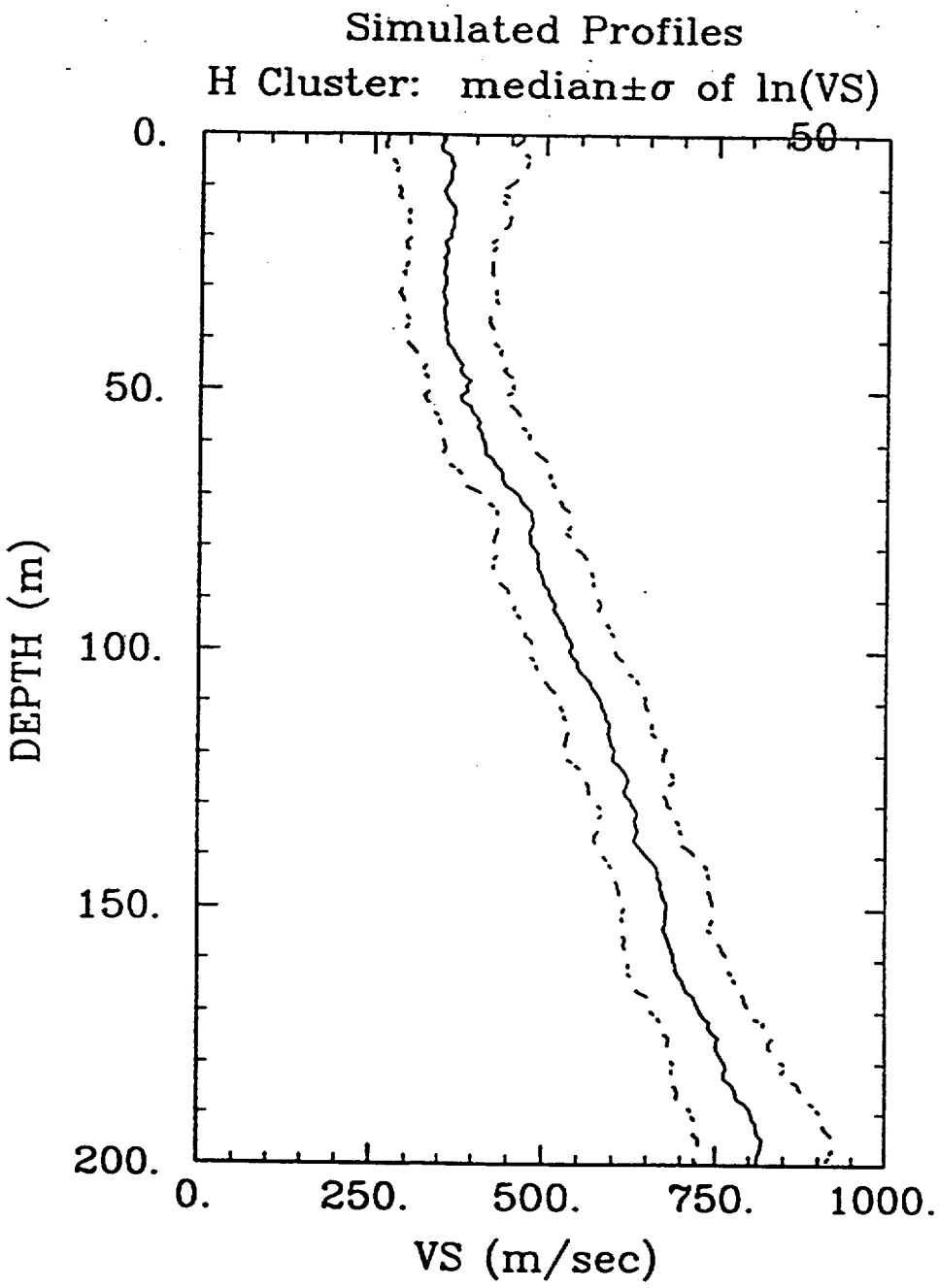

Figure 34. Summary statistics for 50 artificial profiles simulated with the shear-wave velocity model for cluster H: median profile and variability. Solid line, median profile; dashed line, median ± logarithmic standard deviation.

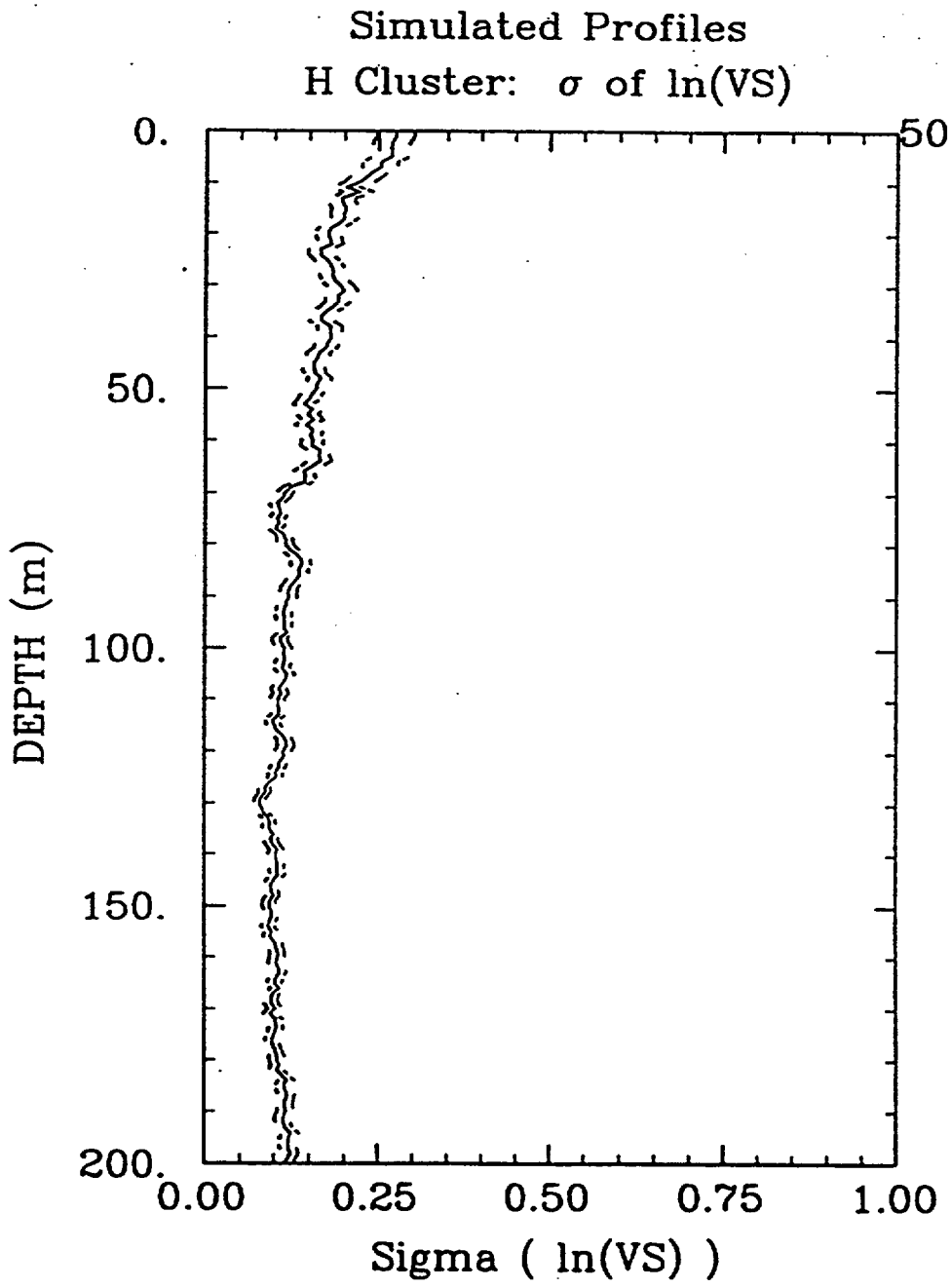

Figure 35. Summary statistics for 50 artificial profiles simulated with the shear-wave velocity model for cluster H: σ_{lnV} vs. depth. Solid line, best estimate; dashed line, best estimate ± standard error of estimation.

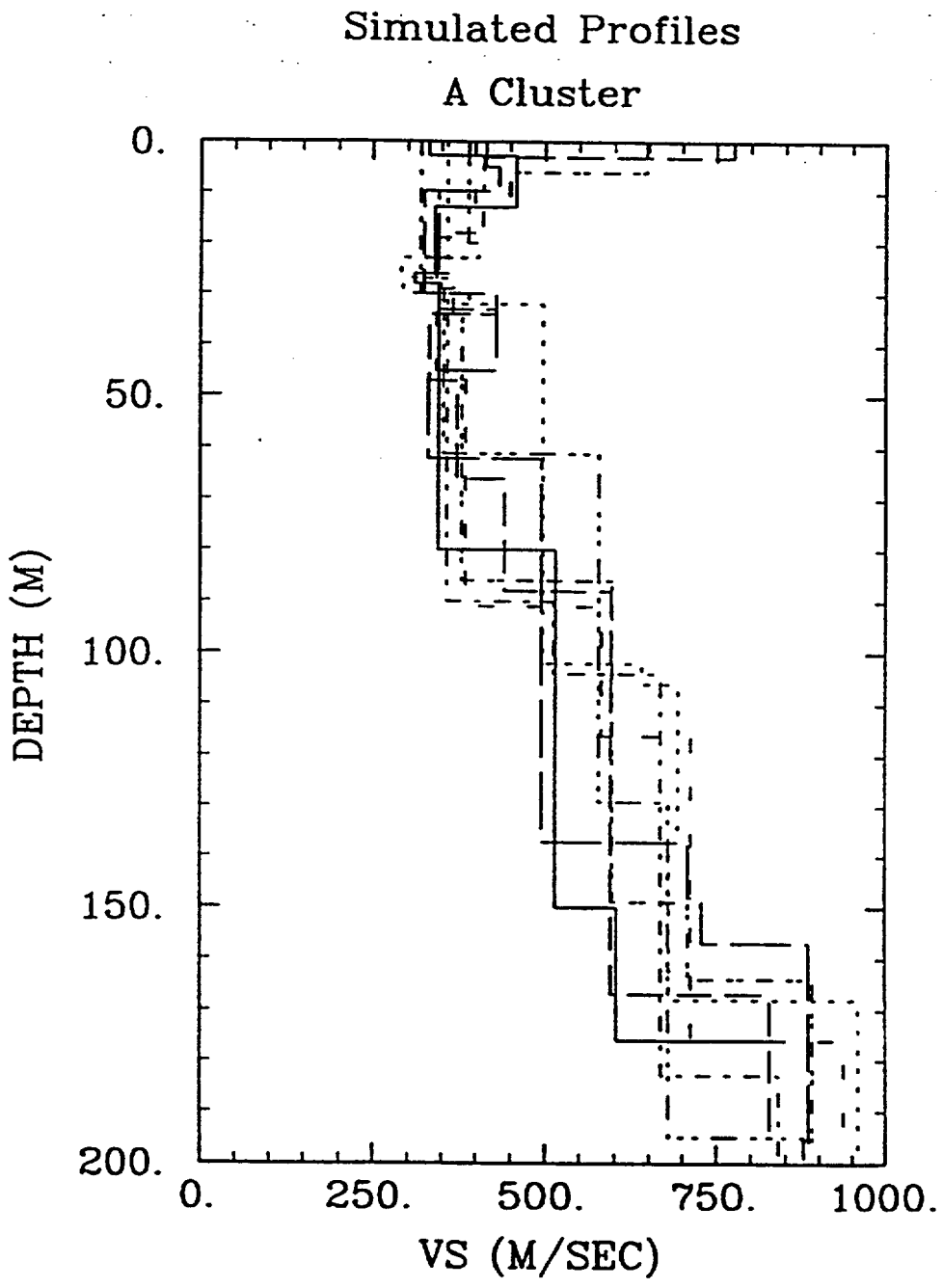

Figure 36. Velocity profiles simulated for cluster A using the site-specific velocity model.

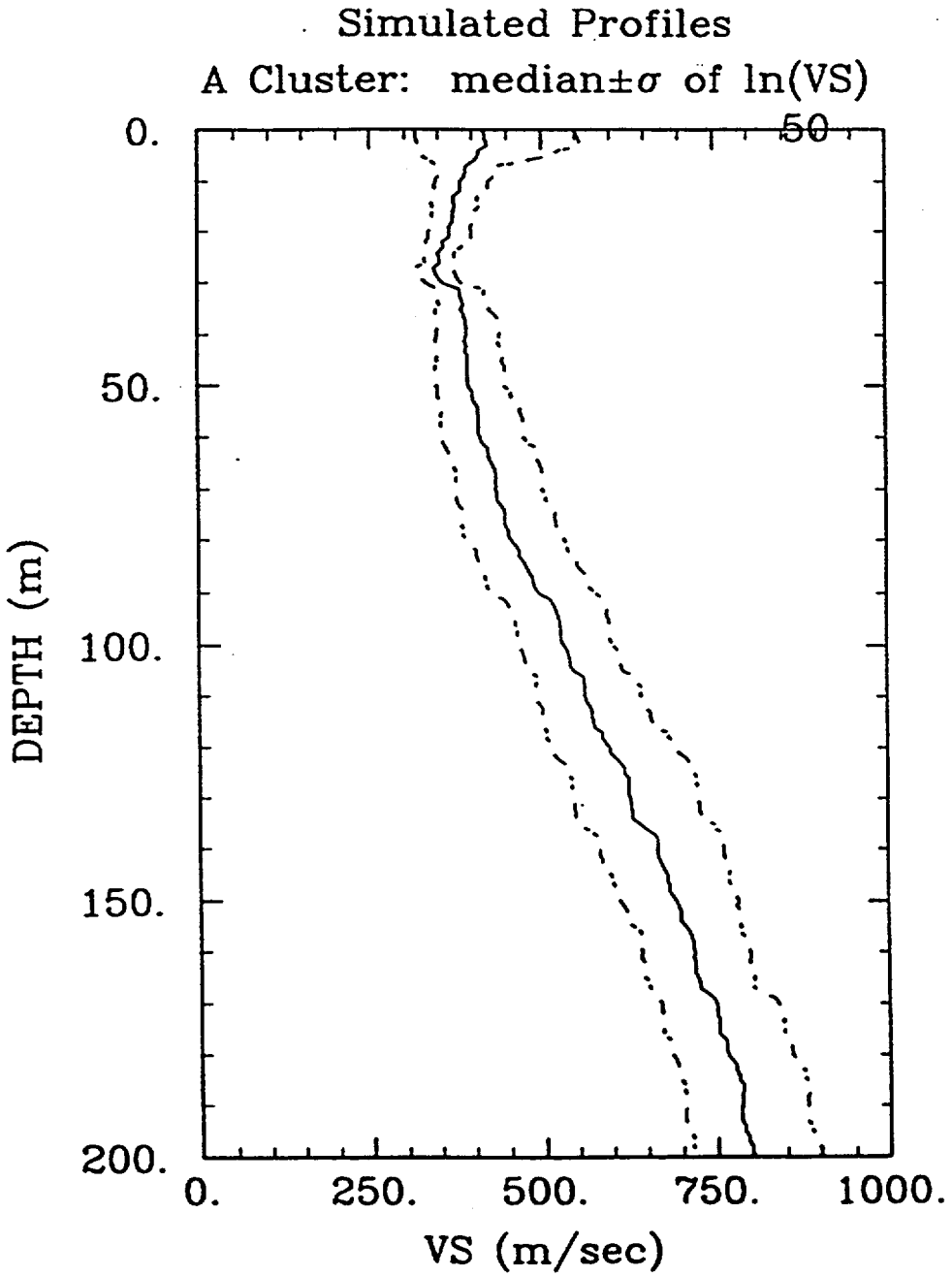

Figure 37. Summary statistics for 50 artificial profiles simulated for cluster A using the site-specific velocity model: median profile and variability. Solid line, median profile; dashed line, median ± logarithmic standard deviation.

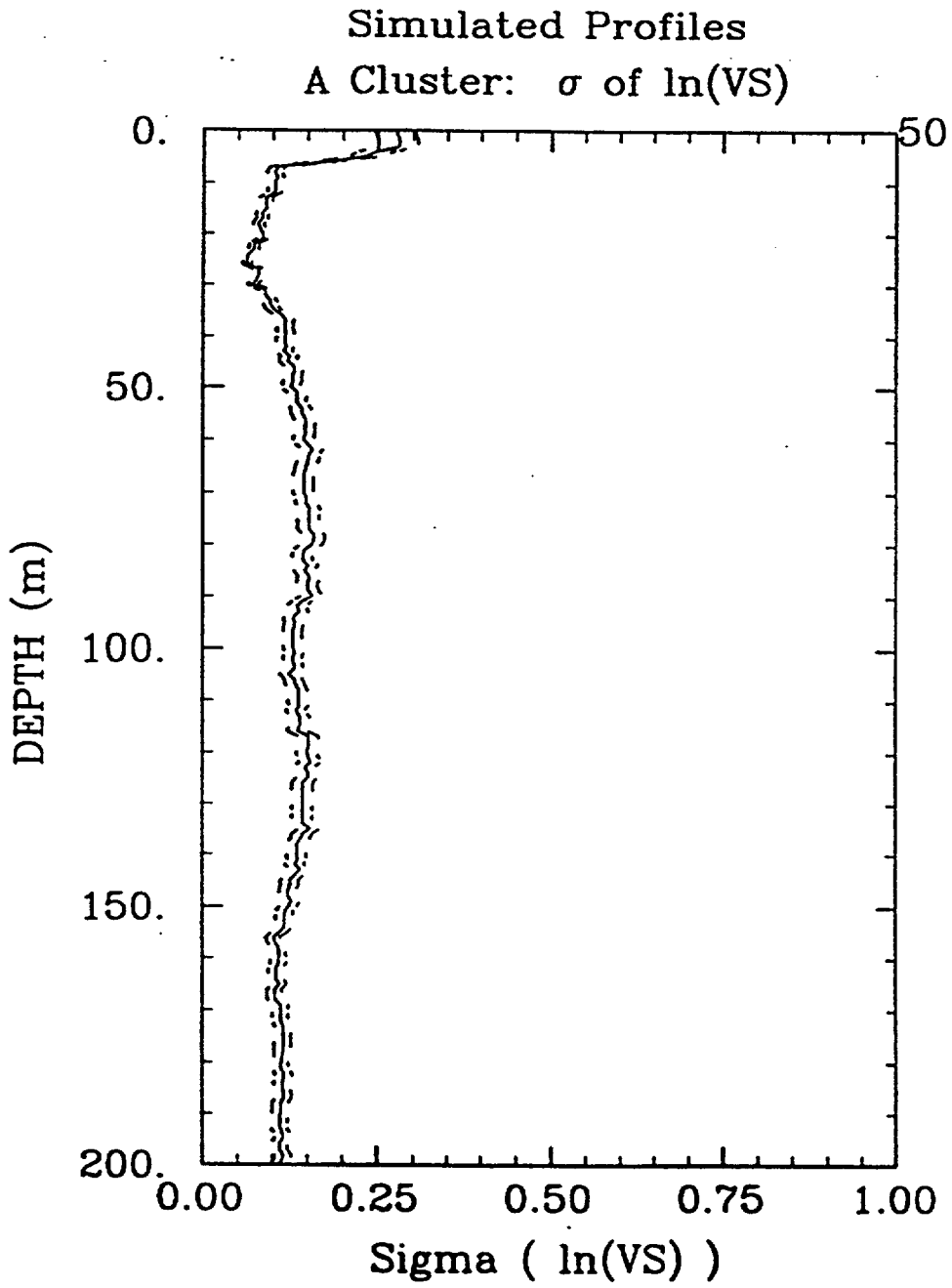

Figure 38. Summary statistics for 50 artificial profiles simulated for cluster A using the site-specific velocity model: σ_{lnV} vs. depth. Solid line, best estimate; dashed line, best estimate ± standard error of estimation.

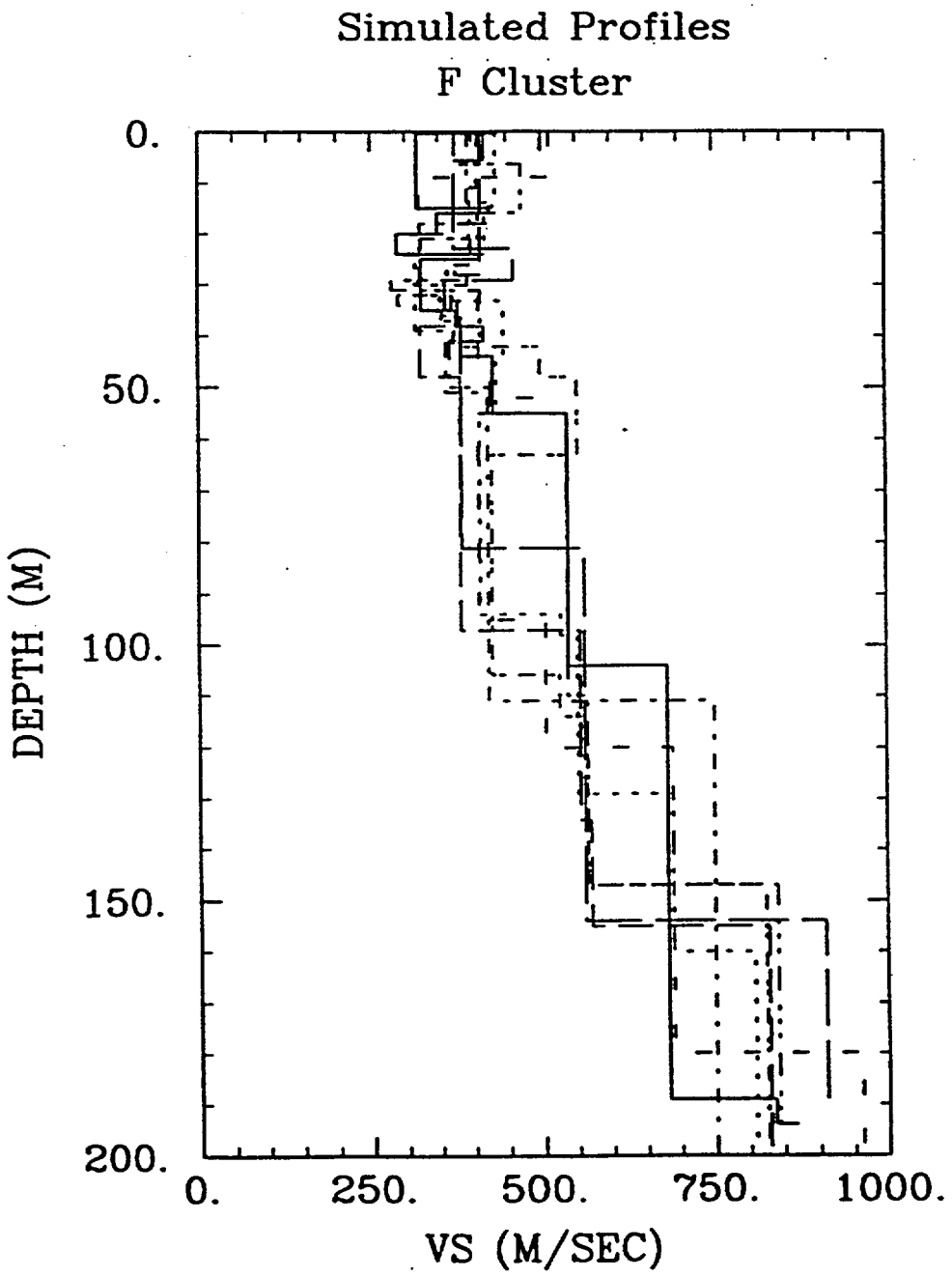

Figure 39. Velocity profiles simulated for cluster F using the site-specific velocity model.

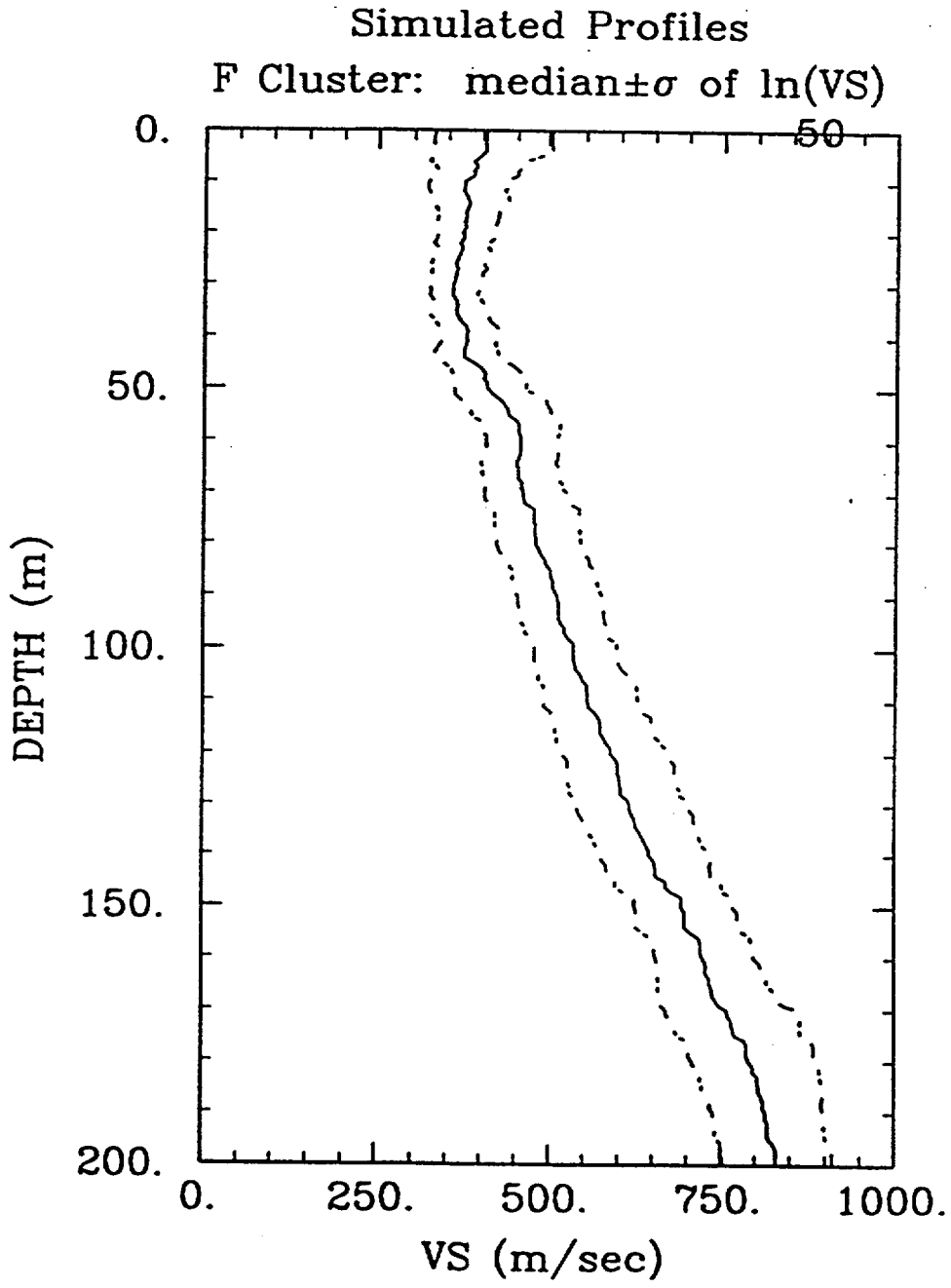

Figure 40. Summary statistics for 50 artificial profiles simulated for cluster F using the site-specific velocity model: median profile and variability. Solid line, median profile; dashed line, median ± logarithmic standard deviation.

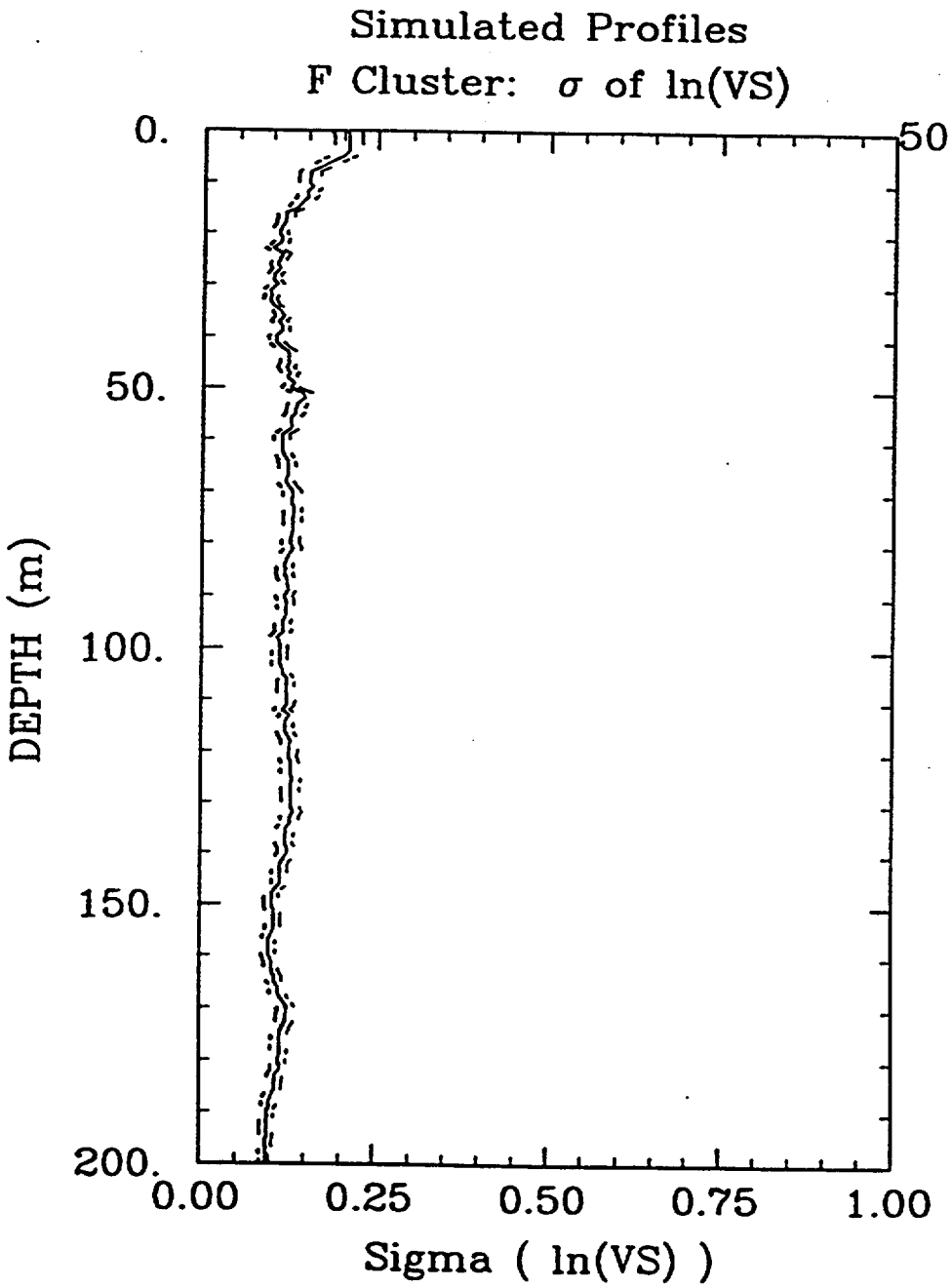

Figure 41. Summary statistics for 50 artificial profiles simulated for cluster F using the site-specific velocity model: σ_{lnV} vs. depth. Solid line, best estimate; dashed line, best estimate ± standard error of estimation.

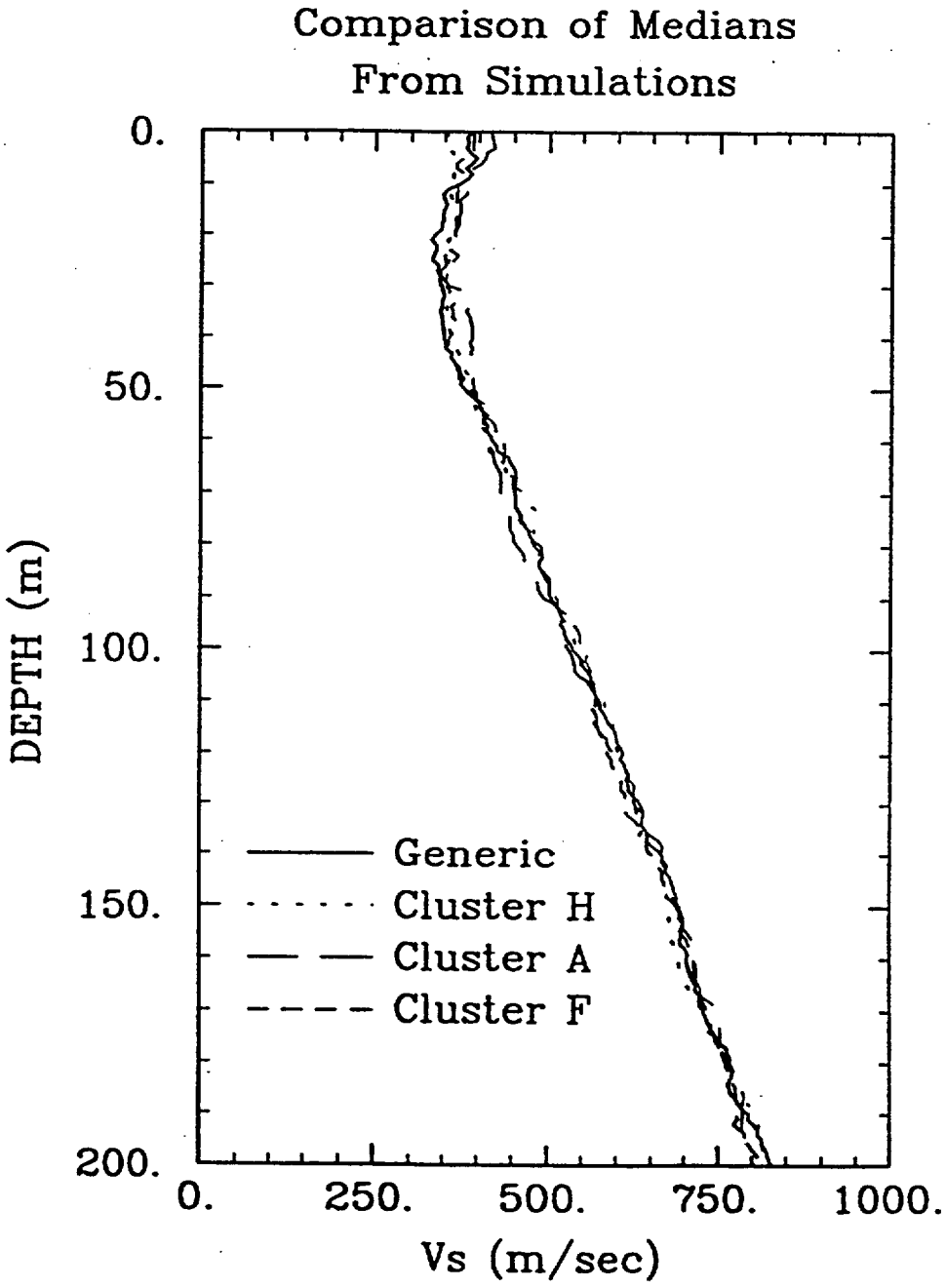

Figure 42. Comparison of median shar-wave velocity profiles from simulations for generic conditions and for clusters A, F, and H.

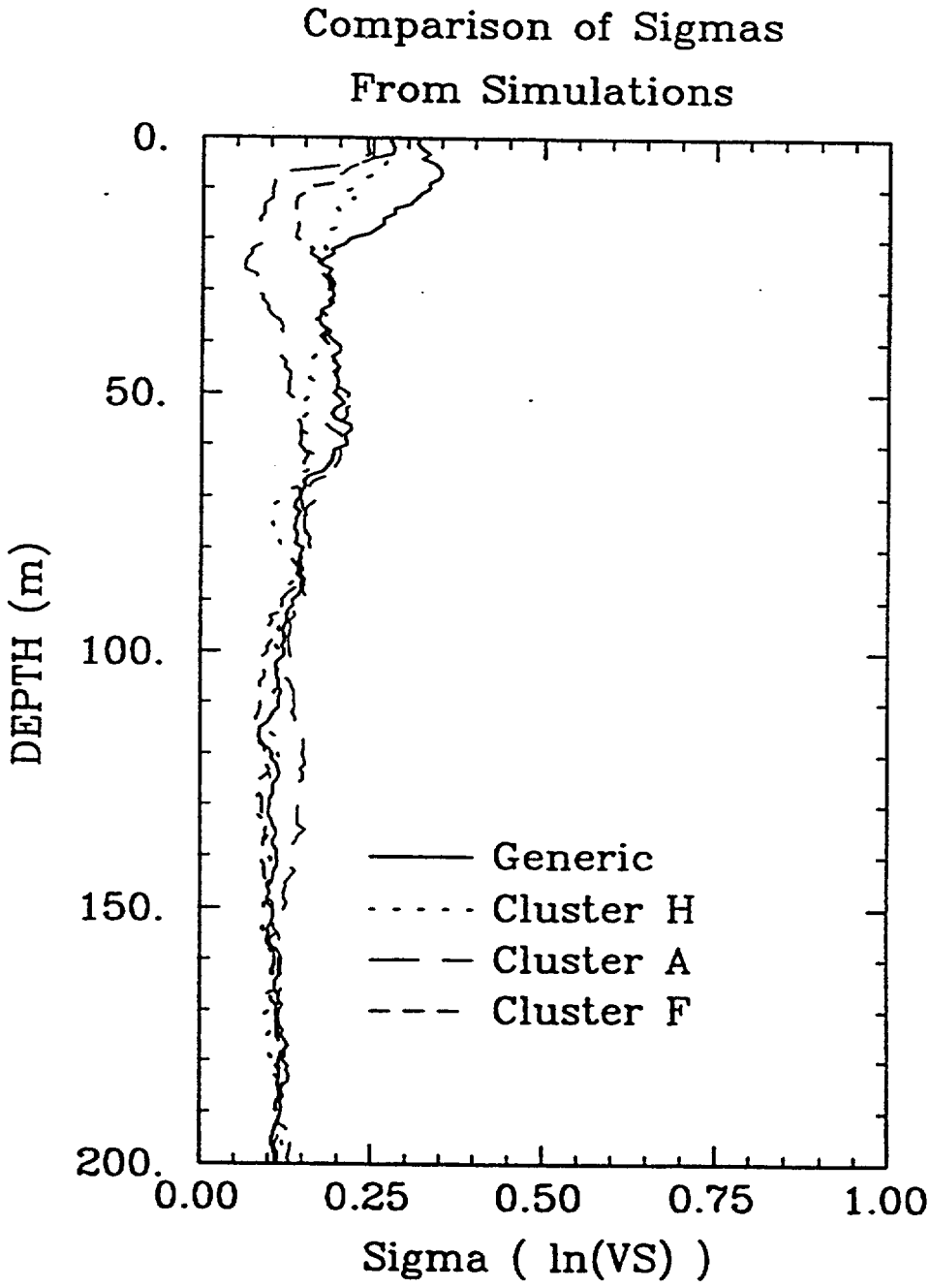

Figure 43. Comparison of σ_{lnV} vs. depth from simulations for generic conditions and for clusters A, F, and H.